EPRI | ELECTRIC POWER RESEARCH INSTITUTE

Fukushima Technical Evaluation

Phase 2—Revised GOTHIC Analysis

3002005295

Fukushima Technical Evaluation

Phase 2—Revised GOTHIC Analysis

3002005295

Technical Update, July 2015

EPRI Project Manager

R. Wachowiak

All or a portion of the requirements of the EPRI Nuclear Quality Assurance Program apply to this product.

YES  NO

ELECTRIC POWER RESEARCH INSTITUTE
3420 Hillview Avenue, Palo Alto, California 94304-1338 ▪ PO Box 10412, Palo Alto, California 94303-0813 ▪ USA
800.313.3774 ▪ 650.855.2121 ▪ askepri@epri.com ▪ www.epri.com

DISCLAIMER OF WARRANTIES AND LIMITATION OF LIABILITIES

THE FOLLOWING ORGANIZATION, UNDER CONTRACT TO EPRI, PREPARED THIS REPORT:

Numerical Applications Division of Zachry Nuclear Engineering

THE TECHNICAL CONTENTS OF THIS PRODUCT WERE NOT PREPARED IN ACCORDANCE WITH THE EPRI QUALITY PROGRAM MANUAL THAT FULFILLS THE REQUIREMENTS OF 10 CFR 50, APPENDIX B. THIS PRODUCT IS NOT SUBJECT TO THE REQUIREMENTS OF 10 CFR PART 21.

This is an EPRI Technical Update report. A Technical Update report is intended as an informal report of continuing research, a meeting, or a topical study. It is not a final EPRI technical report.

NOTE

For further information about EPRI, call the EPRI Customer Assistance Center at 800.313.3774 or e-mail askepri@epri.com.

ACKNOWLEDGMENTS

The following organization, under contract to the Electric Power Research Institute (EPRI), prepared this report:

Numerical Applications Division of Zachry Nuclear Engineering
1955 Jadwin Ave, Suite 470
Richland, WA 99354

Principal Investigators
T. L. George
M. Marshall
O. E. Ozdemir
J. Zankowski
M. S. Lanza
S. W. Claybrook

This report describes research sponsored by EPRI.

This publication is a corporate document that should be cited in the literature in the following manner:

Fukushima Technical Evaluation, Phase 2— Revised GOTHIC Analysis, EPRI, Palo Alto, CA: 2015. 3002005295.

ABSTRACT

This report describes investigations on various aspects of the 2011 Fukushima Daiichi event using the GOTHIC code. GOTHIC is a general-purpose thermal hydraulics code that has the capability to model 3-dimensional flow behavior including the effects of turbulence, diffusion, and buoyancy. This allows GOTHIC to be used in cases where mixing effects and stratification are important.

Five aspects of the Fukushima event are considered here:

- Mixing and local heat transfer effects in the 1F1 drywell
- Mixing effects in the wetwell of 1F3
- Mixing effects in the 1F1 reactor building
- Wetwell venting and interaction with the standby gas treatment system and reactor building ventilation system
- Plant flooding from the tsunami surge

Based on the investigations described in this report, it was found that for this type of event, the containment pressure and temperature response is sensitive to phenomena not typically included in BWR design basis containment analysis. These include:

- Stratification in the suppression pool and in the drywell gas space
- Heat transfer from the drywell vents, header and downcomers to the wetwell gas space, with condensation in the vent system
- Heat transfer from the wetwell gas space to the torus room and surrounding structures
- Leakage between the drywell and wetwell gas space (steam bypass)

The sensitivity of the containment pressure to details such as these may have implications for the understanding of the primary system response during the Fukushima event. These should be considered when evaluating the event using integrated severe accident computer simulations, such as MAAP.

Keywords
Containment
Fukushima
GOTHIC
Severe accident management
Stratification

CONTENTS

LIST OF FIGURES

LIST OF TABLES

1
INTRODUCTION

1.1 The Event

On March 11, 2011, at 14:46 Japan Standard Time (JST), the Fukushima Daiichi Nuclear Power Station experienced a seismic event of historic magnitude. The earthquake—known as the *Tohoku-Chihou-Taiheiyo-Oki Earthquake*—originated offshore with an epicenter located 178 km from Fukushima Daiichi. This earthquake, with a magnitude of 9.0 on the Richter scale, was the largest ever recorded in Japan and the fourth largest ever recorded in the world. The earthquake and subsequent events at the Daiichi site have been extensively documented by the Tokyo Electric Power Company (TEPCO).

At the time of the earthquake, three of the six reactors at the Fukushima Daiichi (Daiichi loosely translates as "number one") Nuclear Power Station were operating at full power, while the remaining three were in various shutdown operational modes. Units 1, 2, and 3 (referred to as 1F1, 1F2, and 1F3 in this report) were operating at full power at the time of the seismic event. Units 4, 5, and 6 were in shutdown mode. Unit 4 (1F4) had been in shutdown mode for a reactor pressure vessel (RPV) shroud replacement since November 30, 2010. Because of the shroud maintenance work, all fuel had been removed from the RPV and stored in the spent fuel pool (SFP). Unit 5 (1F5) had been in shutdown since January 3, 2011, but was being readied for a return to power operation. The fuel was loaded into the RPV, the upper head reassembled, and the vessel pressurized in preparation for leak testing. As with 1F5, Unit 6 (1F6) was also being prepared for a return to power operation, with fuel loaded into the RPV and the upper head reassembled.

For all operating units (1F1, 1F2, and 1F3), the available evidence indicates that the safety systems functioned as required immediately after the seismic event. Following the loss of offsite power after the seismic event, the required emergency diesel generators (EDGs) loaded. The safety systems providing core cooling started according to design. The cooling of the SFPs at each unit was maintained. In addition, at each of the Fukushima Daiichi units, post-accident investigations have not identified any structural damage that could have compromised the reactor coolant system (RCS) pressure boundary, containment envelope, or SFP integrity following the seismic event. Based on the current state of knowledge, the key safety functions at the Fukushima Daiichi plants were not compromised by the seismic event.

The event, however, set in motion additional natural phenomena that would cause the most critical challenge to plant safety functions. As a result of the seismic event, several tsunamis inundated the station starting at 15:27 JST (41 minutes after the earthquake). By 55 minutes after the earthquake, the inundation of the plant by these tsunamis was so severe that a loss of all alternating current (ac) power occurred at 1F1, 1F2, 1F3, and 1F4. The flooding also resulted in all direct current (dc) power being lost at 1F1 and 1F2. Some dc power sources survived at 1F3. Of the five EDGs at Units 5 and 6, one air-cooled EDG for 1F6 continued to produce power. This EDG was later used to supply power to 1F5.

Without sufficient power, critical safety functions were either lost or significantly impaired. The loss of power together with the severity of the aftershocks and risks of additional tsunamis restricted the initial response to the accident. The seismic events and tsunami surges significantly damaged roads and associated infrastructure at the site and surrounding areas. This made it nearly impossible, in the hours after the tsunami arrived, to supplement each unit's capabilities to cope with the challenge to critical safety functions caused by the loss of power.

The need for rapid response to restore or maintain critical safety functions was most pressing at the three units operating at the time of the seismic event (1F1, 1F2, and 1F3). With the 1F1/2 control room and associated reactor buildings (RBs) in darkness, and operators at 1F3 attempting to maintain core cooling with limited battery power, the capability to identify and maintain the condition of the reactor cores was severely compromised. With limited ways to cope with the most severe challenge to a nuclear power plant's critical safety functions, the conditions at 1F1, 1F2, and 1F3 worsened over the hours and days following the initial seismic event. The extreme temperatures and pressures that had developed inside the respective containments resulted in a partial loss of containment function. Fission products and flammable gases that had evolved during the degradation of the 1F1, 1F2, and 1F3 reactor cores were released from the containment into adjacent structures. Severe damage occurred at the site as a result of combustion of the flammable gases inside RBs, and off-site radiological releases occurred before the condition of the three severely damaged reactor cores could be stabilized. The valiant efforts of operators at the Fukushima Daiichi plant to restore cooling to the cores eventually stabilized conditions at the site over the ensuing weeks.

1.2 Scope of This Report

This report describes investigations on various aspects of the Fukushima Daiichi event using the GOTHIC code. The investigation is intended to support and augment analysis of the event using the MAAP computer code (EPRI, 2013).

The analysis presented here takes advantage of the capability of GOTHIC to model certain aspects of the system geometry and behavior in more detail than considered in the MAAP analysis. GOTHIC is a general purpose thermal hydraulics code that is used extensively in the nuclear industry for system design support, licensing support and safety analysis. It has the capability to model 3-dimensional flow behavior including the effects of turbulence, diffusion and buoyancy. This allows GOTHIC to be used in cases where mixing effects and stratification are important.

The results presented in this report are based on limited information for the plant physical parameters and the results from preliminary assessments of the accident scenario developed by others using the MAAP codes. Results may change as more detailed information becomes available and the accident scenario is refined.

Five aspects of the Fukushima event are considered here:

1.2.1 Mixing and Local Heat Transfer Effects in the 1F1 Drywell

The release of combustible gases and radioactive material from the primary containment system (drywell and wetwell) depends on the mixing within the drywell, local heat transfer and condensation rates, and the location of the leak points. A 3-dimensional model of the 1F1

drywell was constructed to investigate local temperature and gas concentrations in the drywell using estimated mass and energy release rates from the reactor vessel.

1.2.2 Mixing Effects in the Wetwell of 1F3

In the early part of the event, energy was transferred to the wetwell via steam from the Safety Relief Valves or from the reactor core isolation cooling (RCIC) pump exhaust for all three units. Mixing in the wetwell pool affects the pool surface temperature and therefore the steam content, temperature, and pressure of the gas space above the pool. In this section, the focus is on the performance of the 1F3 suppression pool during the operation of the RCIC system over the first 24 hours of the event.

1.2.3 Mixing effects in the 1F1 Reactor Building

The explosion in the 1F1 reactor building was the result of the release of combustible gases from the primary containment vessel. Various scenarios are investigated for the release points, estimated release rates, and the subsequent mixing in the reactor building. A 3-dimensional model for the reactor building is used to predict the gas distribution for the assumed release conditions.

1.2.4 Wetwell Venting and Interaction with the Standby Gas Treatment System and Reactor Building Ventilation System

The reactor building model includes the building ventilation system, Standby Gas Treatment System (SGTS), and the wetwell vent system. It is expected that at the time the wetwell was vented that there was significant amounts of combustible gases in the wetwell gas space. The explosion in the 1F1 reactor building occurred about 30 minutes after the wetwell venting occurred, leading to the conjecture that some of the combustible gases in the wetwell made their way into to the reactor building. Various scenarios were investigated for the venting operation and possible mechanisms for gas release into the reactor building.

1.2.5 Plant Flooding from the Tsunami Surge

A 3-dimensional model of the 1F1 and 1F2 plant buildings was constructed to investigate the intrusion of water from the tsunami and the migration of water within the building. Various scenarios were run to investigate flooding of various rooms in the plant with focus on the torus rooms.

2
1F1 DRYWELL PERFORMANCE

2.1 Introduction

The objective of this task is to investigate the impact on the calculated containment behavior when multidimensional effects and vent heat transfer details are included in the analysis. The investigation is intended to support and expand analysis of the event using the MAAP5 computer code. The investigation began with construction of a multidimensional GOTHIC model that includes subdivided volumes for the wetwell, drywell and vent system. The detailed model was then reduced to lumped model that is comparable to the MAAP5 model. The lumped model relies on mass and energy source terms calculated by MAAP5 for the steam, H_2 and CO released to the drywell, and the heat flux from the RPV to the drywell. With some minor adjustments to the MAAP5 source terms results comparable to those from MAAP5 were obtained.

Using the GOTHIC lumped model as a baseline for comparison; the effects of multidimensional behavior in the drywell and vent heat transfer were investigated with the subdivided model. The analysis presented here takes advantage of the capability of GOTHIC to model certain aspects of the system geometry and behavior in more detail than typically considered in traditional containment analysis.

As a result of the seismic event, several tsunamis inundated the station (41 minutes after the earth quake). Following the arrival of the tsunami and flooding of the 1F1 turbine building, a Station Blackout (SBO) started 55 minutes from the time of the earthquake with a loss of all the alternating current (ac) power and direct current (dc) power circuits (TEPCO, 2013). Because power was not restored to the 1F1 control, core cooling was lost for a significant period of time. According to MAAP5 baseline scenario (EPRI, 2013), the following assumptions are made in GOTHIC benchmark analysis:

1. No Reactor Pressure Vessel (RPV) seal leakage is assumed to occur.
2. H2 leak and steam leak through the in-core instrument structures is assumed to occur when the maximum core temperature surpasses the melting point of the stainless steel; around 4 hours into the event. (Figure 2-2)
3. RPV depressurization through Safety Relief Valves (SRV) starts around 6 hours
4. RPV lower head failure occurs around 9 hours into the event (Figure 2-5)
5. Leakage from the Pressure Containment Vessel (PCV) occurs through the drywell head gasket. Drywell head lifting starts around 12 hours into the event, with an assumed leakage area of about 10 cm2.
6. Venting of the Suppression Chamber (SC) to the environment is assumed to occur around 24 hours and continues until drywell pressure falls to ~520 kPa (75 psia).

The MAAP5 calculated drywell pressure is shown in Figure 2-1 with the recorded pressure. The calculated progression of core damage results in earlier containment pressurization than indicated by the measured pressure but, overall, the containment response is closely matched. It

must be recognized that there are many unknowns and uncertainties in this analysis and the good agreement with the recorded data is achieved by adjusting the unknown inputs within reasonable limits.

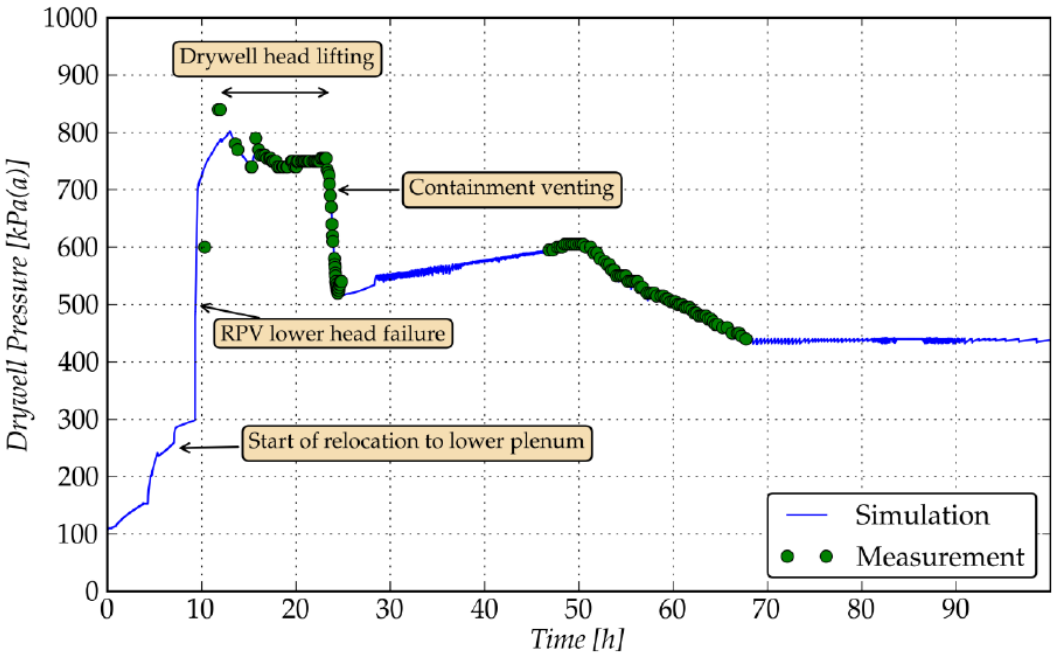

Figure 2-1
1F1 MAAP5 Baseline Scenario—Simulated Drywell Pressure Transient (EPRI, 2013)

Figure 2-2, Figure 2-3, Figure 2-4 and Figure 2-5 show the MAAP5 calculated total gas (Steam, H_2, and CO) and heat release from RPV to DW respectively (EPRI, 2013). These predictions are used as inputs to model the RPV response in the GOTHIC models.

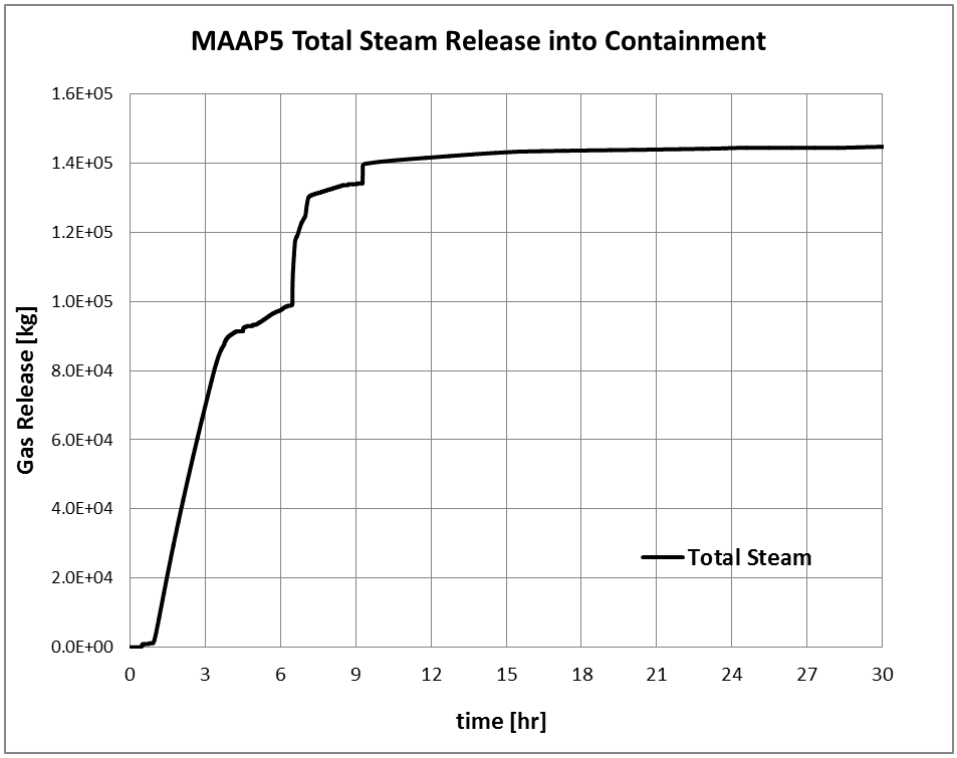

Figure 2-2
1F1 MAAP5 Baseline Scenario—Total Steam Release into Containment (EPRI,2013)

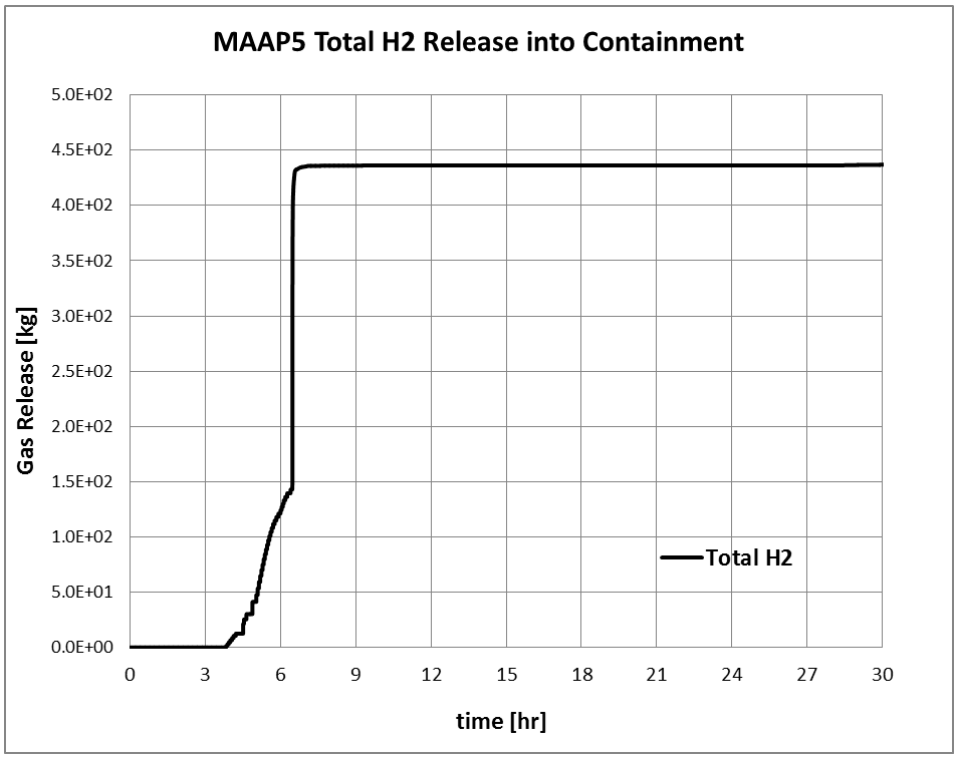

Figure 2-3
1F1 MAAP5 Baseline Scenario—Total H_2 Release into Containment (EPRI,2013)

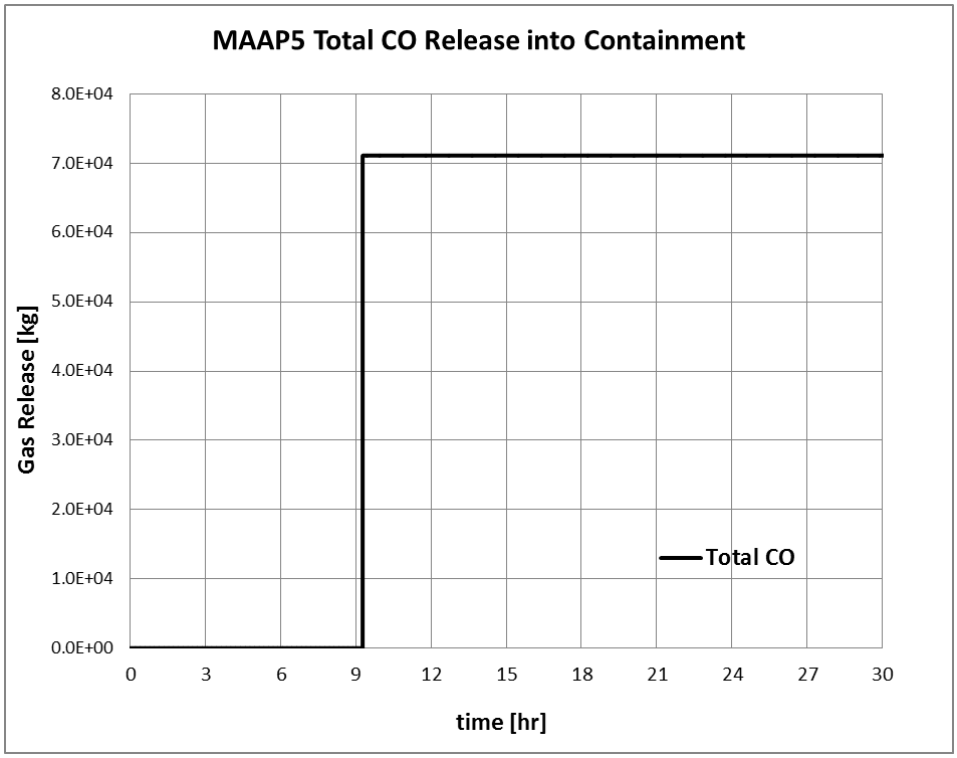

Figure 2-4
1F1 MAAP5 Baseline Scenario—Total CO Release into Containment (EPRI,2013)

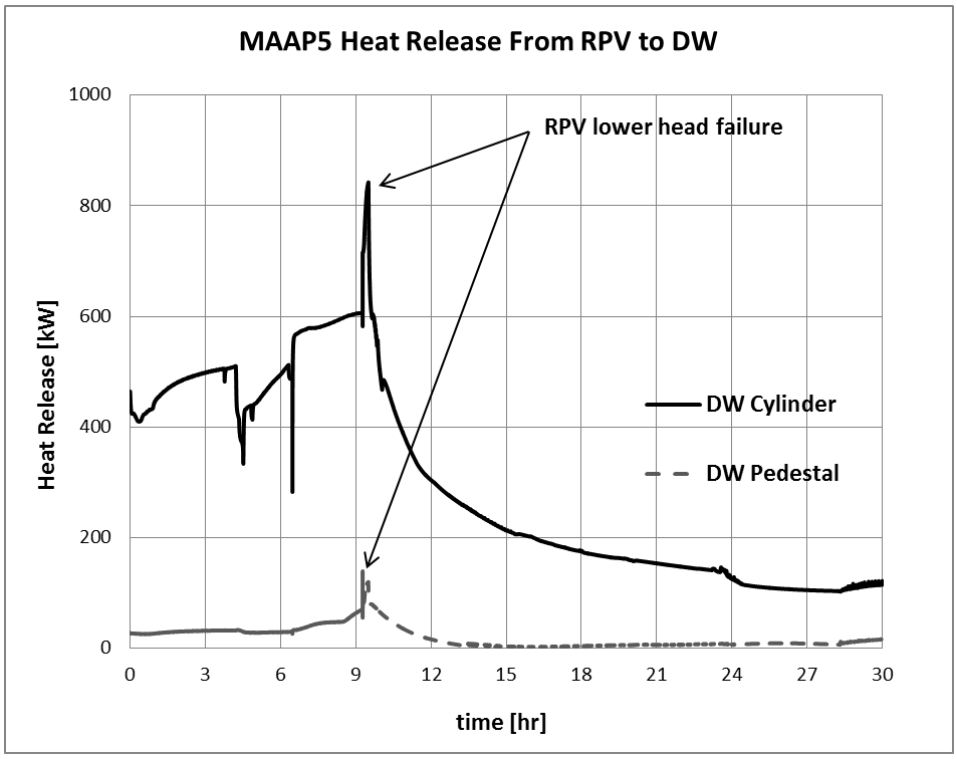

Figure 2-5
1F1 MAAP5 Baseline Scenario—Heat Release from RPV (EPRI,2013)

2.2 GOTHIC Model

GOTHIC Version 8.1 was used to model the 1F1 containment system. The multidimensional model for the containment is described below. The containment model is designed to address drywell mixing and the heat transfer between the drywell vent system and the wetwell during the postulated 1F1 scenario. The scope is limited to the containment response and does not include prediction of the fuel or RPV response. The MAAP5 1F1 baseline simulation of the event is used to provide input to the GOTHIC model for to the steam, H_2 and CO release and heat transfer from the RPV to the containment (Figure 2-2 and Figure 2-5). A graphical representation of the GOTHIC model is shown in Figure 2-6 with pertinent information for the GOTHIC volumes shown in Table 2-1.

In order to reduce the runtime of the multidimensional simulation, a 1/8 sector of the total containment geometry is modeled using an assumed 3D axisymmetric treatment of a generic Mark 1 containment geometry. The geometric parameters of the model are consistent with the Unit 1 measurements (OECD-NEA, 2012). Other unknown parameters, such as the SRV T-Quencher geometry, are estimated from the Monticello plant Mark 1 design (Patterson, B. 1979).

Table 2-1
Unit 1 Volume Data

Volume 1	DW Inner Cylinder
Volume 2	DW Outer Sphere
Volume 3	RPV Leak Mix Volume
Volume 4	DW Head Exit Chamber
Volume 5	DW Head Chamber
Volume 6	Suppression Pool Vent Pipe
Volume 7	Torus Room
Volume 8	Torus Tube
Volume 9	Vent inside Torus Tube
Volume 10	Vent Inside Torus Room
Volume 11	Inner Downcomers
Volume 12	Outer Downcomers
Volume 13	T-Quencher

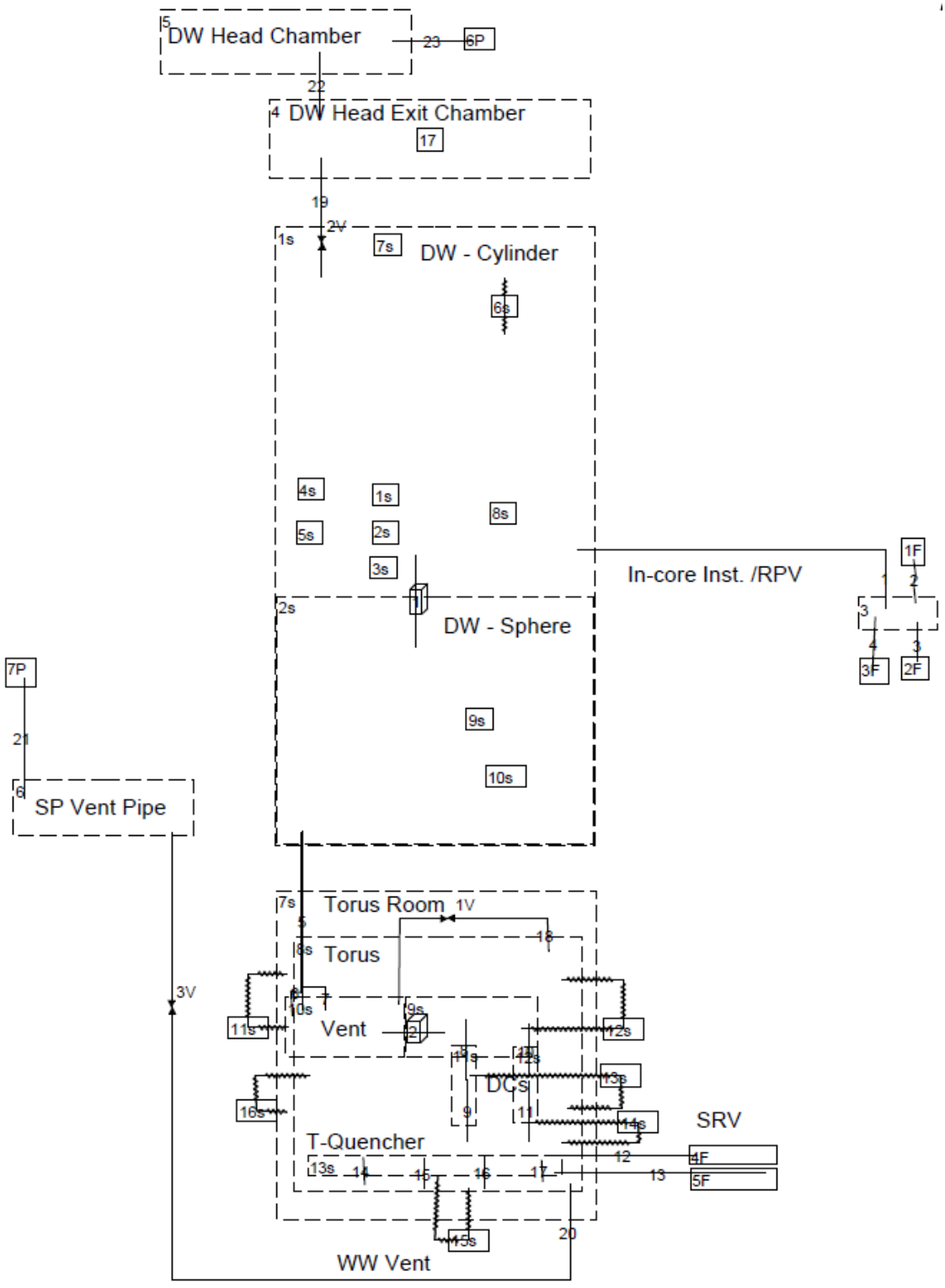

Figure 2-6
1F1 Containment Noding Diagram

2.2.1 Drywell Model Description

A subdivided drywell model was constructed for a 3D representation of the cylindrical and lower spherical portions of the drywell including the RPV, bioshield wall, and major flow paths for natural circulation that exist within the drywell. The important aspects of the drywell model are listed as follows:

1. The drywell model is divided into a central cylindrical volume (Volume 1s), representing the interior cylindrical volume from the drywell top to bottom (including the pedestal region), and a volume representing the outer spherical portion of the lower drywell (Volume 2s). These two volumes are subdivided with sufficient detail to model the natural circulation paths within the drywell. The inner and outer drywell volumes are connected via a 3-D flow connector, allowing unrestricted flow between the inner and outer portions of the lower spherical portion of the drywell.

As shown in Figure 2-7, blockages represent the RPV and Main Steam piping within the DW as well as the bioshield wall supporting and surrounding the lower RPV. The approximate 8 inch gap between the RPV and the bioshield wall may create a potential chimney effect as the hot vessel heats the surrounding air that would enhance mixing in the drywell by bouncy driven flow. However, in some Mark I containment designs, there is a skirt at the bottom of the bioshield annulus that effectively blocks flow into the annulus from below. Annulus details were not available for 1F1. As shown in Figure 2-7, the annular opening is assumed to be blocked by a thin plate from the pedestal region. Therefore, the annulus is open to the drywell at the top, but not at the bottom. This assumption will tend to reduce the drywell mixing by natural convection.

1. Shell conductors 1, 2 and 3 are assigned to RPV blockages, providing a heat source for the upper DW upper cylindrical region, lower DW spherical region and bottom pedestal region, respectively. For the GOTHIC lumped model analysis, the MAAP5 baseline simulation heat flux results (Figure 2-5) were used to specify the heat flux on the RPV side of the conductor. In the subdivided model analysis, however, the local RPV heat flux varies as the DW gas temperature changes in each region. Thus, the uniform heat flux assumption is not appropriate in subdivided models. Instead, the conductor surface temperatures that were obtained from the lumped model were specified as input for the RPV side of the conductors in the 3D model.
2. The convective heat transfer from the main steam lines and recirculation lines to the drywell is modeled using conductors 4 and 5 located at appropriate positions within the drywell. The heat sources are modeled with multi-region conductors including an interior metal wall, estimated air gap (2 inch) and an insulation layer. In the lumped model, an estimated constant 550 F (287 C) internal temperature is used as boundary condition for conductors 4 and 5. In the subdivided model, the internal temperature of the RPV side of the conductor 1 is used as a boundary condition for conductors 4 and 5.

The drywell metal liner for the cylindrical and spherical regions is modeled by conductors 8 and 9, respectively. It is assumed that the material for the metal liner includes a 2 inch air gap between the steel and the structural concrete that is several feet thick. Convective heat loss to the ambient air is assumed for the outside surface of this conductor.

Boundary conditions (1F, 2F and 3F) and flow paths (1, 2, 3 and 4) are included to simulate the postulated sources for steam, H_2 and CO to the drywell. In the MAAP5 analysis, the early release is from an assumed leak through the in-core instrument structures (4 hours into the event). The later sources follow the RPV lower head failure (9 hours into the event) (Figure 2-2). It is assumed that for all of these sources that the release occurs inside the RPV support pedestal.

Valved flow path (19) is included to simulate the postulated leak from the drywell flange to the Refueling Pool Compartment in the Reactor Building when the DW head lifting starts (12 hours into the event).

In the subdivided model, the DW head region above the RPV is modeled as shown in Figure 2-7. The cylindrical region is separated from the head region with a thin flange plate. The heat transfer through the flange plate is modeled with external conductor 6. There is a 3 foot diameter open manway in the plate. This opening is assumed as the only flow passageway from the cylindrical region to the upper head region. The opening is assumed to be located in the modeled 1/8 sector of the drywell. Therefore, the opening size, relative to the modeled dome region is overly large and the calculated mixing between the dome region and the lower drywell may not be as much as indicated in the GOTHIC analysis.

The drywell dome metal liner is modeled by thermal conductor 7, including a 58.5 inch air gap between steel and concrete layers. The surface-to-surface radiation across the air layer is included in the GOTHIC model.

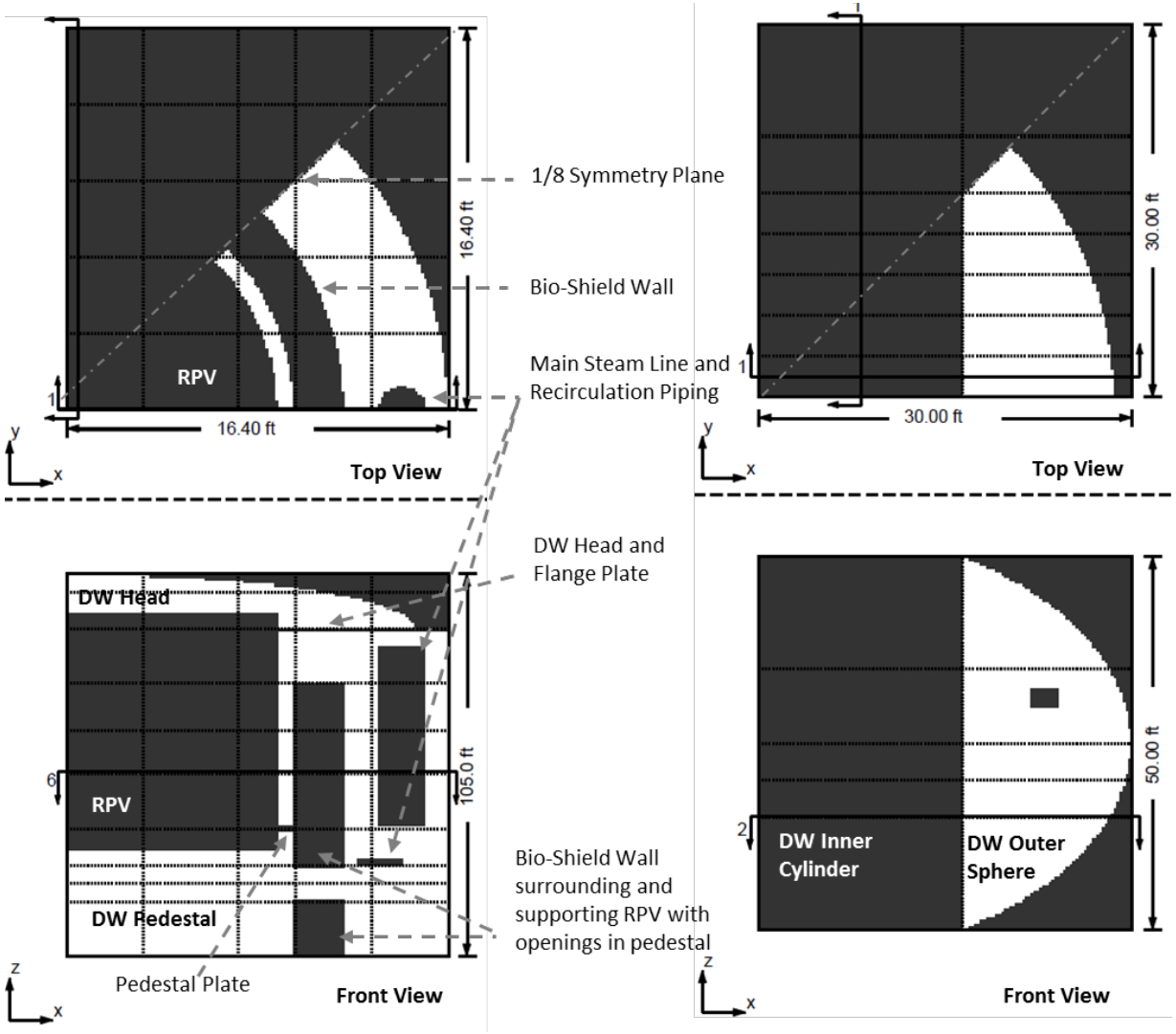

(a) (b)

Figure 2-7
1F1 Inner DW Cylinder Volume 1s (a) and Outer DW Sphere Volume 2s (b)

2.2.2 Wetwell Model Description

The Wetwell (WW) model consists of seven individual subdivided volumes that are connected to each other with 3D connecters and flow paths. To calculate the steam condensation inside the vent and its potential impacts on steam and noncondensable gas flow into the suppression pool, each system is modeled individually in detail as described below:

The Torus model is divided into two main sections; the Torus Room (Volume 7s) which represents the concrete and air space surrounding the vent and torus, and the Torus Tube (Volume 8s). A graphical representation of the Torus and Torus Room is shown in Figure 2-8 (a) and (b) respectively. The average vertical grid spacing both in the suppression pool and gas space above the pool surface is 1.1 feet (0.33 m). The horizontal grid spacing is 4.1ft (1.25 m). The grid spacing across the torus minor diameter is 4.1 feet (1.25 m). It should be noted that the grid spacing inside the torus is fine enough to investigate the vent and downcomer heat transfer effect but it is too coarse to accurately predict the stratification inside the suppression pool.

The vent system is modeled with two subdivided volumes; one inside the Torus Tube (Volume 9s) and one inside the Torus Room (Volume10s). Flow paths from the outer spherical portion of the drywell model represent the main vent lines from the drywell to the Vent Ring Header pipe that resides in the wetwell gas space and distributes the steam/gas/liquid flow from the drywell around the circumference of the suppression pool during a LOCA. The Torus Room Vent and Torus Tube Vent volumes are connected via 3-D flow connectors.

There are 40 inner downcomers and 40 outer downcomers in the 1F1 DW system (OECD-NEA, 2012). Based on the 1/8 axisymmetric modelling approach, 5 downcomers are modeled by each of Volumes Volume 11s and 12s for the inner and outer downcomers, respectively.

Volume 13s represents the T-Quenchers near the bottom of the pool. The Monticello Nuclear Plant (Patterson, B. 1979), was used for the geometric parameters.

Shell conductors (11, 12, 13, 14 and 15) are assigned to the blockages inside each subdivided volume to model the heat transfer across the vent system to the torus room, torus air space and pressure suppression pool.

Flow path 18 and the associated valve model the vacuum breaker (VB) line from the wetwell into the drywell via the drywell vent header.

1. Flow path 20 and associated valve models the manual wetwell venting operation performed at about 24 hours into the event at 1F1.

The GOTHIC model includes heat conductors that model the heat transfer from the steam and gases inside the vent header and the downcomers to the wetwell gas space. Although this feature is of little significance in many scenarios (e.g., Large Break LOCA), for the small steam breaks postulated in the 1F1 scenario, inclusion of this direct heat transfer via conduction through the piping wall has the following potentially significant impacts on the postulated 1F1 scenario:

The vent heat transfer model provides the opportunity for steam within the vent system to condense prior to being released into the suppression pool. Since this steam flow provides the primary mechanism to transport the noncondensable gases (including H_2) from the drywell to the

wetwell, the condensation within the vent system may significantly reduce the transport of noncondensable gases from the drywell to the wetwell.

The heat transfer from the vent system to the wetwell gas space heats the gas space which contributes to the pressurization of the containment system.

The heating of the wetwell gas space has consequences similar to pool thermal stratification since the pool surface would be heated by the gas space with no mechanism to mix the pool. This would tend to reduce any cooling effect the pool might have on the wetwell gas space.

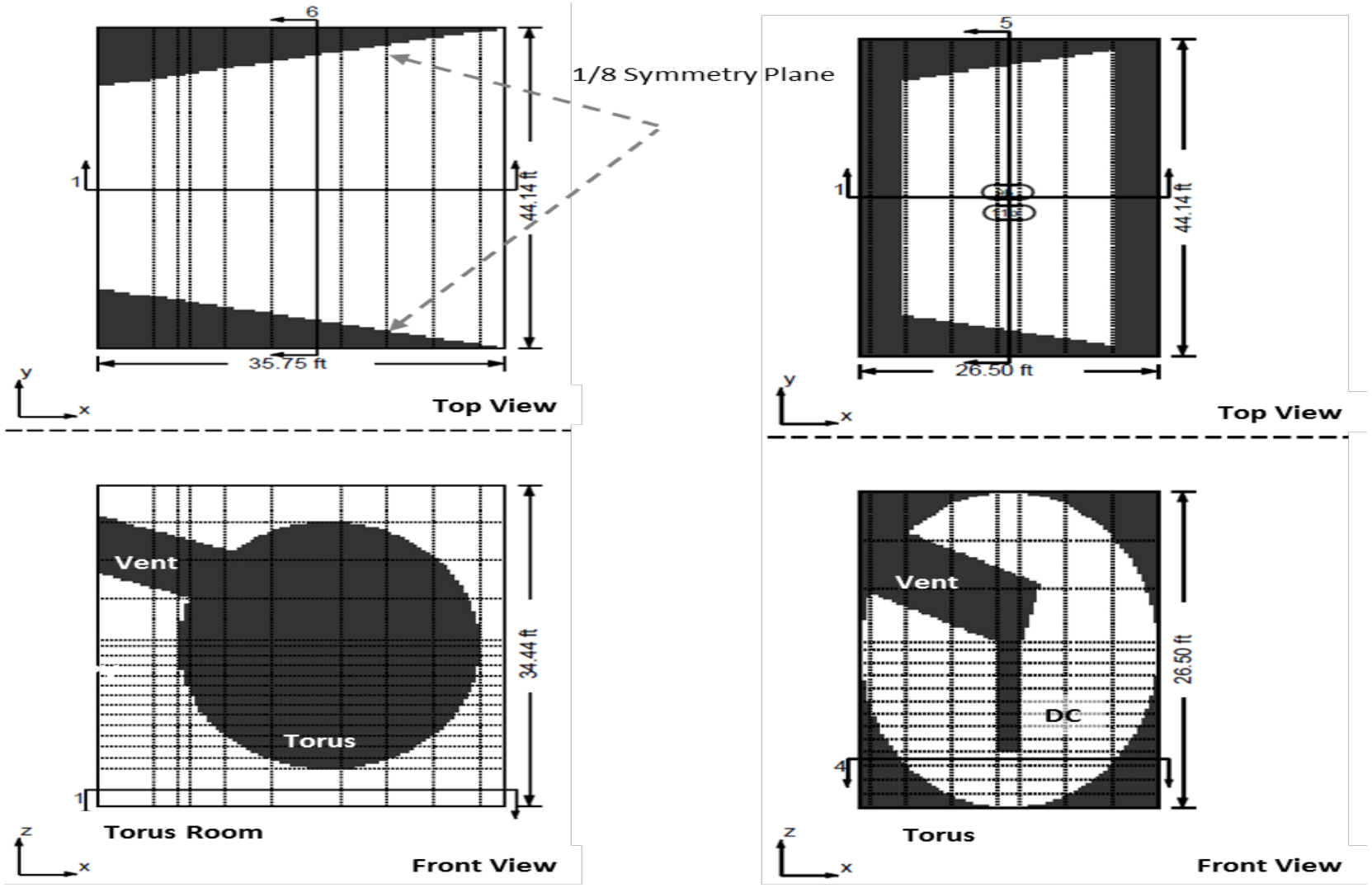

Figure 2-8
1F1 Torus Room Volume 7s (a) and Torus Volume 8s (b)

2.3 GOTHIC Simulation Results

The following discussion compares the GOTHIC lumped model results against the results from the MAAP5 1F1 baseline scenario analysis. Then, the relative effects of drywell mixing and vent heat transfer are investigated by comparing the subdivided model results with the lumped GOTHIC model results.

2.3.1 1F1 Lumped GOTHIC Model without Vent Heat Transfer

Before investigating the multidimensional and vent heat transfer effects, a lumped GOTHIC model was created for the containment that is comparable to the MAAP5 model. This lumped model serves as a baseline for investigating multidimensional and vents heat transfer effects.

The 1F1 Lumped GOTHIC model was generated from the detailed subdivided model nodalization (Figure 2-6). Each subdivided volume was reverted to a lumped volume, preserving the net free volume. The vent system heat transfer was deactivated. Similar to the MAAP5 nodalization, the DW head and DW upper cylindrical regions are represented by Volume 1, and DW pedestal and DW lower spherical regions are represented by Volume 2. By doing so, the MAAP5 calculated heat fluxes (Figure 2-5) from the RPV could be used as boundary conditions in the lumped GOTHIC model.

In order to achieve agreement between the MAAP5 and GOTHIC lumped model results, especially during RPV lower head failure, some adjustments to the specified release rates from the MAAP5 analysis were made. The flow rate functions are defined based on MAAP5 total amount of steam and noncondensable gas predictions. The total steam release during vessel breach was tuned (about 10% more than MAAP5) to match the containment pressure response. In Figure 2-9, the DW and WW pressure response calculated by GOTHIC is compared to the MAAP5 results. The agreement between these two models provides reasonable confidence that the major components of the GOTHIC 1F1 containment model as well as the basic elements of the accident scenarios are appropriately addressed in the GOTHIC lumped model.

As shown in Figure 2-10 , the DW Pedestal/Spherical volume temperature remained higher than the DW Cylindrical/Head volume during the first 16 hours into the event. This difference can be explained by modelling limitations. In the GOTHIC lumped model approach a single flow path is used to connect the pedestal/spherical region to the remainder of the DW. The flow through the connection is driven by the pressure differential between the connected volumes and does not allow bi-directional flow through the connection. Therefore, the mixing in the lumped model will typically be underestimated under natural convection conditions by this lumped GOTHIC model.

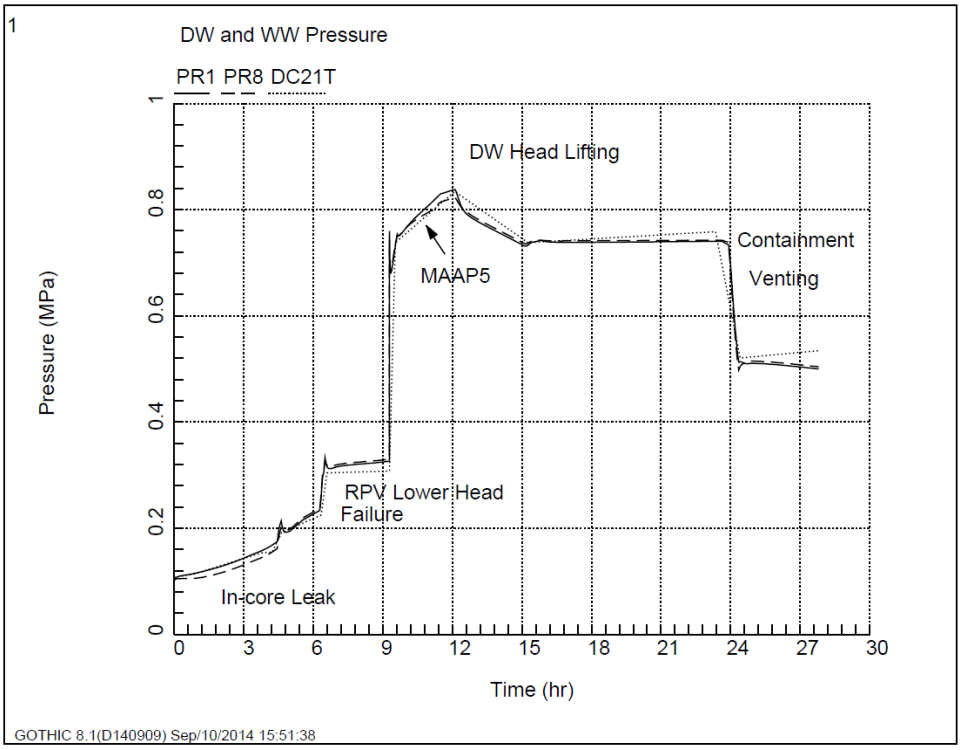

Figure 2-9
GOTHIC Lumped Model – Containment Pressure Prediction

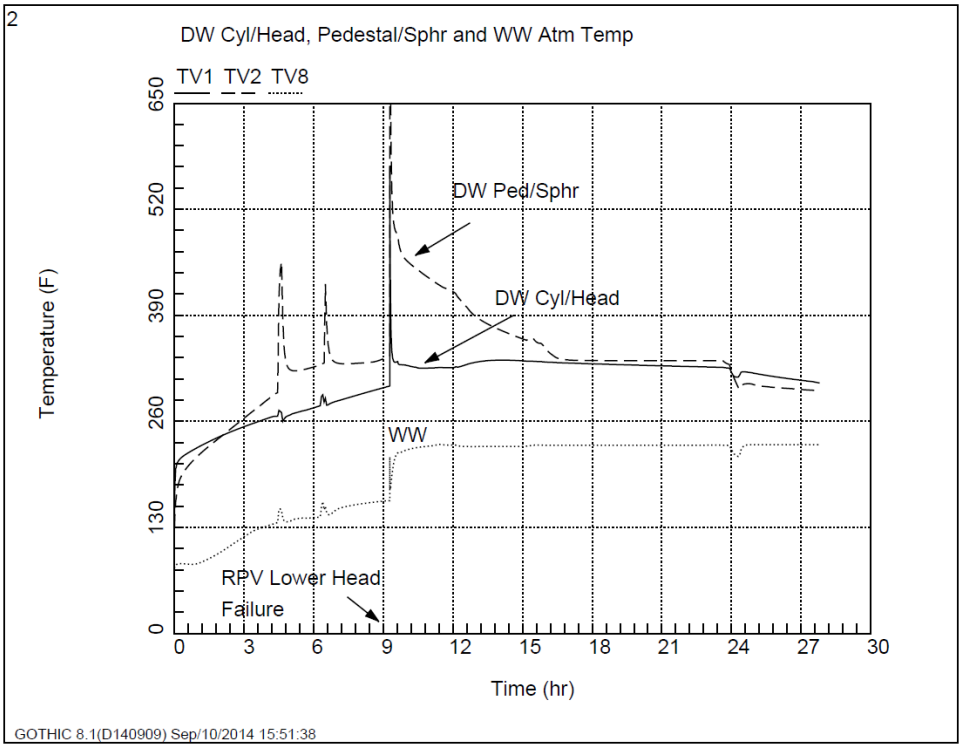

Figure 2-10
GOTHIC Lumped Model – Containment Temperature Prediction

As shown in Figure 2-11, Figure 2-12 and Figure 2-13, the H_2 concentration in the DW starts to build up around 4 hours (in-core instrument leak) and suddenly rises around 6 hours (SRV release in WW) and then drops around 9 hours (RPV lover head failure) into the event. Figure 2-14 and Figure 2-15 show the vent flow and vacuum breaker flow, respectively.

The initial release of hydrogen is from the in-core instrument leakage starting at 4 hours. There is a small amount of flow from the wetwell to the drywell through the vacuum breaker until 6 hours when steam and hydrogen are released to the pool through the SRV T-quenchers, resulting in a significant increase in flow through the vacuum breaker. When the RPV is breached at 9 hours, there is a short duration pressure peak in the drywell. The steam flow carries noncondensing gases (N_2, H_2 and CO) into wetwell, eventually transferring nearly all of the H_2 and CO into the wetwell. When the pressure falls from the peak due to heat loss through the containment shell, there is a large flow from the wetwell to the drywell though the vacuum breaker, resulting in an increase in the hydrogen concentration in the drywell.

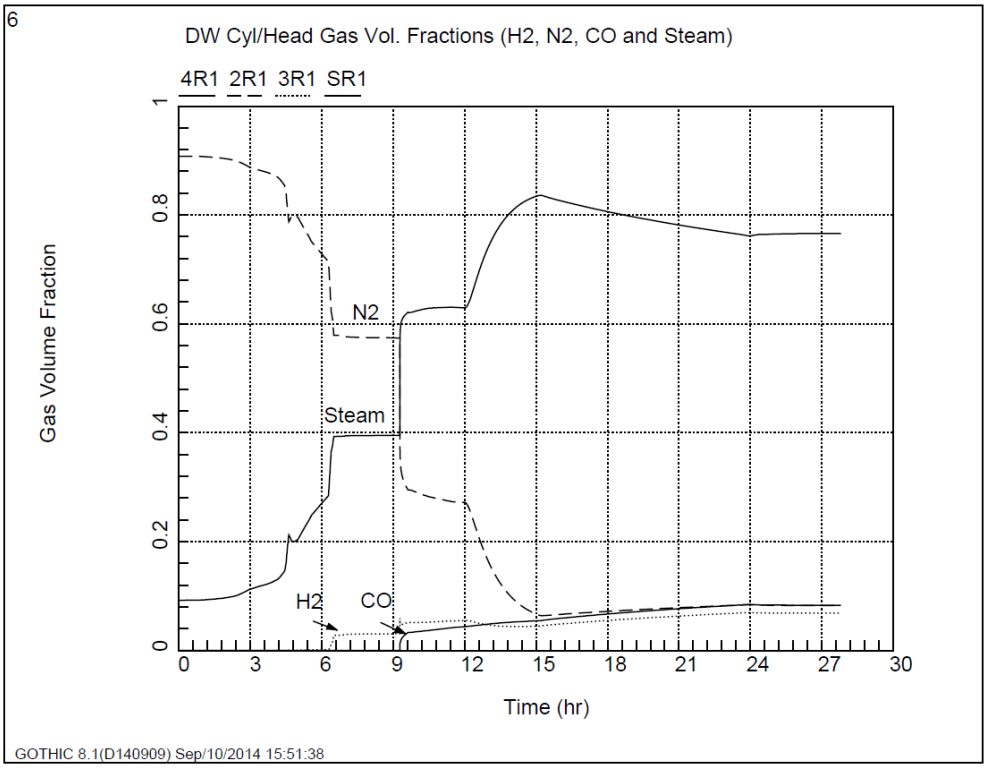

Figure 2-11
GOTHIC Lumped Model DW Head & Cylindrical Region Gas Volume Fractions

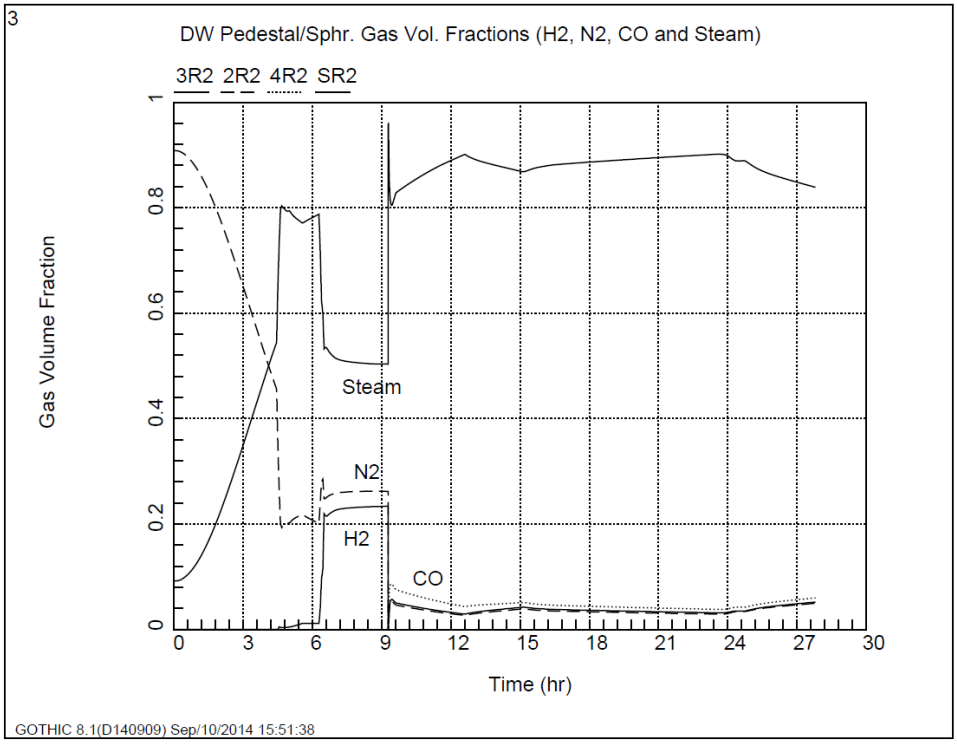

Figure 2-12
GOTHIC Lumped Model DW Pedestal & Sphrical Region Gas Volume Fractions

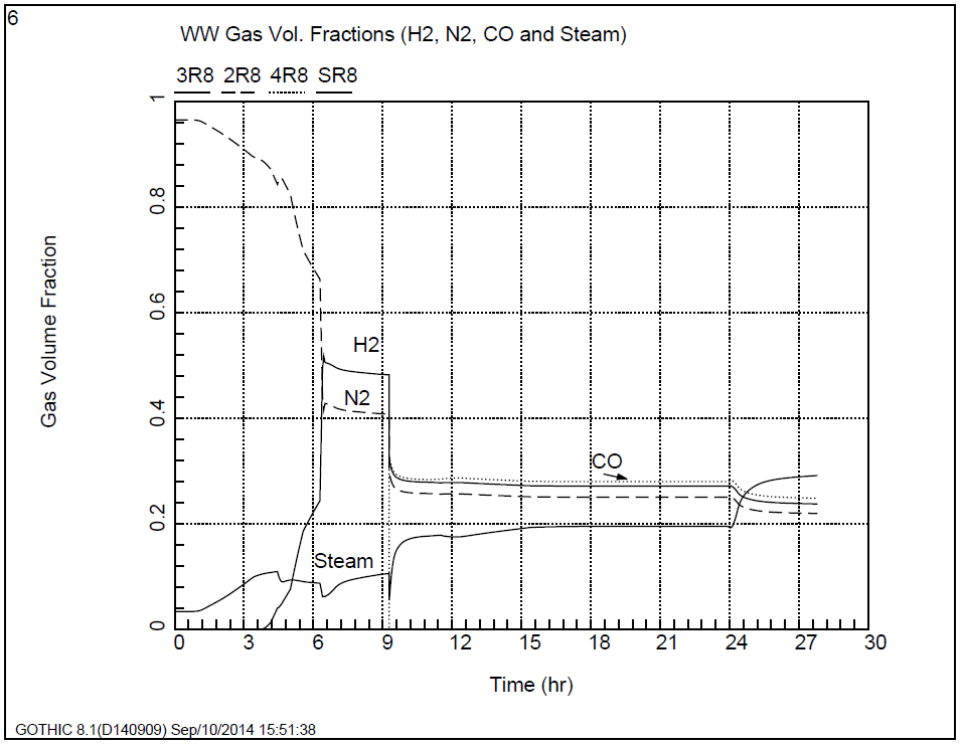

Figure 2-13
GOTHIC Lumped Model WW Gas Volume Fractions

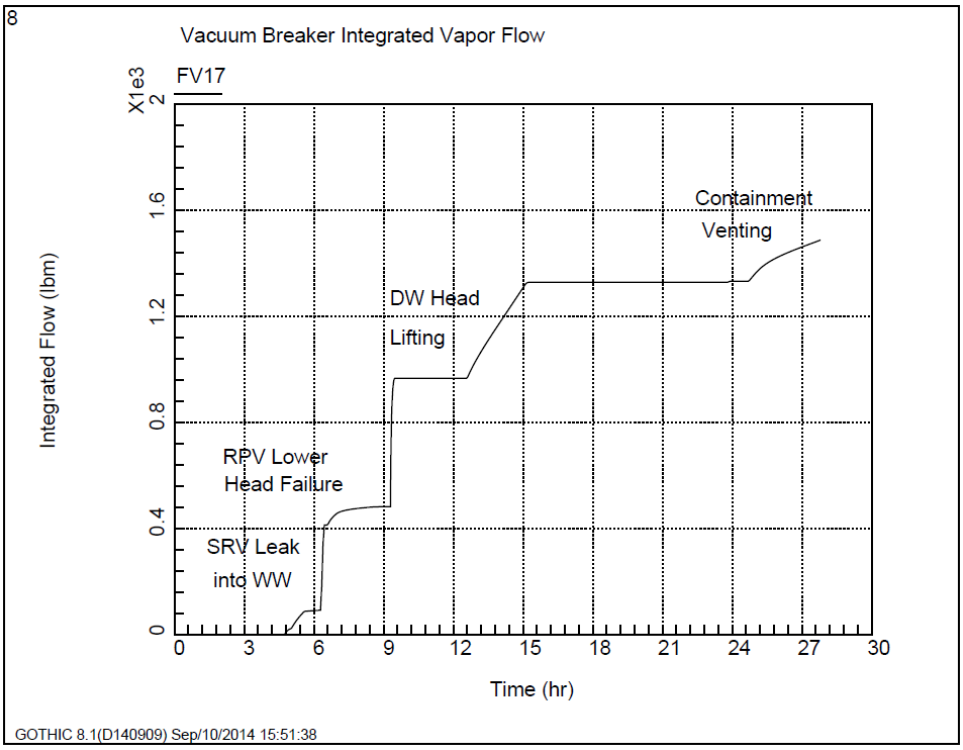

Figure 2-14
GOTHIC Lumped Model Vacuum Breaker Integrated Vapor Flow

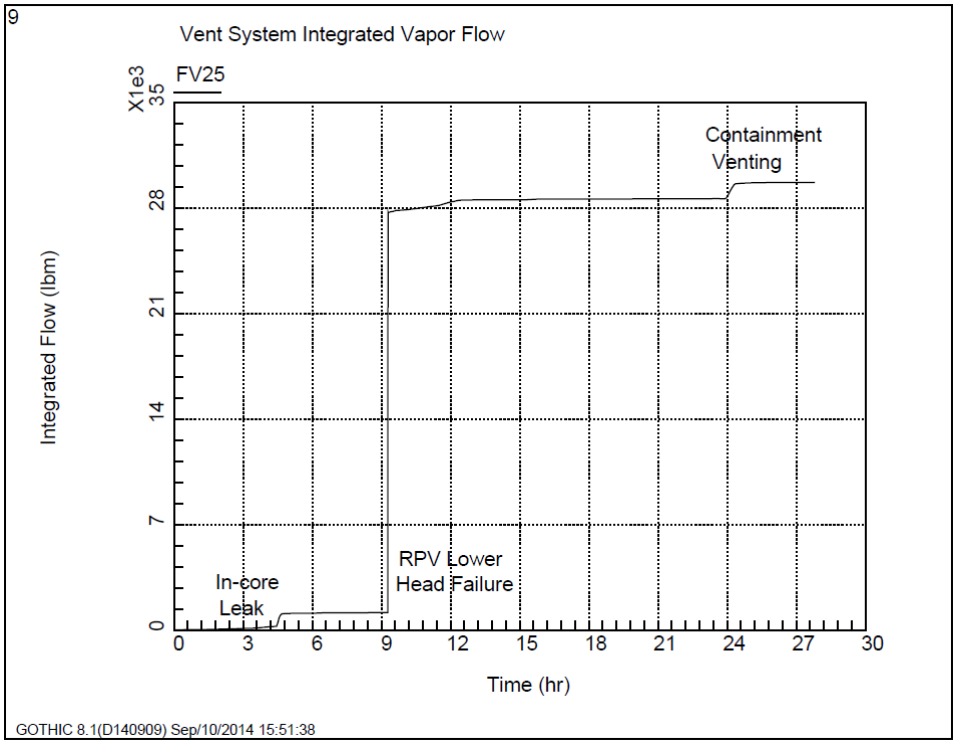

Figure 2-15
GOTHIC Lumped Model Vent System Integrated Vapor Flow

2.3.2 1F1 Subdivided GOTHIC Model without Vent Heat Transfer

The subdivided GOTHIC model was used to investigate the localized gas concentrations, the temperature distribution and the containment pressure response. Figure 2-16 shows the subdivided model DW pressure response and compares it with the lumped GOTHIC model predictions. The pressure prediction agrees with the shape of 1F1 baseline model. However, the multidimensional GOTHIC model predicts the containment pressures that are generally lower than the lumped model results. To investigate the decrease in subdivided model pressure, local containment responses are compared with the lumped model results and discussed in this section.

Compared to the lumped model, a larger pressure spike is calculated by the 3D drywell model during the vessel breach. This is due to the very rapid release of steam into lower DW resulting the magnitude of the peak depending on the rate of change in the release.

Figure 2-17 shows the DW temperatures at different elevations. The DW is generally well-mixed (thermally) with some modest variation during the initial heat up. Between 6-9 hours, the DW sphere region temperature is low due to the increase in gas flow from WW through VB (Figure 2-18). Before the RPV lower head failure occurs around 9 hours, the averaged DW temperature difference between pedestal and head regions was around 20 F (11 C). In the lumped model approach, limited mixing between two regions resulted in a higher temperature difference of around 40 F (22 C).

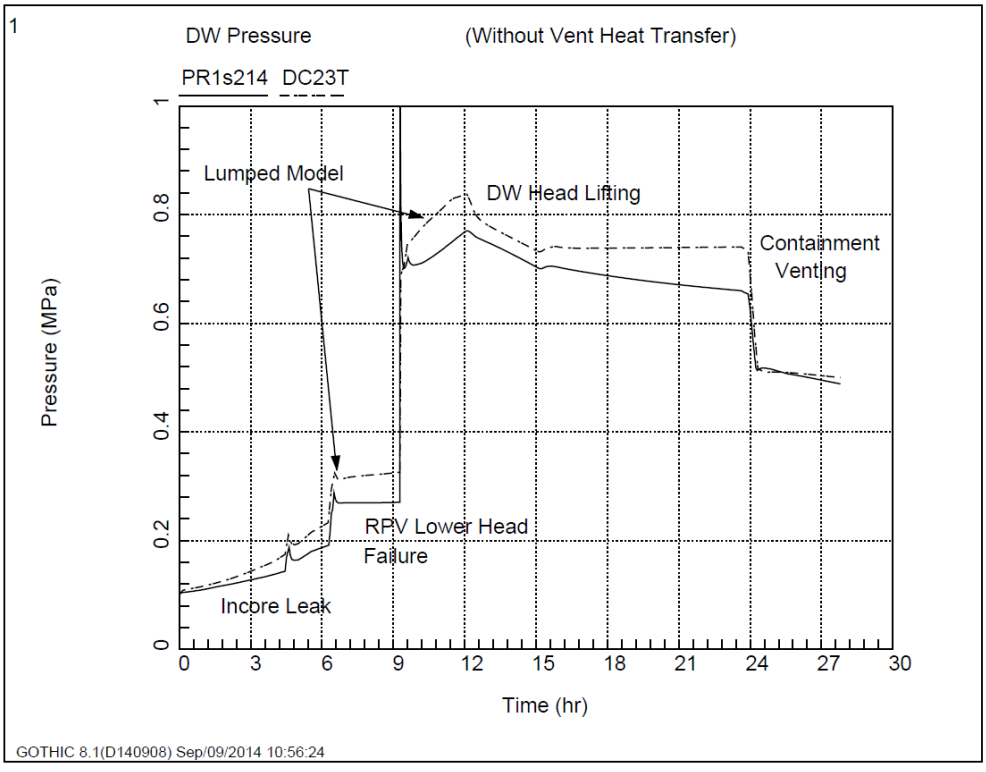

Figure 2-16
3D Model DW Pressure without Vent Heat Transfer

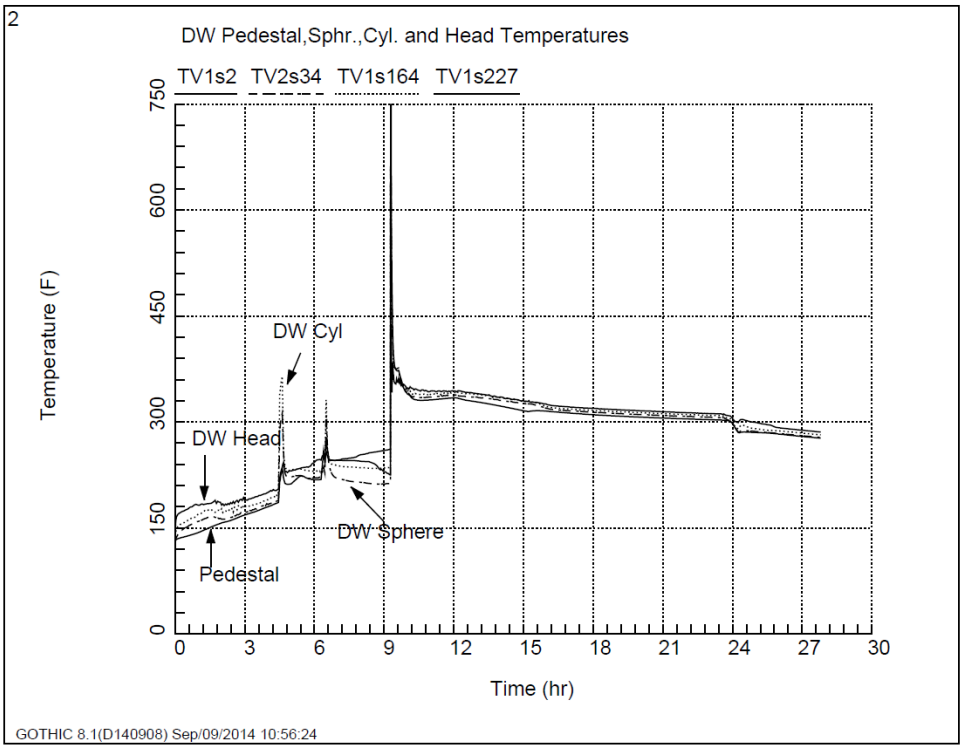

Figure 2-17
3D Model DW Temperature without Vent Heat Transfer

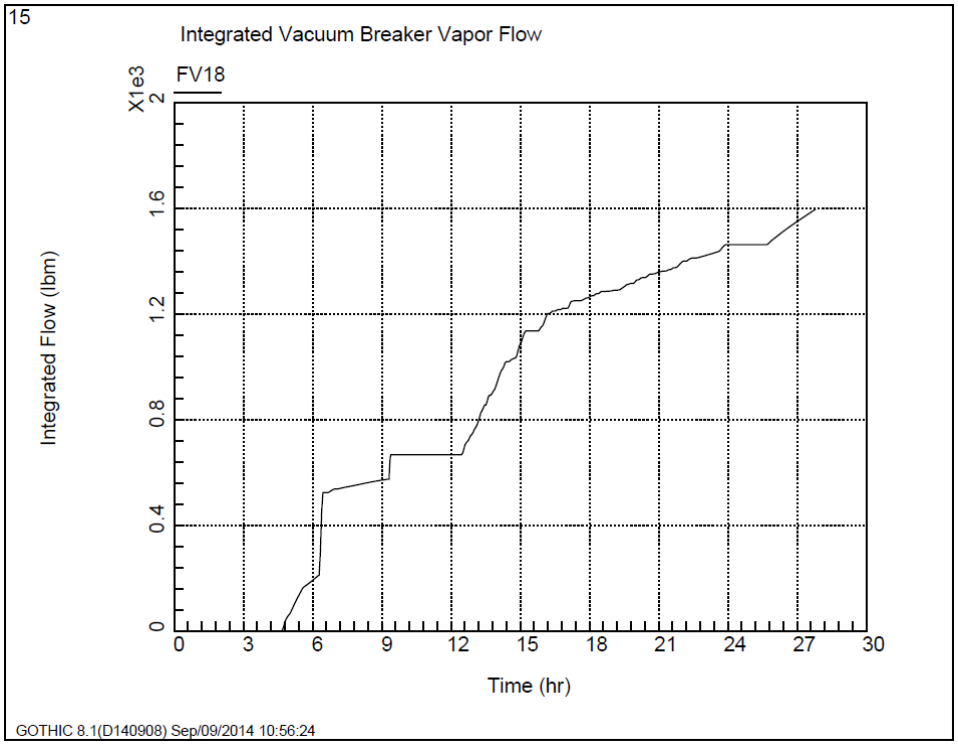

Figure 2-18
3D Model Integrated Vacuum Breaker Vapor Flow without Vent Heat Transfer

Figure 2-19 and Figure 2-20 show local temperature comparisons between the lumped and subdivided GOTHIC models. Similar to the pressure comparison (Figure 2-16) the subdivided DW temperature results are lower than the lumped model predictions, especially in the lower DW pedestal/spherical region.

Figure 2-21 and Figure 2-22 show the subdivided model liquid and gas temperature response in WW and compares them with the lumped model results. As shown in Figure 2-21, the suppression pool bottom and surface temperatures are nearly equal as expected and agree with the lumped model results. When the RPV lower head failure occurs, a large amount of hot steam and noncondensable gases (N_2, H_2 and CO) is transferred to the SC thorough the DW vents and heats up the pool temperature from 170 F to 230 F (77 C to 110 C).

During this period the steam condenses in the pool and the noncondensable gases end up in the suppression chamber gas space. As shown in Figure 2-22, in subdivided model, the suppression chamber gas temperature remains lower than the lumped model prediction throughout the transient. Without heat transfer across the vents the SC gas temperature is predominately a function of the pool temperature and the SC pressure. The lower temperature in the subdivided model is consistent with the lower pressure prediction.

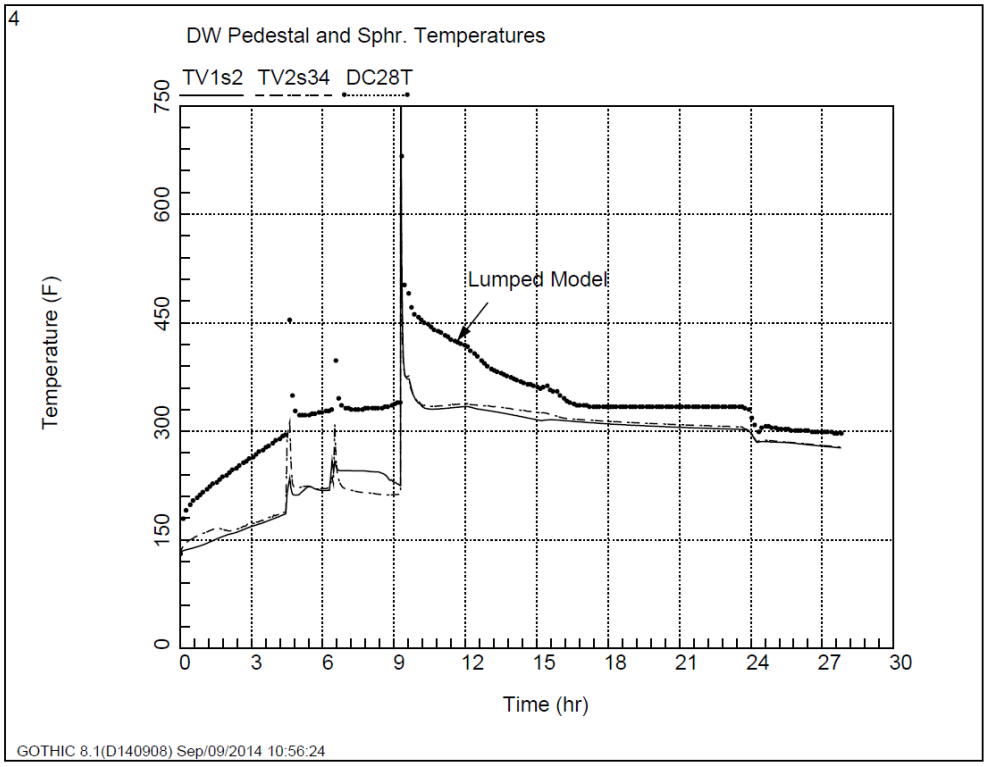

Figure 2-19
3D Model DW Pedestal & Spherical Region Temperature without Vent Heat Transfer

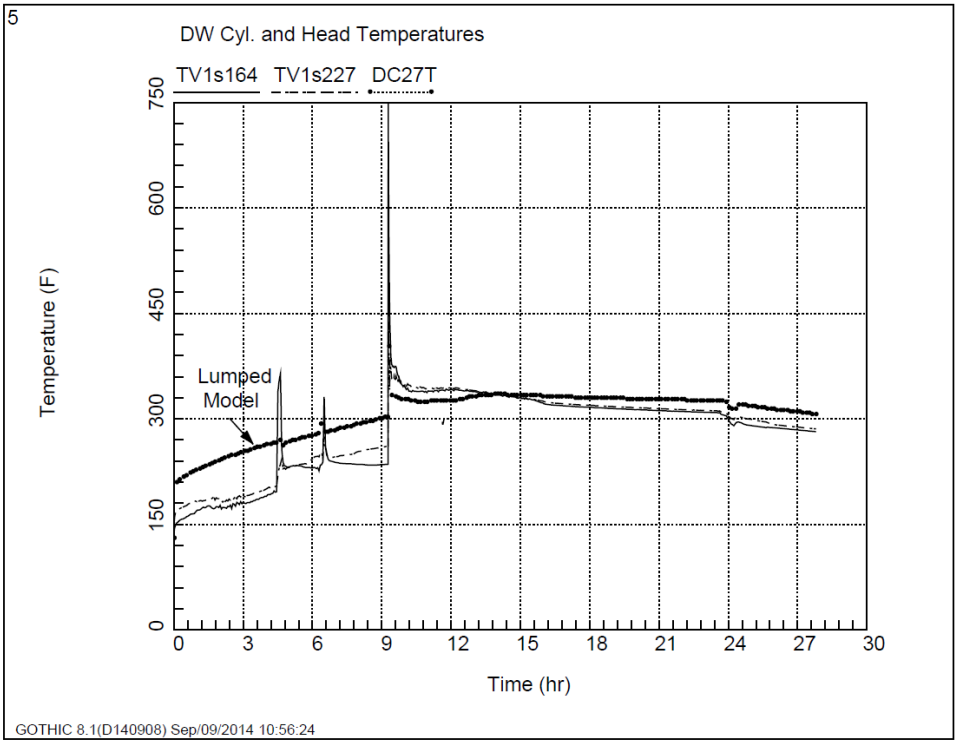

Figure 2-20
3D Model DW Head & Cylindrical Region Temperature without Vent Heat Transfer

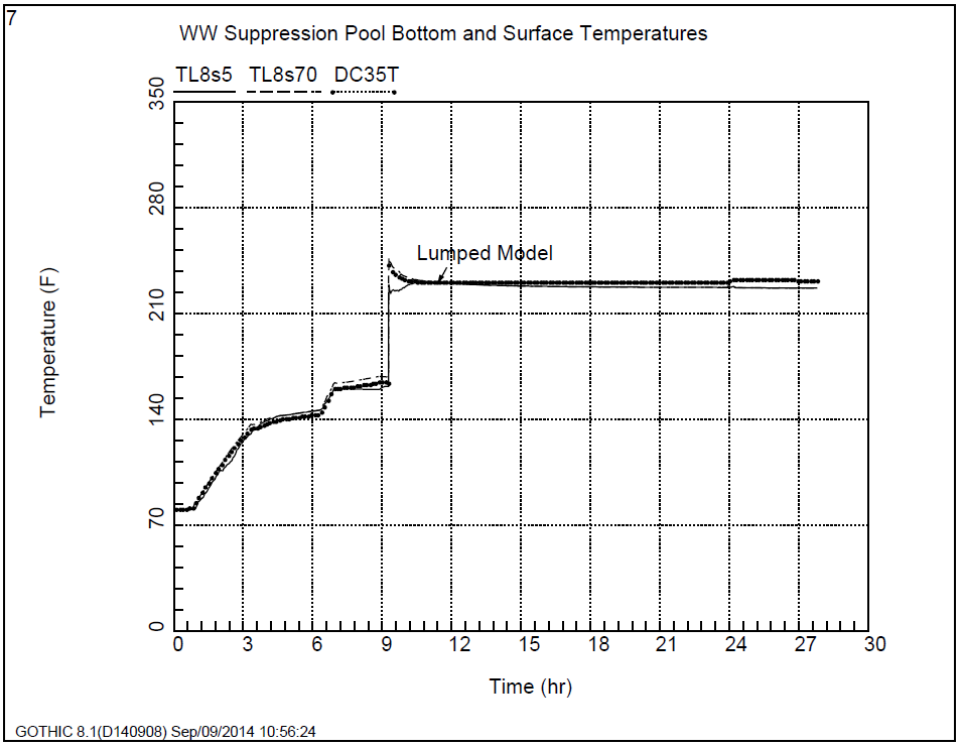

Figure 2-21
3D Model Suppression Pool Temperature without Vent Heat Transfer

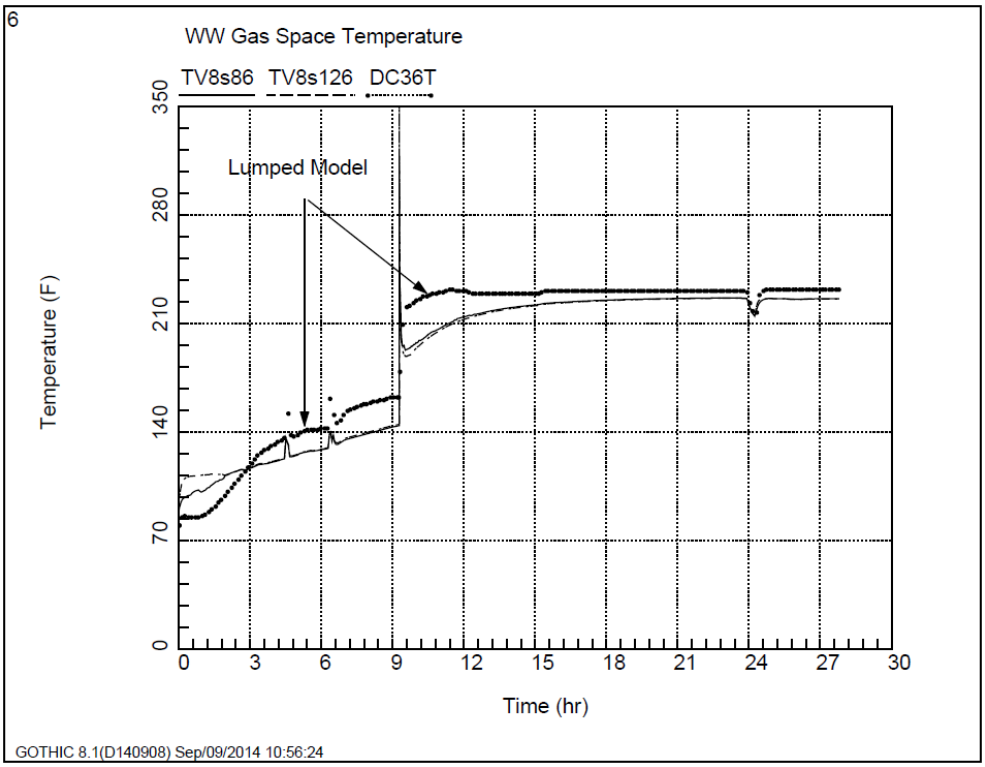

Figure 2-22
3D Model WW Gas Space Vapor Temperature without Vent Heat Transfer

Vector plots (Figure 2-23 and Figure 2-24) show that there is substantial mixing inside the DW and SC. High velocities toward the DW vents are seen when the RPV lower head failure occurs. The rapid gas flow into suppression pool disturbs the mixing patterns in the pool.

Figure 2-25, Figure 2-26, Figure 2-27 and Figure 2-28 present the steam and noncondensable gas distribution within the DW head, cylindrical region, pedestal and spherical region, respectively. Compared to the lumped model results, in the subdivided model the gas concentrations in the DW are generally more uniform with lower steam and H_2 concentrations and higher in N_2 before the RPV failure. In the lumped model, due to limited mixing between two regions, more N_2 was trapped in the DW head/cylindrical volume (Figure 2-11) and the steam concentration is larger in the pedestal/spherical volume due to the in-core instrument leak (Figure 2-12).

Figure 2-29 shows that the subdivided model gas concentration predictions in WW gas space are similar to the lumped model results in Figure 2-13. However, it should be noted that, even though both models show similar gas concentration in WW, the higher WW pressure in the lumped model indicates a larger amount of gas transfer from DW to WW. As shown in Figure 2-30, the total amount of gas transferred from DW into WW through the vent system is higher in lumped model than the subdivided model.

In summary, the subdivided model shows generally well mixed conditions in the DW. The pressurization of the containment for this scenario depends on the amount of noncondensable gases that are transferred to the WW. The limited mixing in the lumped model affects this gas transfer to the WW. For the postulated scenario, with the mass and energy sources low in the

DW, a single volume lumped model for the DW would provide a reasonable estimate for the gas transfer to the WW and the containment pressurization. However, in other possible scenarios, (e.g., a steam/H_2 leak high in DW) a highly stratified condition is possible and a multivolume lumped model or subdivided model would be required.

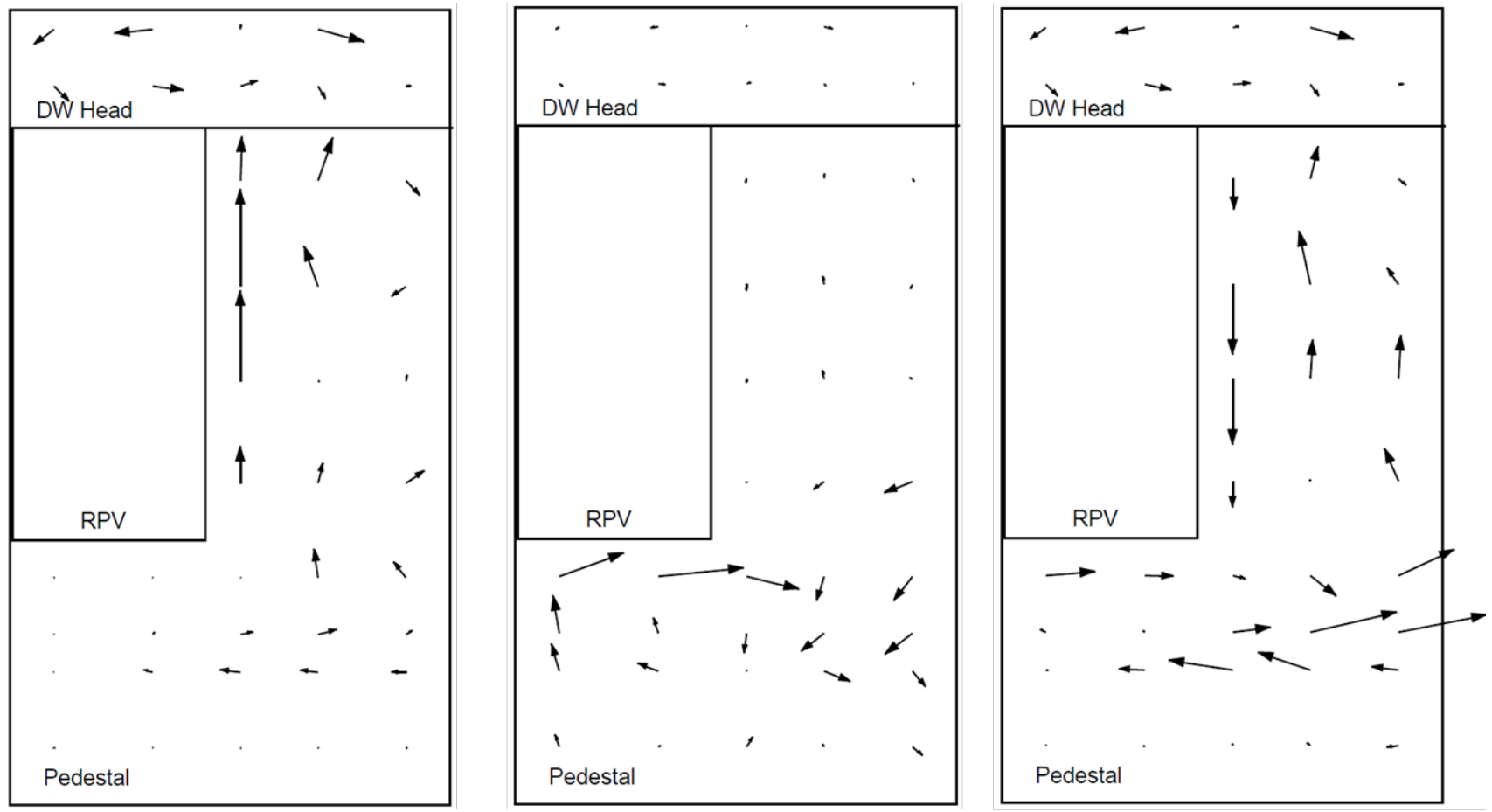

Figure 2-23
1F1 DW Mixing Before, During and After RPV Lower Head Failure

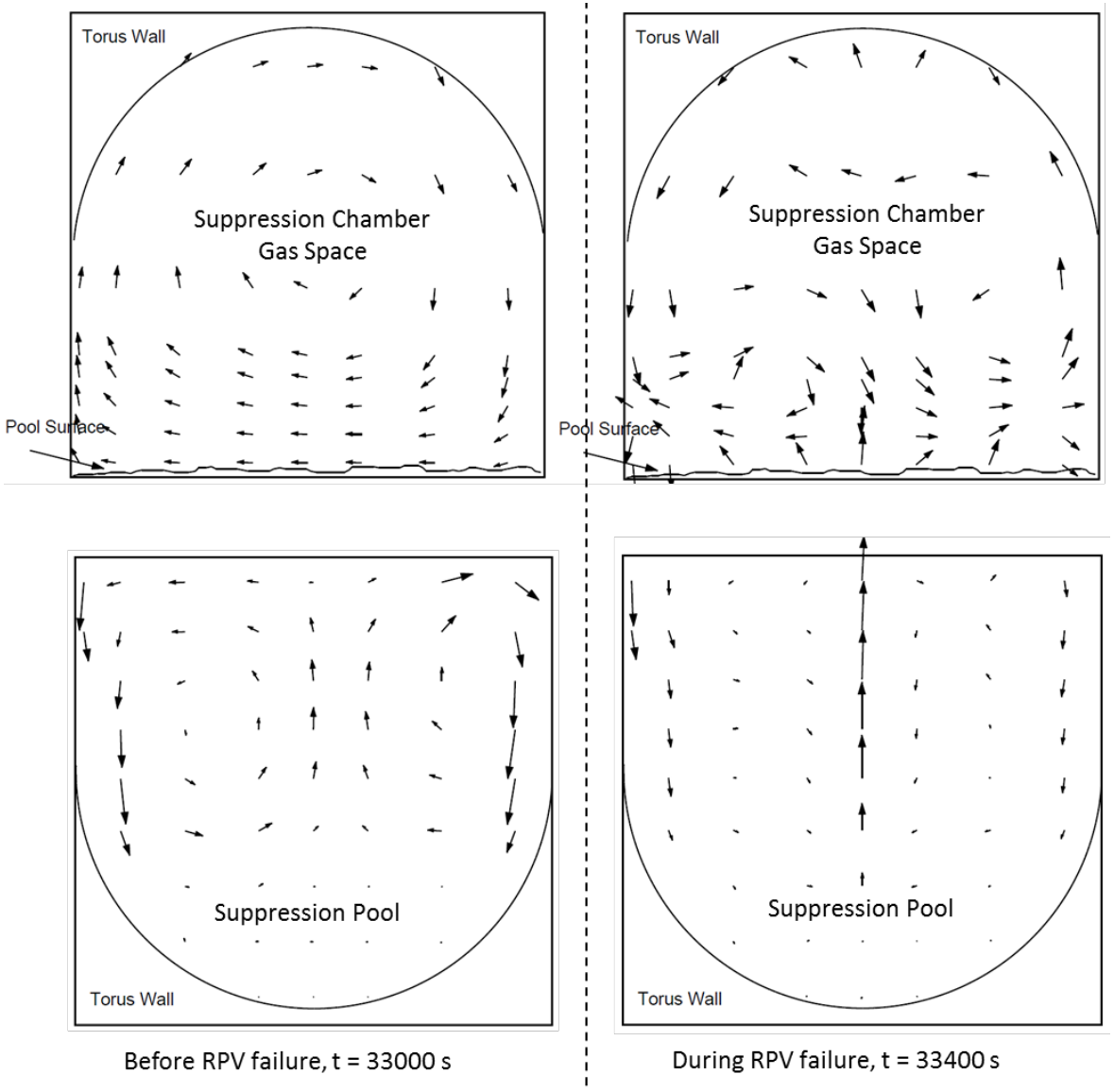

Figure 2-24
1F1 1F1 WW Pool and Gas Space Mixing Before, and After RPV Lower Head Failure

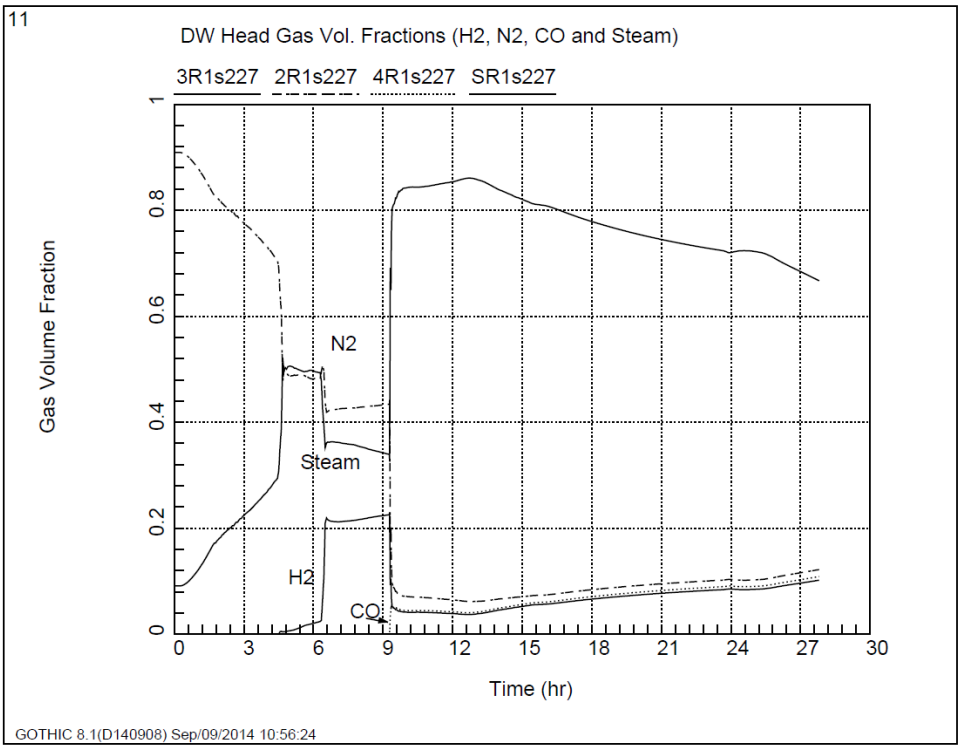

Figure 2-25
3D Model DW Head Gas Volume Fractions without Vent Heat Transfer

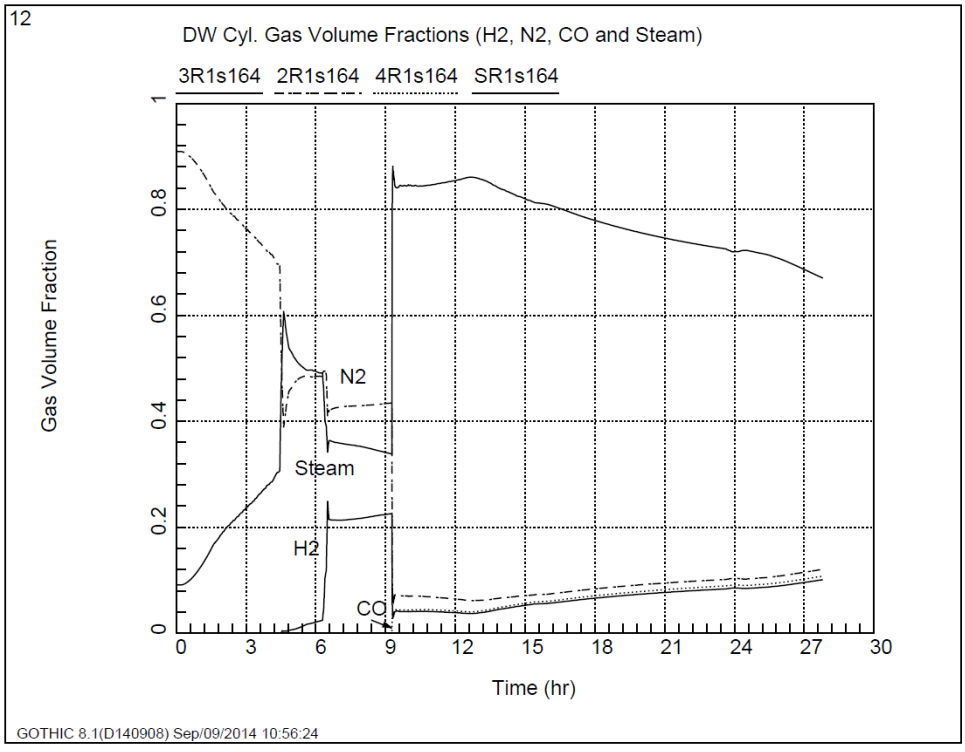

Figure 2-26
3D Model DW Cylindrical Region Gas Volume Fractions without Vent Heat Transfer

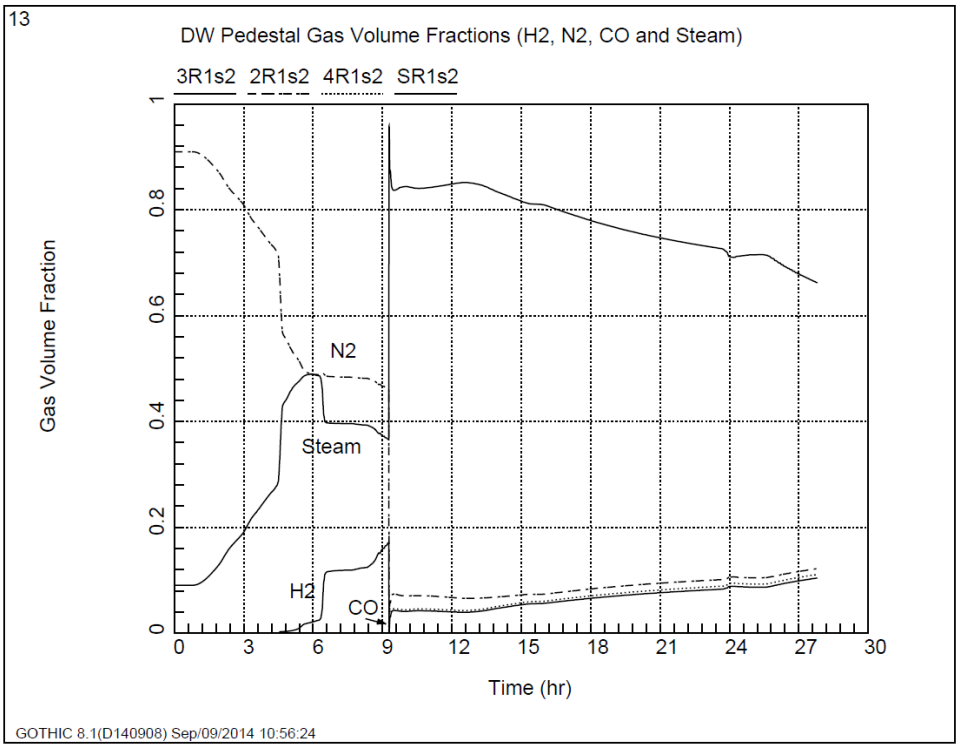

Figure 2-27
3D Model Pedestal Gas Volume Fractions without Vent Heat Transfer

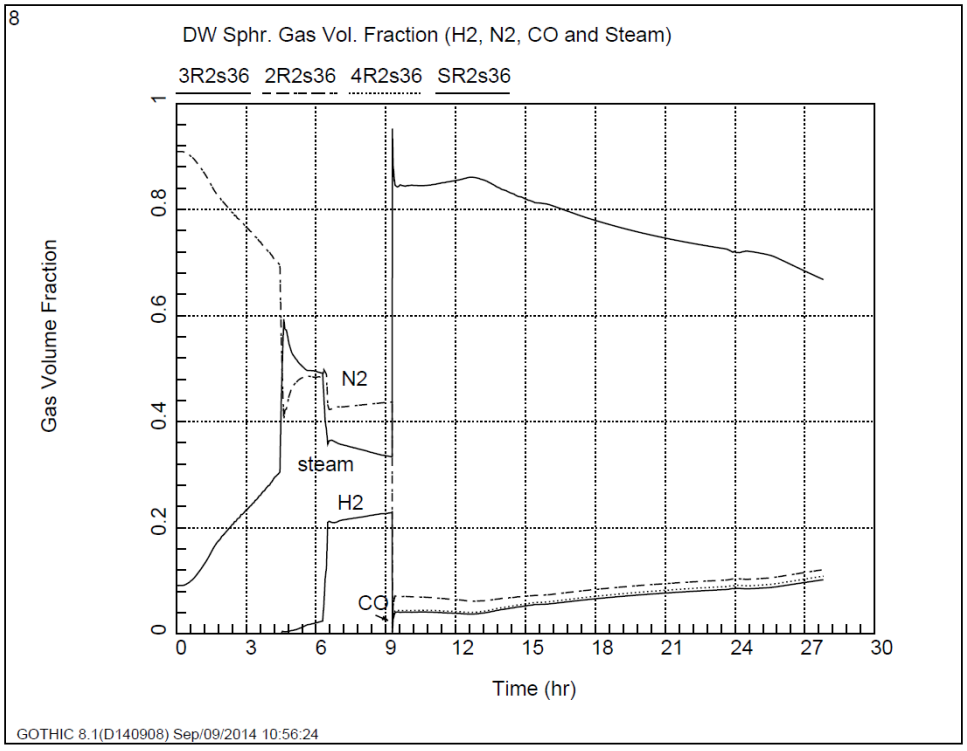

Figure 2-28
3D Model DW Spherical Region Gas Volume Fractions without Vent Heat Transfer

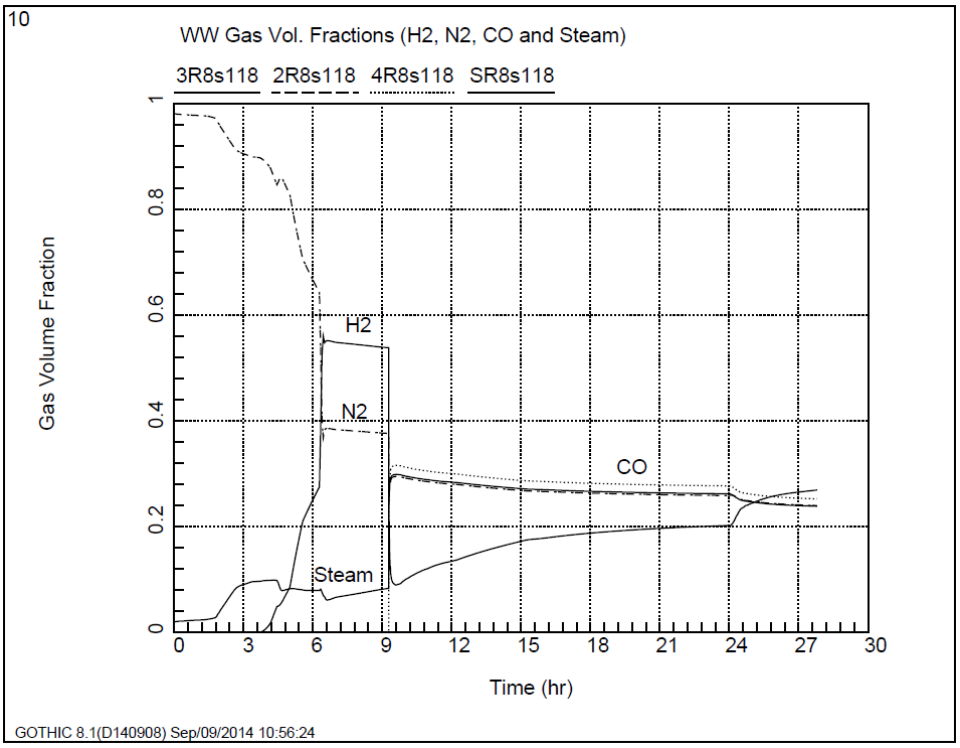

Figure 2-29
3D Model WW Gas Volume Fractions without Vent Heat Transfer

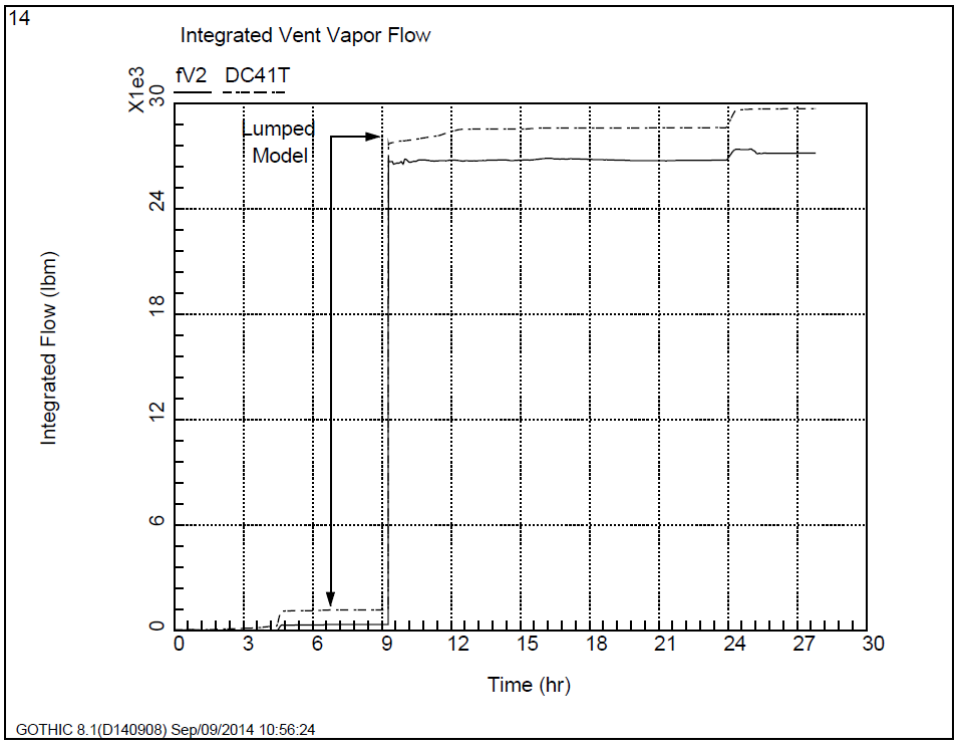

Figure 2-30
3D Model Integrated Vent Vapor Flow without Vent Heat Transfer

2.3.3 1F1 Subdivided GOTHIC Model with Vent Heat Transfer

This model and scenario are identical to the 3D model described in Section 2.3.1 except that the heat transfer between the drywell vent system and the wetwell gas space is included. Figure 2-31 shows the subdivided GOTHIC containment pressure response in DW and compares it with the subdivided model without the vent heat transfer. The pressure predictions agree until the RPV lower head failure at about 9 hours into the event. After the vessel breach, the inclusion of vent heat transfer results in lower containment pressure.

Comparing Figure 2-32 to Figure 2-17 , the heat transfer across the vent does not have a significant impact on DW temperature. However, as shown in Figure 2-33, vent heat transfer does result in increased WW gas space temperature. Even though, the WW gas temperature has a direct relationship to the containment pressure response, the temperature increase effect was more than offset by a reduction in gas transfer to the WW as described below.

Figure 2-34 shows that the calculated gas concentrations in WW gas space are similar in the two cases (Figure 2-29). However, even though both models give similar gas concentration in WW the lower pressure in the case with vent heat transfer indicates less gas transfer from the DW to the. Figure 2-35 shows that the total amount of gas transferred from DW into WW through the vent system is reduced when vent heat transfer is included. In addition, Figure 2-36 shows a continuous liquid flow through the vent, indicative of the condensation that occurs in the vent.

The steam condensation in the vent system reduces the amount of noncondensing gases that are transferred to the WW and the backflow from the WW to the DW via the vacuum breaker (Figure 2-37). As shown in Figure 2-38, compared to the lumped and subdivided GOTHIC model results without the vent heat transfer, this results in a substantially higher concentration of hydrogen in the drywell during the time when drywell flange leakage is postulated to occur. This would be an important factor in assessing the potential for drywell head leakage to lead to the 1F1 hydrogen explosion in the Reactor Building.

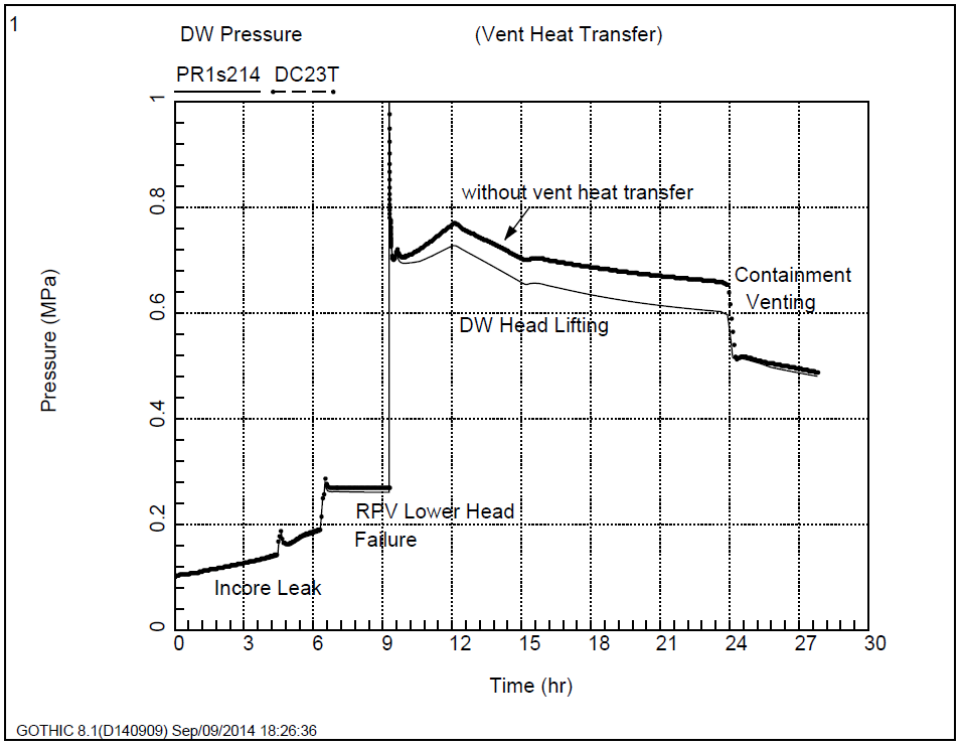

Figure 2-31
3D Model DW Pressure with and without Vent Heat Transfer

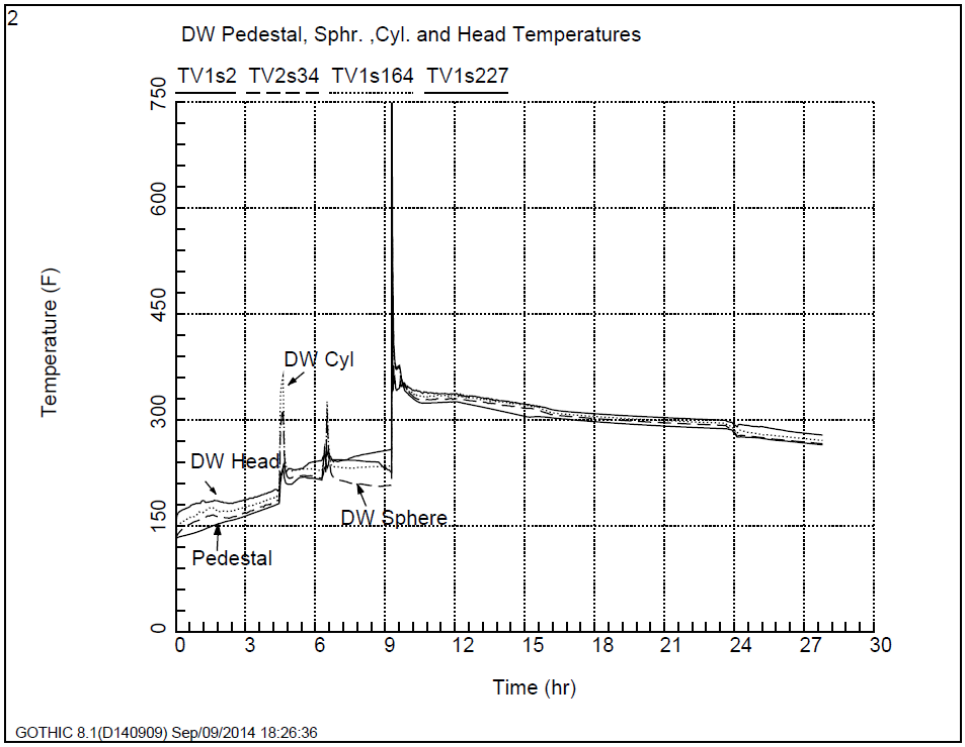

Figure 2-32
3D Model DW Temperature with Vent Heat Transfer

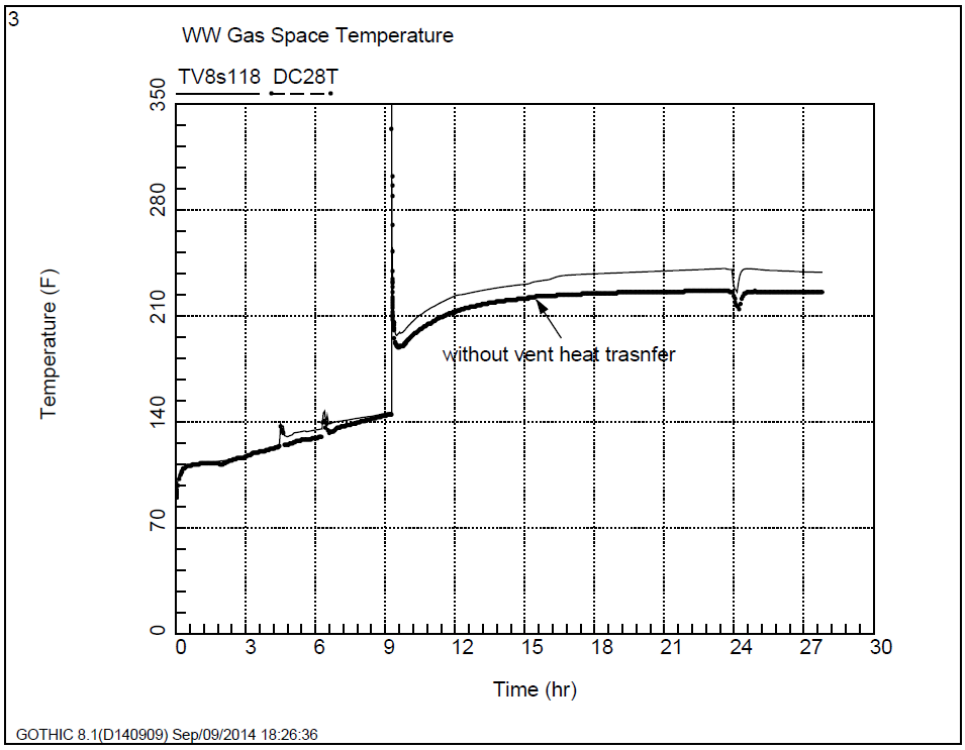

Figure 2-33
3D Model WW Gas Temperature with and without Vent Heat Transfer

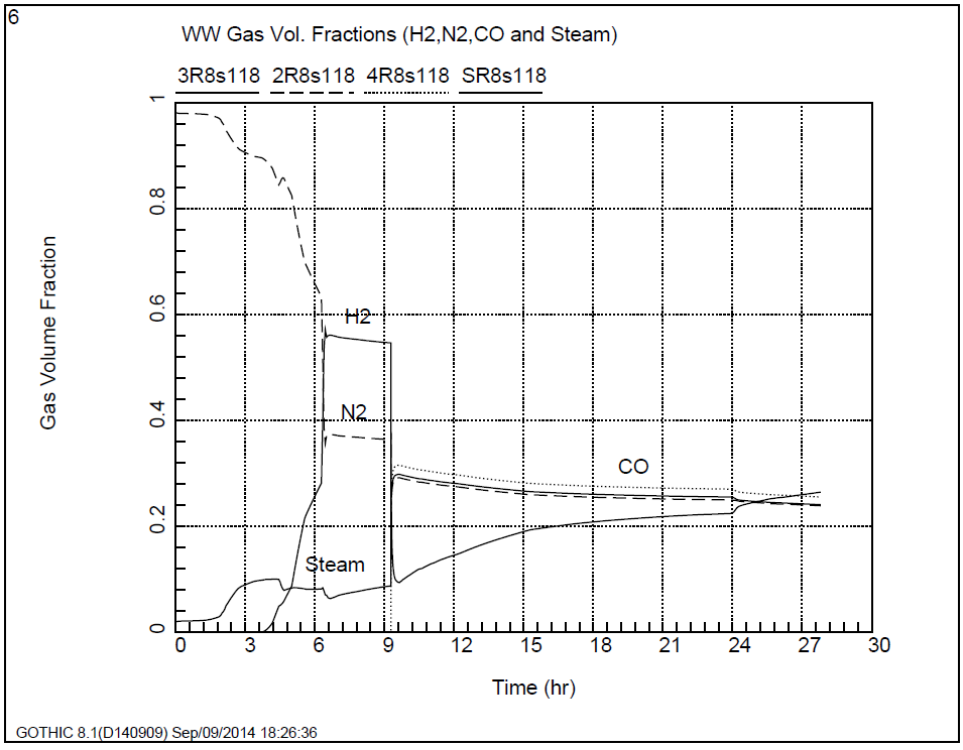

Figure 2-34
3D Model WW Gas Volume Fractions with Vent Heat Tansfer

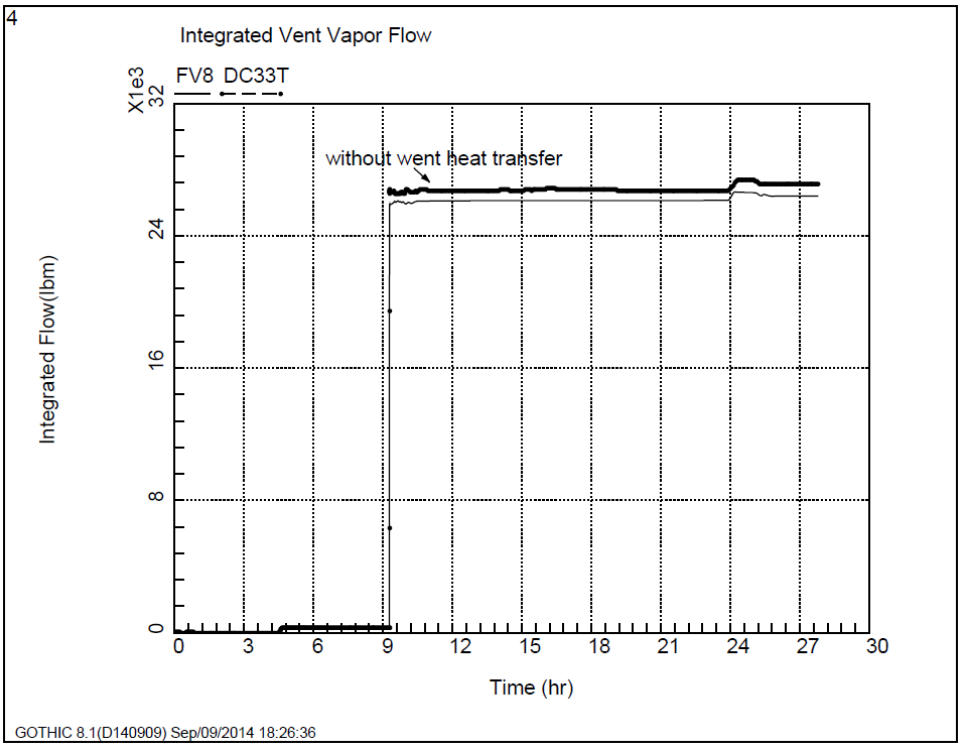

Figure 2-35
3D Model Integrated Vent Vapor Flow with and without Vent Heat Transfer

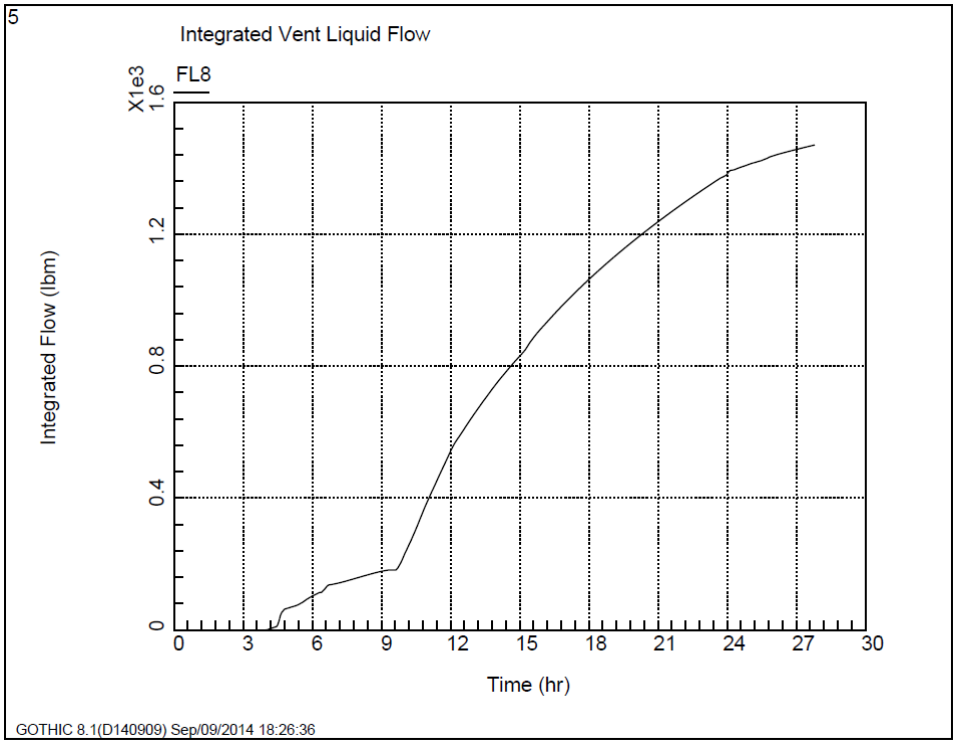

Figure 2-36
3D Model Integrated Vent Liquid Flow with Vent Heat Transfer

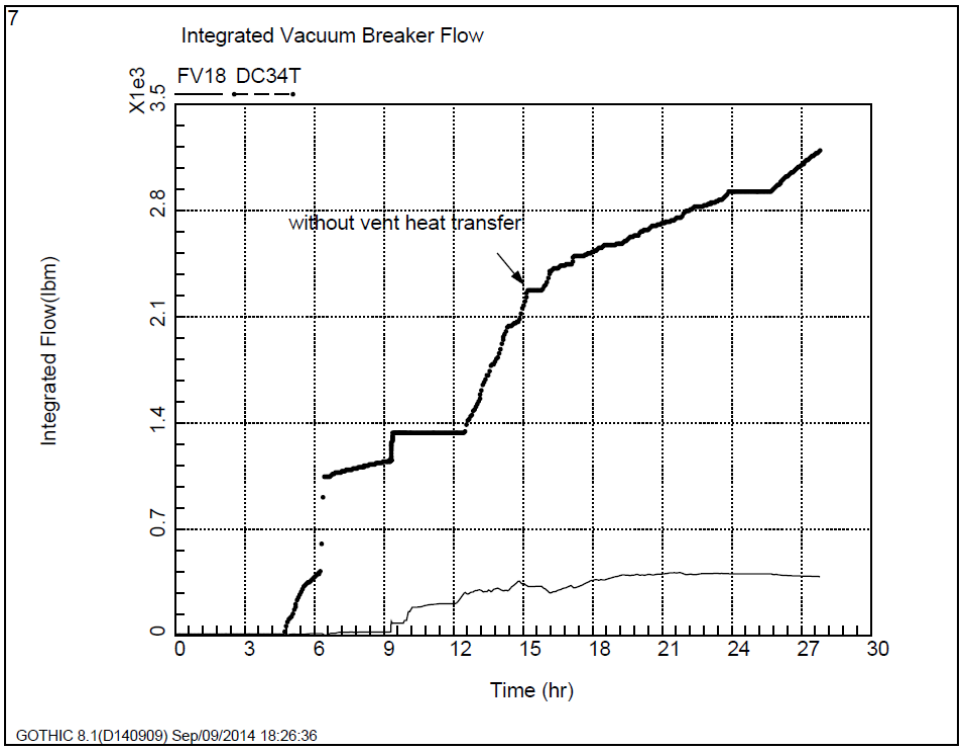

Figure 2-37
3D Model Integrated Vacuum Breaker Flow with and without Vent Heat Transfer

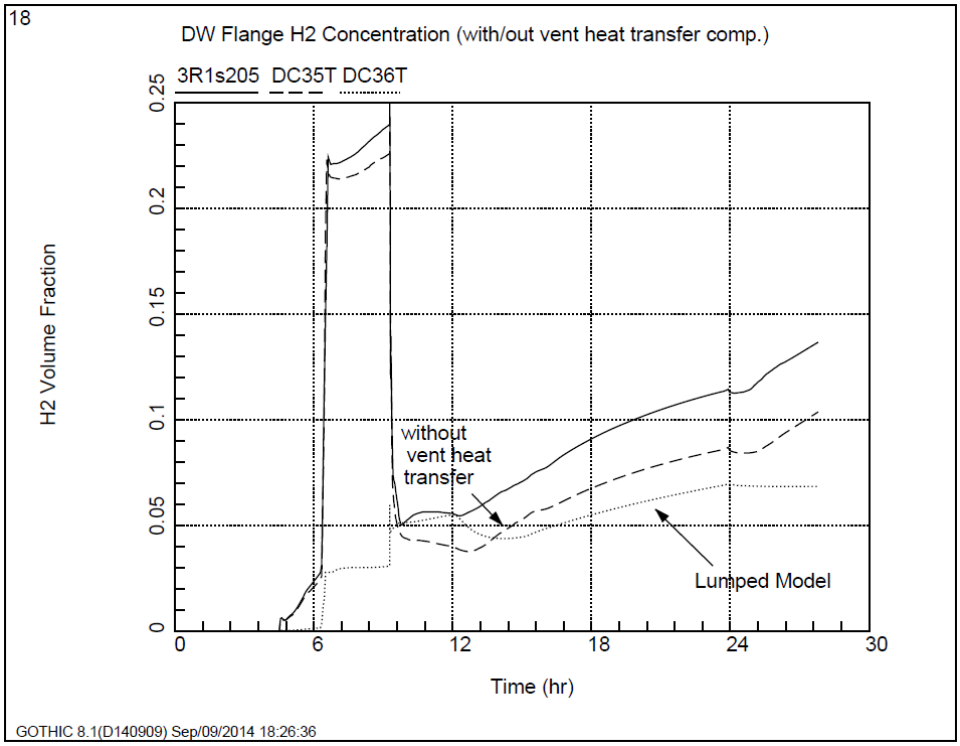

Figure 2-38
3D Model H_2 Concentration at DW Flange with and without Vent Heat Transfer

2.4 Conclusions

The effects of multidimensional modelling and vent heat transfer on the 1F1 event simulation through the WW venting have been investigated. The model incorporates a subdivided drywell model that can predict the 3-dimensional flow pattern, temperature and gas distribution within the drywell. To capture the major coupling effects of other system components, the model also includes the drywell vent system, wetwell with the suppression pool, leakage to the surrounding reactor building and the wetwell vent to the stack.

The postulated scenario, with the mass and energy sources low in the drywell, results in a fairly well-mixed drywell, although there are still some variations in the temperature and gas concentrations that influence the containment pressurization and the hydrogen release to the reactor building. Compared to lumped model approach, the increased mixing in the drywell subdivided model results in less gas transfer to the wetwell and lower containment pressures. In other possible scenarios, (e.g., a steam/H_2 leak high in drywell) a highly stratified condition is possible and a properly configured multivolume lumped model or subdivided model would be required for a realistic estimate of the containment performance.

The containment system model was modified to consider heat transfer from the steam and gas in the drywell vent system to the wetwell and torus room. The inclusion of vent heat transfer had a significant impact on the overall containment response for the 1F1 scenario, particularly during RPV lower head failure and the subsequent steam flow from the vessel to the drywell. In spite of the increase in wetwell gas temperature, the vent heat transfer model predicted continued condensation of the steam in the vent system and a smaller amount of noncondensable gas transfer to the wetwell compared to the model without the vent heat transfer. The net result was a reduction in the containment pressure.

Symmetrical modeling of the vent system doesn't take into account some steam/gas circulations between vents through vent header circumferentially. GOTHIC results indicate well mixed conditions exist in drywell throughout the transient; therefore this potential vent header mixing effect would not have a significant impact in the behavior of the results.

Compared to a two volume lumped model that restricts mixing, the subdivided model gives lower containment pressure. Including the vent heat transfer further reduces the containment pressure. This implies that the tuned steam, hydrogen and CO release rates used in the MAAP5 simulation for the event may be lower than necessary to replicate the measured containment pressure. Further, the more detailed modeling used here indicates that the hydrogen concentration in the upper drywell at the time of the postulated DW head flange leak is larger than indicated in the lumped model. Taken together, this investigation indicates that the hydrogen release to the reactor building may have been significantly larger than estimated in the MAAP5 simulation.

3
1F3 WETWELL PERFORMANCE

3.1 Introduction

The pressure in the containment is directly related to the pressure in the wetwell gas volume. The gas volume pressure is determined primarily by the amount of noncondensing gases that have been transferred to the wetwell via the drywell vents or other mechanisms. It is also influenced by the temperature rise due to the compression of the gas in the wetwell gas space and by heat transfer from the pool and other hot surfaces. Steam from pool evaporation or other sources will also contribute to the pressure rise.

In this section, focus is on the performance of the 1F3 the suppression pool and the wetwell gas space during the event as described in Attachment A-5. In 1F3, the primary source of mass and energy to the wetwell was the exhaust steam from the RCIC turbine pump. The RCIC injection first started at 15:05 on March 11 and ran for 20 minutes. It was restarted at 16:03 on March 11 and ran continuously until 11:36 on March 12. The wetwell spray was first started at 12:06 on during this period is shown in Figure 3-1 with the system start and stop points indicated (starting with the second start of the RCIC system). This study considers the performance only through the end of the wetwell spray period when the pressure rise is much larger than expected under normal shutdown conditions with RCIC operation.

Several different models for the containment system are presented in the subsections that follow. The models take advantage of geometric symmetry and therefore include only one-half or smaller section of the full geometry and the appropriately scaled system flow and leak rate. However, all system flow and leak rates reported in this section are scaled up to the full containment values for reader convenience.

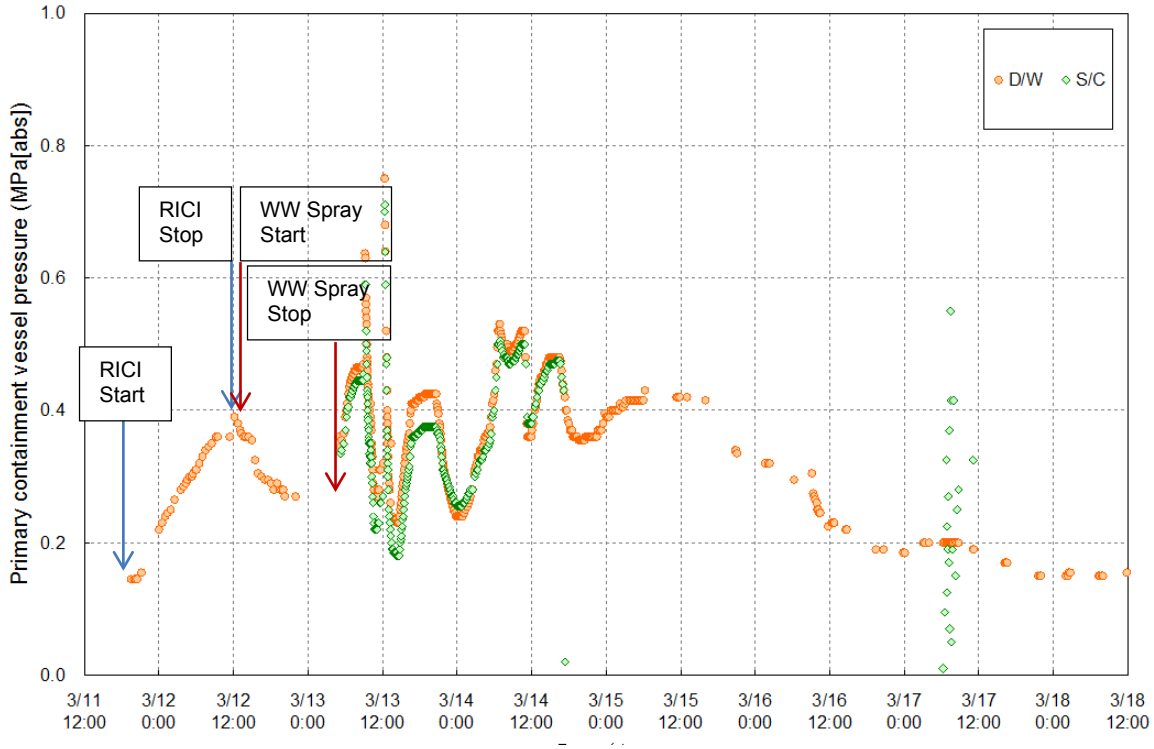

Figure 3-1
1F3 Measured Containment Pressure Response

3.2 Simplified Scoping Model

A simple GOTHIC model was constructed to get a rough idea of the impact of various mechanisms for the containment pressurization. The noding diagram is shown in Figure 3-2. The modeling elements include:

- Volumes (dashed line boxes)
  - 1 – Torus Gas Space
  - 2s - Drywell
  - 3 - Drywell Vents
  - 4 – Distributor Volume for steam release
  - 5 – Torus Room
  - 6 – Torus Pool
  - 7 - RCIC Pipe
- Boundary Conditions (solid line boxes)
  - 1F - Steam flow from RPV
  - 2F – HPCI Exhaust to Suppression Pool

- 3F/4C – Drywell Leak
- 5F– Drywell Spray
- 6F – Wetwell Spray
- 7P – Torus Room Pressure
- 8F/9C – RCIC Exhaust to Suppression Pool.

- Conductors
  - 1s in Volume 2 represents heat transfer from the primary system
  - 2 Vent to torus heat transfer
  - 3 Torus to Torus Room heat transfer
  - 4 Torus Room to Torus Room walls heat transfer

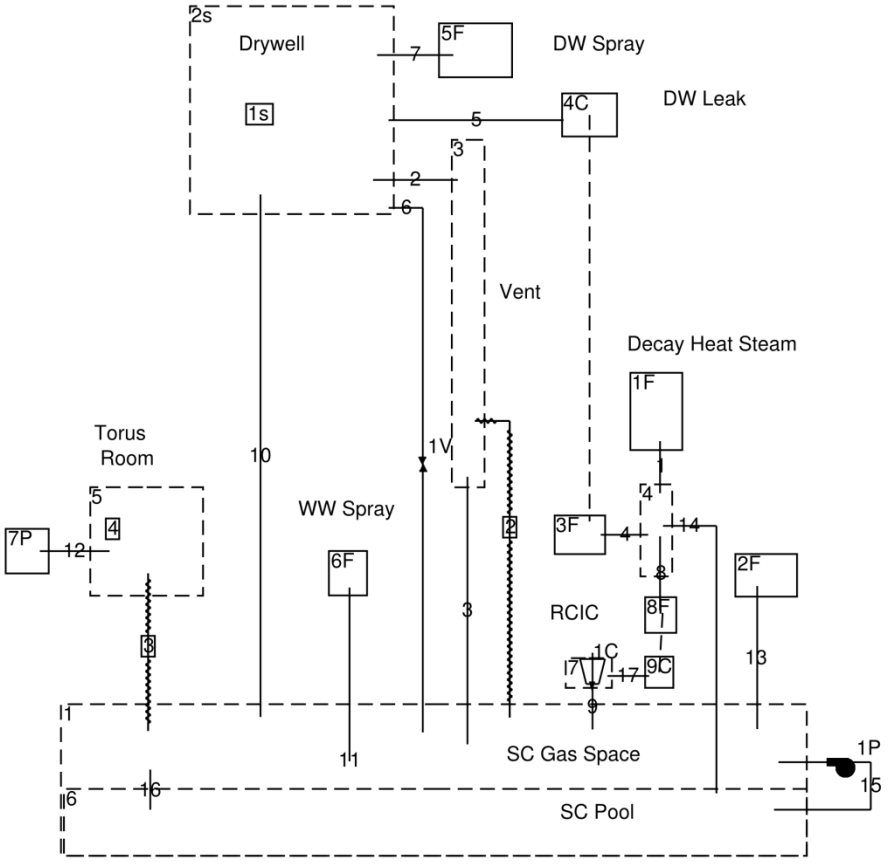

Figure 3-2
1F3 Lumped Containment Model

The connecting lines between the volumes and boundary conditions represent Flow Paths. Flow Paths 2 and 3 connect the Vent volume to the drywell and wetwell, respectively. Flow Path 6

represents the vacuum breaker line between the wetwell gas space and the Dry Well. Valve component 1V models the vacuum breakers.

The heat loss from the RPV and hot piping was model with a simple steel conductor with insulation on the side exposed to the drywell atmosphere. The RPV side of the conductor was held at the RPV saturation temperature. The estimated total surface area of the conductor is 300 m^2.

Heat transfer between the vent piping and the torus air space and pool was included. The heat transfer from the torus to the torus room was included. In the base model, the torus room was assumed to be filled with air and only the heat transfer between the torus gas space and the room air was modeled. Subsequent sensitivity cases investigated the effects of heat transfer between the torus pool and a partially flooded torus room.

The steam flow rate from the RPV was derived from the decay heat (TEPCO, 2013) assuming all of the decay heat went to heating and boiling the 10° C water injected by the RCIC water at 7.25 MPa. The estimated RCIC turbine pump exhaust flow is 4.1 kg/s with the injection water into the RPV at 10°C (OECD-NEA, 2012). The total steam flow from the RPV is routed to distributor Volume 4 in the simplified model. The RCIC exhaust flow is controlled by boundary condition 8F. For some sensitivity cases, some of the steam from the RPV was redirected to the drywell via boundary condition 8F. In all cases, the remaining steam is assumed to go to the suppression pool through the SRV spargers, represented by flow path 14. It is assumed that the RCIC turbine exhaust steam enters the pool at saturation conditions at the suppression chamber pressure. Cooler 1C is included in volume 7 to reduce the enthalpy of the steam coming from the RPV to the saturation value.

The wetwell spray starts at about 76,740 seconds. The spray flow is 13.8 kg/s at 10°C with a 2 mm drop diameter (OECD-NEA, 2012).

The HPCI flow starts at 78,480 seconds and the RPV vessel depressurizes over the next 6 hours. The HPCI flows (on either side of the pump) are not known (OECD-NEA, 2012). An assumed value of 6 kg/s was used. This results in a drywell pressure that is close to the recorded value at 110,000 seconds assuming a well-mixed suppression pool.

To investigate pool stratification effects, the pressure suppression chamber is split into two volumes (Volumes 1 and 6). The upper level (Volume 1) includes the wetwell gas space and the top 50 centimeters of the pool. The lower level models the remainder of the pool. To account for possible convective mixing between the pool near surface and the rest of the pool, Flow Path 15 and the associated pump component 1P are included in the model with Flow Path 16 completing the loop. The surface-to-pool mixing is controlled by the specified flow rate through the pump. All of the RCIC exhaust flow is added to the near surface water in the upper subvolume.

By adjusting the boundary condition flows and the pump flow rate, this simple model can be used to get a first order estimate of the containment pressure response due to pool stratification with or without a steam leak in the drywell.

Typical analysis for containment pressure and temperature response during a plant event uses a model similar to the one above except that the wetwell is modeled with a lumped volume. Inherent in this modeling approach is a well-mixed suppression pool. This situation can be

simulated with the GOTHIC lumped model by using a high flow rate for the pump so that the near surface water temperature is close to the pool average temperature. During the period of interest, measured pressure is reported only for the containment drywell. However, assuming that the containment systems are operating as expected, the difference between the drywell and wetwell gas space pressure is limited. Except for the vent clearing period during a LOCA, the positive pressure differential (drywell to wetwell) is limited by the submergence of the drywell vents. For a nominal pool level, this is equivalent to about 12.5 kPa. On the negative side, the pressure differential is limited by the operation of the vacuum breakers between the wetwell gas space and the drywell. The vacuum breakers open at 1 psi (6.9 kPa) or less. Therefore, the measured drywell pressure should be a reasonable indicator of the wetwell gas space pressure.

The drywell pressure and wetwell temperature results for the simple lumped model are shown in Figures 3-3 and 3-4. The initial rise in drywell temperature is due to the heat up of the drywell atmosphere by convection from the RPV and associated piping. In this analysis it was assumed that the containment air coolers were off throughout the event. Starting at around 25,000 seconds and before the wetwell spray is activated at about 77,000 seconds, the measured pressure rises much more than calculated. With the wetwell sprays on, the measured pressure gradually falls, eventually coming into agreement with the calculated pressure. It is expected that the sprays would cool the wetwell gas space and the pool surface. Cooling the pool surface would promote circulation in the pool and the pool would tend toward the well mixed condition, consistent with the calculation assumptions.

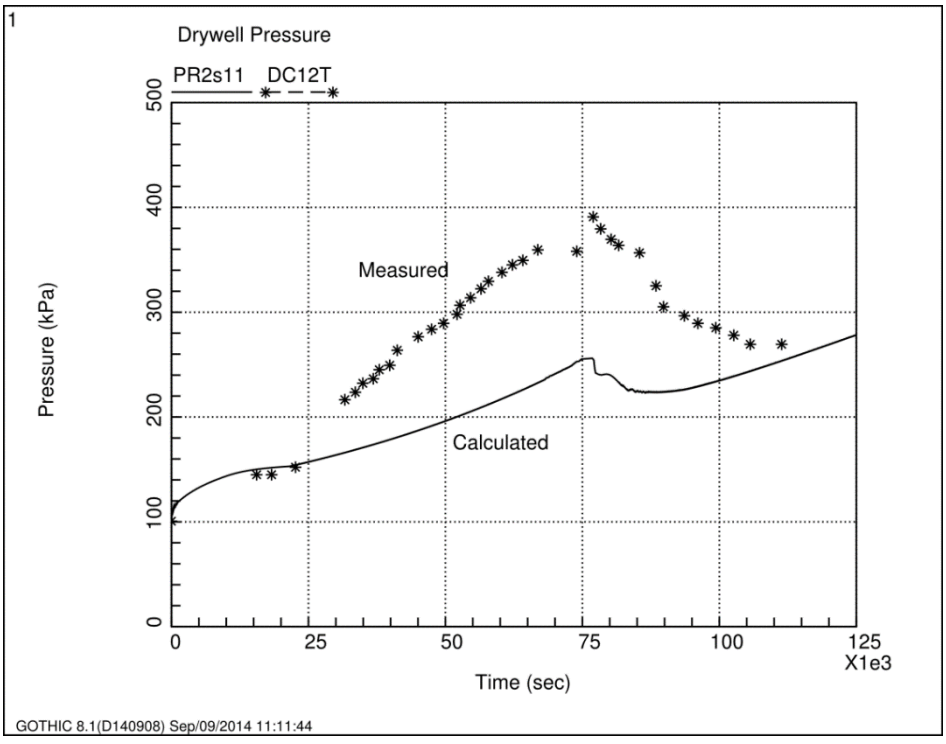

Figure 3-3
1F3 Drywell Pressure - Typical Lumped Model

The temperature results show that the gas space temperature is close to the pool temperature until the wetwell sprays are activated. The gas space temperature then drops below the pool

temperature due to sensible heat transfer to the cold drops. As expected, the pool surface and bulk temperature are nearly equal due to the imposed pool mixing.

It is not clear what causes the large discrepancy between the measured and calculated pressure. Since the well mixed pool condition at around 110,000 seconds is in good agreement with the measured data, the total amount of mass and energy transferred to the wetwell over that period is likely consistent with what actually happened during the event. Therefore, the difference in the results is likely due to differences in the partitioning of the energy in the pool and gas spaces.

Possible causes for the discrepancy in the measured and calculated results are thermal stratification of the pool, incomplete steam condensation, a leak in the drywell, or some combination of these. Each of these effects is discussed below.

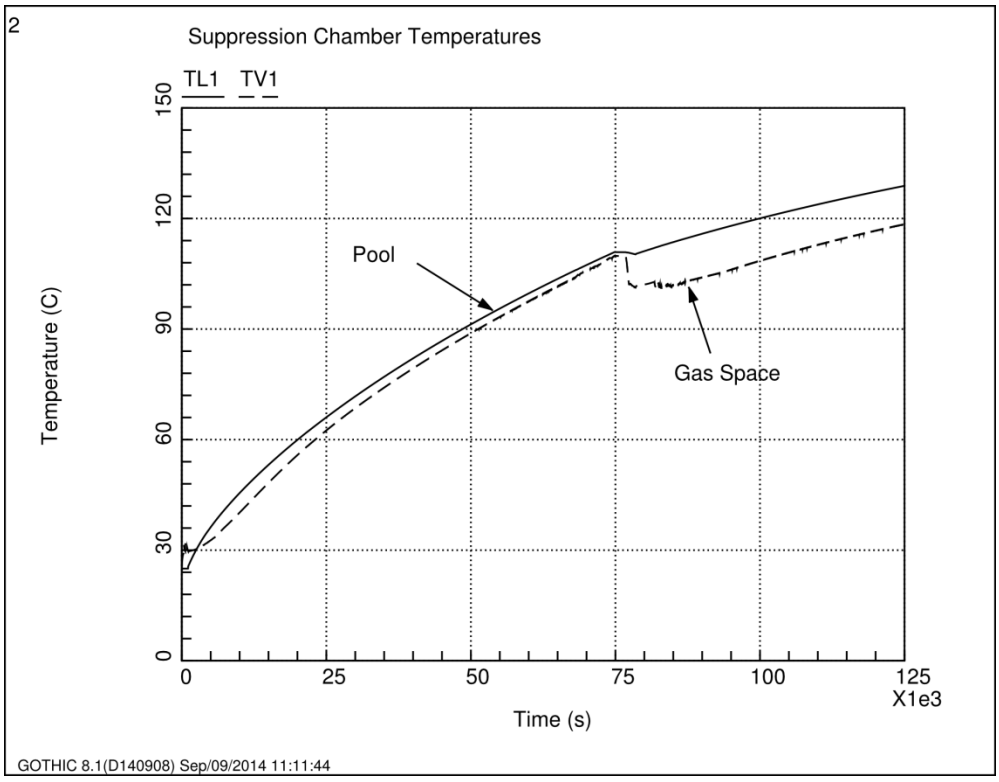

Figure 3-4
1F3 Wetwell Temperatures - Typical Lumped Model

3.3 Pool Thermal Stratification

During a large break LOCA, there are high flow rates of steam and noncondensing gases through the drywell vents into the pool. The large flow rates and the uniform distribution of the vents in the pool result in a well-mixed pool and little or no thermal stratification. This is the basis for the lumped modeling approach for containment Design Basis Accident analysis. However, in situations where there are lower steam flow rates to the pool, significant thermal stratification is a recognized possibility. Top to bottom temperature differences on the order of 33°C were observed in a short term (11 minute) steam release from a single Safety Relief Valve at the Monticello plant (Cook, 1984) (Patterson, 1979). Studies at the POOLEX facility indicate that significant stratification can occur under certain conditions (Laine & Puustinen, 2006) (Li,

Kudinov, & Villanueva, 2011) (Li, Kudinov, & Villaneva, 2010) (Li & Kudinov, 2009) for longer periods of steam injection. During an RPV pressure control test at the Browns Ferry Nuclear Plant, with continuous operation of the RCIC system for approximately 24 hours, significant stratification of the suppression pool was observed. These tests are described in detail in Appendix B with comparisons to GOTHIC results for the test simulations.

For a steam injection into the pool from a single SRV or a turbine exhaust line, the steam condenses near the injection point and the hot water (along with some steam bubbles) rises to the surface. The hot water spreads across the pool surface and the surface can be significantly hotter than the bulk of the water in the pool. The hot surface contributes to high wetwell pressure in two ways; 1) the pool surface heats the gas in the gas space and 2) the higher vapor pressure of the hot surface water causes more steam to be released to the wetwell gas space. The plume induced by the hot source in the pool entrains some of the surrounding fluid as it rises to the surface. In a closed volume, such as a pressure suppression pool, the entrained fluid must be replaced by flow that comes from the upper part of the pool to complete the circulation loop. During sustained injections, this entrainment and circulation results in heating all of the pool above the lowest injection point as observed in the test described in Appendices A-3, A-4 and A-5.

The simple GOTHIC containment model can be used to investigate the amount of stratification (surface to bulk temperature difference) that would be required to give the measured pressure response. In this analysis, a control system is installed in the model that automatically adjusts the mixing pump flow so that the calculated gas space pressure agrees with the measured pressure.

The pressure and temperature results for this case are shown in Figure 3-5 and Figure 3-6. As expected, the calculated pressure is close to the measured pressure up to the time of the spray activation. With the spray on, the calculated gas space pressure drops rather quickly. At this time the control system shuts off the mixing pump because further mixing would only cause the calculated pressure to fall even more quickly. Even with no pool mixing, the calculated pressure is below the measured pressure. With the activation of the HPCI system, the pool resumes its temperature rise and the mixing pump adjusts to match the measured pressure.

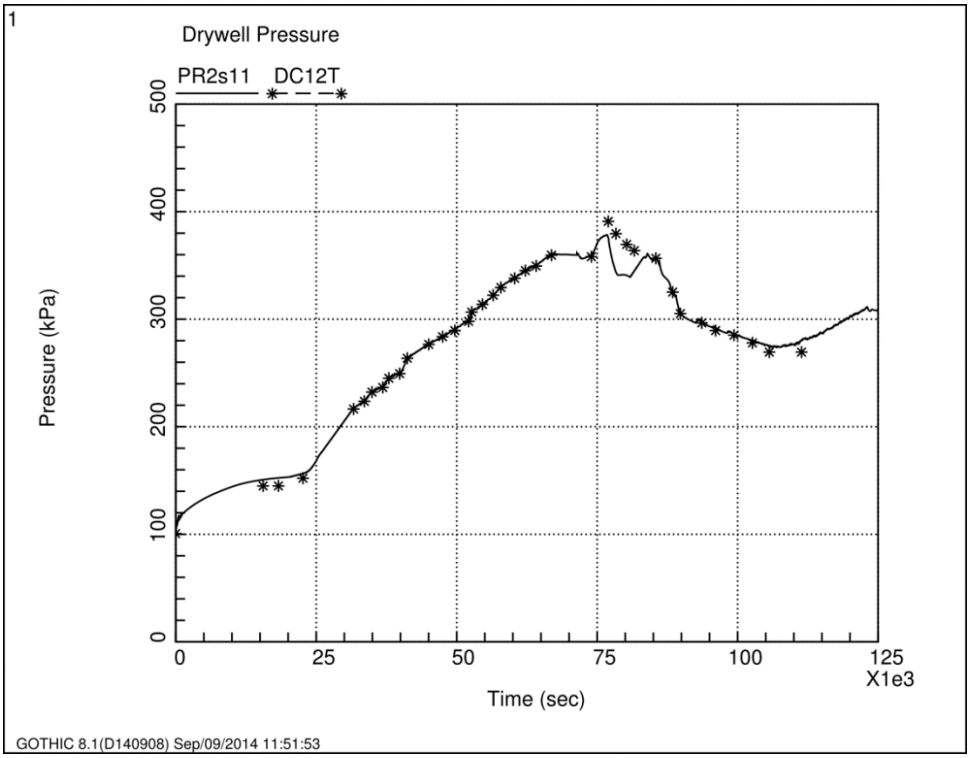

Figure 3-5
1F3 Drywell Pressure - Lumped Model with Stratification

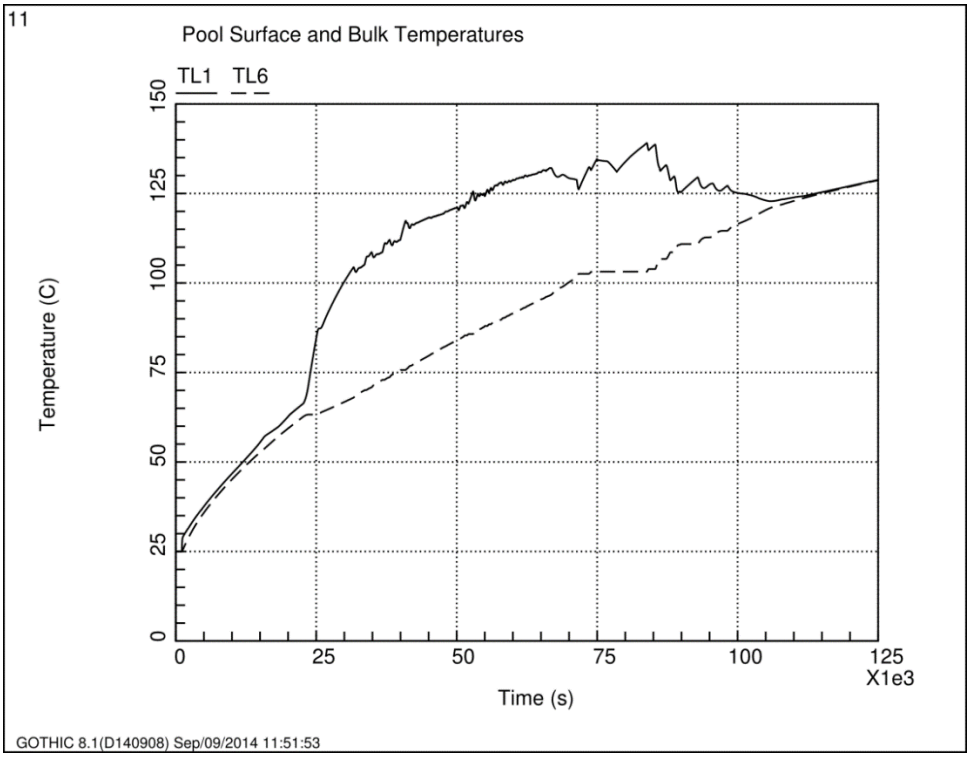

Figure 3-6
1F3 Wetwell Temperature - Lumped Model with Stratification

The temperature results indicate that surface-to-bulk temperature differences on the order of 45°C are needed to get the observed containment pressures. In this calculation, the near surface water approaches the boiling temperature starting at around 50,000 seconds.

The question now is whether or not the magnitude of the thermal stratification forced in the lumped analysis could actually occur in the 1F3 pool due to the RCIC exhaust flow to the pool. Thermal stratification is numerically difficult to predict because the differential forces that keep the system in balance are very small and the stratification can be disturbed by details in the physical system and numerical noise. GOTHIC has been used extensively for modeling buoyancy dominated flow, particularly for gas distribution and building heat up. To prepare for the pool stratification analysis, additional validation of GOTHIC was conducted. Attachment A-3 describes a GOTHIC simulation for one of the POOLEX tests, Attachment A-4 presents results from a GOTHIC simulation of a Monticello SRV discharge tests and Attachment A-5 compares GOTHIC with observed behavior for a Browns Ferry RPV pressure control test with RCIC discharge. These results confirm that GOTHIC is well suited for this investigation.

A 3-dimensional GOTHIC model was constructed for the 1F3 wetwell. This model is essentially the same as the lumped model described above except that the pressure suppression chamber was modeled with a 3D mesh. The overall noding diagram is shown in Figure 3-7. The model includes the drywell, wetwell and vents. Provisional boundary conditions for a postulated drywell steam leak and for the drywell spray are included in the model but these were not activated in the results presented here.

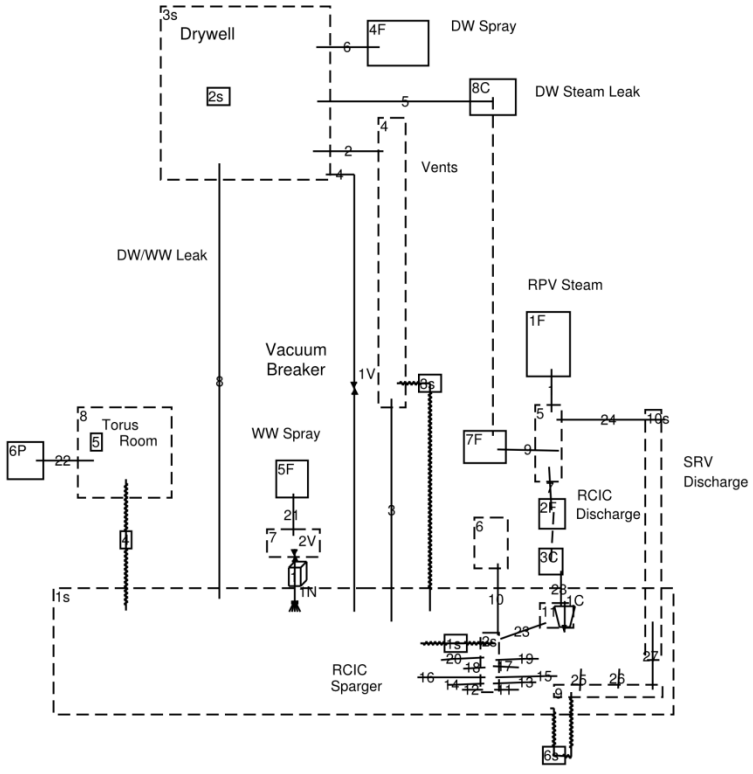

Figure 3-7
1F3 3D Model for Pool Stratification Evaluation

Volume 2s represents the RCIC sparger with a flow path at each grid level in the pool within the range of the sparger holds. Volume 9 is the SRV T-quencher. Volume 7 and the attached 3D connector are used to uniformly distribute the spray in the wetwell gas space.

Although GOTHIC can model the toroidal geometry of the wetwell, a slightly simplified approach was used to reduce simulation time. One half of the SC is modeled as a horizontal cylinder, ignoring the curvature effects of the actual torus. The noding for the wetwell is shown in Figure 3-8. The left boundary of the volume cuts through the RCIC exhaust sparger. The nominal grid spacing in the pool is 0.2 m in the vertical direction. A rather coarse grid is used in the gas with the expectation that it will be fairly well-mixed.

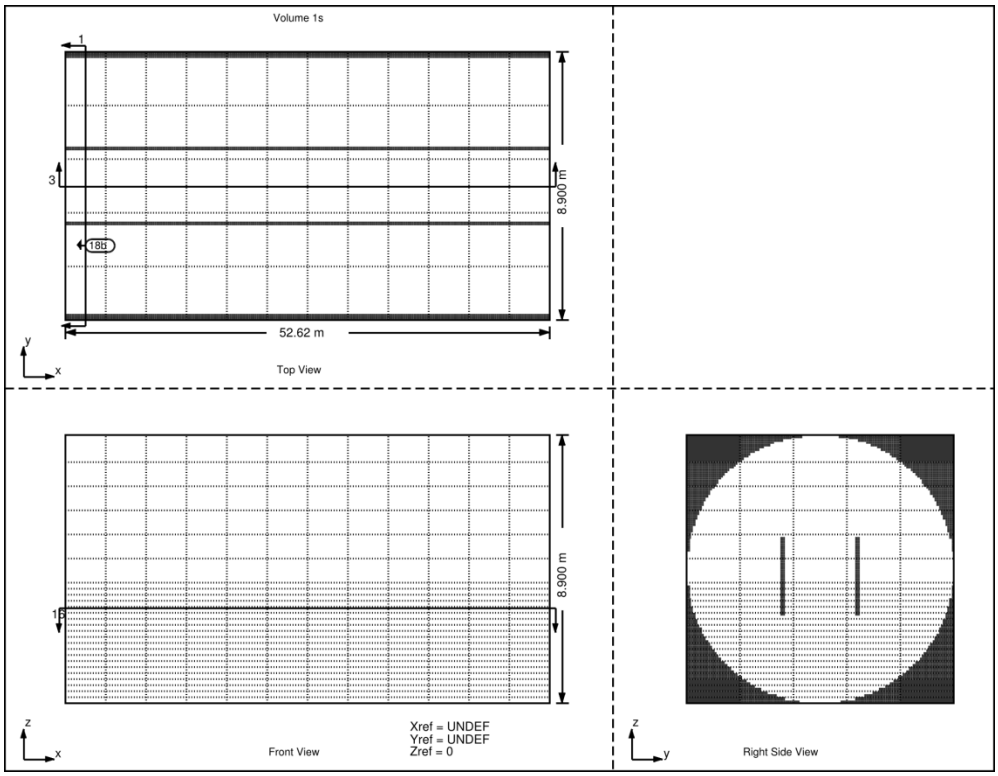

Figure 3-8
1F3 3D Wetwell Model for Pool Stratification Evaluation

The stratification depends on the steam injection depth. The GOTHIC model splits the steam flow between the RCIC and the SRV T-quencher. The RCIC flow is assumed constant at the specified times as indicated in the OECD benchmark prescription. The remaining steam flow from the decay heat goes to the SRV T-quencher. The total steam flow and the RCIC flow are shown in Figure 3-9. As the decay heat decreases, the fraction of the total steam flow going to the SRV T-quencher decreases. At the end of the RCIC operation, the decay heat was just a little more than necessary to provide the specified RCIC turbine exhaust flow.

With the steam source rates shown in Figure 3-9, the steam flow to the SRV T-quencher is decreasing, but continuous. In the actual event it is expected that the SRV flow was intermittent with the same total steam release. Intermittent releases at much higher rates would like induce more mixing in the pool than shown in the result presented below.

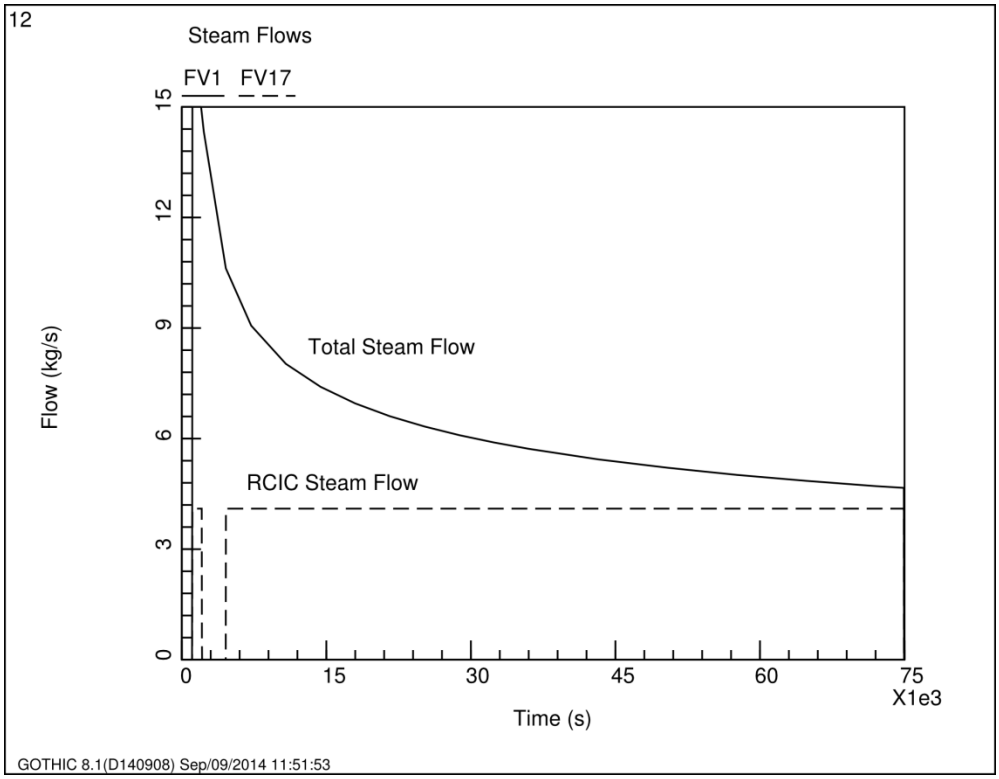

Figure 3-9
1F3 Steam Flows

To investigate the stratification effects, two cases were run. The first case assumes that the steam split between the RCIC and the SRV T-quencher is the same as in the lumped model. The steam to the T-quencher located near the bottom of the pool will tend to mix the pool and reduce stratification. The second case assumes that all of the steam goes to the RCIC sparger. This case maximizes the stratification in the pool.

3.3.1 Stratification Case 1 – RCIC and SRV Injection

Figure 3-10 shows surface and bulk pool temperature. Although a small amount of stratification slowly develops, at 20 hours the surface to bulk temperature difference is less than 2°C. Even the small flow to the SRV T-quencher at the end of the transient simulation is sufficient to keep the pool nearly well-mixed. The temperature and velocity distribution in the pool at 10 hours are shown in Figures 3-11 and 3-12. The longest vector in Figure 3-12 represents a velocity of 0.08 m/s. The predicted containment pressure is shown in Figure 3-13.

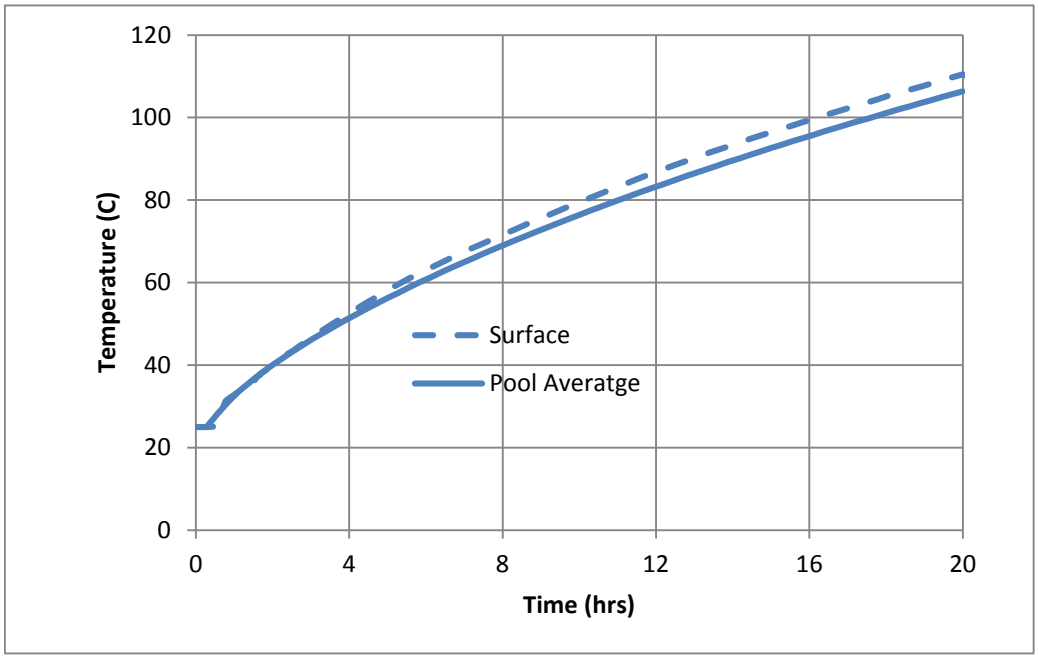

Figure 3-10
1F3 3D Pool Stratification – Case 1

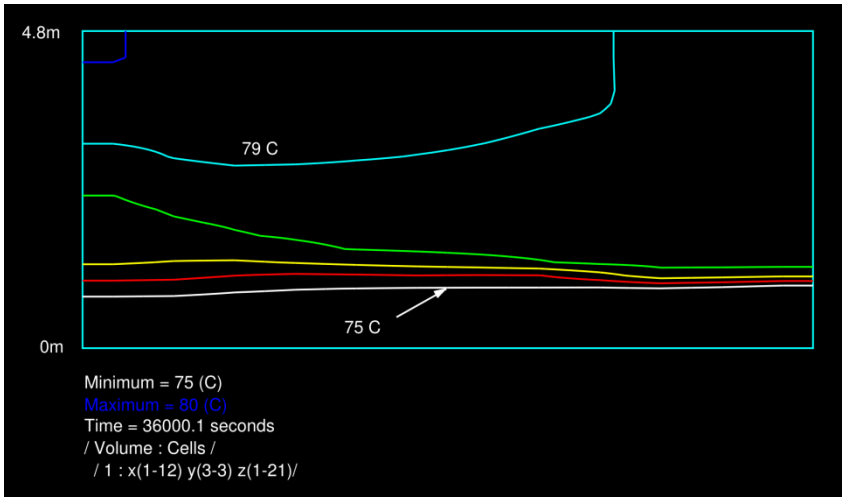

Figure 3-11
1F3 3D Pool Temperature Distribution at 10 hours – Stratification Case 1

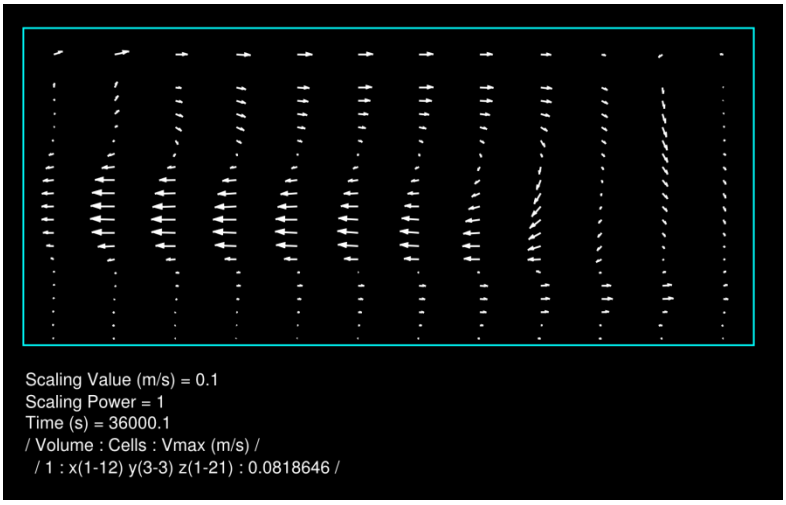

Figure 3-12
1F3 3D Pool Velocity Distribution at 10 hours – Stratification Case 1

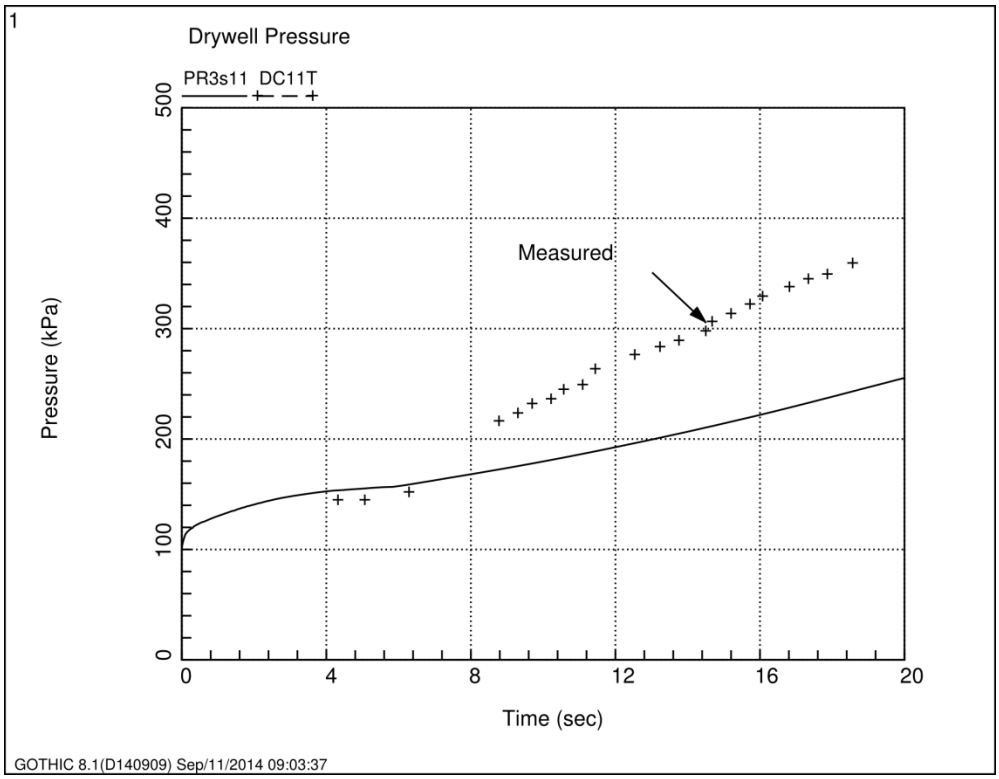

Figure 3-13
1F3 Containment Pressure with 3D Pool Model – Stratification Case 1

3.3.2 Stratification Case 2 – RCIC Injection Only

In this case, all of the heat from the decay heat was assumed to enter the pool through the RCIC sparger. As the injection flow decrease the steam will exit the sparger higher and higher in the pool. Without the SRV injection low in the pool, the potential for stratification is greater than in Case 1.

Figure 3-14 shows surface and bulk pool temperature for the first 20 hours of the 1F3 event. The stratification reaches a maximum at around 10 hours with a surface to bulk pool temperature difference of about 9°C. The temperature and velocity distribution in the pool at 10 hours into the event are shown in Figures 3-11 and 3-12. The longest vector in Figure 3-12 represents a velocity of 0.09 m/s. The predicted containment pressure rise (Figure 3-17) is slightly higher than for Case 1.

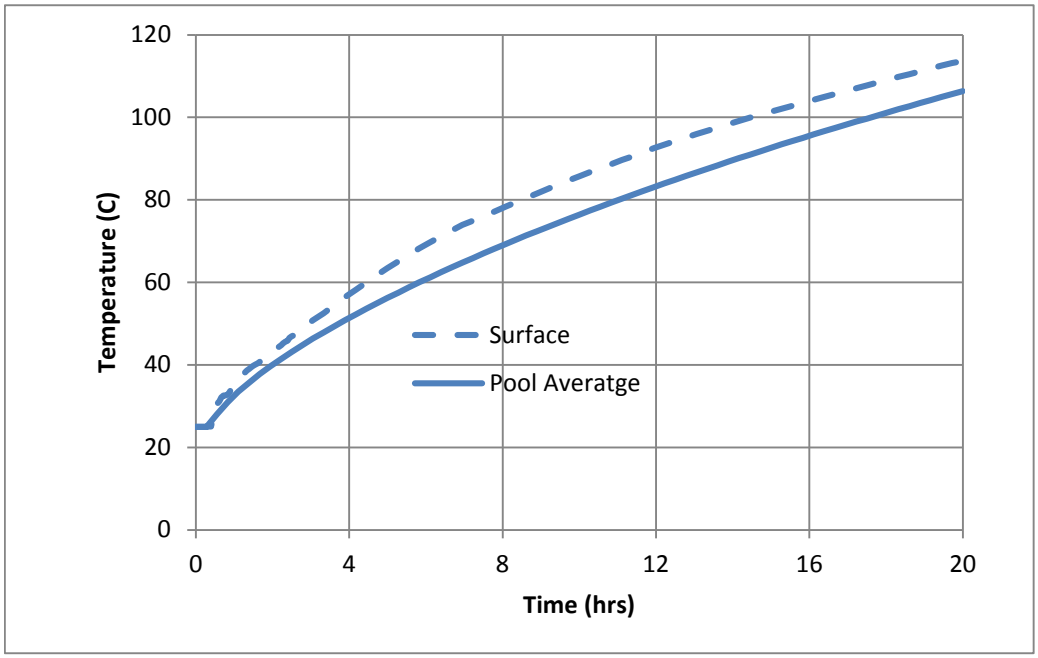

Figure 3-14
1F3 3D Pool Stratification – Case 2

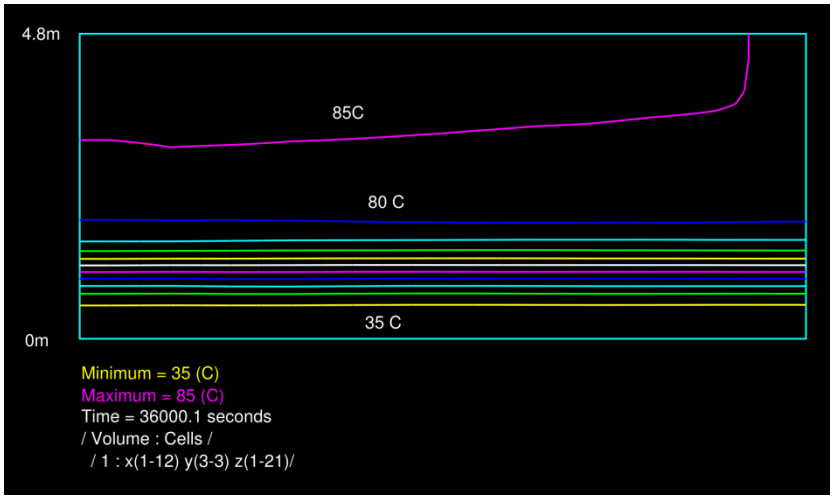

Figure 3-15
1F3 3D Pool Temperature Distribution at 10 hours – Stratification Case 2

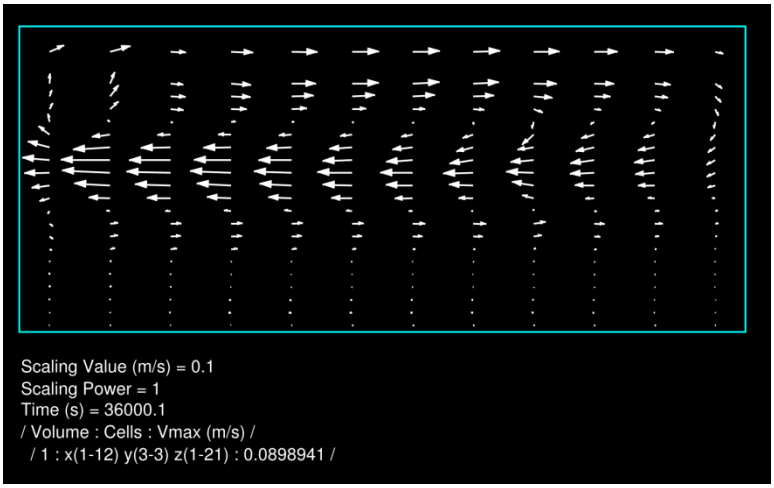

Figure 3-16
1F3 3D Pool Velocity Distribution at 10 hours – Stratification Case 2

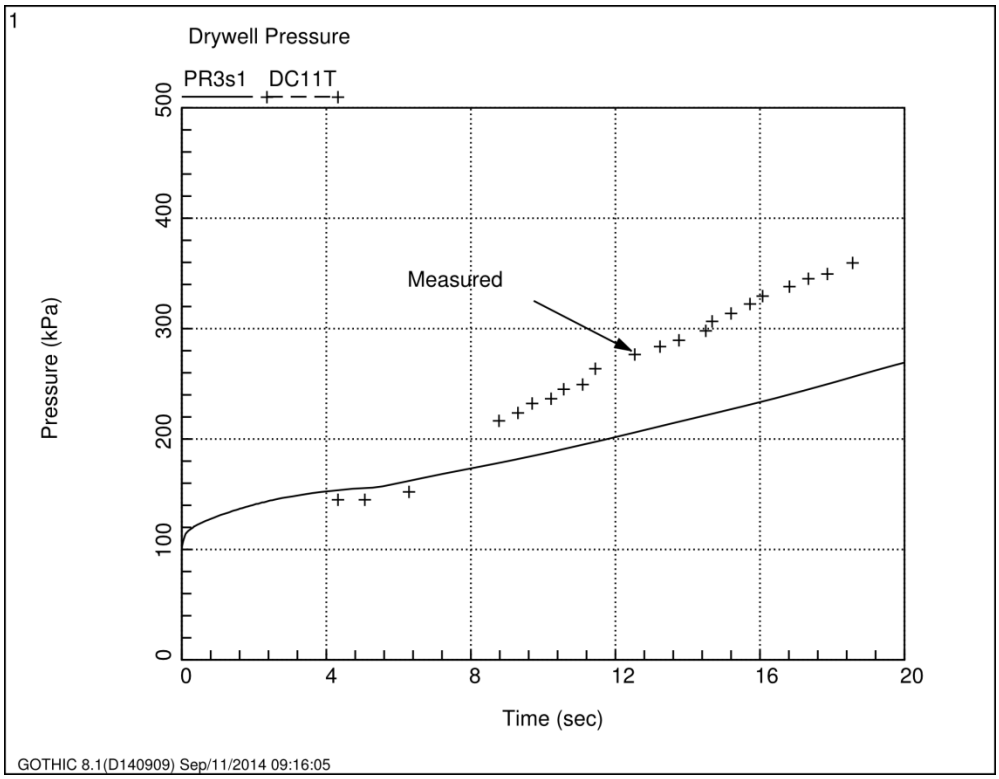

Figure 3-17
1F3 Containment Pressure with 3D Pool – Stratification Case 2

As expected, these results show more stratification than Case 1. However, even in this case designed to maximize the stratification, the surface to bulk temperature difference is much less than needed to produce the observed containment pressure rise. From these results is it apparent that the high containment pressure is not due to pool thermal stratification alone.

The GOTHIC calculated results for stratification presented here might seem inconsistent with the benchmarking results presented in the attachments which indicate substantially more prominent stratification. In the POOLEX test, the stratification zone (region of largest temperature gradient) was at the bottom of the injection pipe, i.e., at the bottom of the heat (buoyancy) source. This is typical of any buoyancy driven flow pattern. Given enough time, the region above the buoyancy source will generally be well mixed. The steam flow rate in the POOLEX test was relatively much smaller than postulated for 1F3. Essentially all of the injected steam in the POOLEX test condensed in the discharge pipe and the discharge pipe did not include an end sparger. The Monticello test shows significant stratification nearer the surface. In this case the discharge from the SRV T-quencher lasted for only 11 minutes. This was barely enough time for the temperature front to make its way to the opposite side of the torus. The steam flow was then shut off and the stratification persisted in the upper part of the pool as predicted by GOTHIC. Had the steam flow been allowed to continue in the test, the stratification zone would gradually move down to the level of the T-quencher, similar to the effect observed in the POOLEX test. The Browns Ferry test indicates significantly more stratification than predicted here (~20 °C, surface to bulk temperature difference). However, the stratification was much less than needed to produce pressurization observed in 1F3 even though the RCIC steam flow per unit torus volume for Browns Ferry test was about 50% lower than postulated for 1F3. The higher steam injection rate in 1F3 would result in less stratification than observed in the Browns Ferry test.

Based on these analyses, observations and comparison, it is highly unlikely that pool stratification was a major factor in the high containment pressure observed in 1F3 during the first 24 hours.

3.4 Incomplete Steam Condensation in the Pressure Suppression Pool

Another possible cause for the high measured containment temperature is incomplete condensation of the RCIC exhaust steam. It is conceivable that large steam bubbles could form from the closely spaced holes in the sparger and that some fraction of the steam would escape the pool surface. The steam entering the wetwell gas space would cause the pressure and temperature in the gas space to rise. Some of the steam could enter the drywell via the vacuum breakers and some would condense on the pool surface. The condensation on the pool surface would depend on the stratification within the pool as well as the steam and liquid temperature distribution in the gas space.

To investigate the possibility of incomplete steam condensation, a 2D model was constructed with a fine grid around the sparger and coarser grid away from the sparger. The overall noding is shown in Figure 3-18. The detailed noding for the wetwell is shown in Figure 3-19. The idealized 2D model includes one 10° sector of radius 1 m surrounding the sparger and the associated volume of the remainder of the torus. The modeled length in the x-direction is one-half the circumference of the torus to preserve the pool mixing time scale. For the near sparger sector region, the radial grid lines are nominally spaced at 10 cm. The vertical grid spacing in the pool and the gas region immediately above the pool is also 10 cm. Flow Boundary Condition 1F represents the RCIC exhaust flow and Pressure Boundary Condition 2P is a vent to constant pressure. Cell face area porosity fractions were specified to model the exhaust pipe and the sparger holes. This gives a good representation of the velocity (and, therefore, momentum) of the steam entering the pool.

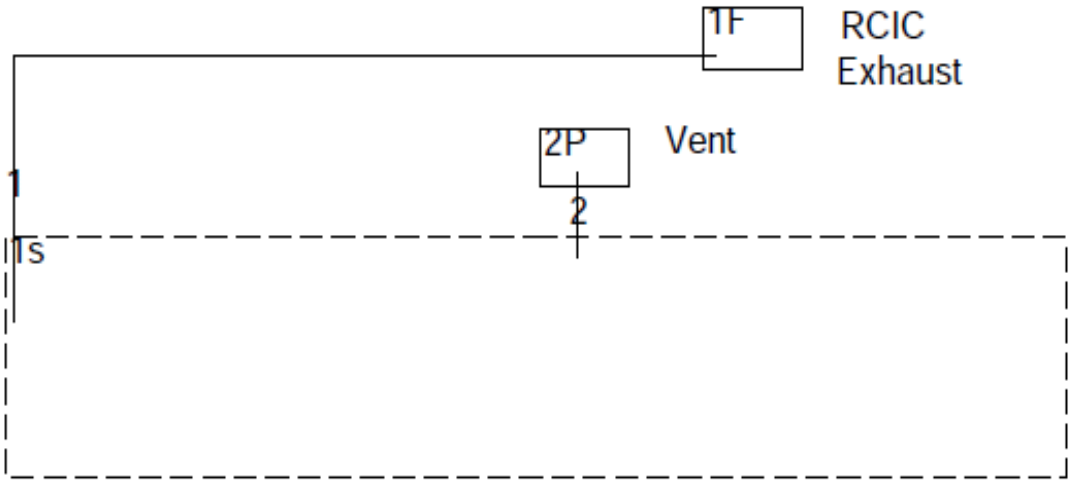

Figure 3-18
1F3 2D Incomplete Steam Condensation Model – Overall Noding

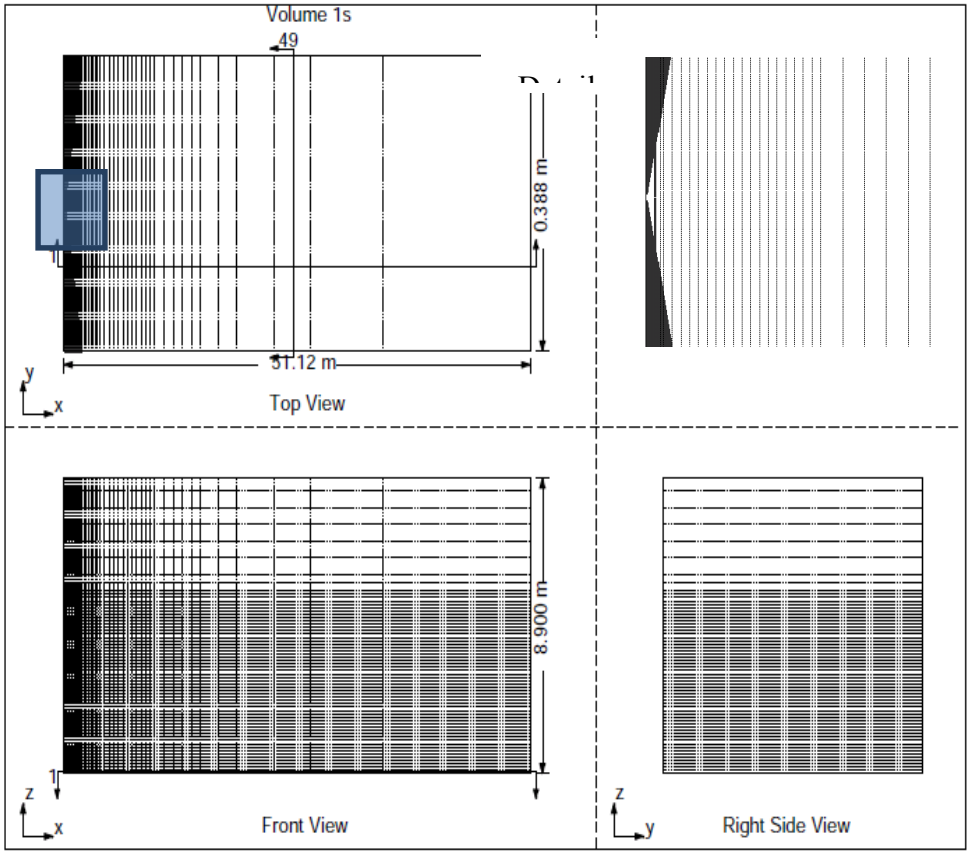

Figure 3-19
1F3 2D Incomplete Steam Condensation Model –Noding Detail

For this simulation, the pool was initialized at 75°C and vent pressure was 1 atm. The bubble formation and condensation process around the sparger is very unsteady and pool bypass, if it does occur, would likely be in spurts as some bubbles break the pool surface. To estimate the

non-steady steam leaving the pool, the flow through the vent was monitored using control variables that capture the lagged mass flow rate through the vent. This averaged vent flow, as a percent for the RCIC exhaust flow and adjusted for the difference in the vapor density at the vent and the steam density exiting the pool is shown in Figure 3-20.

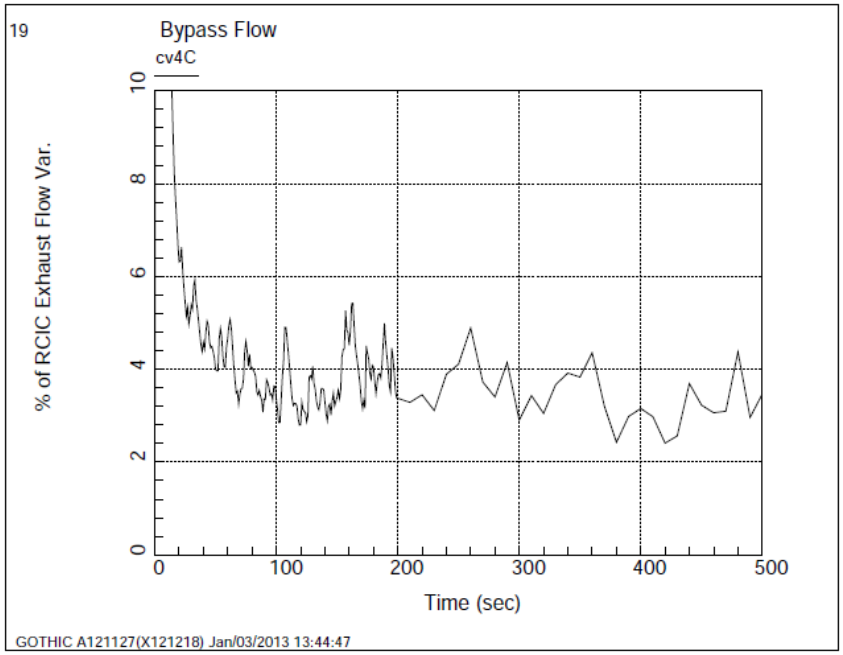

Figure 3-20
1F3 RCIC Exhaust Uncondensed Steam

Early in the transient there apparently is some significant steam exiting the pool, but as the circulation flow in the pool becomes established, the outflow drops rather quickly to an average value of around 3% of the RCIC exhaust flow. The near sparger void, temperature and velocity distribution at 150 seconds are shown in Figures 3-21, 3-22 and 3-23. The region shown is 6 m by 6 m. Figure 3-24 is a frame taken from a TecPlot® movie showing the vapor fraction and liquid velocity profile near the RCIC sparger at 150 seconds. These patterns are oscillatory as can be seen in the animation clip for the startup transient. The animation can be seen by following the link: RCIC_discharge (NAI, 2013). The URL is available in the reference section. From these particular images, it appears that a significant fraction of the steam is breaking through the surface. However, the additional condensation on the water falling back to the pool and the pool surface is sufficient to condense most of the steam that might escape the pool. Although the GOTHIC results appear reasonable, there is significant uncertainty in this simulation. In the subsequent analyses, we will investigate the consequences of incomplete steam condensation on the system pressurization.

Figure 3-21
1F3 Void Distribution near RCIC Sparger at 150 seconds

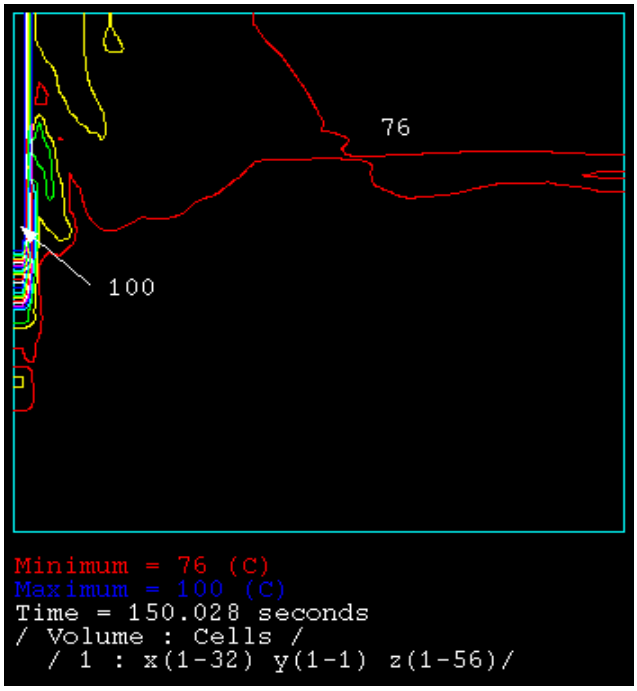

Figure 3-22
1F3 Temperature near RCIC Sparger at 150 seconds

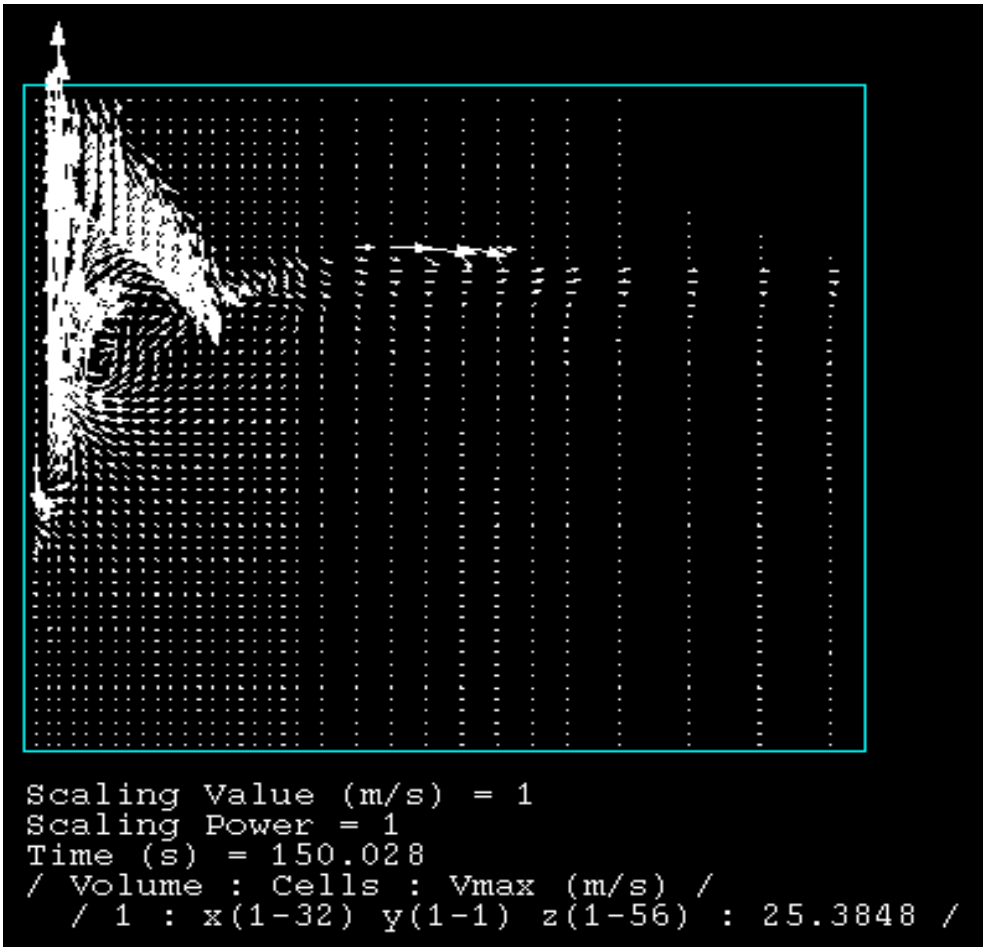

Figure 3-23
1F3 Liquid Velocity Pattern near RCIC Sparger at 150 seconds

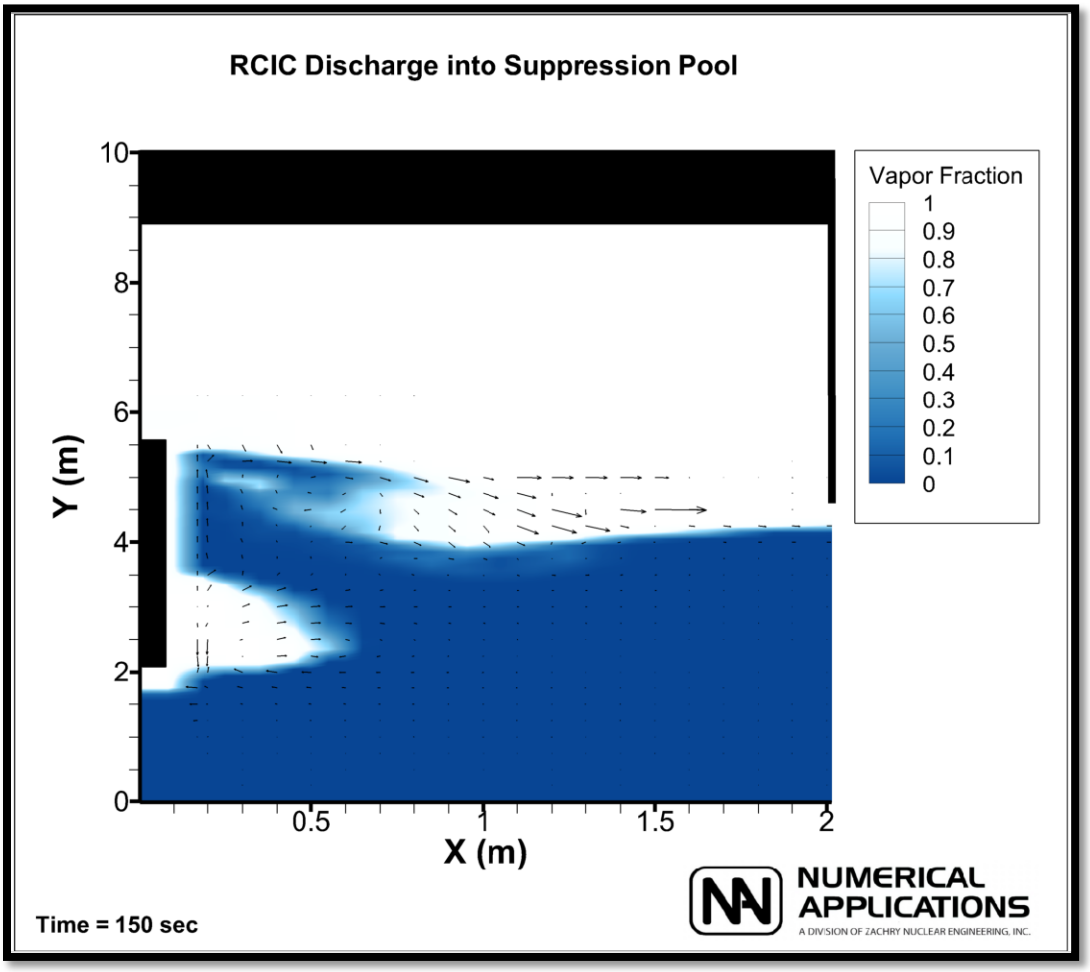

Figure 3-24
Frame Showing Vapor Fraction and Liquid Velocity Profile

The model shown in Figure 3-18 was used to investigate the system pressurization due to incomplete steam condensation. In this model, the cells are large relative to the bubbles that would form around the sparger and the model predicts nearly 100% condensation of the injected steam. The model was modified slightly so that a portion of the RCIC exhaust was injected just above the pool to simulate the possible steam escaping the pool. To minimize mixing (and, consequently, maximize the pressure rise) the gas space steam injection was configured so there was no momentum source. The first run assumed a steaming rate of 3% of the RCIC exhaust flow for consistency with the detailed analysis discussed above. In this simulation, the pressure rise rate was less than 2 kPa per hour compared with ~15 kPa per hour measured. Either the steam escape rate is much higher or the pressurization is not due to this effect alone. A second run was made with 15% steam escape. The wetwell pressure is shown in Figure 3-25. This run was not intended to track the actual event transient. The RCIC flow and gas space steam injection were on constantly from the beginning of the simulation. The intent was to investigate the pressurization rate corresponding to the event time between 25,000 and 75,000 seconds.

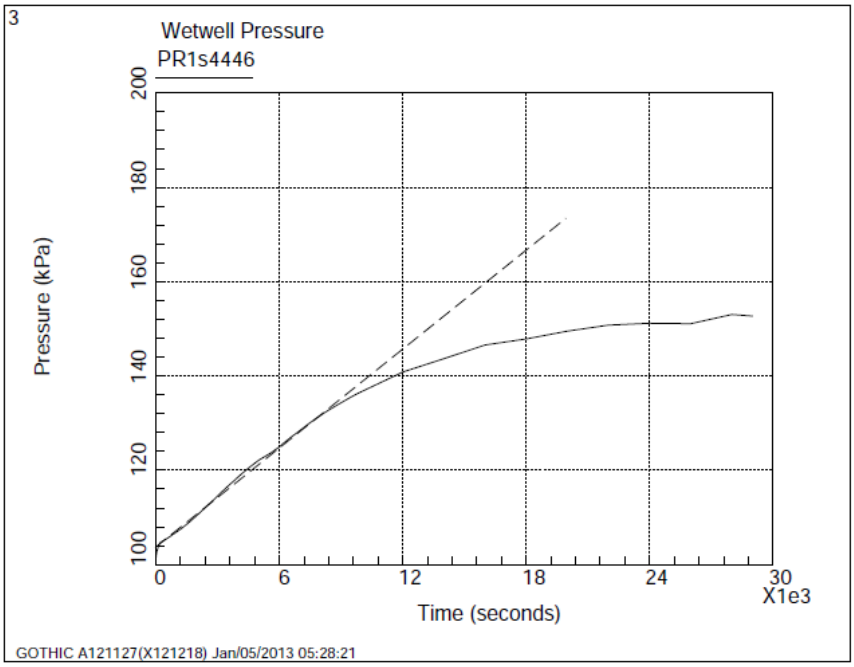

Figure 3-25
1F3 Wetwell Pressure with 15% RCIC Exhaust Not Condensed

For the first 9,000 seconds, the pressurization rate is in fairly good agreement with the measured drywell pressurization rate indicated by the dashed line in the graph. However, the pressurization then tapers off and quits as the wetwell gas space becomes predominately steam. Figure 3-26 shows the steam volume fraction at various elevations in the wetwell gas space. The initial nitrogen is gradually carried out of the wetwell (with steam) via the vacuum breakers as the system pressurizes. The nitrogen tends to reduce the condensation rate on the pool and other cold surfaces and, as it is depleted, the condensation on the pool surface increases, limiting the pressurization. The atmosphere is fairly well mixed at and above the injection elevation of the escaping steam. At the pool surface elevation the steam concentration is low. The relatively thin layer of high nitrogen concentration at the pool surface is not sufficient to keep the steam from condensing. If the steam had been injected at the level with the pool surface, the mixing in the wetwell gas space would be even more complete resulting in a lower pressure rise than seen here. Clearly, the containment pressurization cannot be explained by incomplete steam condensation alone. Furthermore, the detailed analysis indicates that the incomplete condensation potential is minimal, much less than the 15% of the RCIC exhaust flow used in this case.

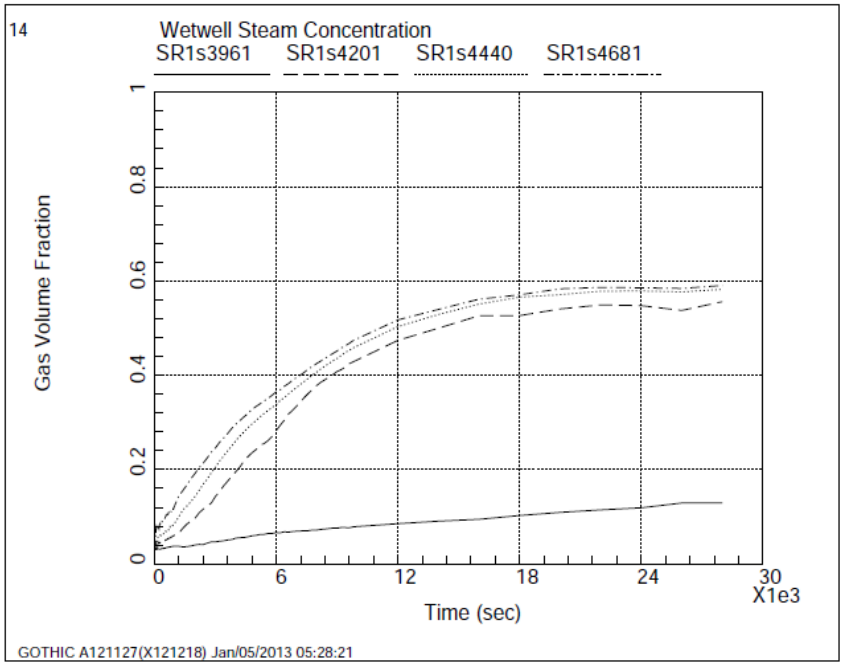

Figure 3-26
1F3 Wetwell Steam Concentrations with 15% RCIC Exhaust Not Condensed

3.5 Leak to Drywell

The MAAP simulation for the 1F3 event approximated the pressure rise in the drywell by assuming a high energy leak in the drywell, possibly from the recirculation pump seals. The lumped model was used to investigate this possibility. The leak to the drywell is deducted from the total steam flow to the wetwell. The leak to the drywell will pressurize the drywell and if the pressure exceeds the wetwell pressure, plus the vent submergence head, the steam and nitrogen will vent to the wetwell. The steam will condense and the nitrogen will be trapped in the wetwell contributing to the pressure rise.

Figure 3-27 shows the drywell pressure assuming a 0.1 kg/s (2.4% of the RCIC exhaust flow) steam leak linearly ramped in between 23,000 and 25,000 seconds and terminating with the depressurization of the RPV at 75,000 seconds. For this model it is assumed that the drywell is well-mixed.

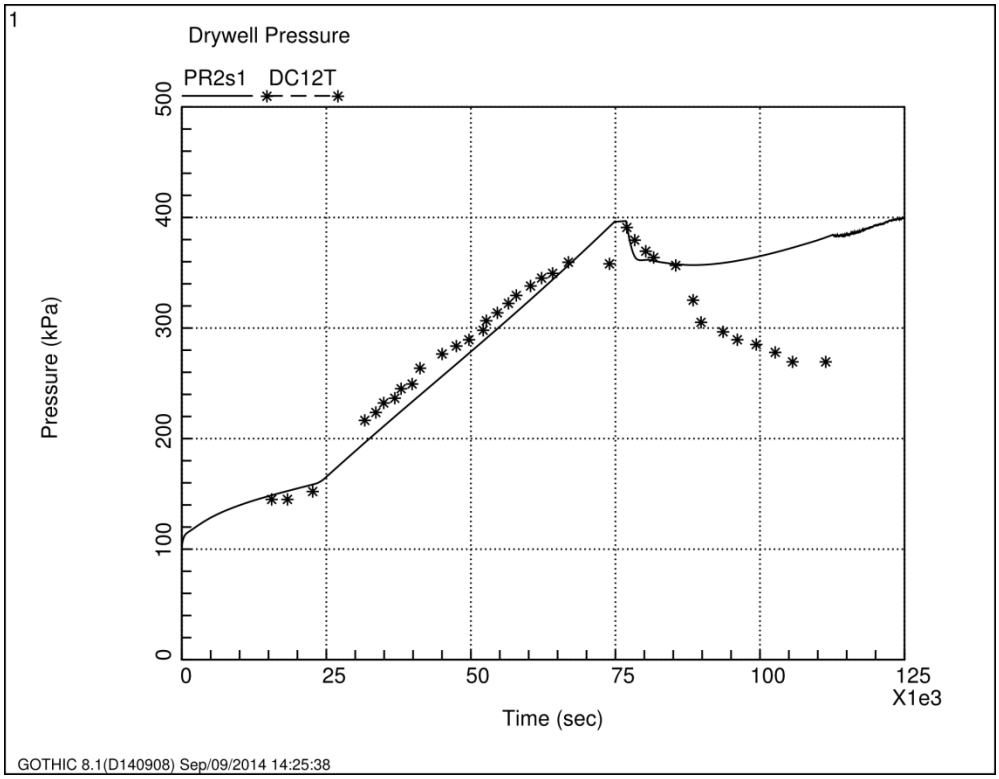

Figure 3-27
1F3 Lumped Model Drywell Pressure with 0.1 kg/s Leak to Drywell

The pressurization to 75,000 seconds can be easily matched by adjusting the leak rate to the DW. The initial depressurization after the wetwell spray is activated matches the measured pressure in the drywell but the pressure then begins to increase due to the injection of the HPCI exhaust flow. As previously indicated, the HPCI exhaust flow is not known. To provide an understanding of the impact of the HPCI flow, Figure 3-28 shows the drywell pressure response when the HPCI exhaust flow is entirely neglected. In this case the agreement is better but this scenario requires that the HPCI exhaust be diverted to somewhere other than the suppression pool.

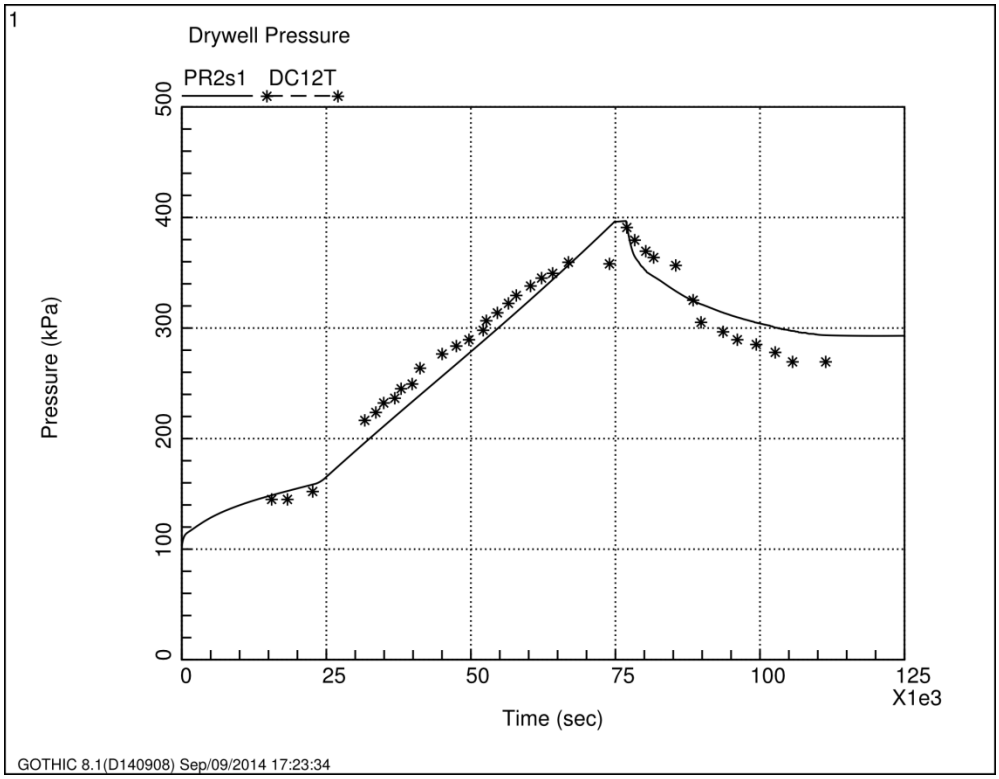

Figure 3-28
1F3 Drywell Pressure with 0.1 kg/s Leak to Drywell without HPCI

3.6 Drywell to Wetwell Leak

Earlier investigations of the 1F3 pressurization event examined the impact of a direct leak between the drywell and the pressure suppression chamber gas space. It was found that the leak, in conjunction with a steam leak to the drywell was necessary to get the observed 1F3 pressurization. However, the prior analysis did not account for the full decay heat. With the assumption that all of the decay heat is converted to steam that goes to the suppression chamber via the RCIC exhaust, SRV discharge, or leak to the drywell it is not necessary to include a drywell to wetwell gas space leak. Using the simplified lumped model, the containment pressure response is not substantially different with or without a small bypass leakage. The potential for a bypass leak combined with multidimensional effects in the pressure suppression chamber gas space is examined in the next section.

3.7 Multidimensional Effects in the Suppression Chamber Gas Space

It has been established with some certainty that stratification in the pressure suppression pool was not the primary cause for the containment pressure rise during the first 24 hours of the 1F3 event. In this section, the possibility of multidimensional effects in the gas space is considered.

NRC guidance allows for leakage between the drywell and suppression chamber equivalent to a 1 inch (2.54 cm) diameter hole for a Mark I containment. It is conceivable that a small leak to the suppression chamber gas space would allow hot steam and gases from the drywell to collect and stratify in the upper regions of the suppression chamber gas space. A multidimensional model was constructed to investigate this and other possible multidimensional effects in the suppression

chamber gas space. The model used for this analysis is the same as that used for the pool stratification study except for the noding in torus and the inclusion of the DW to SC leak.

The noding for the suppression chamber is shown in Figure 3-29. The pool is modeled with a rather coarse grid with the expectation that the pool will be fairly well-mixed. Vertical grid spacing in the gas space is 0.2 m.

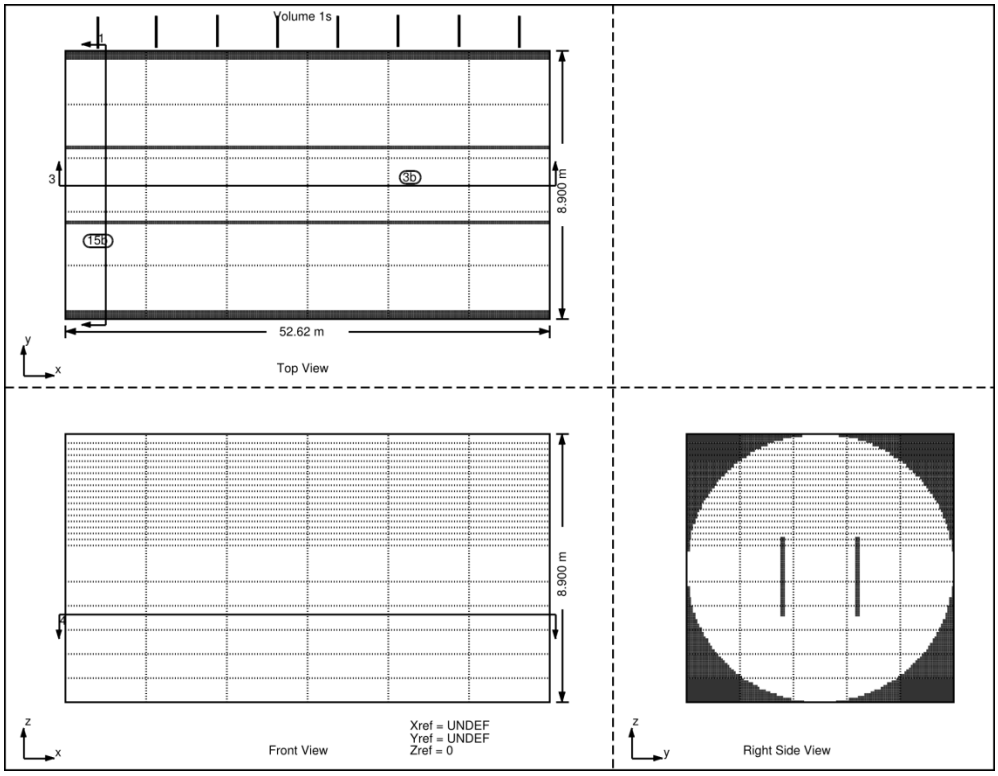

Figure 3-29
1F3 SC Noding for Multidimensional Gas Space Effect I

The predicted drywell pressure for the 1F3 event is shown in Figure 3-30. The pressure rise before the spray activation is a little lower than in the comparable lumped model, most likely due to reduced heat transfer between the pool and the gas space. It is important to note that this model does not include the HPCI injection. It is expected that with the HPCI injection included, the pressure at the end of the 125,000 simulation would be significantly higher than the measure pressure, similar to that shown for the lumped model (Figure 3-27).

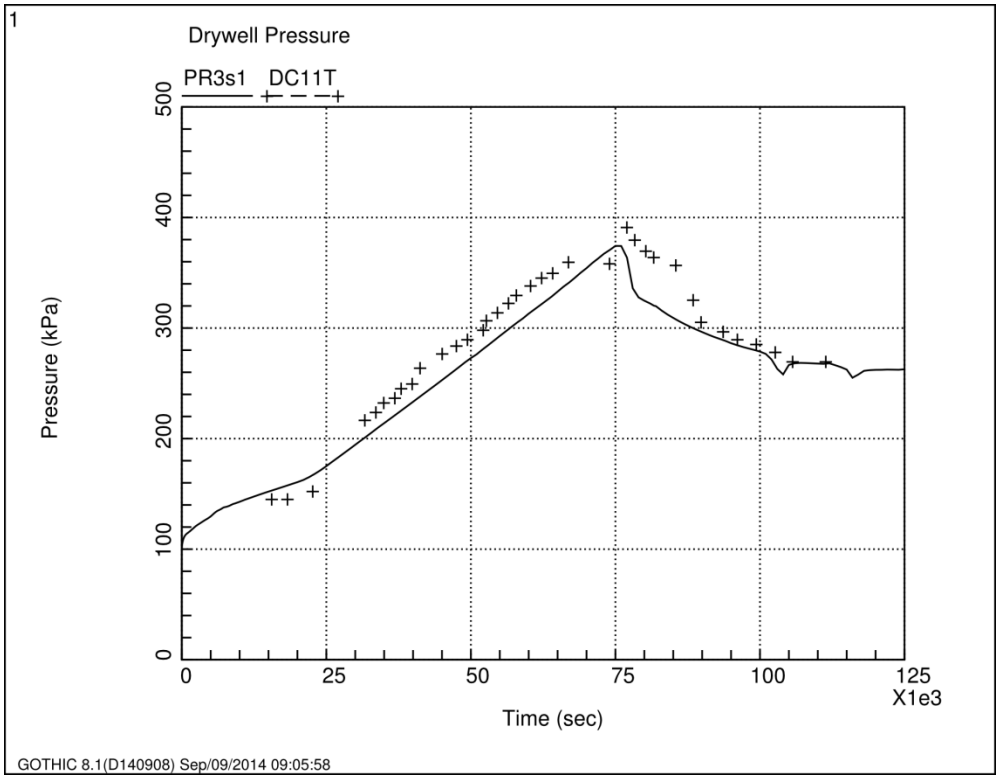

Figure 3-30
1F3 DW Pressure for Multidimensional Gas Space Model I

Selected temperatures in the gas space are shown in Figure 3-31. The select locations are just above the pool surface, at the top of the suppression chamber and one point midway between these two points. The pool surface temperature is also shown in the plot. The results indicate a well-mixed gas space throughout the 125,000 simulation. The apparent departure from well-mixed conditions starting at 80,000 seconds occurs when the pool level approaches the top of the grid level that initially contained the pool surface. As the liquid level fills a grid level, the interfacial heat and mass transfer is artificially reduced because the small amount of vapor in the level approaches the surface conditions. This allows the upper part of the gas space to be temporarily cooled by the spray as indicated by the temperature dips after 80,000s. There is a corresponding artificial dip in pressure in Figure 3-30.

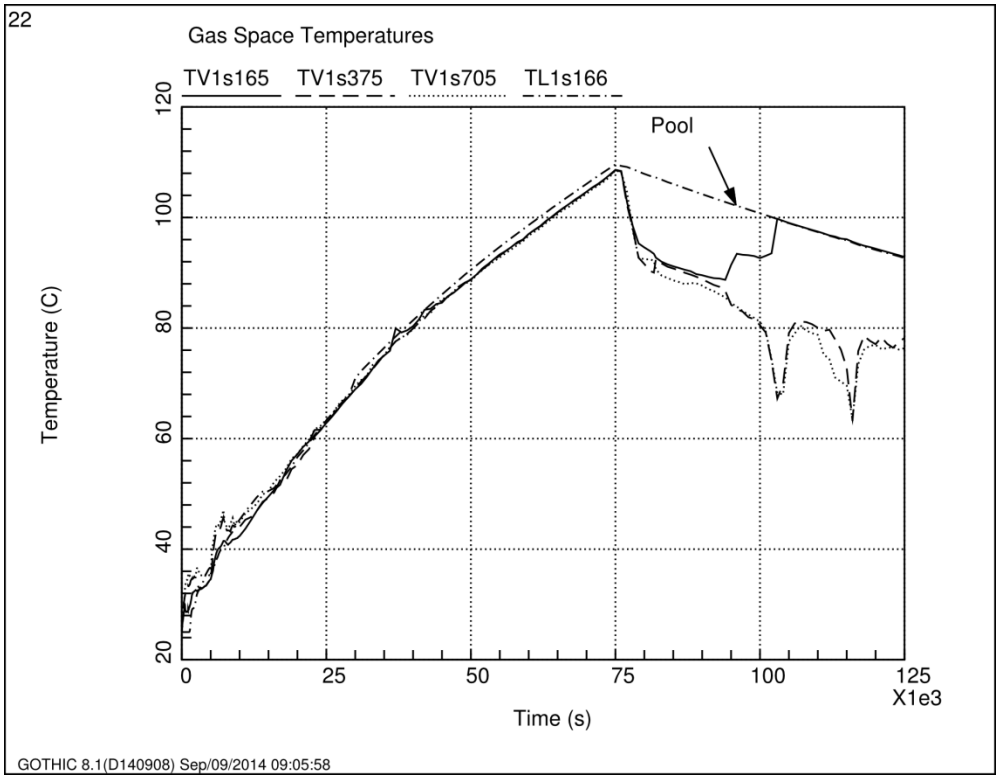

Figure 3-31
1F3 SC Gas Space Temperatures for Multidimensional Gas Space Model I

From these results it is apparent that the multidimensional effects in the gas space are minimal for 1F3 event.

3.8 Conclusions on the 1F3 Initial 36 Hour Containment Pressure.

Based on the investigations using lumped and subdivided modeling for the 1F3 containment pressure response during the first 36 hours of the event, the following observations are offered:

1. Although significant pool stratification can develop during RCIC turbine exhaust injection to the pool, as shown in the Browns Ferry test, it is not likely that stratification of the pool was a dominate contributor to the unexpected containment pressure rise during the first 24 hours of the event at 1F3. Analysis indicates that a surface to bulk temperature difference of about 45 °C would be needed to give the observed containment pressurization. Multidimensional GOTHIC analyses indicated that the stratification would be less than 10 °C if all of the decay heat goes through the RCIC sparger. With the decay heat split between the RCIC sparger and the stratification is minimal.
2. It is not likely that incomplete condensation of the RCIC steam discharge to the pool was responsible for the containment pressure rise. Using the lumped model, the observed containment pressure response could not be duplicated assuming some fraction of the injected steam did not condense in the pool. Multidimensional GOTHIC analyses showed that the fraction of the steam that could potentially escape the pool was small and could not account for the containment pressurization.

3. A high energy leak to the drywell can result in the observed containment pressurization. In the analysis presented here, a constant steam leak at 0.1 kg/s (<2 gpm) starting at around 25,000 seconds and continuing until the RPV depressurization at 75,000 seconds gives good agreement with the observed pressurization. A high temperature water leak, resulting in an equivalent amount of steam would give a similar effect. The steam pressurizes the drywell and enters the suppression pool through the containment vent system, carrying along non condensing gas. The buildup of noncondensables in the suppression chamber gas space causes the entire containment pressure to increase.
4. The activation of the SC spray gives the observed initial containment pressure reduction. However, the addition of the postulated HPCI turbine exhaust flow to the suppression pool soon overwhelms the spray effect and the calculated containment pressure resumes its rise. Multidimensional effects in the SC gas space are not significant during the spray depressurization period. A variable, increasing spray rate can improve the match with the observed pressurization rate but the spray rate must go to levels that are substantially higher than suggested and eventually the SC begins to repressurize due to the gas space volume reduction resulting from the rising pool level.
5. The only effective means found for matching the observed containment depressurization during the SC spray period was the total neglect of the HPCI turbine exhaust flow to the suppression pool. It is unlikely that the HPCI turbine exhaust was not discharged to the pool and other causes should be sought.
6. For the 1F3 pressurization event it appears that multidimensional effects in the suppression chamber are not a major contributor to the containment pressurization. However, in the course of this investigation and validation of GOTHIC for stratification, it is clear that there are cases where pool stratification may be significant, primarily when the steam discharge rate is small. A correlation has been developed (see Section 3.9) that can be used to simulate pool stratification effects in a lumped parameter model.
7. In this investigation, it was assumed that the drywell was well mixed. However, if the steam leak is high in the drywell, the pressurization may be more pronounced because of stratification in the drywell and a higher fraction of noncondensable gas flow to the vents.

3.9 Modeling Pool Stratification in a Lumped Volume Model

During Loss of Coolant Accident (LOCA) at lower steam flow rate conditions, there is a risk of thermal stratification above the discharge pipe exit. Previously, 3D GOTHIC models have been benchmarked against different pool stratification scenarios and documented in the appendices (Appendix A-3, A4 and A-5). In this section, focus is on the development of a correlation that can be used to estimate pool stratification in a lumped modelling approach.

With the ability to predict stratification established, GOTHIC was used to simulate a variety of conditions for steam injection into a half Mark I suppression pool (symmetry plane through the RCIC sparger). The suppression chamber model was based on the Browns Ferry Nuclear Plant (BFNP) Unit 2 geometric parameters (Appendix-A5). A simplified lumped GOTIC model was constructed using the same geometric parameters. The lumped model includes a two zone model for the suppression pool. The steam is injected into the upper volume. A pump and associated flow connections are included to provide some mixing between the upper and lower pool volumes, similar to the scoping model described in 3.2. Using the numerically generated data set

a correlation was developed for the mixing rate (pump flow rate) between the upper and lower pool volumes.

The lumped model nodalization is given in Figure 3-32. Volume 1, representing the suppression chamber is subdivided into two levels. The upper level includes the SC gas space and the top 20% of the SP. The lower level models the remainder of the pool. In a 1D subdivided model, flow is allowed between the two volumes but the 1D nature of the noding does not allow for circulation between the upper and lower volumes. To account for possible convective mixing between the pool near surface and the rest of the pool, Flow Path 7 and an associated pump component 1P are included in the model. The surface-to-pool mixing is controlled by the specified flow rate through the pump.

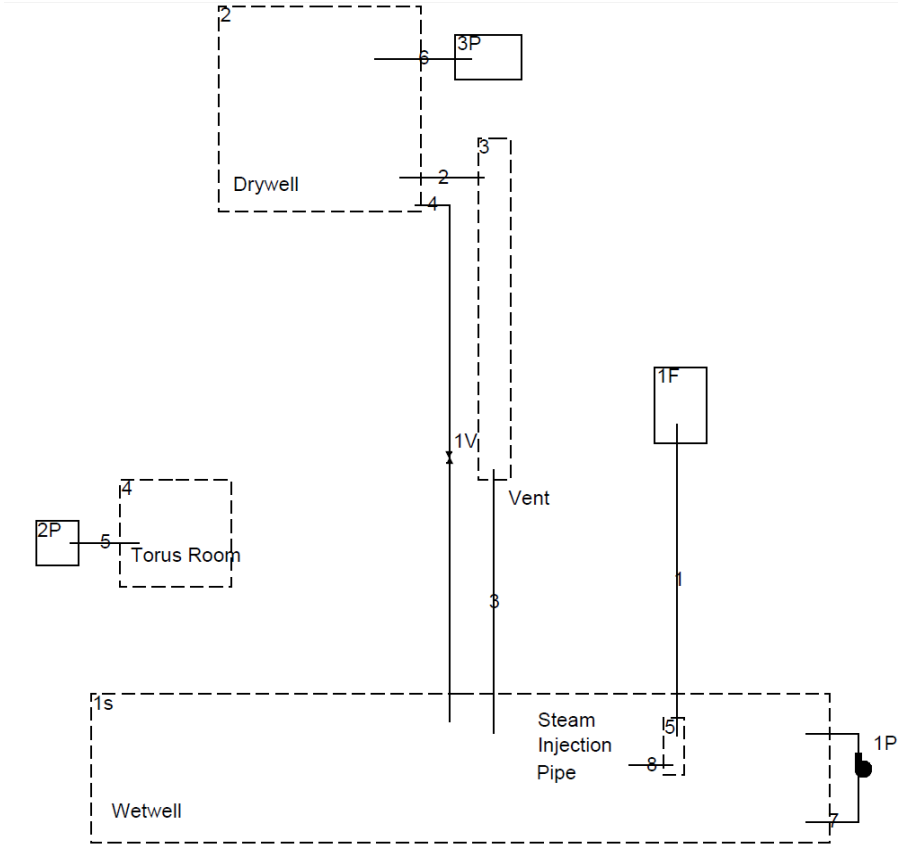

Figure 3-32
BFNP Unit 2 GOTHIC ½ BFNP Unit 2 Lumped Model Nodalization

Flow Paths 2 and 3 connect the vent volume to the drywell and wetwell, respectively. Flow Path 4 represents the vacuum breaker line between the wetwell gas space and the drywell. Valve component 1V models the vacuum breakers. Lumped Volume 2 represents the DW, Volume 3 represents the DW Vent and Volume 4 represents the Torus Room. Conductors were added for heat transfer between the wetwell gas space and the Torus Room and between the Torus Room air and the Torus Room concrete walls.

Volume 5 represents the submerged steam injection pipe. The pipe volume is connected to the pool with a single Flow Path 8. The assumed initial conditions were 30 °C (86 °F) and 101.3 kPa

(1.47 psia). Steam was injected from boundary condition 1F into the steam injection pipe. The steam enthalpy is estimated at 2,785 kJ/kg based on the measured BFNP Unit 2 RPV pressure (5,962kPa) (saturation conditions assumed).

During the steam injection into the pool, the steam condenses near the injection point and the hot water (along with some steam bubbles) rises to the surface. During the early phase of steam injection, hot water spreads across the pool surface and the surface can be significantly hotter than the bulk pool water. As the steam injection continues, the water above the source becomes fairly well mixed. As seen in the GOTHIC simulation of the BFNP Unit 2 RCIC test (Appendix A-5), steam was released only from the first two levels of the sparger and heated up the pool above the source without significantly mixing the water below that level bottom. In order to capture this effect in a simplified lumped model, the steam flow is added to the near surface water in the upper subvolume. The surface-to-lower-pool mixing is controlled by a pump that circulates flow between the upper and lower volumes. The mixing rate correlation described in this section controls the pump flow rate. The mixing rate is assumed to be a function of following parameters:

1. The flow rate of the steam ($\dot{m}_s$)
2. The submergence ratio (injection depth divided by the total pool depth (d / d_t), see Figure 2-33)
3. The temperature difference between the condensed steam and the lower pool ($\Delta T = T_s - T_l$), and the thermal expansion coefficient of the pool water (ε_t)

i.e., $$\dot{m}_p = f_1\left(d/d_t\right) f_2\left(\dot{m}_s\right) f_3\left(\Delta T, \varepsilon_t\right) \qquad (3\text{-}1)$$

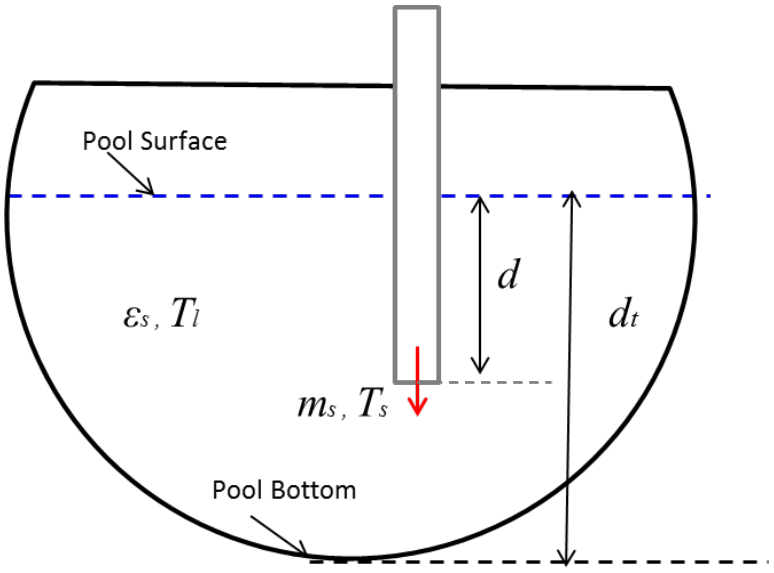

Figure 3-33:
Suppression Pool Parameters

Based on the BFNP Unit 2 geometric specifications and initial conditions (Appendix A-5), a series of sensitivity studies were conducted to investigate each individual parameter;

- Case Series I: The injection pipe submergence ratio (d/d_t) was varied between 0.1 to 1 at constant steam injection flow rate.
- Case Series II: The steam flow rate, $\dot{m}_s$ was varied between 0.01 and 2 kg/s at a fixed steam injection location.
- Case Series III: Variations in pool temperature ΔT and its effect on the thermal expansion term ε_t were studied.

For all the case studies, 3D GOTHIC models were run to give transient predictions of the pool surface. Then, the 3D temperature predictions were used to drive the pump flow rate via a system of control variables in the simplified lumped model. The control system automatically adjusts the pump flow rate so that the calculated lumped model pool surface temperatures agree with the 3D temperature predictions. By doing so, the required pump flow rates are obtained for all simplified GOTHIC models

3.9.1 Case Series I: Steam Injection Location Case Study

In Case Series I, steam is injected at a fixed flow rate of 1.54 kg/s (equivalent to 3.08 kg/s steam flow for a full scale typical MARK I containment with 3382 m^3 pool volume) for 7,200 seconds (2 hours) from boundary condition 1F into the pool at nine different depths. As shown in Figure 3-34, when the steam injection depth was increased, the pool surface temperature predicted by the GOTHIC 3D model decreased.

In the simplified GOTHIC model, the steam was injected into the upper level of the WW control volume which contains only the 20% of the total pool water. The surface-to-pool mixing was controlled by a specified flow from the lower level of the pool through the pump. As the steam injection depth was increased, higher pump flow was needed in the simplified GOTHIC models to maintain the pool surface temperature to match the GOTHIC 3D predictions. The maximum required pump flow rate for each case is presented in Figure 3-35. Using the curve fitting function available in Excel the relation between the submergence ratio and the normalized maximum pump flow rate is approximated by,

$$\frac{\dot{m}_{p-\max}}{\dot{m}_{p-d/d_t\max}} = \left(d/d_t\right)^{1.25} \tag{3-2}$$

$\dot{m}_{p-d/d_t\max}$ is the maximum pump flow rate when d/d_{tmax} = 0.93 (the maximum pool depth ratio) that is used to normalize the results in Figure 3-35. The relationship between the location of the steam injection and the pump flow rate in the simplified GOTHIC models can be written as,

$$\dot{m}_p \sim \left(d/d_t\right)^{1.25} \tag{3-3}$$

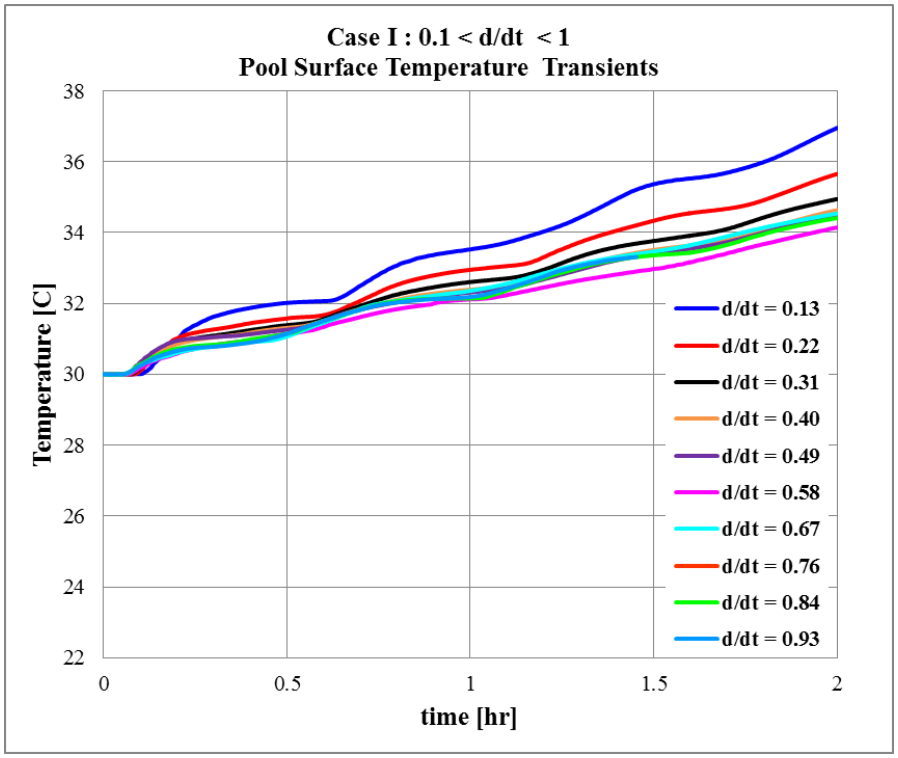

Figure 3-34
Case I GOTHIC 3D Pool Surface Temperature Predictions

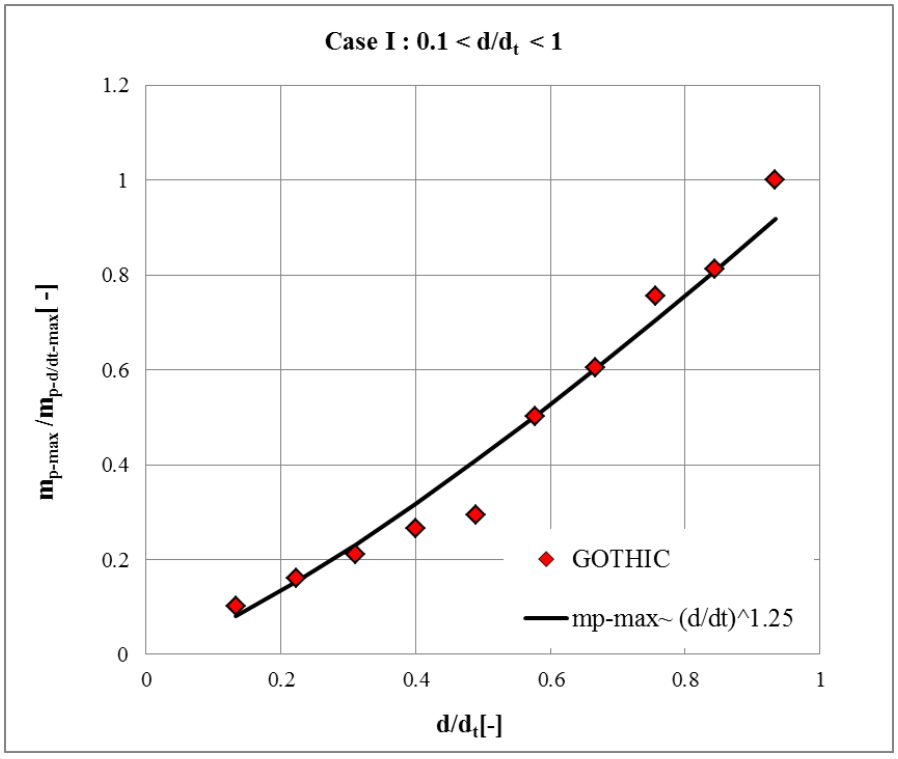

Figure 3-35
Case I GOTHIC Maximum Required Mixing Rate

3.9.2 Case Series II: Steam Injection Rate Case Study

In Case Series II, the steam flow was varied between 0.01 and 2 kg/s (equivalent to 0.02 and 4kg/s steam flow for a full scale typical MARK I containment with 3382 m3 pool volume) and injected for 7,200 seconds (2 hours) at a fixed elevation, d/dt = 0.47. (This is a typical injection depth for RCIC exhaust). From Figure 3-36, it can be seen that at lower injection rates ($\dot{m}_s \leq 0.1$ kg/s) there was only a moderate effect on the pool surface temperature whereas at higher steam injection ($\dot{m}_s$ >0.1 kg/s), the pool surface temperature increased more rapidly.

Using the 3D GOTHIC surface temperature predictions as a target control for the controlled circulation flow, the required maximum pump flow ($\dot{m}_{p-\max}$) was obtained for each simplified GOTHIC model. Then, the $\dot{m}_{p-\max}$ predictions were divided by $(d/d_t)^{1.25}$ to exclude the steam release location effect. To scale the mixing rate to the pool volume, the steam injection rates ($\dot{m}_s$) were divided by the total pool water mass (m_{pool}). As shown in Figure 3-37, $\dot{m}_{p-\max} \Big/ \left(m_{pool} (d/d_t)^{1.25} \right)$ results are plotted against $\dot{m}_s / m_{pool}$. The relationship is defined by three linear correlations between $\dot{m}_{p-\max}$ and $\dot{m}_s / m_{pool}$:

$$\frac{\dot{m}_{p-\max}}{m_{pool}} = 3.27\times10^{4}\left(\frac{\dot{m}_s}{m_{pool}}\right)(d/d_t)^{1.25} \quad \text{for} \quad 0 \leq \dot{m}_s / m_{pool} < 1.6\times10^{-8}\ s^{-1} \tag{3-4}$$

$$\frac{\dot{m}_{p-\max}}{m_{pool}} = \left(3.97\times10^{3}\left(\frac{\dot{m}_s}{m_{pool}}\right) + 4.61\times10^{-4}\right)(d/d_t)^{1.25} \quad \text{for} \quad 1.6\times10^{-8} \leq \dot{m}_s / m_{pool} < 6\times10^{-8}\ s^{-1} \tag{3-5}$$

$$\frac{\dot{m}_{p-\max}}{m_{pool}} = \left(2.38\times10^{3}\left(\frac{\dot{m}_s}{m_{pool}}\right) + 5.55\times10^{-4}\right)(d/d_t)^{1.25} \quad \text{for} \quad 6\times10^{-8} \leq \dot{m}_s / m_{pool} < 1.2\times10^{-6}\ s^{-1} \tag{3-6}$$

where $\dot{m}_{p-\max}$ is in kg/s and m_{pool} is in kg.

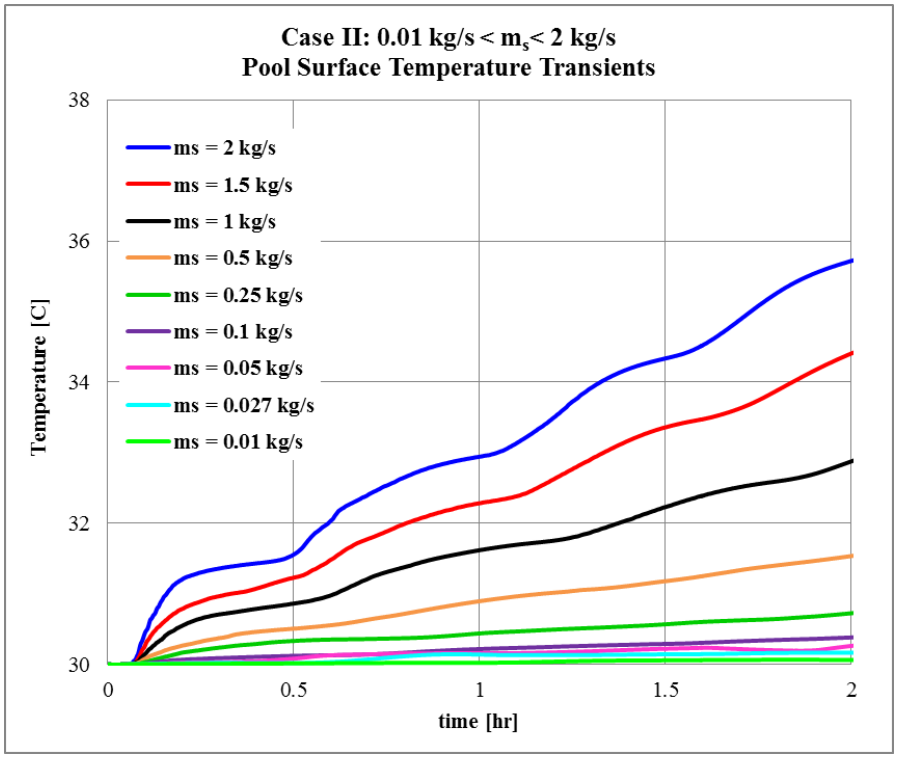

Figure 3-36
Case II GOTHIC 3D Pool Surface Temperature Predictions

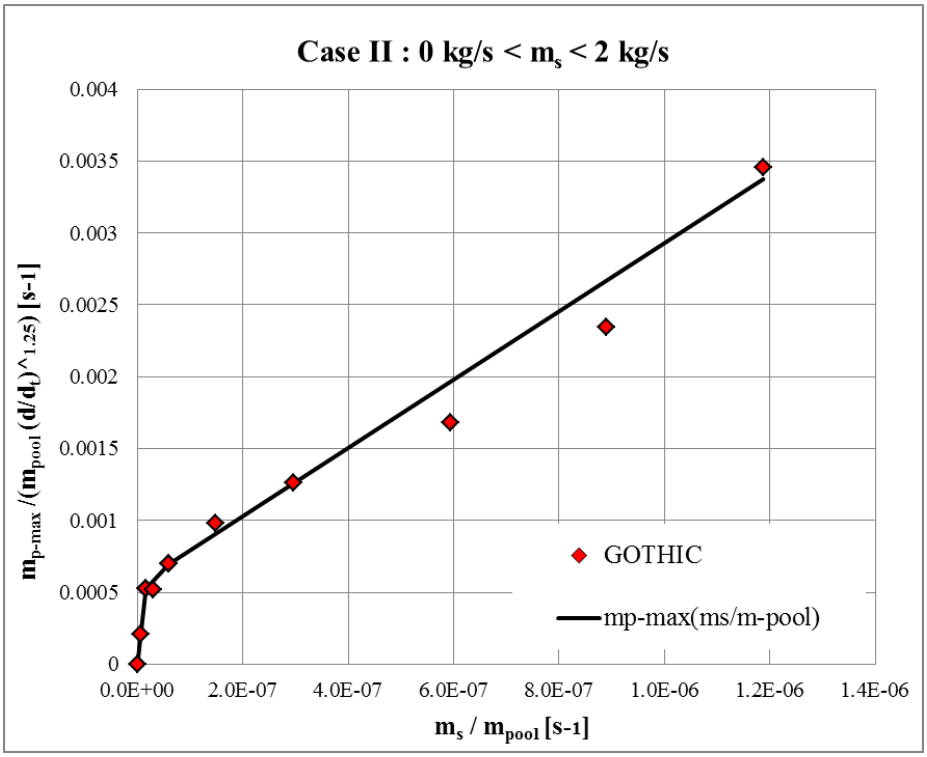

Figure 3-37
Case II GOTHIC Required Maximum Pump Flow Rate

3.9.3 Case III: Pool Temperature and Thermal Expansion Case Study

In Case Series III, the previously presented Browns Ferry Nuclear Plant (BFNP) Unit 2 3D GOTHIC model was used for steam injection through the RCIC sparger at four different steam injection rates: 0.5, 0.75, 1.0 and 1.54 kg/s (equivalent to 1, 1.5, 2 and 3.08 kg/s steam flow for a full scale typical MARK I containment with 3382 m^3 pool volume). Steam is injected for 122,400 seconds (34 hours).The RCIC sparger is modeled with a 1D subdivide pipe volume and the sparger volume is connected to the pool with nine Flow Paths (FP) spanning the range of the sparger length (Appendix A-5).

The 3D GOTHIC model results showed differences in steam release depth (d) based on variances in steam injection rate ($\dot{m}_s$). At lower injection rates, steam was released through only the highest level of the sparger openings. As the steam flow rate increases, the water level in the sparger if further depressed and the steam injection extends to lower levels of the sparger. These injection depths were supplied as input for the lumped model pump circulation flow rate calculation. In general, the injection depth will not be known. Therefore, it is essential to understand the relationship between injection rate and the injection depth for a sparger. Using the known geometric parameters as shown in Figure 3-38 and listed in Table 3-1, an analytical correlation between $\dot{m}_s$ and d can be developed:

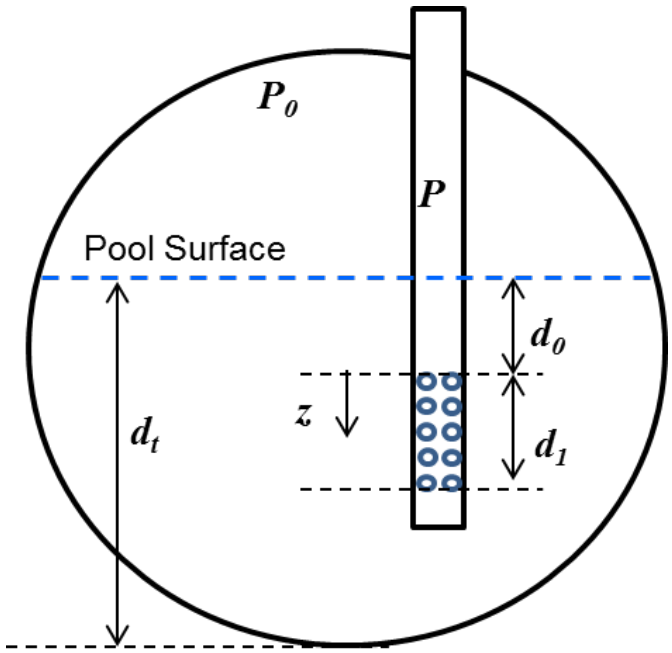

Figure 3-38
CASE III Suppression Pool Geometric Parameters

Table 3-1
CASE III Suppression Pool Geometric Parameters

$\dot{M}_0$	Steam mass flow rate into the sparger
u	Steam velocity in the sparger
v	Steam velocity through the sparger holes
P	Steam pressure in the sparger
P_o	Suppression chamber gas space pressure
ρ_w	Suppression pool density
ρ	Steam density
A_h'	Sparger hole area per unit length
A_p	Sparger cross section area
k	Loss factor for the sparger holes
d_0	Submergence to the top of the sparger hole region
d_1	Distance from the top of the sparger hole region to the depressed water level in the sparger
d	Total release depth
g	Gravitational acceleration
R	Steam gas constant
T	Steam temperature

Assuming constant steam density, at any distance, *z*, from the top of the sparger hole region, the mass balance for the steam flow in the sparger is

$$A_p \rho \frac{du}{dz} = -A_h' \rho v \tag{3-7}$$

or

$$v = -\frac{A_p}{A_h'} \frac{du}{dz} \tag{3-8}$$

The force balance for the steam flow through the holes is

$$P - \left(P_0 + \left(d_0 + z\right) \rho_w \boldsymbol{g}\right) = \frac{k}{2} \rho v^2 \tag{3-9}$$

giving

$$\frac{dP}{dz} - \rho_w \boldsymbol{g} = k\rho v \frac{dv}{dz} \tag{3-10}$$

Combining this equation with Equation 3-8 gives

$$\frac{dP}{dz} - \rho_w \boldsymbol{g} = k\rho \left(\frac{A_p}{A_h^{'}} \right)^2 \frac{du}{dz} \frac{d^2u}{dz^2} \tag{3-11}$$

Neglecting the wall friction, the momentum balance for the flow down the sparger is

$$A_p \left(P_z - P_{z+\Delta z} \right) + A_p \rho \left(u_z^2 - u_{z+\Delta z}^2 \right) = A_h^{'} \Delta z v \rho u \tag{3-12}$$

giving

$$-A_p \frac{dP}{dz} - A_p \rho \frac{du^2}{dz} = A_h^{'} v \rho u \tag{3-13}$$

Combining this equation with Equation 3-8 gives

$$\frac{dP}{dz} + \rho \frac{du^2}{dz} = \rho u \frac{du}{dz} \tag{3-14}$$

or

$$\frac{dP}{dz} = -\rho u \frac{du}{dz} \tag{3-15}$$

At the top of the sparger section (z=0)

$$\dot{M}_0 = A_p \rho u_{z=0} \tag{3-16}$$

Also

$$\dot{M}_0 = \int_0^{d_1} A_h^{'} \rho v dz \tag{3-17}$$

Assuming that the hole velocity varies linearly with *z*, i.e.,

$$v = v_{z=0} (1 - \frac{z}{d_1}) \tag{3-18}$$

Equation 3-17 reduces to

$$\dot{M}_0 = A_h^{'} \rho v_{z=0} \frac{d_1}{2} \tag{3-19}$$

The unknown pressure gradient can be eliminated by combining Equations 3-11 and 3-15, giving

$$-\rho u\frac{du}{dz}-\rho_w \boldsymbol{g}=k\rho\left(\frac{A_p}{A_h^{'}}\right)^2\frac{du}{dz}\frac{d^2u}{dz^2} \tag{3-20}$$

or

$$-\frac{1}{2}\frac{du^2}{dz}-\frac{\rho_w}{\rho}\boldsymbol{g}=\frac{k}{2}\left(\frac{A_p}{A_h^{'}}\right)^2\frac{d}{dz}\left(\frac{du}{dz}\right)^2 \tag{3-21}$$

Integrating this equation over the sparger hole length gives

$$-\frac{1}{2}\int_0^{d_1}\frac{du^2}{dz}dz-\int_0^{d_1}\frac{\rho_w}{\rho}\boldsymbol{g}dz=\frac{k}{2}\left(\frac{A_p}{A_h^{'}}\right)^2\int_0^{d}\frac{d}{dz}\left(\frac{du}{dz}\right)^2 dz \tag{3-22}$$

Using Equation 3-8 in the right hand side gives

$$-\frac{1}{2}\int_0^{d_1}du^2-\int_0^{d_1}\frac{\rho_w}{\rho}\boldsymbol{g}dz=\frac{k}{2}\int_0^{d}dv^2 \tag{3-23}$$

Carrying out the integration gives

$$u_{z=0}^2-\frac{2\rho_w}{\rho}\boldsymbol{g}d_1=-kv_{z=0}^2 \tag{3-24}$$

Combining this equation with Equations 3-16 and 3-19 gives

$$\frac{\dot{M}_0^2}{A_p^2\rho^2}-\frac{2\rho_w}{\rho}\boldsymbol{g}d_1=-4k\frac{\dot{M}_0^2}{d_1^2\rho^2A_h^{'2}} \tag{3-25}$$

or,

$$\frac{d_1^2}{A_p^2}-\frac{2\rho_w\rho\boldsymbol{g}d_1^3}{\dot{M}_0^2}=-\frac{4k}{A_h^{'2}} \tag{3-26}$$

If ρ is known, then the above equation can be solved for d_1.

The average steam density in the sparger can be estimated from

$$\rho=\frac{P_0+\left(d_0+d_1\right)\rho_w\boldsymbol{g}+\dfrac{2k\dot{M}_0^2}{\rho\left(A_h^{'}d_1\right)^2}}{RT} \tag{3-27}$$

or,

$$RT\rho^2-\left(d_0+d_1\right)\rho_w\boldsymbol{g}\rho-\frac{2k\dot{M}_0^2}{\left(A_h^{'}d_1\right)^2}=0 \tag{3-28}$$

Equations 3-26 and 3-28 can be solved iteratively for d_1.

If the sparger is angled θ from vertical, then the equations to be solved are:

$$\frac{d_1^2}{A_p^2} - \frac{2\rho_w \rho \boldsymbol{g} d_1^3 cos\theta}{\dot{M}_0^2} = -\frac{4k}{A_h^{'2}} \tag{3-29}$$

$$RT\rho^2 - \left(d_0 + d_1\right)\rho_w \boldsymbol{g}\rho cos\theta - \frac{2k\dot{M}_0^2}{\left(A_h^{'} d_1\right)^2} = 0 \tag{3-30}$$

Knowing the geometric parameters and steam injection rate, one can use Eq. 2-30 to estimate the lowest steam release location and calculate the maximum steam release depth *d* as,

$$d = (d_0 + d_1)\cos\theta \tag{3-31}$$

The required submergence ratio for Equations 3-4, 3-5 and 3-6 is

$$d/d_t = \frac{(d_0 + d_1)\cos\theta}{d_t} \tag{3-32}$$

With the known submergence ratio versus steam injection rate for a vertical sparger, the mixing correlation can be used to model the steam release to the pool from a RCIC or HPSI turbine exhaust. Similar to previous case studies, in Case Series III, first the 3D GOTHIC pool surface temperature results were obtained for each steam flow rate. Using pool surface temperatures as control variables, required pump flows were calculated for all simplified GOTHIC models. As shown in Figure 3-39, the general trend of the pump flows started with a maximum flow rate and then decayed exponentially over the time.

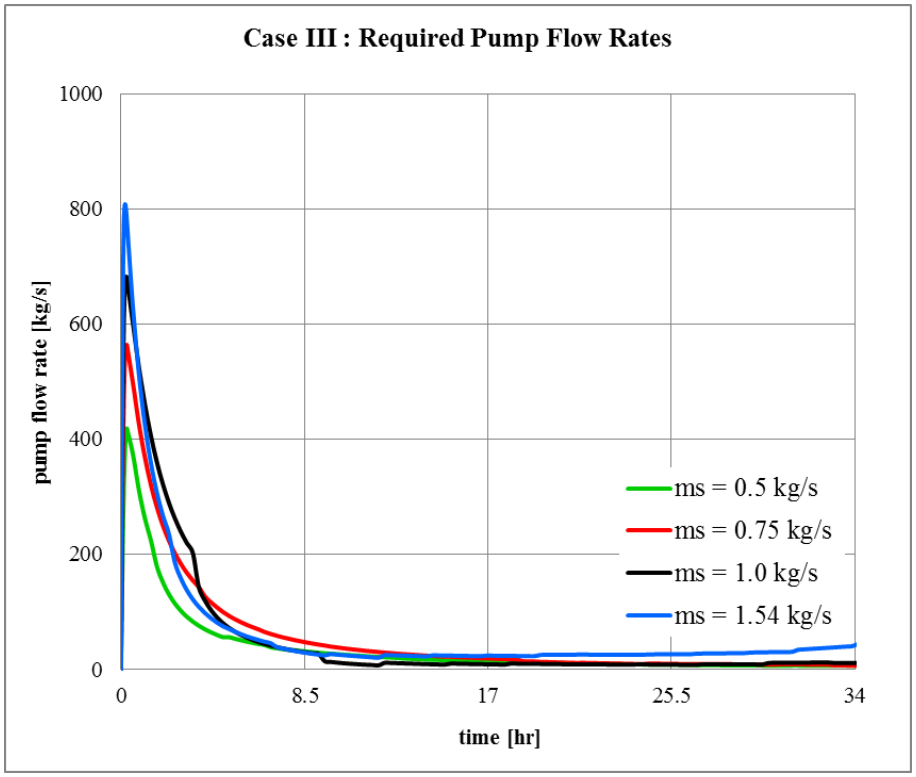

Figure 3-39
CASE III GOTHIC Required Pump Flow Rate Predictions

The mixing induced by the condensed steam is due primarily to the buoyancy force arising from the difference in the condensed liquid density and the pool bulk density. The density difference gradually decreases as the pool temperature increases over the time. Thus, it is expected that the temperature difference between the bulk pool and condensed steam ($\Delta T = T_s - T_l$) as well as the variations in thermal expansion of the pool water (ε_t) over the time are important parameters in the mixing rate.

Based on Figure 3-39 a power function form is assumed,

$$\dot{m}_p = \dot{m}_{p-\max}(d, \dot{m}_s / m_{pool})\lambda(\Delta T \varepsilon_t - \beta)^n \qquad (3\text{-}33)$$

The $\dot{m}_{p\max}(d, \dot{m}_s / m_{pool})$ function was previously defined in Equations 3- 4, 3-5 and 3-6. Based on curve fitting and trial-error methods using the GOTHIC models, the best fit λ, β and n constants are

$\lambda = 2\text{x}10^{-6}$

$\beta = 0.0215$

$n = -1.75$

Substituting these constants back into Equation 3-33 and combining it with 3-4, 3-5 and 3-6 gives the comprehensive form of the required pump flow rate correlations as,

$$\frac{\dot{m}_p}{m_{pool}} = 3.27\times10^{4}\left(\frac{\dot{m}_s}{m_{pool}}\right)\left(d/d_t\right)^{1.25}\,2\times10^{-6}\left(\left(T_s-T_l\right)\varepsilon_t-0.0215\right)^{-1.75} \tag{3-34}$$

for $0 \le \dot{m}_s \Big/ m_{pool} < 1.6\times10^{-8}\ s^{-1}$

$$\frac{\dot{m}_p}{m_{pool}} = \left(3.97\times10^{3}\left(\frac{\dot{m}_s}{m_{pool}}\right)+4.61\times10^{-4}\right)\left(d/d_t\right)^{1.25}\,2\times10^{-6}\left(\left(T_s-T_l\right)\varepsilon_t-0.0215\right)^{-1.75} \tag{3-35}$$

for $1.6\times10^{-8} \le \dot{m}_s \Big/ m_{pool} < 6\times10^{-8}\ s^{-1}$

$$\frac{\dot{m}_p}{m_{pool}} = \left(2.38\times10^{3}\left(\frac{\dot{m}_s}{m_{pool}}\right)+5.55\times10^{-4}\right)\left(d/d_t\right)^{1.25}\,2\times10^{-6}\left(\left(T_s-T_l\right)\varepsilon_t-0.0215\right)^{-1.75} \tag{3-36}$$

for $6\times10^{-8} \le \dot{m}_s \Big/ m_{pool} < 1.2\times10^{-6}\ s^{-1}$

where,

$\dot{m}_p$	Pump Flow Rate, [kg/s]
$\dot{m}_s$	Steam Flow Rate, [kg/s]
m_{pool}	Pool Water Mass, [kg]
T_s	Saturation Temperature of Steam [°C]
T_l	Bulk Temperature of Pool [°C]
ε_t	Thermal Expansion Coefficient of Water [1/°C]
d	Steam Injection Depth [m]
d_t	Total Pool Depth [m]

Using Equations 3-34 to 3-36, pump flow rates are recalculated and results are compared with GOTHIC the flow rates required to match the GOTHIC 3D predictions (Figure 3-39) and presented individually in Figure 3-40(a) – (b) and Figure 3-41(a) - (b).

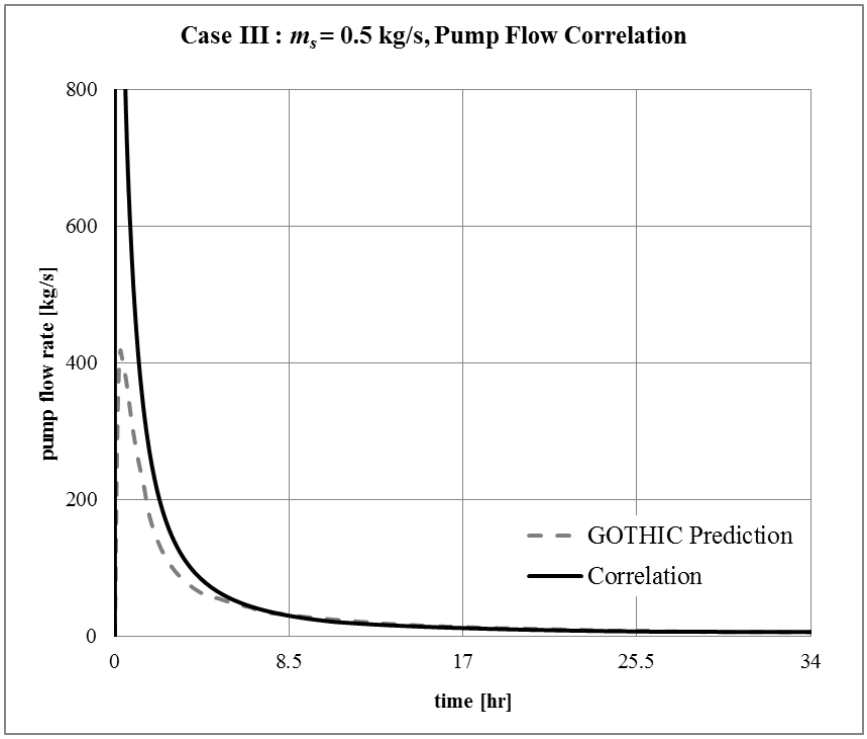

(a) m_s = 0.5 kg/s

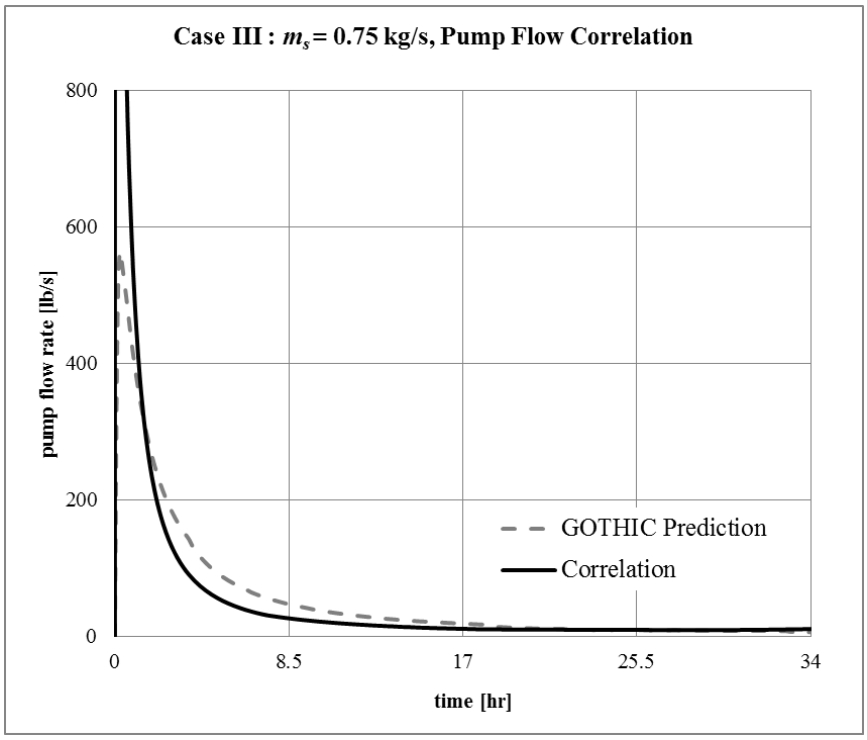

(b) m_s = 0.75 kg/s

Figure 3-40
CASE III GOTHIC Required Pump Flow Rate Predictions (0.5-0.75kg/s)

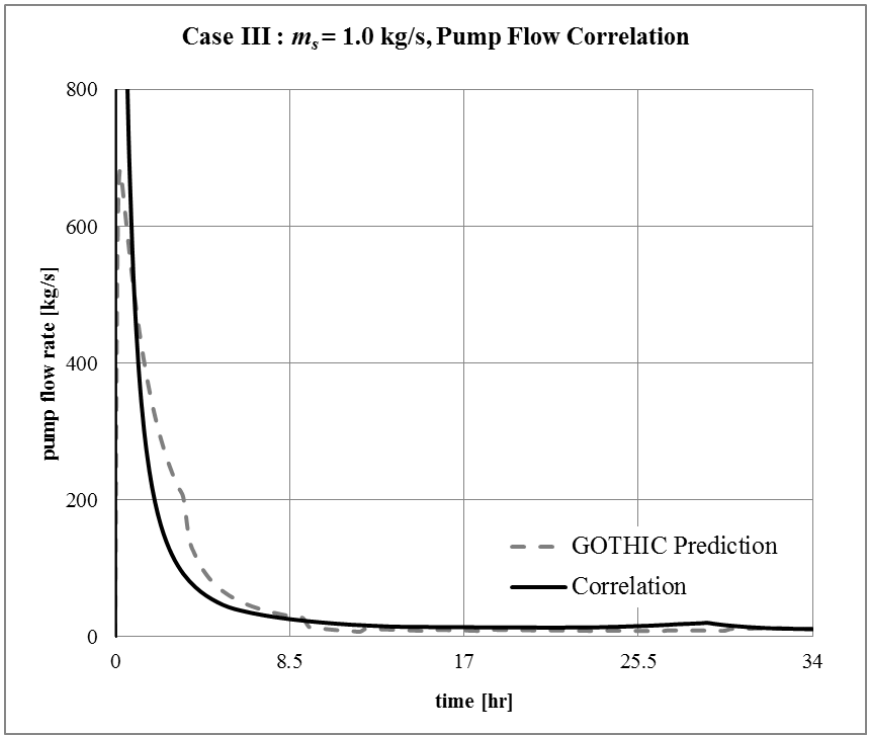

(a) m_s = 1.0 kg/s

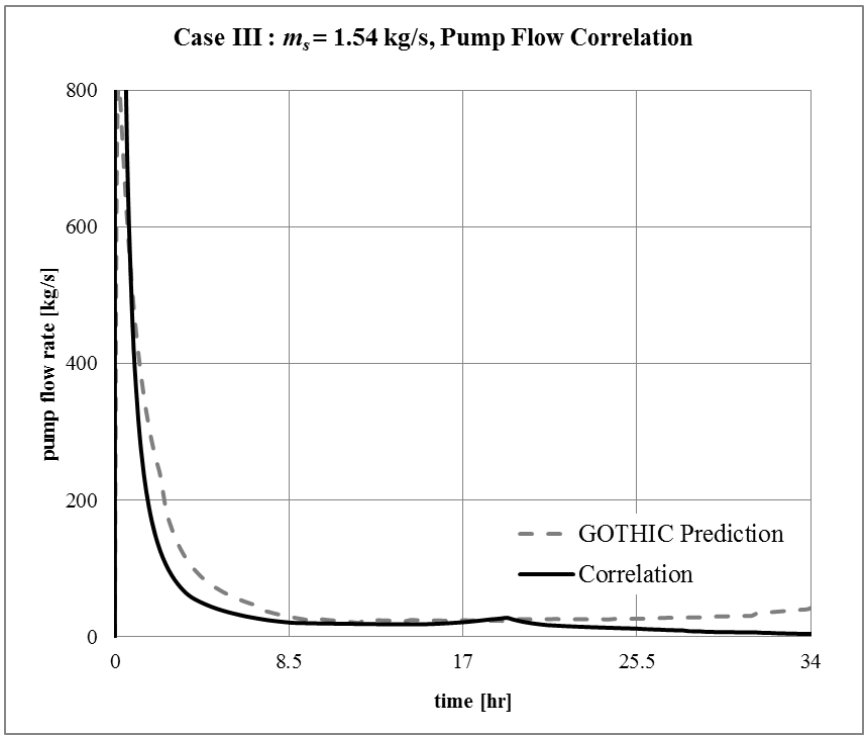

(b) m_s = 1.54 kg/s

Figure 3-41
CASE III GOTHIC Required Pump Flow Rate Predictions (1.0 – 1.54 kg/s)

The 1.54 kg/s steam injection case results were further studied since it provides the largest variation in pool temperature compared to other smaller steam injection scenarios. As shown in Figure 3-43 and Figure 3-43, even though the temperature difference $\Delta T = (T_s - T_l)$ decreases throughout the transient, the thermal expansion term ε_t increases with the increase in pool temperature. From Figure 3-44, it is concluded that during the early stage of the transient, when the pool temperature is cooler, ε_t has a more dominant role in the $(T_s - T_l)\varepsilon_t$ factor. As the pool temperature approaches the boiling point, ε_t approaches its maximum value. However, $(T_s - T_l)$ continues to decrease and controls the $(T_s - T_l)\varepsilon_t$ factor.

It should be noted that for the given correlation (Eqs. 3-21, 3-22 and 3-23) it is necessary to keep $(T_s - T_l)\varepsilon_t > 0.0215$ to avoid unbounded terms. Variations in the $(T_s - T_l)\varepsilon_t$ term with respect to temperature difference (ΔT) are compared against the limiting value (0.0215)in Figure 3-45. The factor reaches the 0.0215 limit when ΔT is around 65.7 °F.

As the $(T_s - T_l)\varepsilon_t$ approaches 0.0215, $\left((T_s - T_l)\varepsilon_t - 0.0215\right)^{-1.75}$ goes to infinity resulting in an excessive pump flow and over mixing of the suppression pool. Thus, a temperature difference limit is needed to avoid unrealistic pump flow. After testing the correlation at different ΔT limits, the most reasonable pump flow rates were obtained when ΔT>90 °F; 90 °F is recommended as a lower limit for the temperature difference ($(T_s - T_l)$) in Equations 3-34 to 3-36.

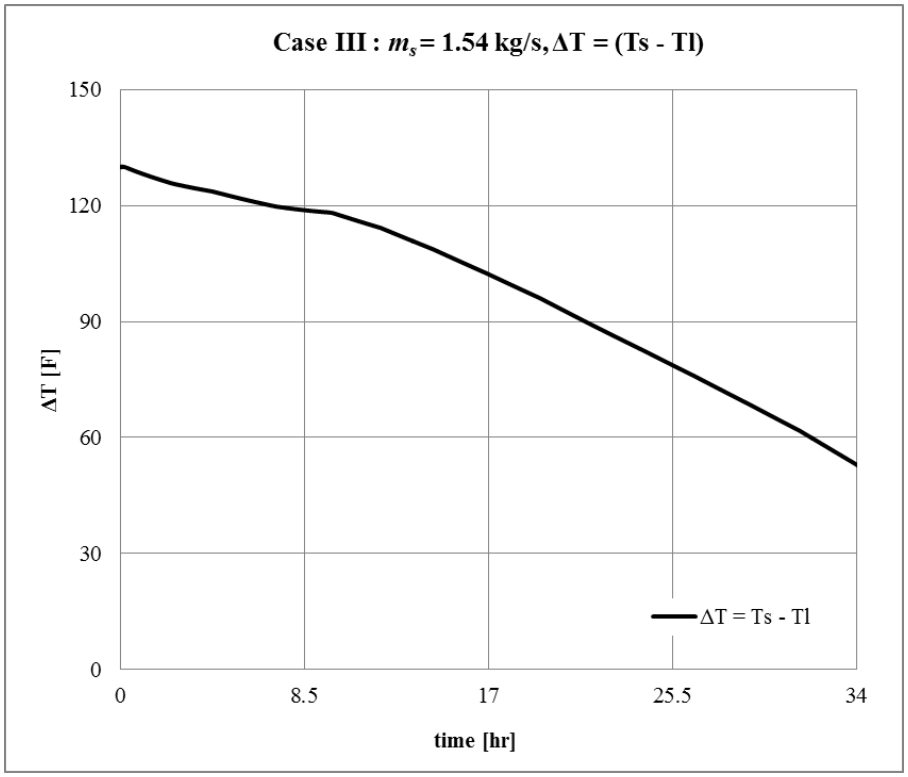

Figure 3-42
CASE III GOTHIC Temperature Difference Predictions, $\Delta T = T_s - T_l$

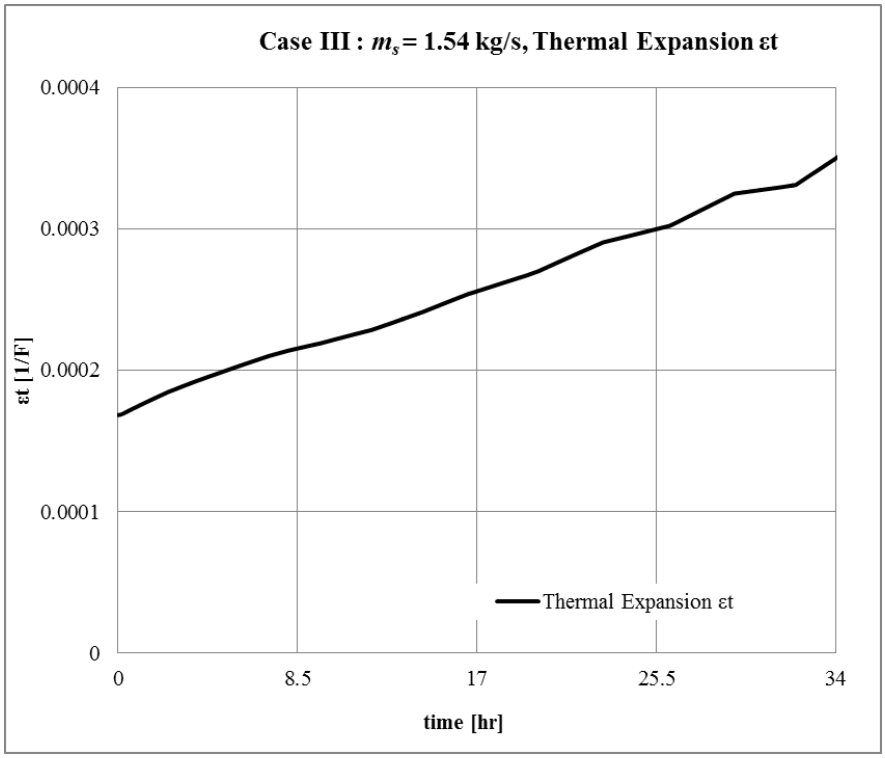

Figure 3-43
CASE III GOTHIC Thermal Expansion Predictions, ε_t

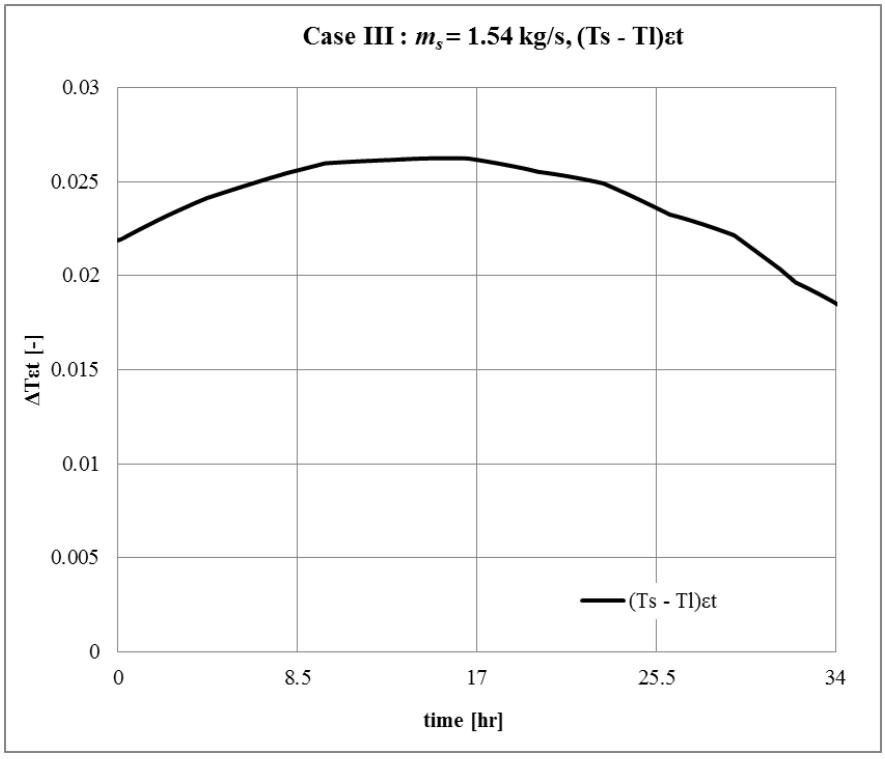

Figure 3-44
CASE III GOTHIC (T_s - T_l)ε_t Predictions

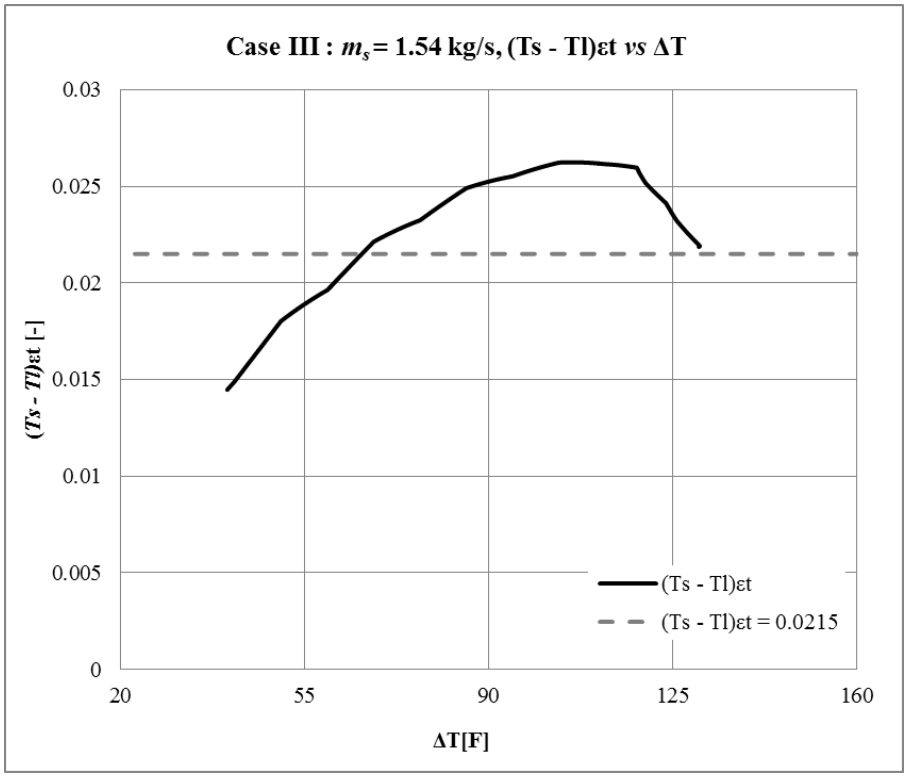

Figure 3-45
CASE III (T_s - T_l)ε_t vs ΔT = T_s - T_l Comparison

Finally, Equations 3-34, 3-35 and 3-36 are set as control variables in the simplified GOTHIC models and used to control the required pump flow rate to circulate the liquid inside suppression pool. In Figure 3-46(a-b) and Figure 3-47(a-b), the suppression pool surface temperature results from the lumped model are compared with previously obtained 3D GOTHIC predictions. At smaller steam injection rates, the mixing flow correlation used in the lumped GOTHIC model gives good agreement with the detailed 3D GOTHIC model calculations. When the steam injection rate is increased, and the pool surface temperature gets closer to its boiling point, discrepancies between the 3D and lumped modeling prediction up to ±5 °C were observed.

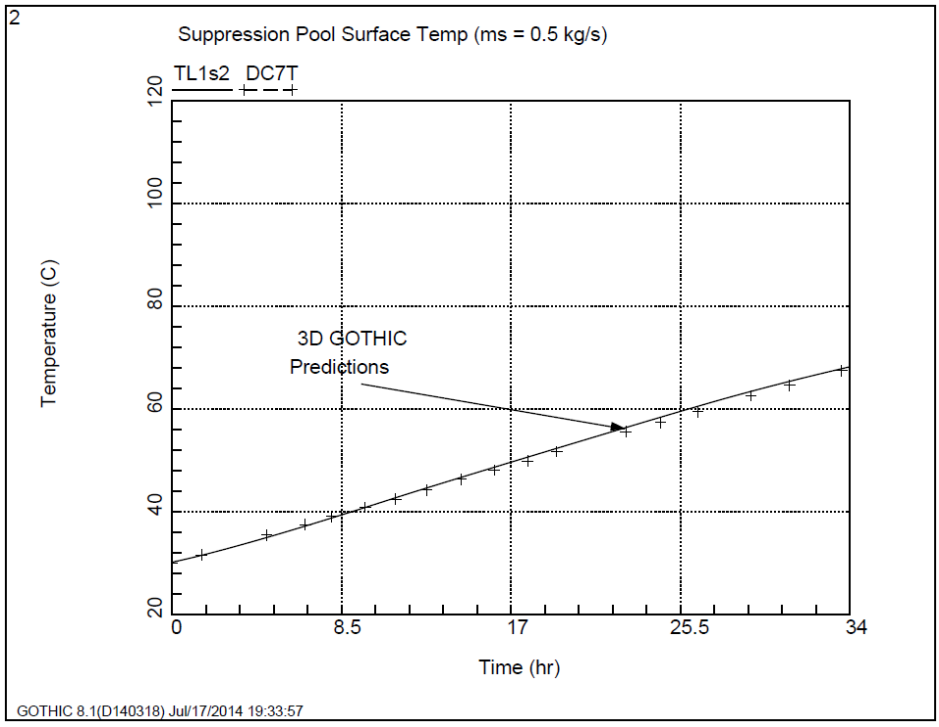

(a) $m_s = 0.5$ kg/s

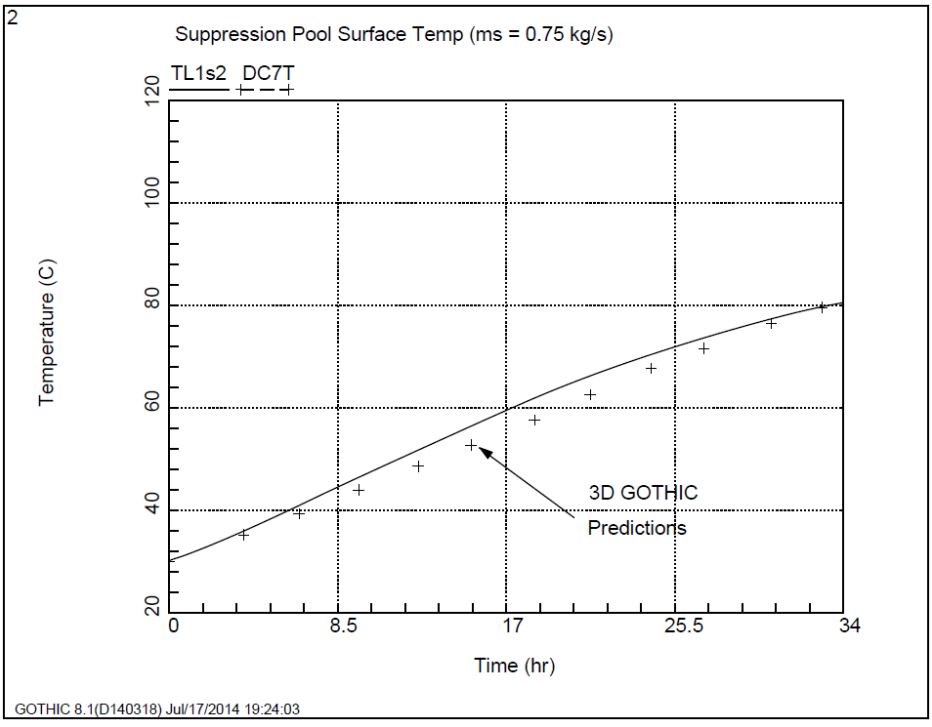

(b) $m_s = 0.75$ kg/s

Figure 3-46
CASE III Comparison of GOTHIC Lumped and 3D Model Results (0.5-0.75 kg/s)

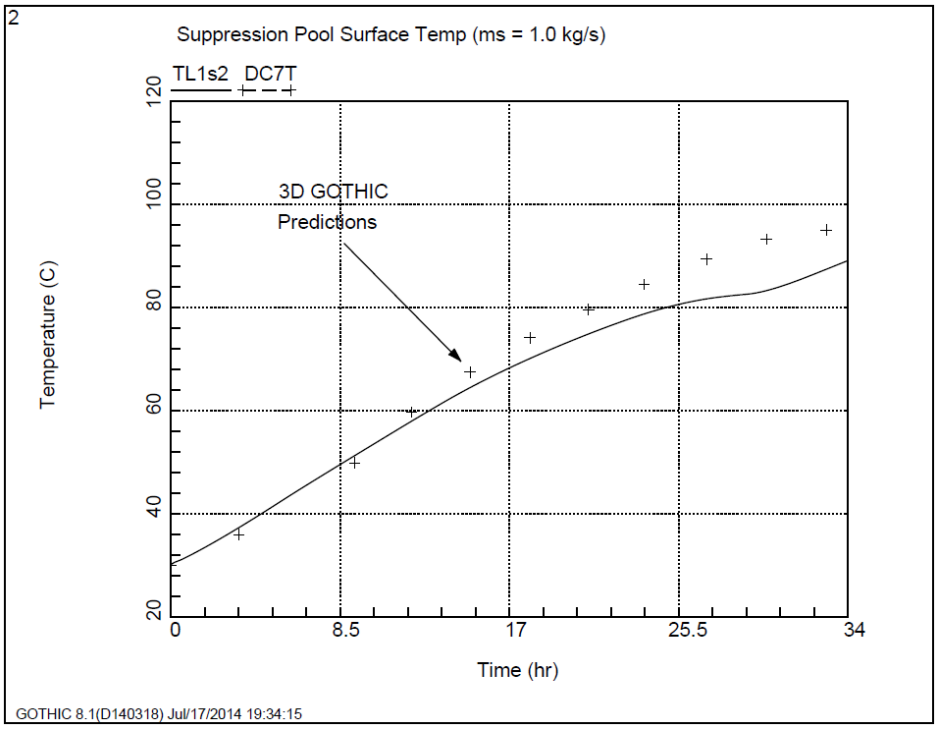

(a) m_s = 1.0 kg/s

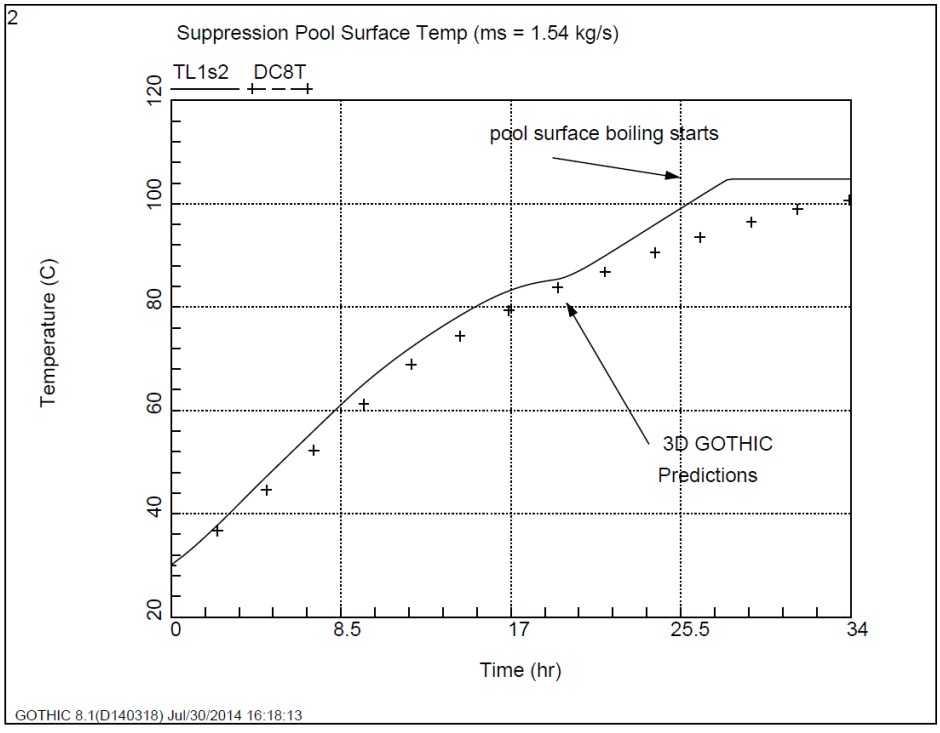

(b) m_s = 1.54 kg/s

Figure 3-47
CASE III Comparison of GOTHIC Lumped and 3D Model Results (1.0-1.54 kg/s)

In order to complete the correlation matrix, two additional cases were studied where the steam was injected near the bottom of the suppression pool, representative of an SRV release. Two different steam injection rates were used; 0.5kg/s and 1.54kg/s. In both cases, the 3D GOTHIC model results showed that the entire pool is nearly well mixed and the pool bottom and surface temperatures remain almost equivalent throughout the transient (Figure 3-48(a)-(b)).

The lumped model suppression pool surface temperature results are compared with the 3D GOTHIC predictions in Figure 3-49(a) (b). For these cases, the simplified GOTHIC model with pump flow correlation results agree well with the detailed 3D GOTHIC model predictions.

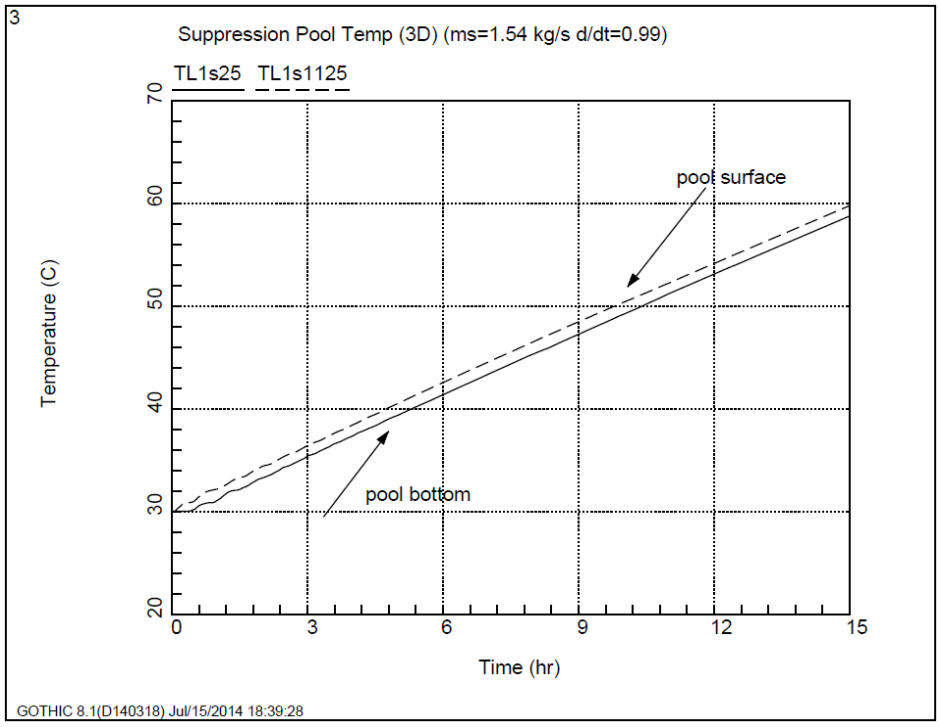

(a) $m_s = 0.5$ kg/s

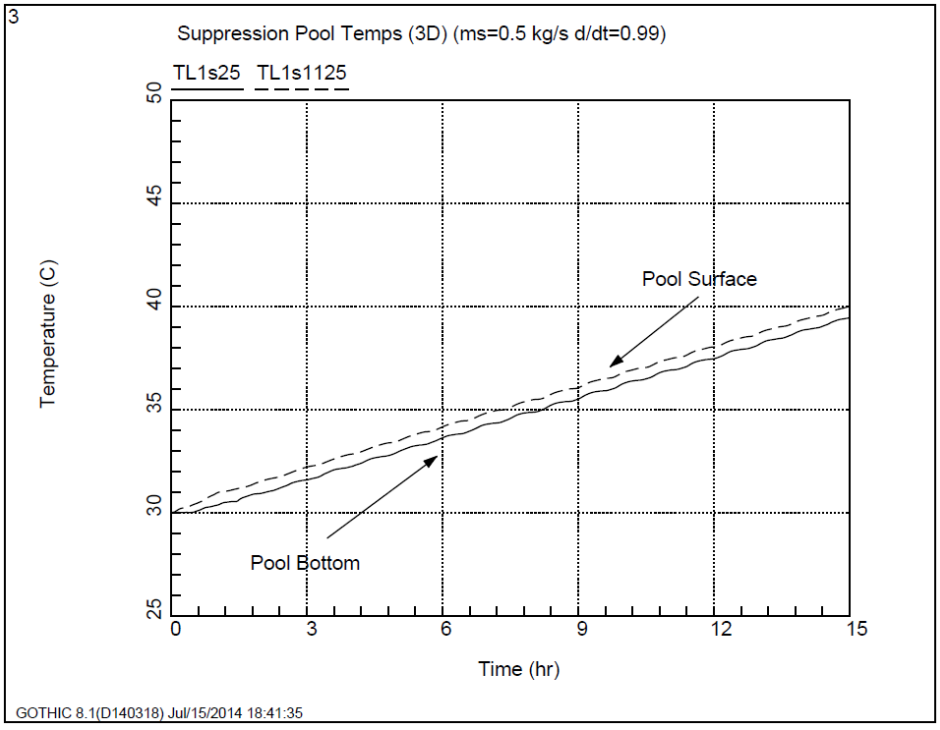

(b) $m_s = 1.54$ kg/s

Figure 3-48
3D GOTHIC Pool Bottom and Surface Temperature Predictions

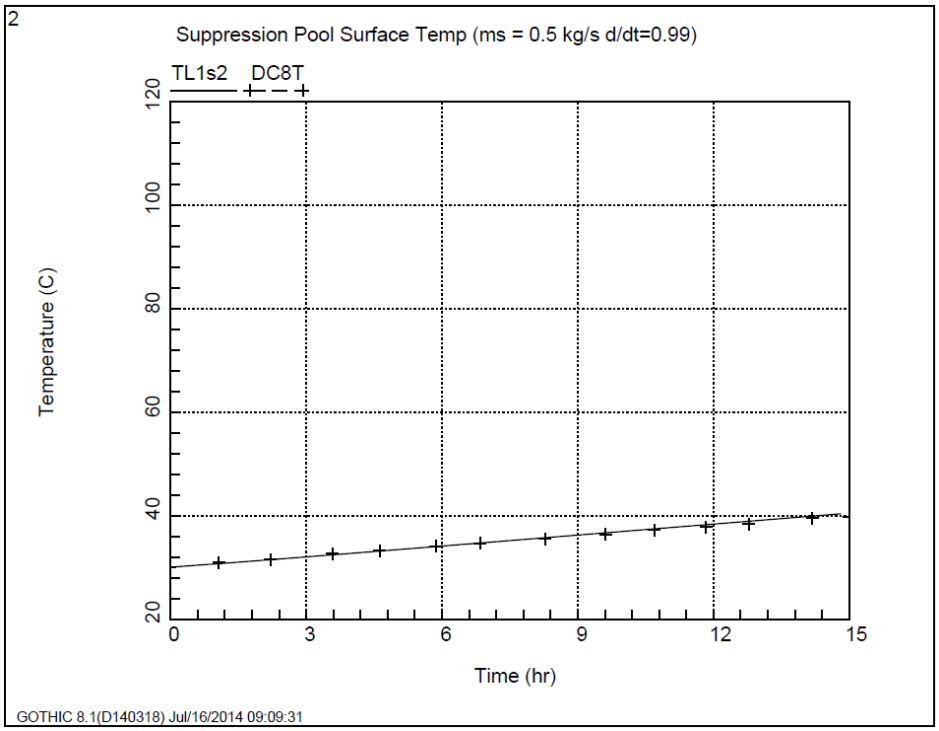

(a) m_s = 0.5 kg/s

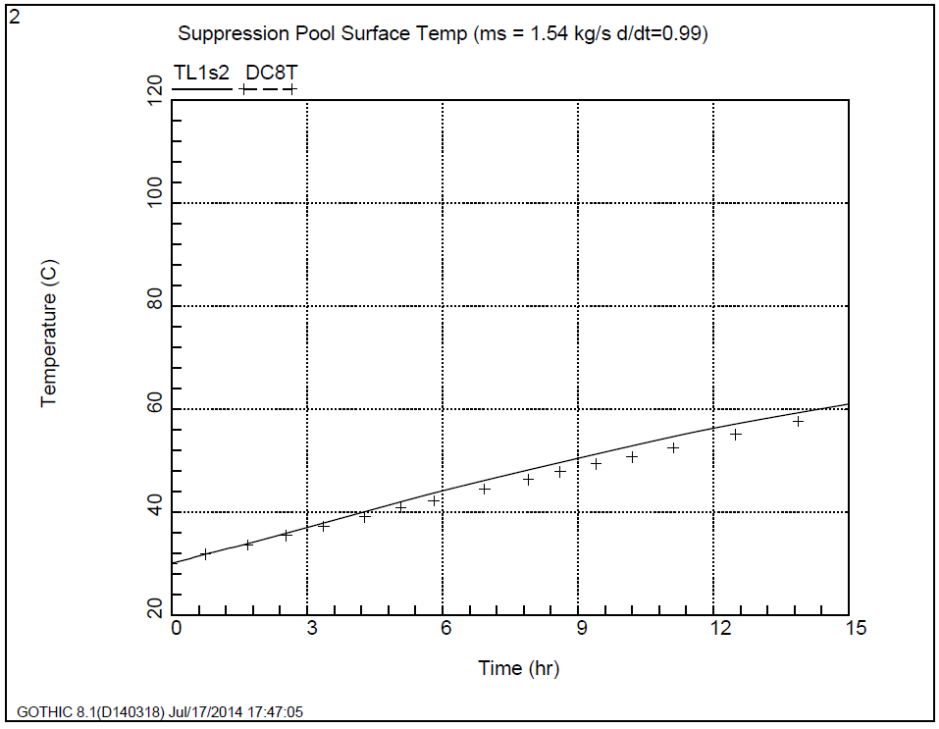

(b) m_s = 1.54 kg/s

Figure 3-49
GOTHIC Surface Temperature Predictions

4
1F1 REACTOR BUILDING PERFORMANCE

4.1 Introduction and Background

Following the tsunami, combustible gas build up in the reactor buildings of 1F1, 1F3, and 1F4 led to significant explosions destroying the fifth floor on each of these buildings. Leaks have been postulated to have occurred along the drywell dome flange. In 1F4 it is thought that the venting from the 1F3 wetwell traveled through the common stack and back into HVAC system or through the Standby Gas Treatment System (SGTS) and into the HVAC system. Post-accident inspection of the 1F4 reactor building revealed extensive damage to the HVAC exhaust ducts. Similarly, in 1F1 a redistribution of combustible gas from the wetwell through the wetwell vent line and back through its own HVAC exhaust system is considered. Additionally, a leak through the flange in the top of the drywell is postulated to increase the gas concentrations in the fifth floor of 1F1.

A multidimensional model of the reactor building was constructed to investigate the mixing and buildup of gasses in the reactor building for several different scenarios. The model contains internal compartments, openings in walls and floors, the exhaust ventilation system, heat transfer and condensation on the walls and structures, and the wetwell vent system including the stack to atmosphere. Three scenarios were run to analyze various potential combustible gas and steam flow paths and the effect on the gas and steam concentrations in the reactor building fifth floor. Hydrogen, mainly from the high temperature oxidation of the zirconium cladding, and carbon monoxide from interaction of concrete and the molten core material are the primary combustible gases considered in this analysis.

The flammability limits of hydrogen-steam-air mixtures can be seen in Figure 4-1 (NRC CR-3486, 1986). The lower burn limit is approximately 4% hydrogen by volume provided there is enough air. Similarly, a mixture containing more than 12.5% carbon monoxide by volume will burn again provided there is enough air (NEA, 2000). The transition to detonation for a hydrogen air mixture is normally at around 18% hydrogen by volume. The addition of carbon monoxide into a hydrogen-air-steam mixture will add to the usable fuel for both flammability and detonation.

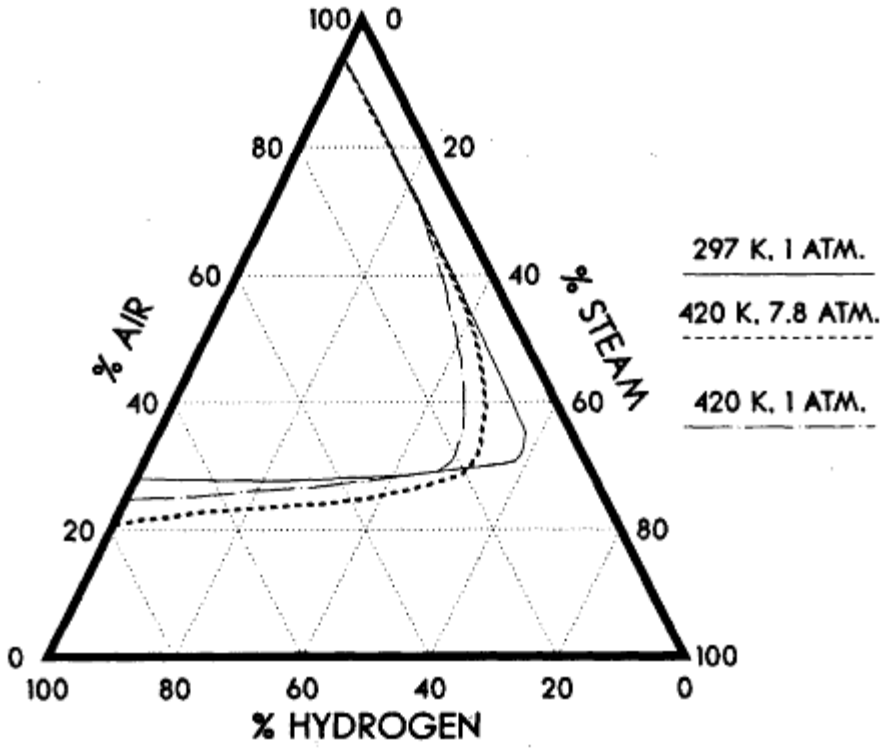

Figure 4-1
Flammability Limits of Hydrogen:Air:Steam Mixtures

The detonation limits of carbon monoxide-hydrogen-air-steam mixtures can be seen in Figure 4-2 (NEA, 2000). The detonation cell width determines many detonation characteristics and is used to determine the composition limits of detonability. As the mixture becomes more reactive the detonation cell width becomes smaller. A mixture of 18% hydrogen in air has a detonation cell width of 5 cm. With 5% CO in the mixture, the same detonation cell width is reached at 16%. With 10% CO the equivalent detonation mixture is about 11% hydrogen.

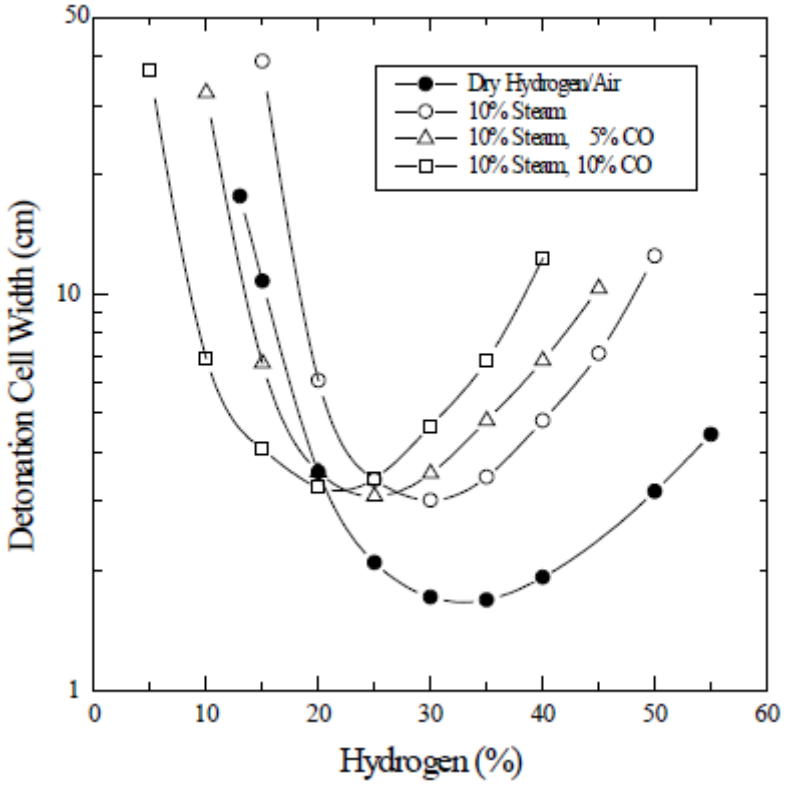

Figure 4-2
Flammability Limits of Carbon Monoxide: Hydrogen:Air:Steam Mixtures

The results for the gas concentration in the Reactor Building strongly depend on results from the MAAP analysis for the gas release and gas mixture composition in the drywell and wetwell. Results and conclusions presented here could change substantially as the simulation of the primary and containment systems are refined.

4.1.1 1F1 Explosion

Footage from a camera set up to monitor the reactor buildings after the Japanese government imposed a 10km evacuation zone captured the explosion in 1F1. Video stills can be taken by stepping through the footage frame by frame. The video was played back at 20 frames per second. Therefore, each frame in the following figures represents a 0.05 second increment in time. The initial frame in Figure 4-3 shows the 1F1 reactor building to the right of the 1F1 and 1F2 the common exhaust stack at the center. The next frame in Figure 4-4 shows what appears to be one of the blowout panels with a small plume of smoke coming from it. Figure 4-5 shows an explosion with visible flames coming out of the fifth floor west facing wall. The amount of smoke grows from the previous frame. Post-accident aerial photographs show what appears to be the remains of the roof slumped onto the fifth floor. Structural beams that had supported the roof are bent inwards indicating a roof collapse. Figure 4-6 shows the possible instant of the roof collapse.

A pressure wave appears to be rising from the building as seen in Figure 4-7. Using the common stack to measure the distance the wave travels and the elapsed time between frames the wave velocity can be estimated at 410 m/s, faster than the speed of sound (340m/s), and is therefore

likely a pressure wave from the explosion and subsequent collapse of the roof. Eventually, the pressure wave slows and dissipates (Figure 4-8) with a peak height several meters below the top of the exhaust stack. Unlike the explosion in 1F3, there does not appear to be any trailing debris behind the pressure wave. The explosion was primarily horizontal, knocking out all of the blowout panels on the fifth floor and subsequently collapsing the roof.

GOTHIC includes modeling capabilities for hydrogen deflagration but the capability does not extend to the transition to detonation. Also, it does not currently include burn rate models for CO or CO/hydrogen mixtures. However, the predicted gas and steam concentrations can be used to evaluate the potential for burn and detonation.

Figure 4-3
1F1 Prior to Explosion

Figure 4-4
1F1 Paneling Blows Off

Figure 4-5
1F1 Hydrogen Explosion

Figure 4-6
1F1 Possible Collapse of Roof

Figure 4-7
1F1 Pressure Wave

Figure 4-8
1F1 Pressure Wave Dissipates

4.2 Inputs

Table 4-1: Reference Drawings lists the references drawings used to construct this model. The input summary below makes reference to this table.

1. The reactor building room dimensions, wall thicknesses and other physical data are taken from the structural drawings 14, 15, 16, and 17.
2. Reactor building HVAC return ducting dimensions are taken from drawings 1, 2, 3, 4, 5, and 6.
3. Reactor building SGTS piping dimensions are taken from drawings 7 and 8.
4. Reactor building wetwell vent line dimensions are taken from drawings 6, 9, 10, 11, 12, and 13.
5. The 1F1 exhaust stack dimensions are taken from drawing 8.
6. The status of valves during loss of offsite power is taken from (EPRI, 2013).
7. Wetwell and drywell release rates and release gas compositions are taken from (EPRI, 2013).
8. Atmospheric conditions are taken from weather data for March 11, 2011.

4.3 Assumptions

1. It is assumed that rooms with closed doors are completely sealed from the building and do not introduce additional flow paths into the model.
2. Building leakage is assumed to be large enough to maintain a drop in building pressure of 0.0623 kPa when exhausting through the SGTS.
3. It is assumed that the dry well leak occurs at a single spot on the fifth floor rather than distributed along the drywell flange.
4. It is assumed that the reactor building roofs have a similar composure to other reactor building roofs and are composed of several inches of insulation, 2-3 inches of gypsum board, and a layer of tar.

Table 4-1
Reference Drawings

REF	Drawing I.D.	Description
1	11F-510-001	HVAC FL OP -2060
2	11F-510-002	HVAC FL OP 10200
3	11F-510-003	HVAC FL OP 18700 & 25900
4	11F-510-004	HVAC FL OP 32300 & 39920
5	11N-510-010	HVAC FL OP 18700
6	10Q-037-601	1F1&2 Common Stack
7	4b-SGTS-5A,B 14B-SGTS-5A,B~8A,B 14B-SGTS-9,10,81	SGTS & HVAC to Stack
8		Exhaust Stack Drawing
9	5514-H36 Rev. 1	Wetwell Vent Line
10	T-1199-X-901	AC SGTS FL OP 18700
11	T-1199-X-902	AC SGTS FL OP 10200
12	T-1199-X-904	SGTS FL OP 10000
13	5501-173 Rev. 1	Wetwell Vent Line
14	G-192414	General Arrangement Reactor Building Op. -1230 & Op. 10200 Floor
15	G-192415	General Arrangement Reactor Building Op. 18700 & Op. 25900 Floor
16	G-192416	General Arrangement Reactor Building Op. 31000 & Op. 38900 Floor
17	G-192417	General Arrangement Reactor Building Sections

4.4 GOTHIC Model

The overall noding for the reactor building and other modeled systems is shown in Figure 4-17. This diagram shows the major volumes modeled and the connecting flow paths representing doorways, hatches and other openings as seen in the building layouts in Figure 4-9 and Figure 4-10.

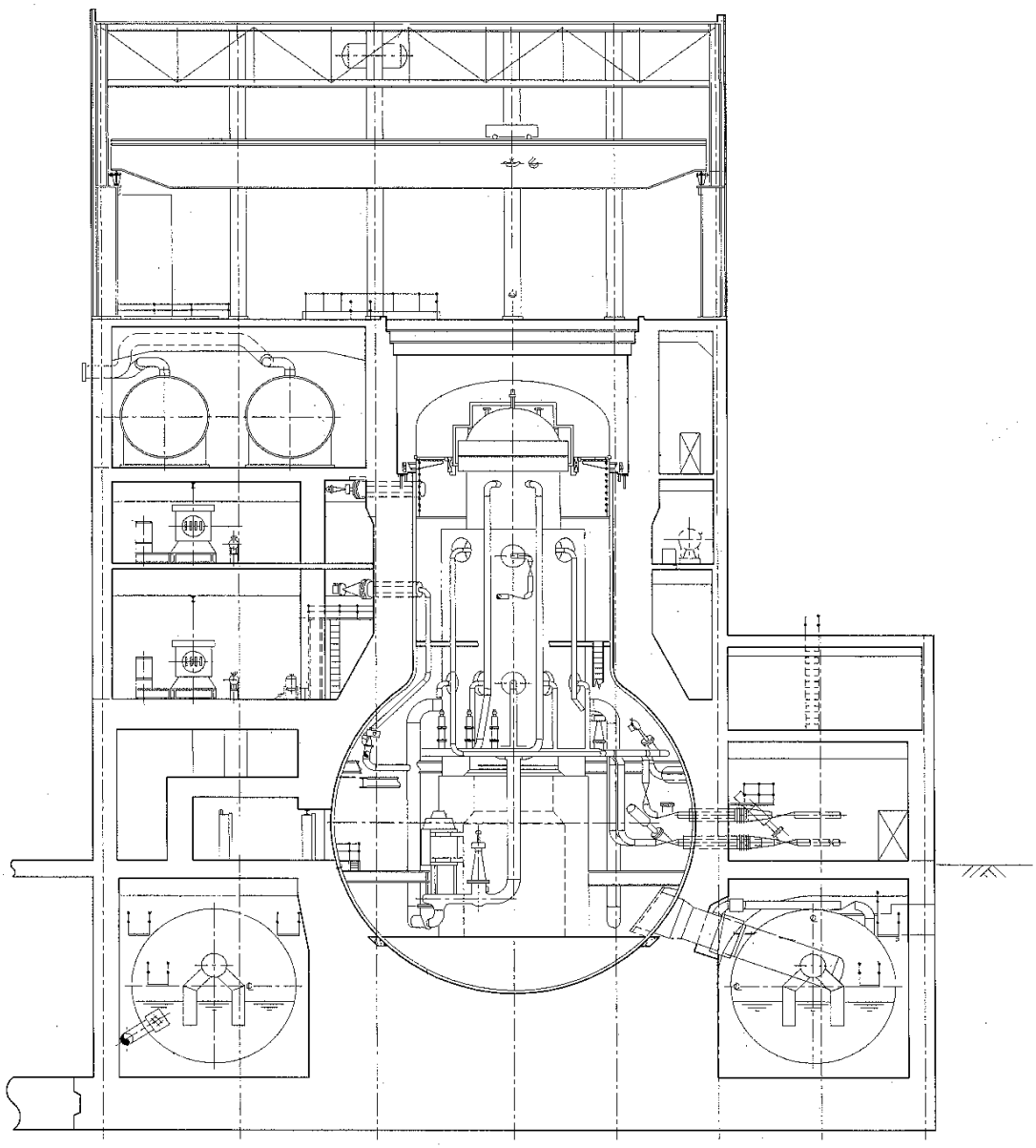

Figure 4-9
1F1 Looking North

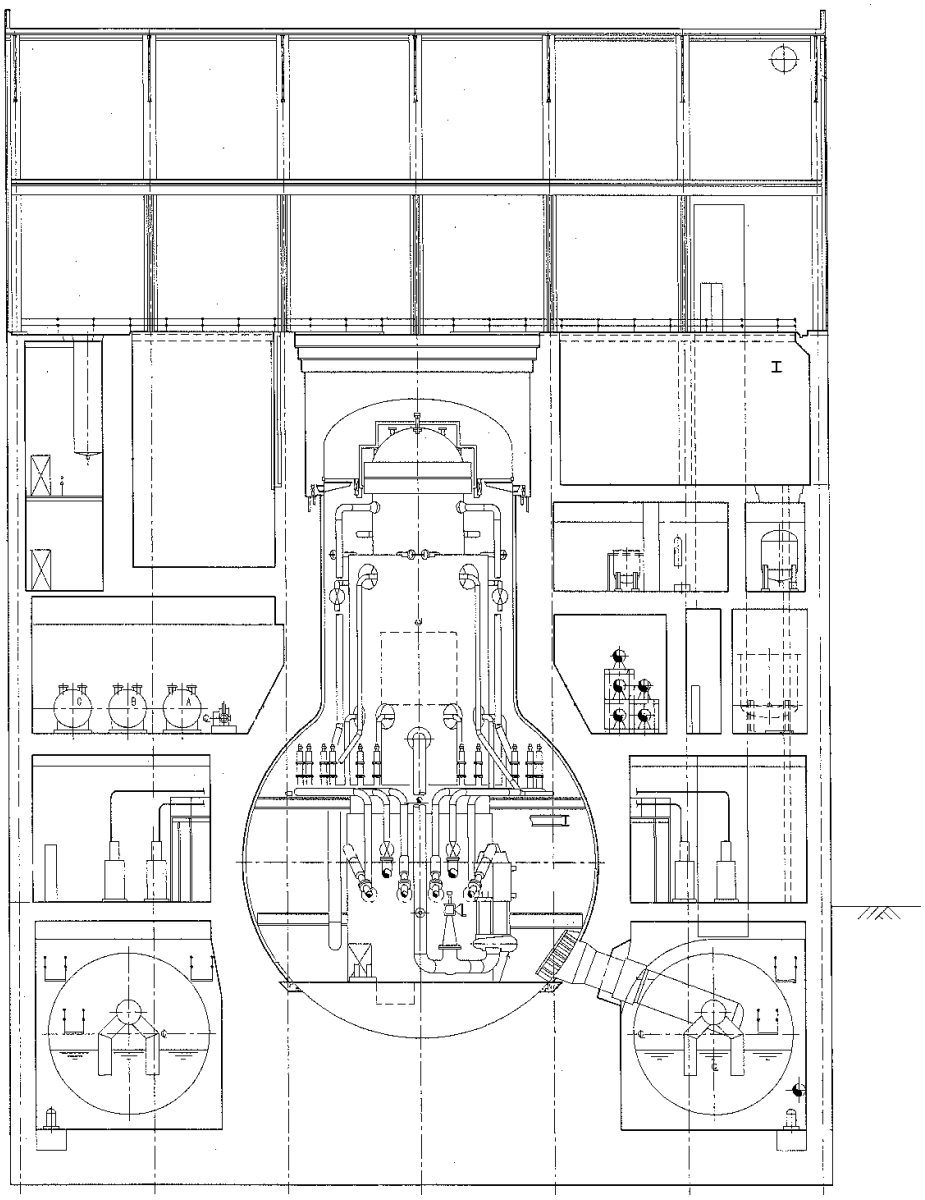

Figure 4-10
1F1 Looking West

A single subdivided volume (Volume 1s) represents the reactor building with blockages placed in lieu of closed rooms and can be seen in Figures 4-11 through 4-16. The door scheduling was confirmed through the assistance of TEPCO personnel to ensure all potential flow paths are modeled.

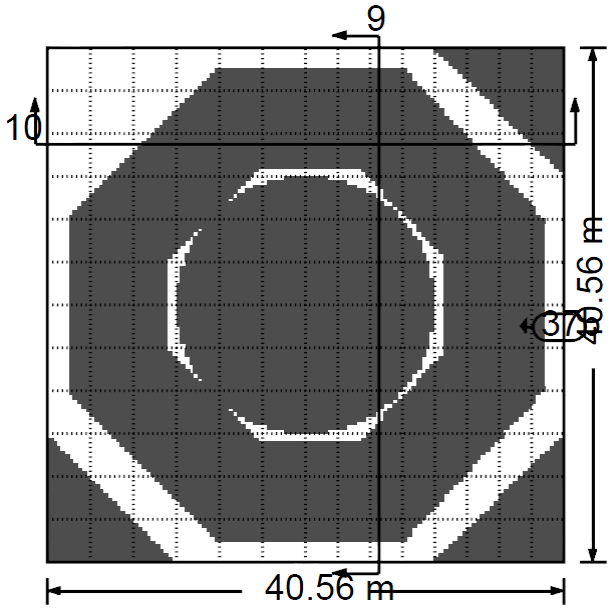

Figure 4-11
Basement Subdivisions and Blockages

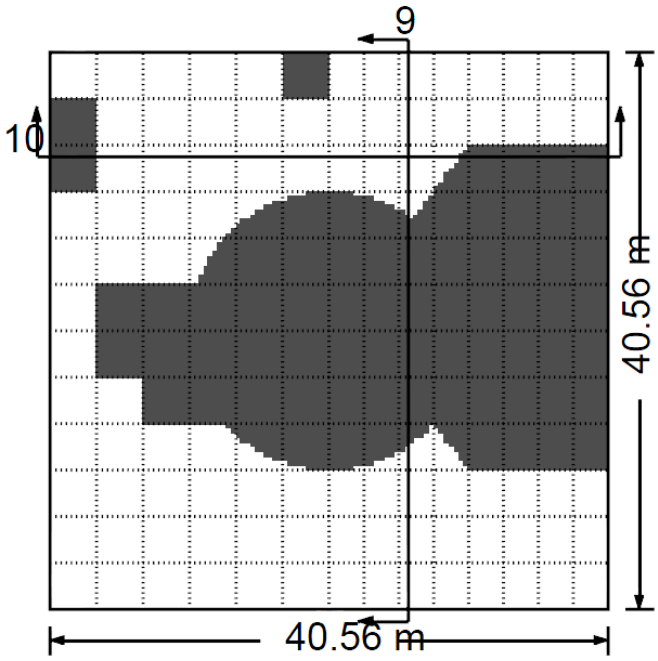

Figure 4-12
First Floor Subdivisions and Blockages

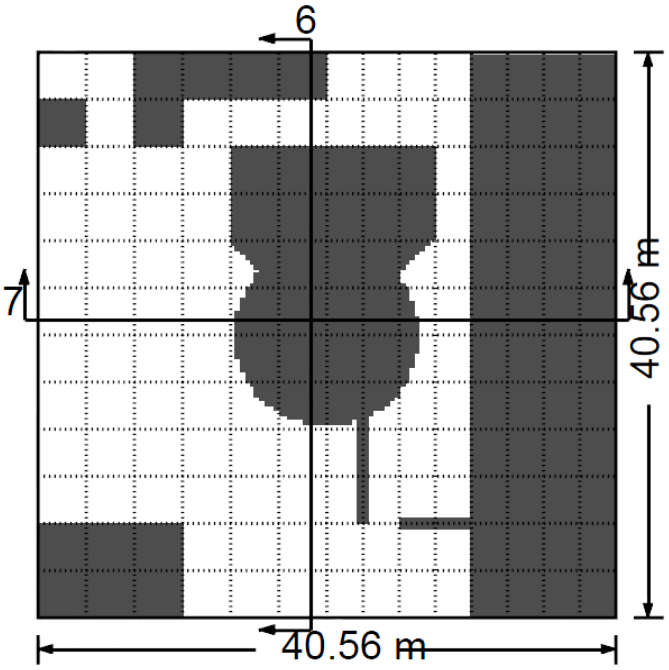

Figure 4-13
Second Floor Subdivisions and Blockages

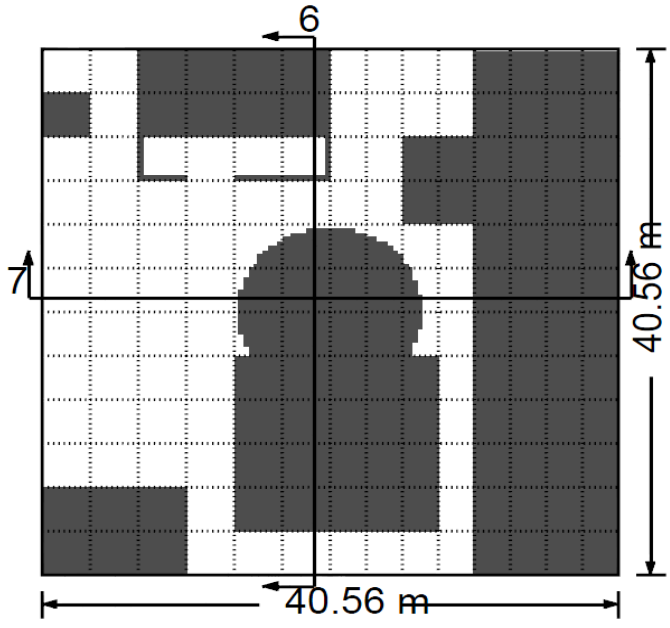

Figure 4-14
Third Floor Subdivisions and Blockages

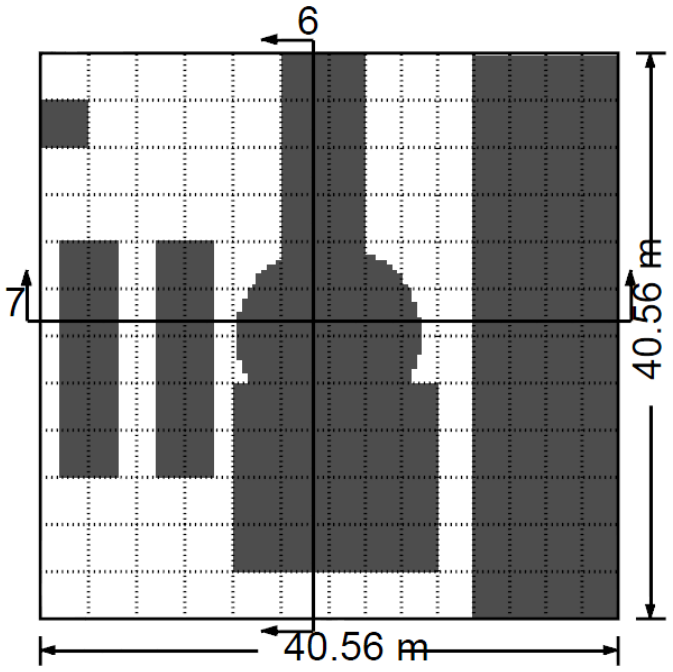

Figure 4-15
Fourth Floor Subdivisions and Blockages

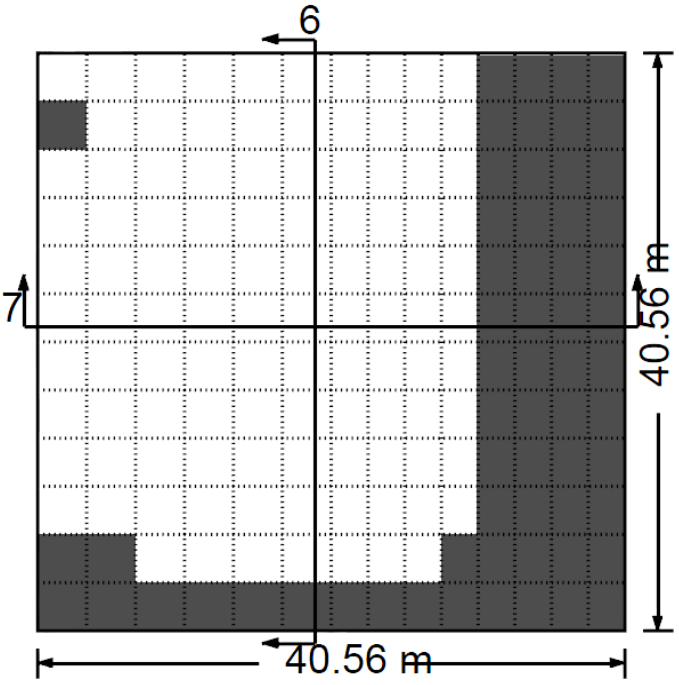

Figure 4-16
Fifth Floor Subdivisions and Blockages

Volume 2 is the elevator shaft with connections to each floor of the reactor building.

Volume 3 is a vertically subdivided volume representing the exhaust stack. The vertical subdivisions in this volume line up with the floors in the reactor building.

Volume 4 is the surrounding atmosphere and Volume 5 represents the SGTS.

Volumes 6 through 18 are various HVAC headers to which the exhaust ducts are connected into the reactor building.

Volumes 19, 22, and 23 are subdivided volumes representing the wetwell vent line. Volumes 21 and 24 are subdivided volumes representing the HVAC exhaust. These volumes are subdivided to allow tracking of the pressure wave when the wetwell pressure relief valve is opened.

Volume 20 is the suppression pool and has conditions equivalent to the data from Input 7. The volume includes the wetwell pool in order to account for flashing and the water entrainment by the flow from the wetwell exhaust duct.

Boundary Conditions 3P and 4F maintain atmospheric conditions. Boundary Condition 1F is the leak from the Drywell flange from Input 7. Boundary Condition 2P provides the suppression pool pressure and temperature conditions.

There are 6 valves in the model. Valve 1 is located on a line that connects the SGTS to the wetwell vent line. Valve 2 isolates the wetwell vent line from the exhaust stack. Valve 3 isolates the second floor HVAC header from the SGTS. Valve 4 isolates the SGTS from the exhaust stack. Valve 5 isolates the second floor HVAC header from the exhaust stack. Valve 6 isolates the wetwell from the wetwell vent line.

Flow path 85 represents the building leakage to the surrounding atmosphere. It was sized so that the SGTS would be able to reduce the building pressure to -1/4” water within 10 minutes as normally required for operating BWR plants. The flow path is positioned on the first floor since most of the building exterior openings are located here.

The various scenarios analyzed all use the same general model but trip different valves open to examine various paths the released hydrogen could have taken.

Leak conditions, including gas composition, are taken from MAAP results. Figure 4-18 is a flow path schematic showing the HVAC, SGTS, and wetwell connections.

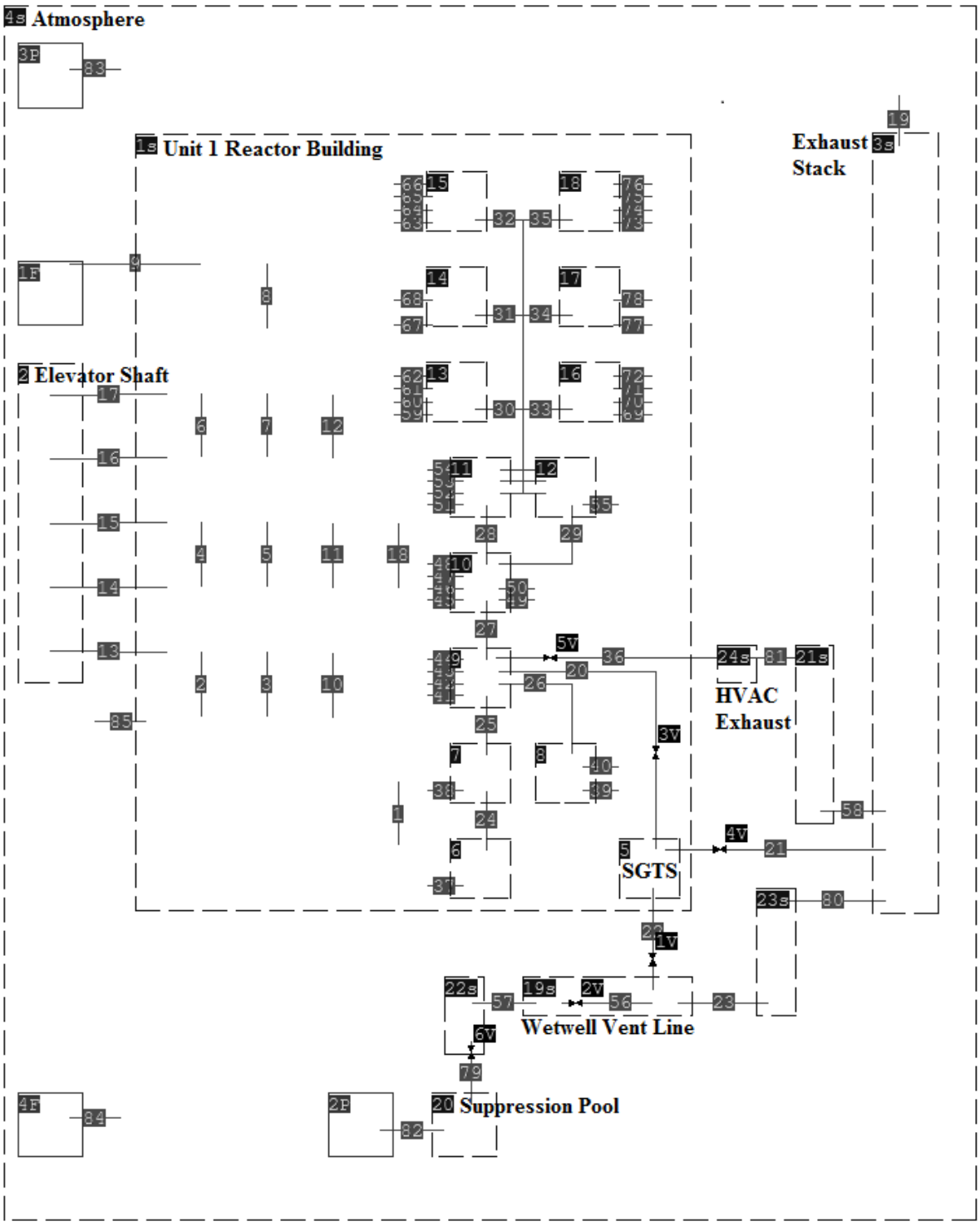

Figure 4-17
Fukushima 1F1 GOTHIC Model

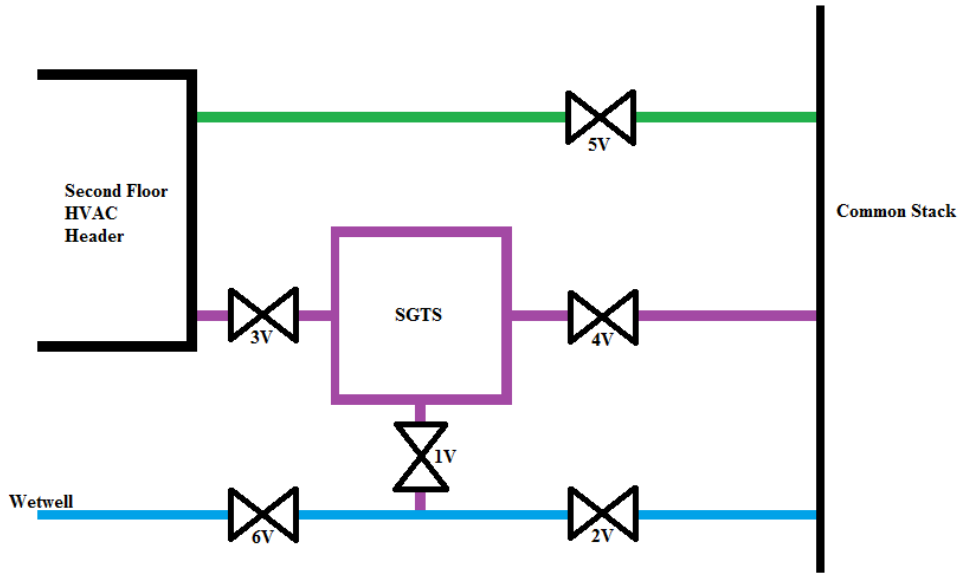

Figure 4-18
HVAC, SGTS, and Wetwell Vent Connections

4.5 Release Rates

The release rates from the drywell and wetwell are show in Figure 4-19 and Figure 4-20. In these graphs, time 0 corresponds to the time of the initial earthquake wave which occurred at 14:46 March 11, 2011.

In the MAAP analysis, the drywell is assumed to begin leaking at 39,657 seconds (approx. 1:47 March 12). At 1:48 March 12, firewater injection had started and it was noticed that the drywell pressure had increased at 2:30 March 12. This increase in drywell pressure could have caused a failure which allowed leakage through the drywell flange. The wetwell release begins at 85,560 seconds (approx. 14:32 March 12) when the wetwell was manually vented.

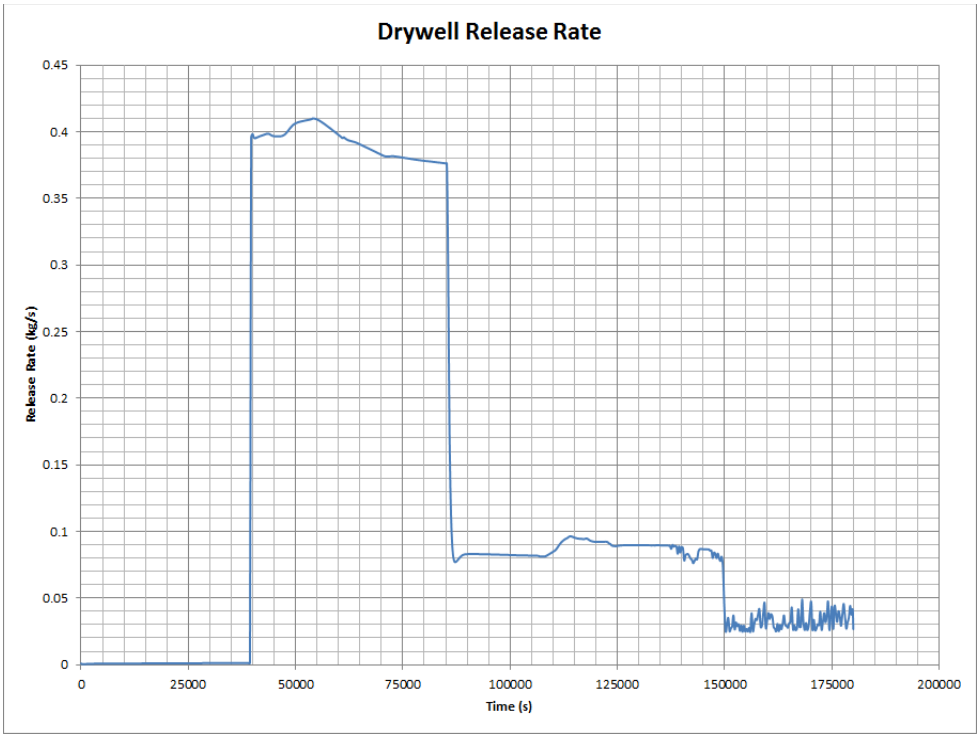

Figure 4-19
Drywell Release Rate (Kg/s)

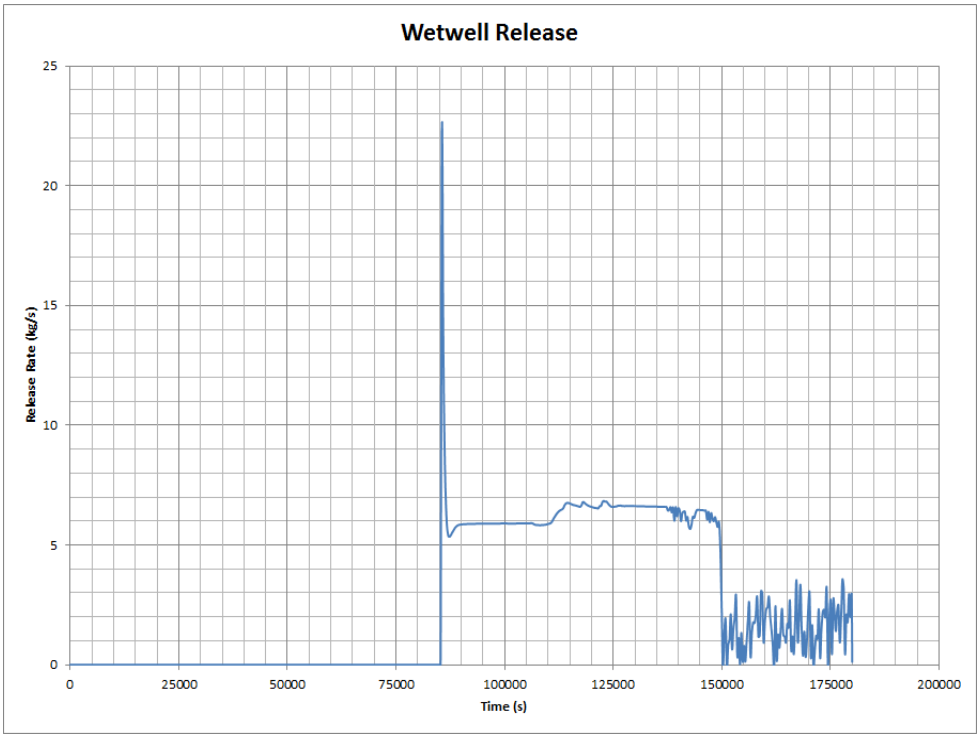

Figure 4-20
Wetwell Release Rate (Kg/s)

The gas concentrations in the drywell and wetwell can be seen in Figure 4-21 and Figure 4-22. This data was generated using the MAAP code and implemented in the model through Boundary Conditions 1F (Drywell) and 2P (Wetwell).

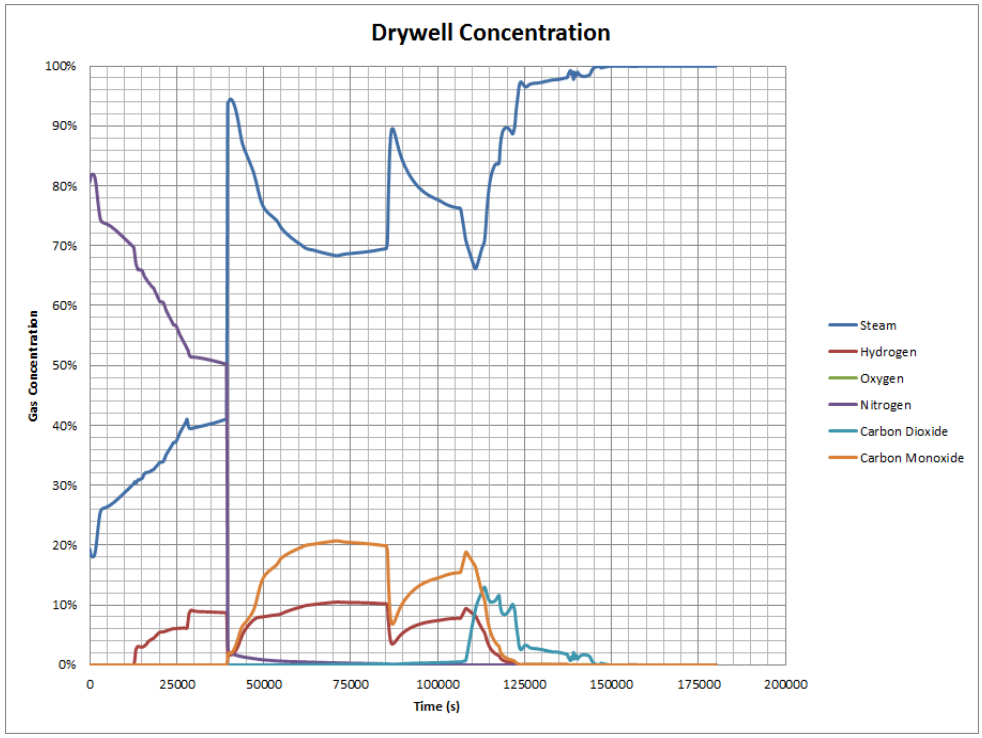

Figure 4-21
Drywell Gas Concentration

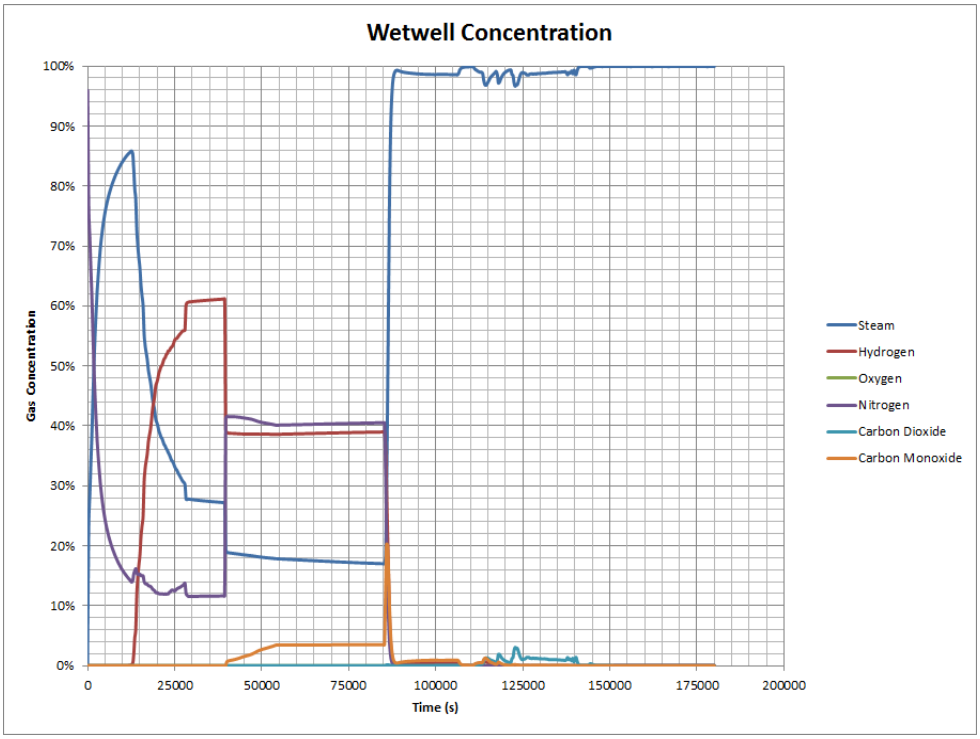

Figure 4-22
Wetwell Gas Concentration

4.6 Simulations and Observations

Each scenario was run to predict the gas concentrations on various floors in the reactor building. It should be noted that the plotted cells are at various heights spanning the fifth floor. All scenarios indicate a well-mixed concentration of combustible gases.

4.6.1 Scenario 1: Fifth Floor Drywell Leak Only

The drywell only leak model sets the valves on the wetwell vent line, HVAC exhaust, and tie between the wetwell vent line and SGTS to the closed position. This includes valves 1V, 2V, 5V, and 6V. The SGTS valves, 3V and 4V, are open during a loss of offsite power (EPRI, 2013). MAAP data is used to introduce a leak into the fifth floor, postulated to have leaked through the flange at the top of the drywell. This leak is modeled using Flow Path 9 and Boundary Condition 1F. The leakage point was hypothesized to have occurred along the drywell flange directly into the fifth floor. The leak is therefore placed approximately in the center of fifth floor above the drywell at the floor level.

Figure 4-23 is a vertical slice spanning the 37.18m length and 15.85m height of the fifth floor which shows an initial small variation in local hydrogen concentration. The high temperature of the released gases also contributes to the natural circulation seen in Figure 4-24 and Figure 4-25. The combustible gases are released so slowly that there is sufficient time for the fifth floor atmosphere to mix by convective currents and diffusion. Velocities in the vertical and horizontal directions are on the order of 0.5 m/s and 0.2 m/s or less, respectively. These are typical velocities for natural convection currents in air. The natural circulation pattern with the addition

of the leak from the drywell flange is sufficient to keep the fifth floor well mixed throughout the transient.

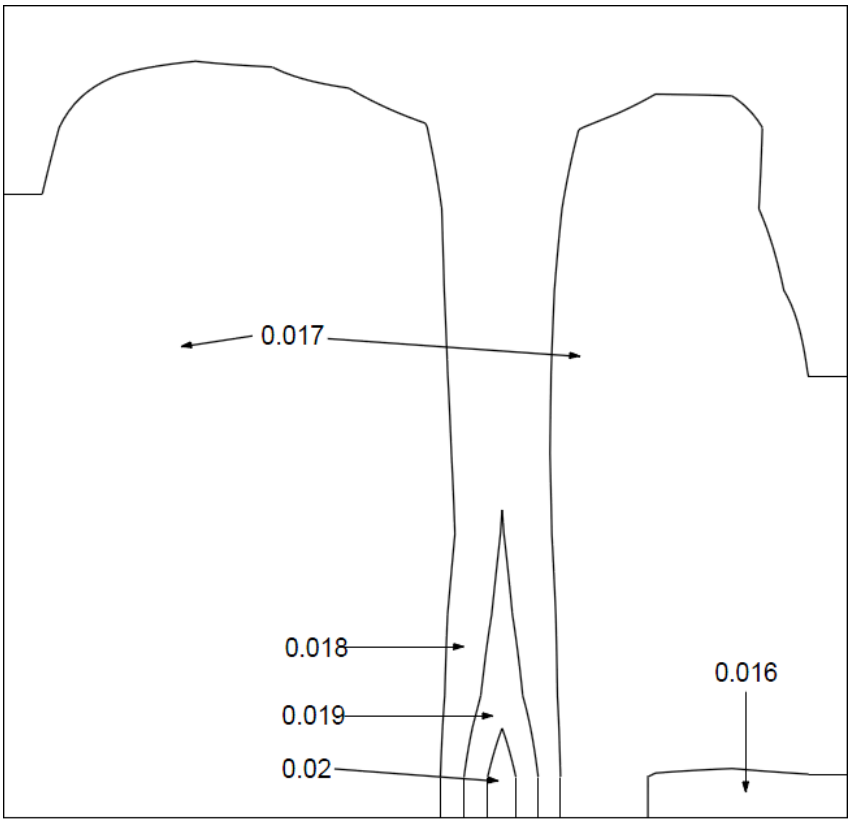

Figure 4-23
Hydrogen Distribution

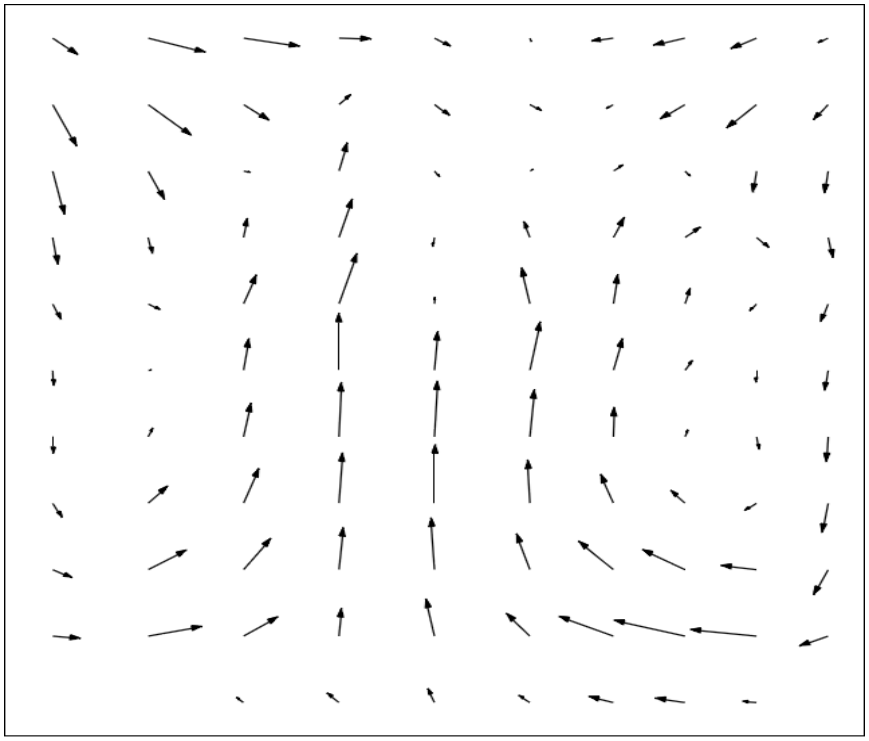

Scaling Velocity (m/s) = 0
Scaling Power = 1
Time (s) = 60002.6
/ Volume : Cells : Vmax (m/s) /
/ 1 : x(1-10) y(2-12) z(26-26) : 0.190158 /

Figure 4-24
Horizontal Circulation in Fifth Floor

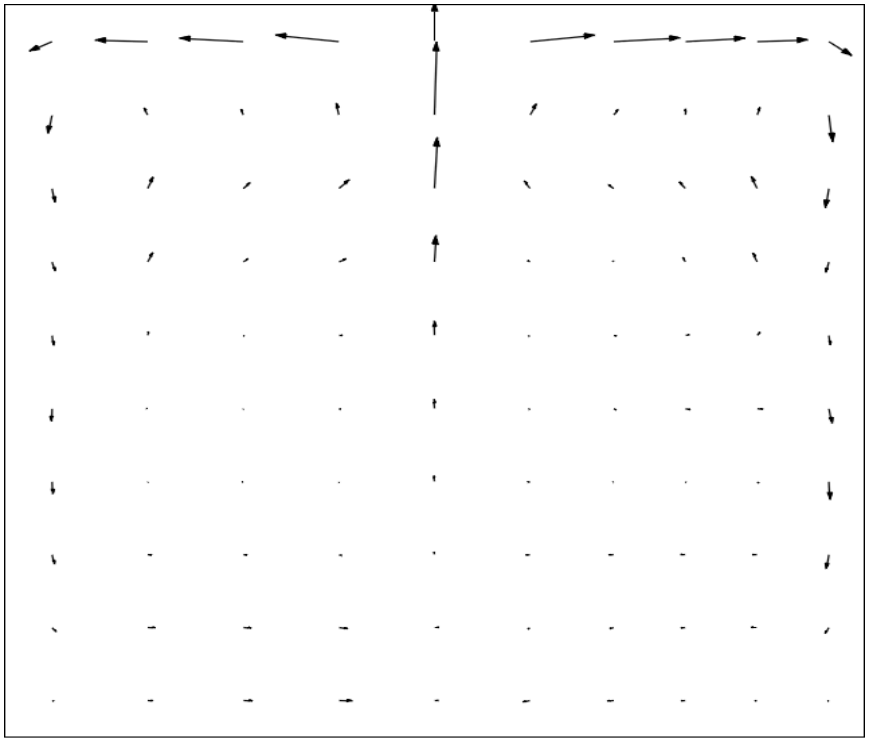

Scaling Velocity (m/s) = 0
Scaling Power = 1
Time (s) = 60002.6
/ Volume : Cells : Vmax (m/s) /
/ 1 : x(1-10) y(9-9) z(21-30) : 0.529303 /

Figure 4-25
Vertical Circulation in Fifth Floor

Figures 4-26, 4-27, and 4-28 show the volume fraction of hydrogen, carbon monoxide, and steam, respectively, taken from varying elevations on the fifth floor. These results indicate that hydrogen and CO are well mixed at the fifth floor throughout the transient. There is a small variation in the steam concentration however the top to bottom variation is no more than about 1%. At 89,400 seconds after the earthquake (time of the explosion) the hydrogen and steam concentrations are about 10% and 7%, respectively. Considering only the hydrogen, this is a flammable mixture but not explosive. However, the CO concentration at the same time is close to 20%. Combined with the hydrogen, this represents a potentially explosive gas mixture. Studies done by the Nuclear Energy Agency Committee on the Safety of Nuclear Installations (NEA/CSNI) indicate that the combination of 5% CO with 10% hydrogen in air can result in detonation (NEA, 2000).

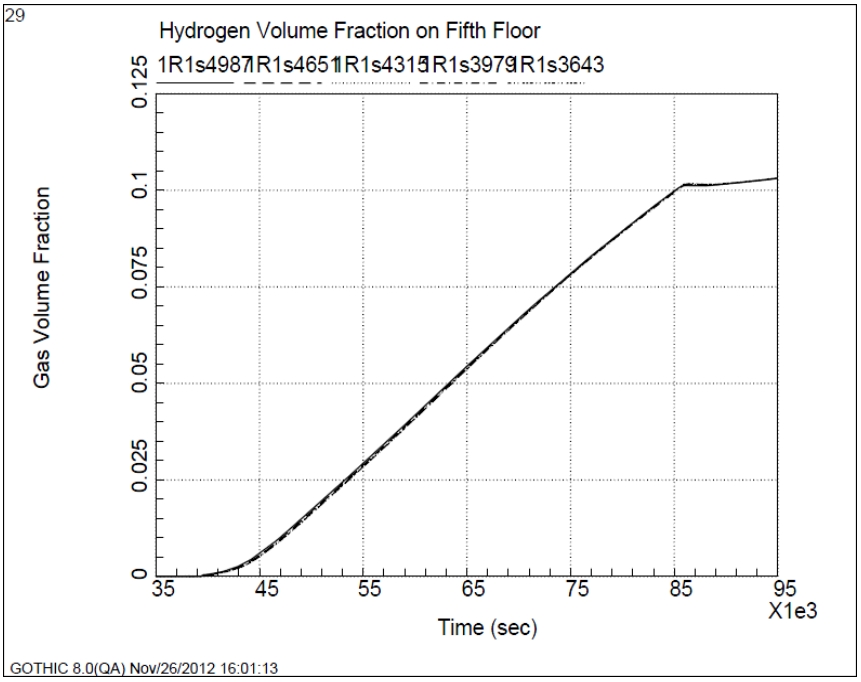

Figure 4-26
Fifth Floor Hydrogen Concentration with release from Drywell Only

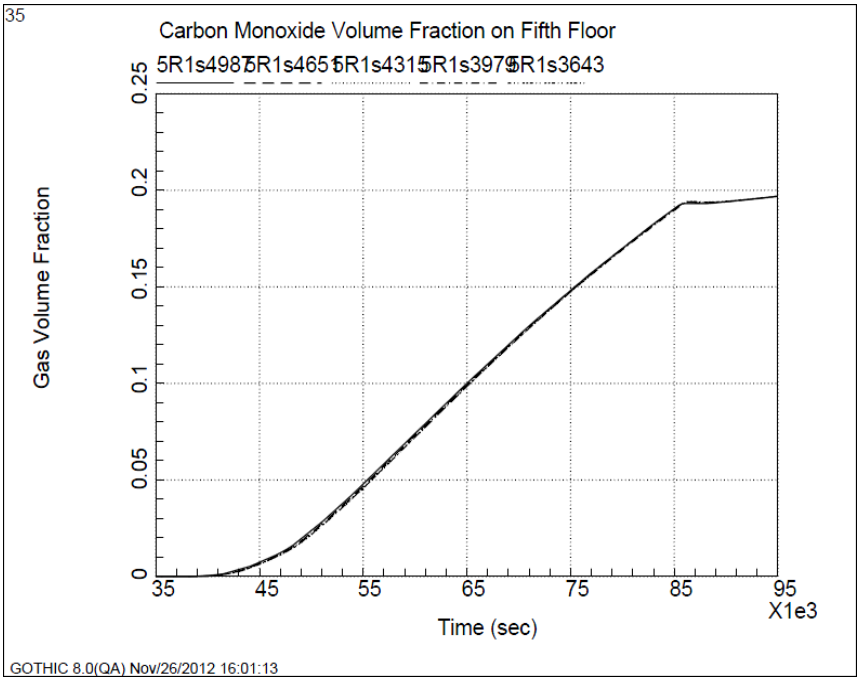

Figure 4-27
Fifth floor Carbon Monoxide concentration with release from Drywell Only

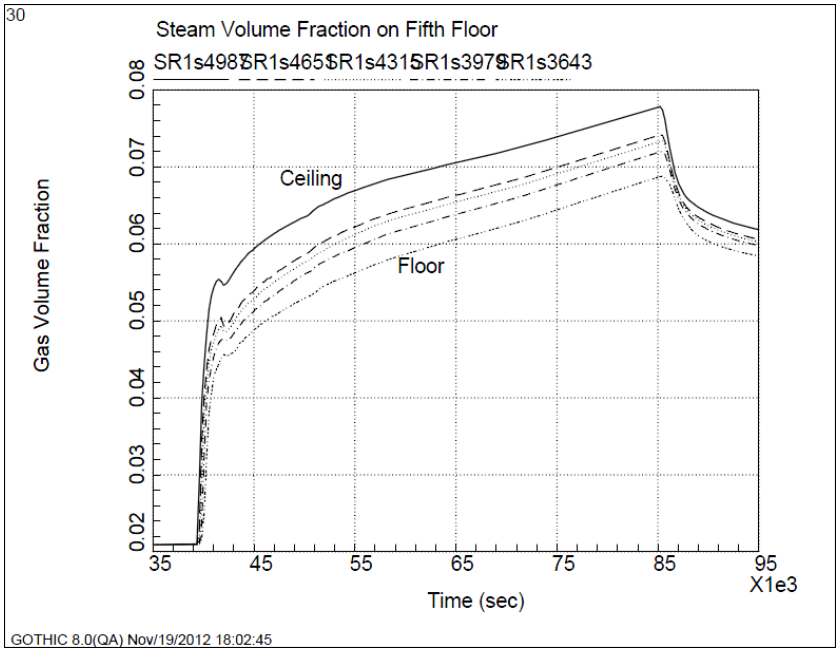

Figure 4-28
FIFTH Floor Steam Volume Fraction for Drywell Only Leak

Plots of the hydrogen volume fraction on the other four levels of the reactor building show low concentrations of hydrogen (below the flammability limit). The low levels are due primarily to molecular diffusion from the mixture at the fifth floor. None of the floors other than the fifth floor accumulate either a flammable or detonable quantity of hydrogen through a drywell only release from the flange.

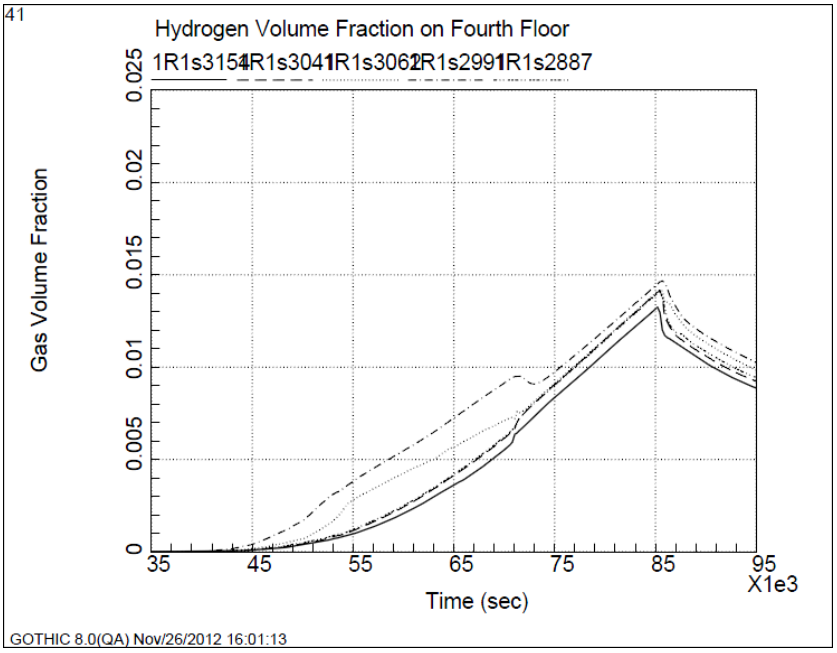

Figure 4-29
Fourth Floor Steam Volume Fraction for Drywell Only Leak

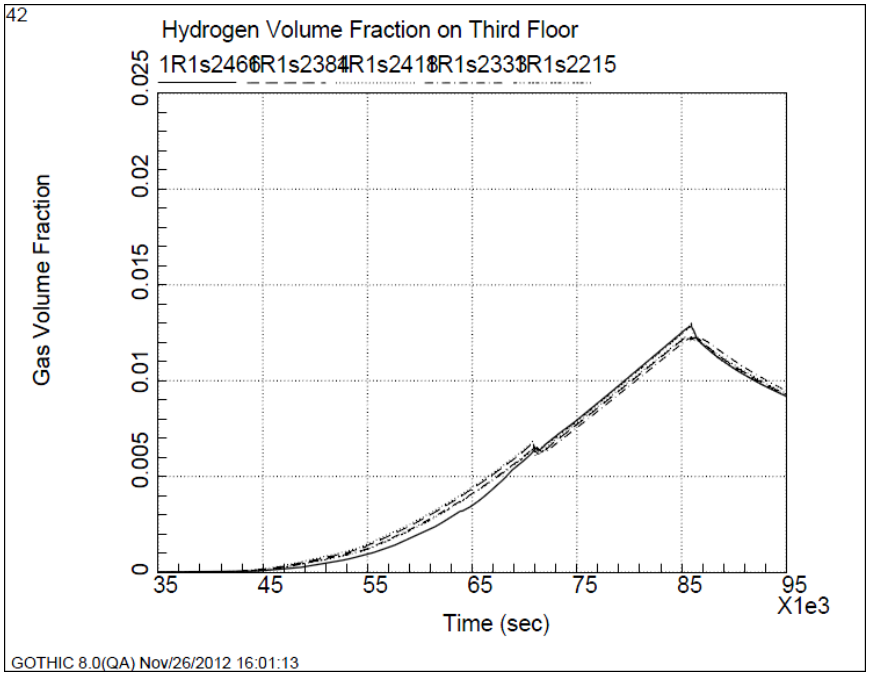

Figure 4-30
Third Floor Steam Volume Fraction for Drywell Only Leak

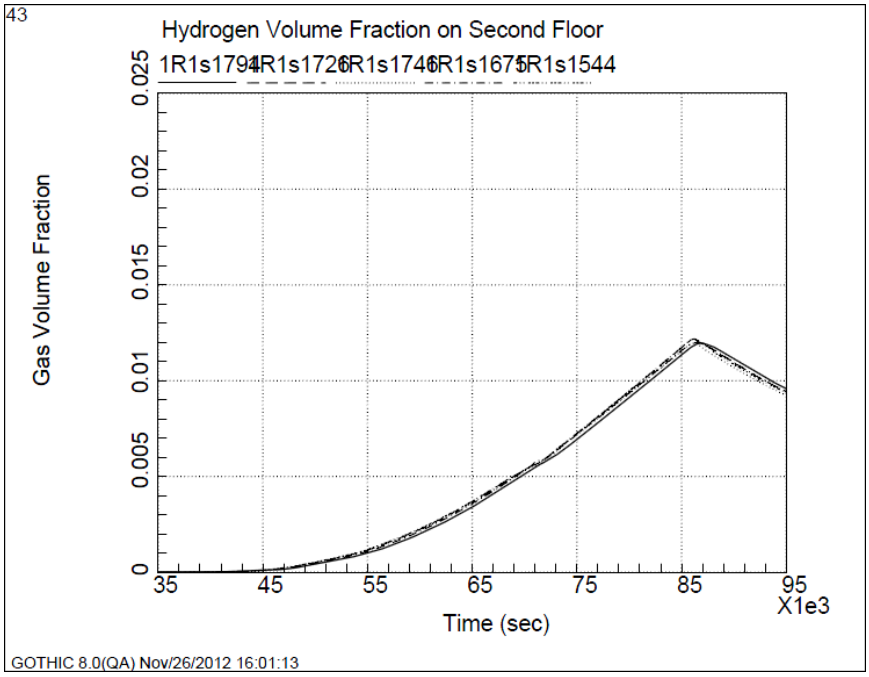

Figure 4-31
Second Floor Steam Volume Fraction for Drywell Only Leak

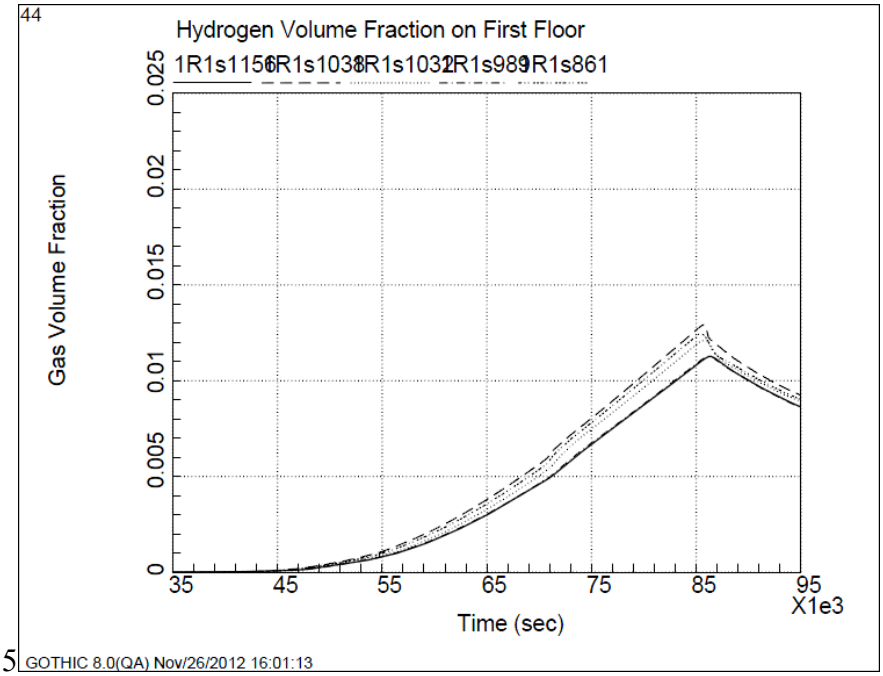

Figure 4-32
First Floor Steam Volume Fraction for Drywell Only Leak

4.6.2 Scenario 2: Drywell Release with Wetwell-Venting and Backflow through SGTS

The hydrogen explosion occurred within about 30 minutes of the manual operation of the wetwell vent. It is expected that the wetwell would have significant levels of hydrogen at that time and it is speculated that some of that hydrogen may have entered the reactor building. In this scenario, hydrogen is postulated to have exhausted to the stack from the wetwell with possible return back into the building through the SGTS. Referring to the valves in Figure 4-18, the HVAC exhaust damper (5V) and tie between the wetwell vent line and SGTS (1V) are held closed. The SGTS valves (3V and 4V) are open during a loss of offsite power (EPRI, 2013). The valves connecting the wetwell to the exhaust stack (2V and 6V) are opened at the time of the wetwell venting.

Figure 4-33 and 4-35 show the volume fraction of hydrogen and steam, respectively, taken from varying elevations on the fifth floor when the valve between the wetwell and SGTS remains closed. In this scenario, flow was allowed to exhaust from the wetwell into the stack through the wetwell vent. The flow is allowed to travel back through the open SGTS and redistributed throughout the building via the exhaust ducting headers as shown in Figure 4-18 of Section 4.4. GOTHIC shows that the hydrogen, carbon monoxide, and steam are again well mixed throughout. There is only slightly more hydrogen in the room than in the case with leakage from the drywell only. The gas composition released from the wetwell lowers the carbon monoxide volume fraction slightly.

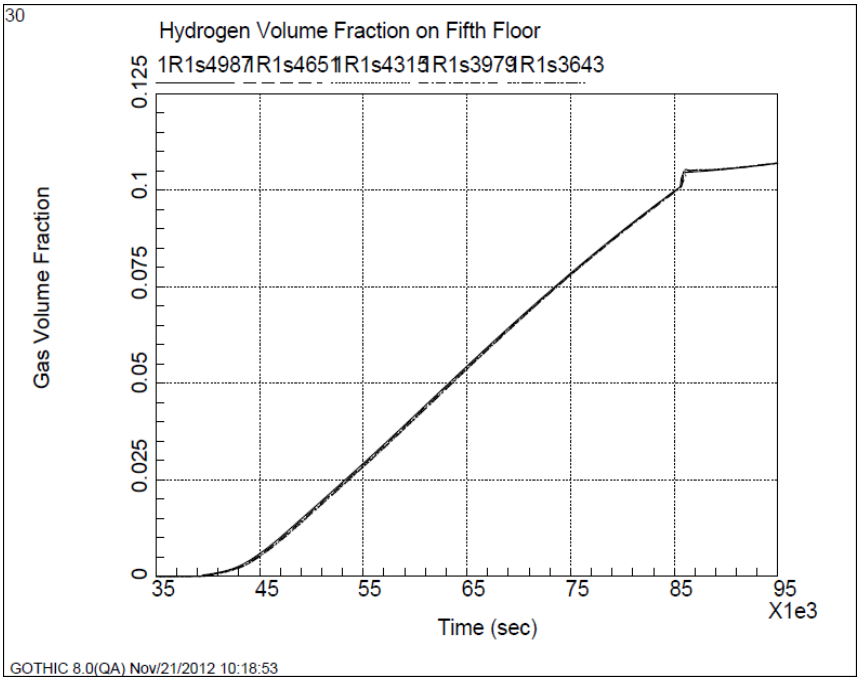

Figure 4-33
Hydrogen Release into Fifth Floor with Closed Wetwell-SGTS Valve

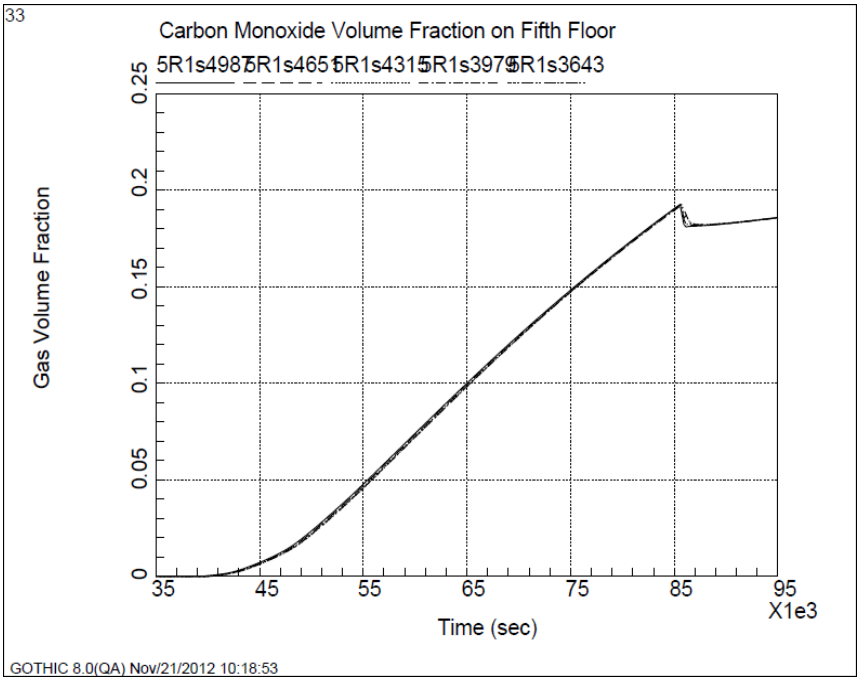

Figure 4-34
Carbon Monoxide Release into Fifth Floor with Closed Wetwell-SGTS Valve

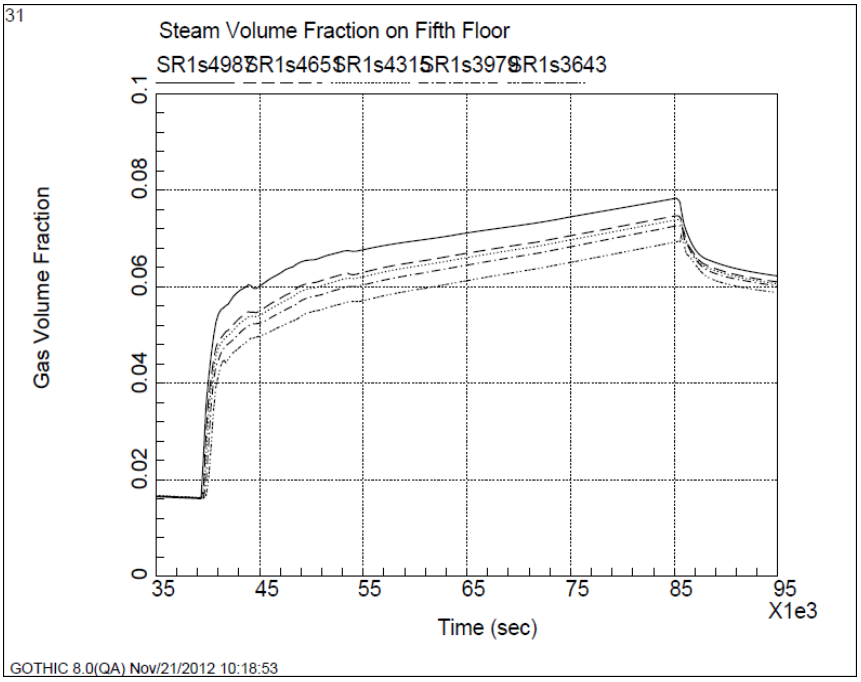

Figure 4-35
Steam Volume Fraction with Closed Wetwell-SGTS Valve

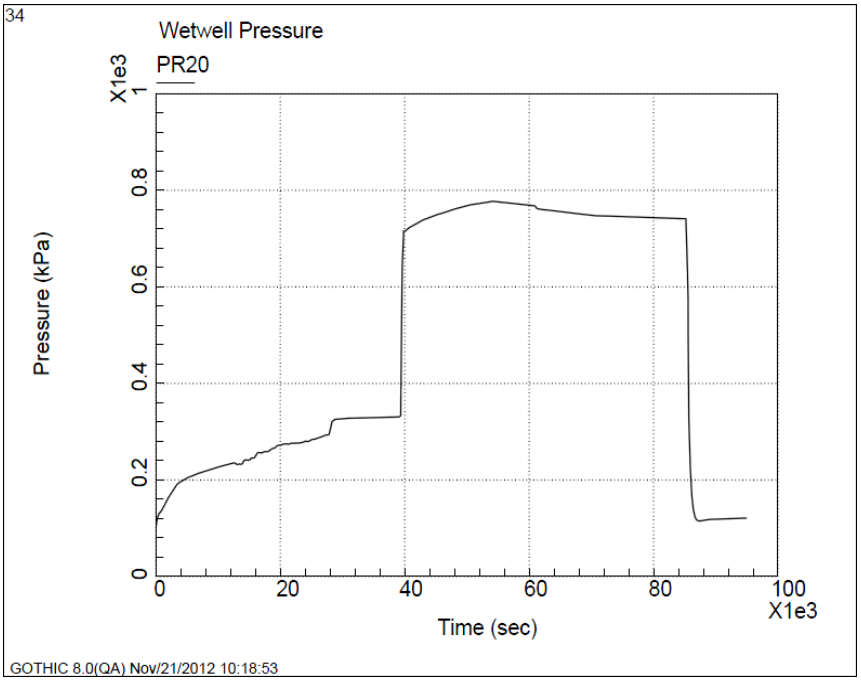

Figure 4-36
Wetwell Pressure

In this simulation, the wetwell pressure transient was specified using results from MAAP shown in Figure 4-36. When the wetwell vent valve is opened, a pressure wave is transmitted downstream. In this analysis it was assumed that the vent valve opened very quickly. If the valve opens more slowly, the downstream pressure differentials would be significantly reduced. The

normally closed valve that connects the wetwell vent to the SGTS (1V), curve "DP22" on Figure 4-37, experiences a differential pressure of approximately 625 kPa. The damper in the exhaust vent line connection to the stack (5V), curve "DP36" on Figure 4-37, experiences a differential pressure of 50kPa. It is unknown whether or not these pressure loads could damage the indicated valves.

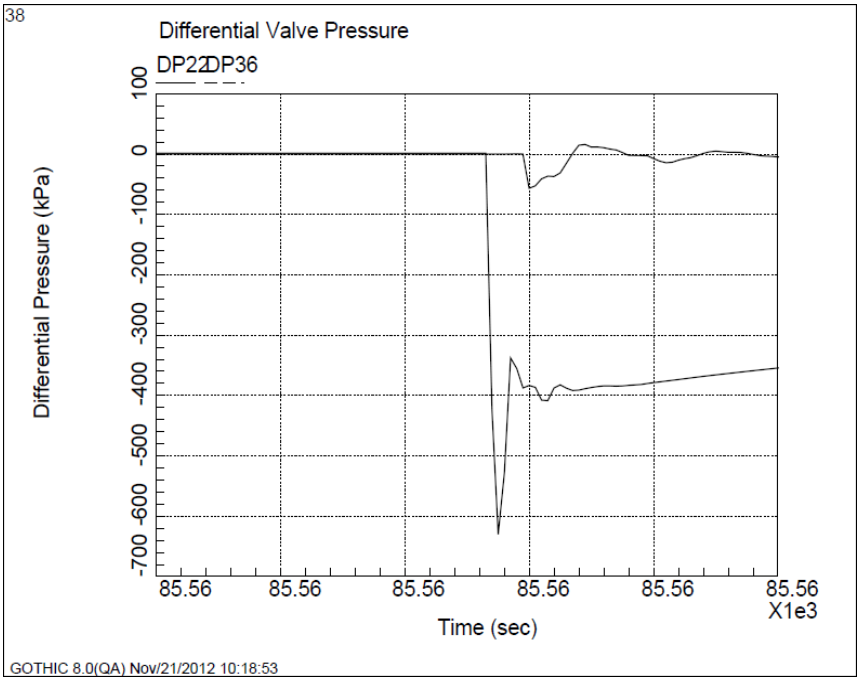

Figure 4-37
Pressure Response of Valves on Potential Flow Paths

When the wetwell vent line is opened the vapor flow, represented in Figure 4-38 as curve "FV19", the majority of the flow is exhausted out of the top of the common stack, curve "FV80". A portion is sent through the SGTS which accounts for the sudden increase in hydrogen before being completely exhausted through the stack. With a concentration of 10.5% hydrogen and 6% steam, the conditions in the fifth floor 89,400 seconds after the earthquake have the potential to be flammable. With the addition of 19% carbon monoxide the mixture has the possibility of being detonable.

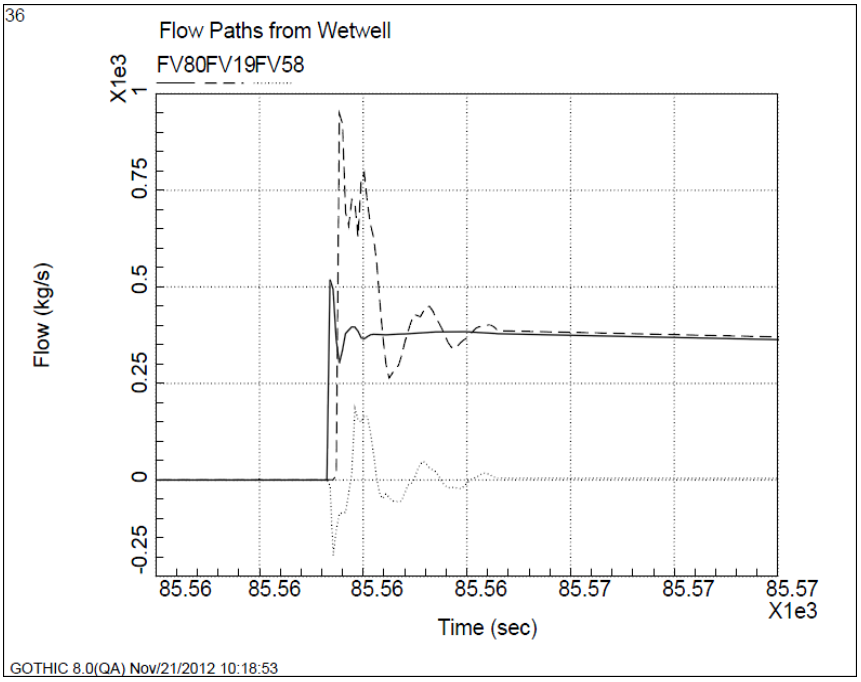

Figure 4-38
Flow Paths from Wetwell

Although there is not a substantial increase in the fifth floor combustible gas concentrations, the added flow increases the combustible gases in the HVAC headers for 500 seconds. Figure 4-40 and Figure 4-41 show the hydrogen and carbon monoxide volume fractions in the HVAC headers, respectively. Prior to the wetwell venting, there is a small amount of combustible gases. The second floor through the fifth floor HVAC ducting experience increases in hydrogen and carbon monoxide above detonable limits when the wetwell is vented. This large increase in hydrogen and is the result of back flow from the stack.

The connection between the SGTS and the exhaust HVAC ducting is on the second floor. All of the ducting in the second floor and above sees detonable gas concentrations. The combustible gas concentrations in the first floor ducting decreased due to buoyancy induced flow into the ducting from the first floor room air. The estimated volume of ducting with detonable gas mixture is 140 m^3.

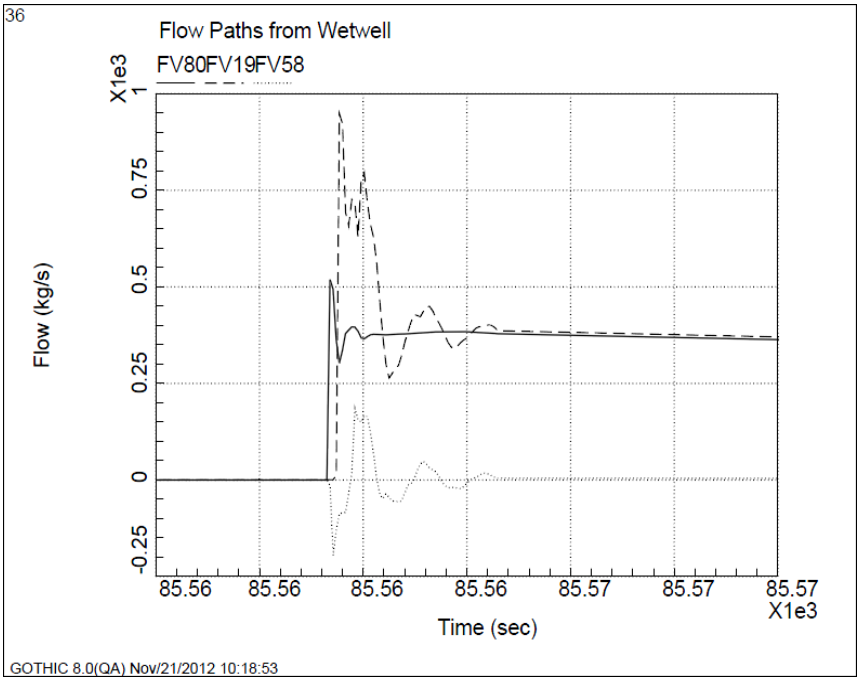

Figure 4-39
Flow from Wetwell via various Pathways

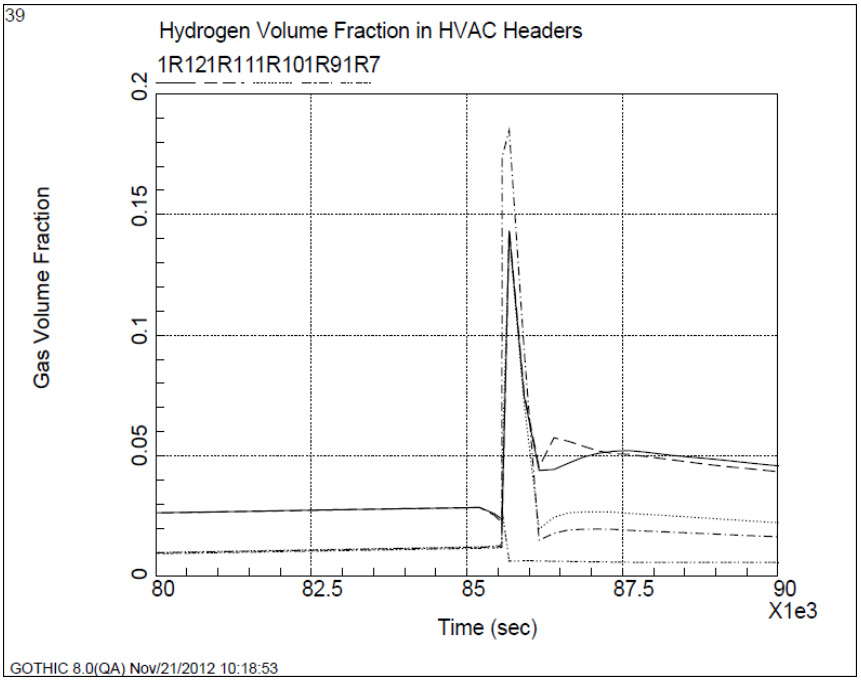

Figure 4-40
Hydrogen Volume Fraction in HVAC Headers

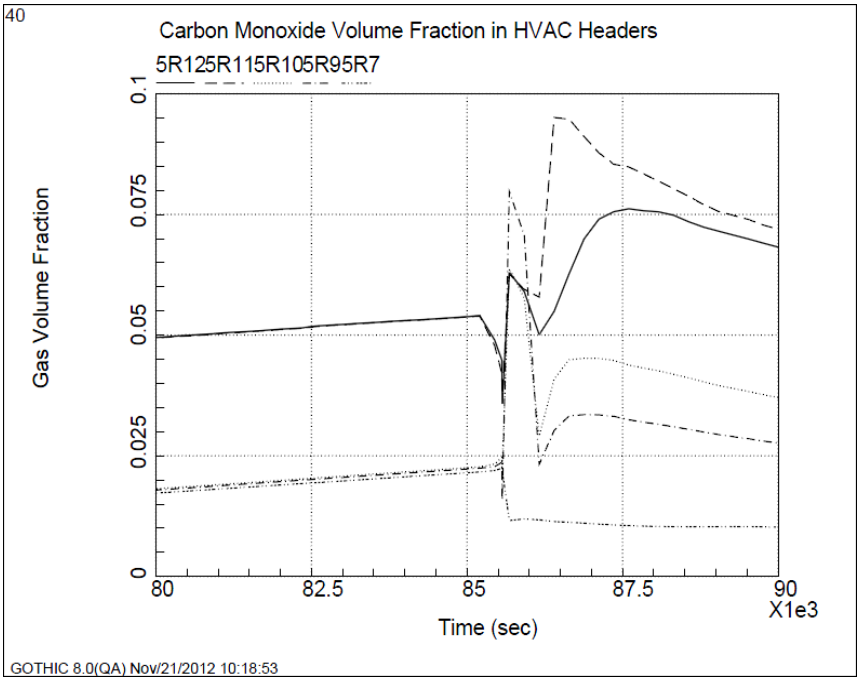

Figure 4-41
Carbon Monoxide Volume Fraction in HVAC Headers

The back flow into the HVAC system is an indication of what might have occurred in 1F4 when the 1F3 wetwell was vented. In this case, the flow would be from 1F3 into the stack and then into the 1F4 SGTS or HVAC exhaust duct. This would require that valves to the 1F4 SGTS or HVAC be in the open position to allow back flow from the stack. The gas concentrations in the ducting presented here for the 1F1 simulation may or may not be representative of the conditions in 1F4. That would depend, to a large extent, on the 1F3 wetwell conditions (gas concentrations) at the time of the 1F3 wetwell venting.

4.6.3 Scenario 3: Wetwell Release with Wetwell-SGTS Tie Open

The wetwell release with wetwell-SGTS tie open model sets the valve on the tie between the wetwell vent line and SGTS (1V) to the open position. The SGTS valves (3V and 4V in Figure 4-18) are open during a loss of offsite power (EPRI, 2013). The valves connecting the wetwell to the exhaust stack (2V and 6V) are opened at the time the MAAP data shows flow leaking from the wetwell. This scenario allows hydrogen the quickest route back into the building and it is expected that this will result in the highest hydrogen concentration.

Figures 4-42, 4-43, and 4-44 show the volume fraction of hydrogen, carbon monoxide, and steam, respectively, taken from varying elevations on the fifth floor with the valve between the wetwell and SGTS failing open. The combustible gases and steam are again well mixed throughout. With a concentration of 21% hydrogen, 30% steam, and 20% carbon monoxide the conditions in the fifth floor after the earthquake are well within the detonable range.

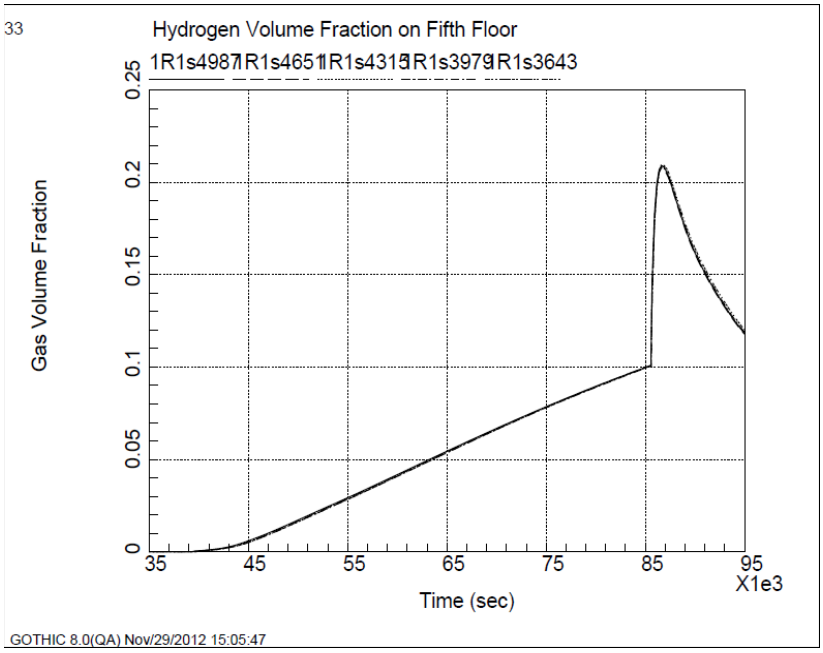

Figure 4-42
Hydrogen Release into Fifth Floor with Open Wetwell-SGTS Valve

The release through the SGTS increases the volume fraction of hydrogen in the fifth floor by two fold. The amount of steam, however, is also increased by five times that of the previous scenarios. At the time of the explosion the predicted mixture is still in a detonable state.

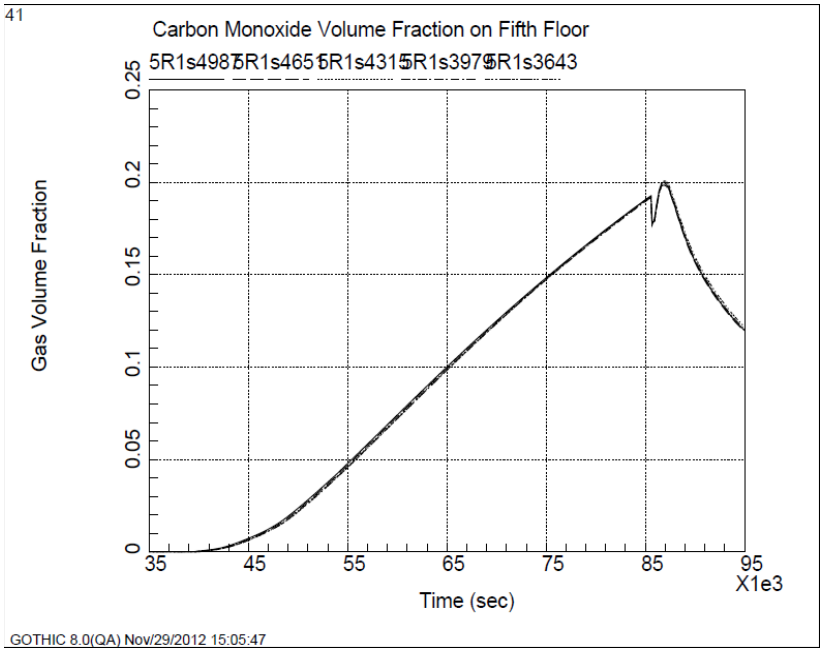

Figure 4-43
Carbon Monoxide Release into Fifth Floor with Open Wetwell-SGTS Valve

Figure 4-45 shows the amount of hydrogen released in the HVAC headers. Figure 4-46 shows the amount of steam released in the HVAC headers. At the time of the postulated break the HVAC headers are inundated with hydrogen and steam. At the time of the explosion, the first floor HVAC headers contain a hydrogen and steam mixture that is detonable.

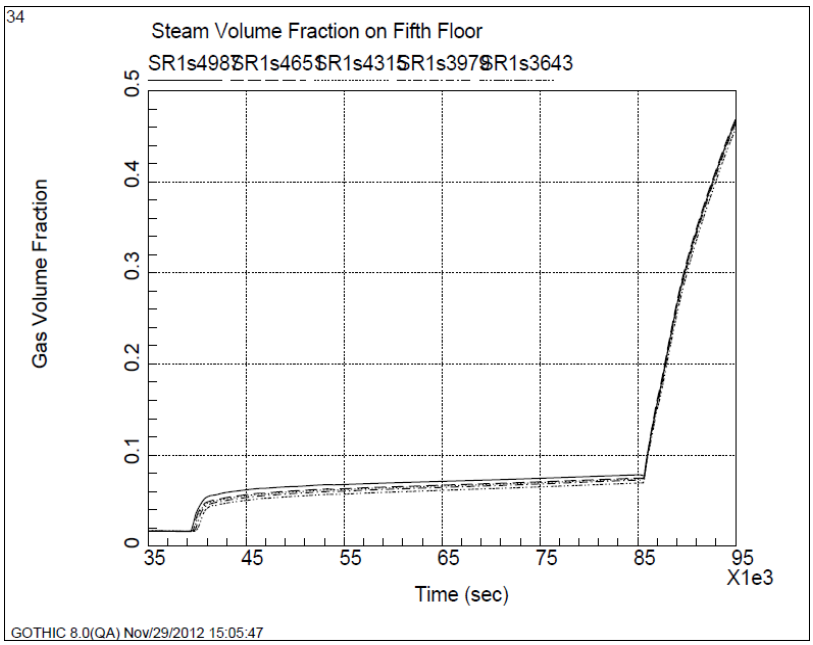

Figure 4-44
Fifth Floor Steam concentration with Open Wetwell-SGTS Valve

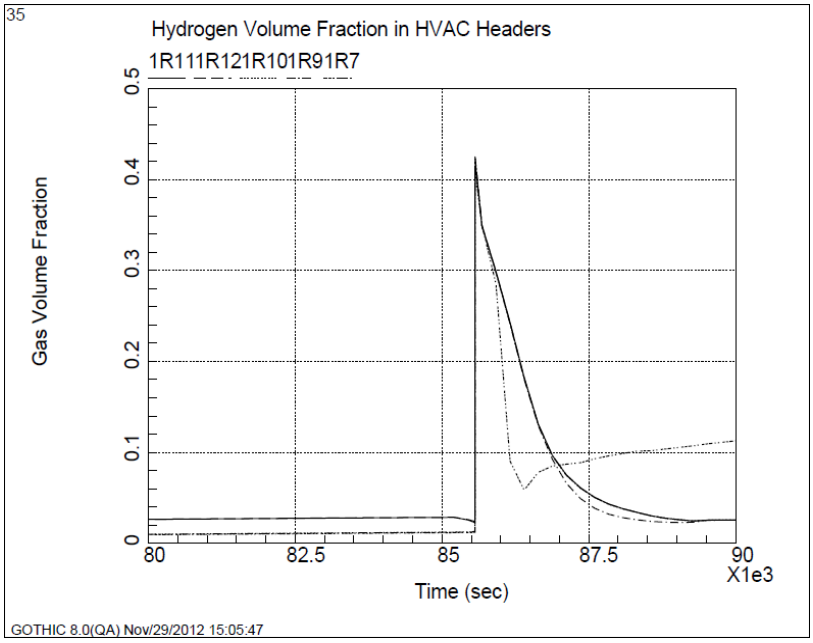

Figure 4-45
Hydrogen Concentration in HVAC Headers

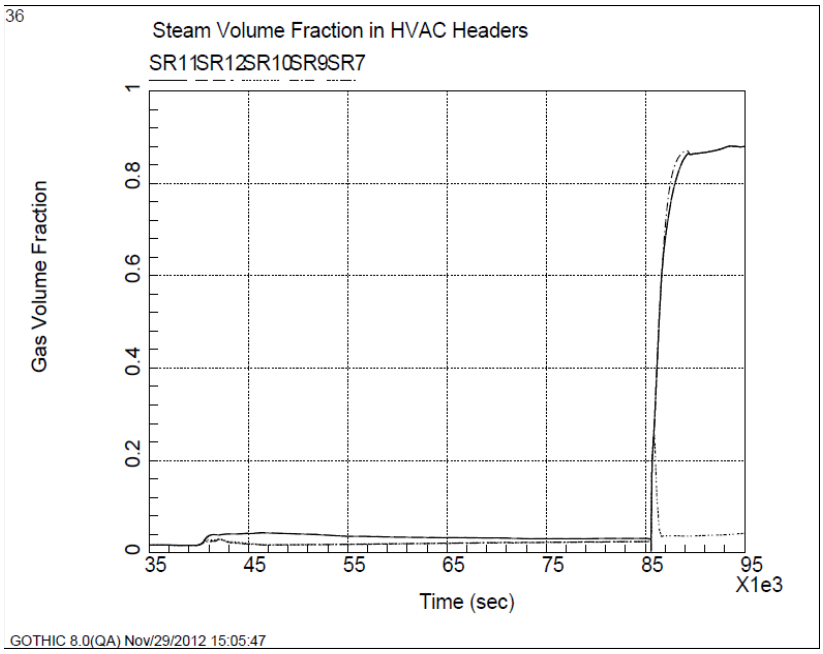

Figure 4-46
Steam Release into HVAC Headers

Figures 4-47 through 4-50 depict the hydrogen volume fraction on the fourth through first floor, respectively. In each case the hydrogen reaches a detonable level. Given the limited damage to the lower elevations of the 1F1 Reactor Building, it is unlikely that this postulated scenario occurred.

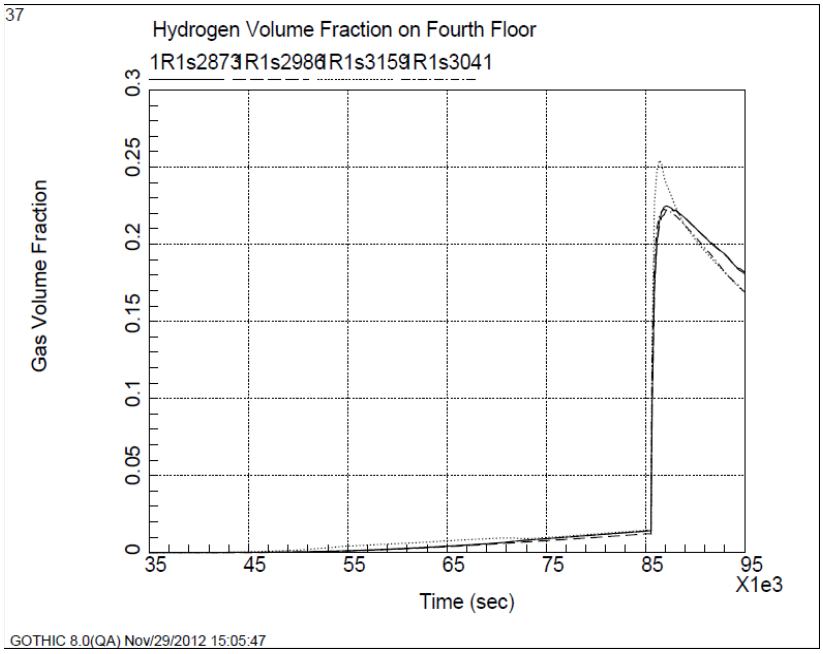

Figure 4-47
Hydrogen Concentration on Fourth Floor

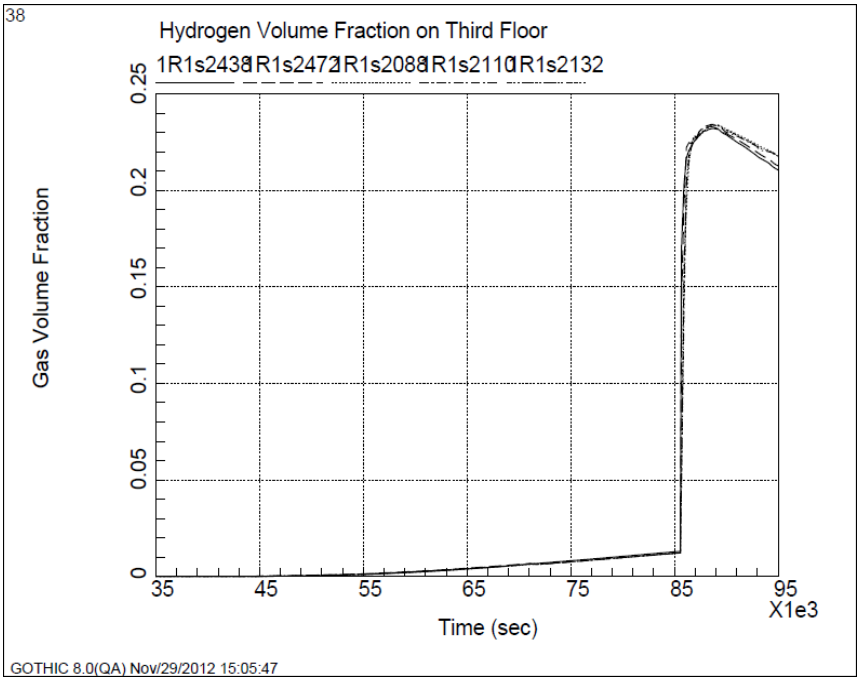

Figure 4-48
Hydrogen Concentration on Third Floor

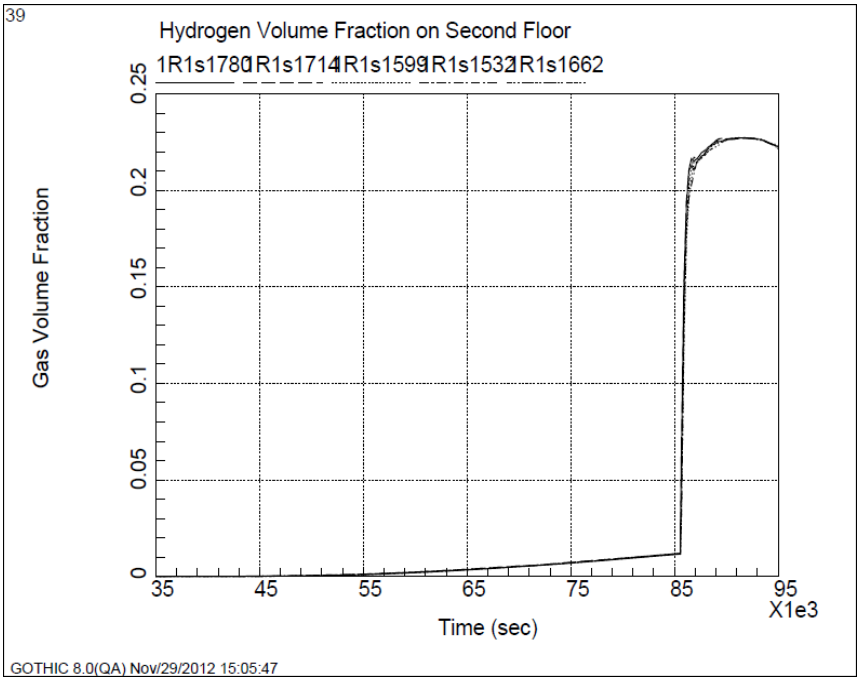

Figure 4-49
Hydrogen Concentration on Second Floor

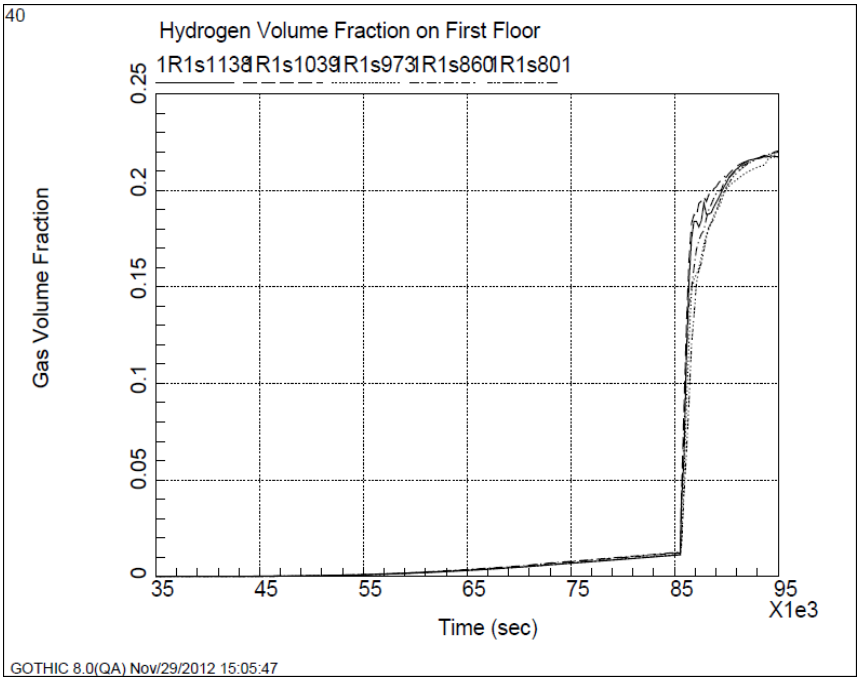

Figure 4-50
Hydrogen Concentration on First Floor

4.6.4 Scenario 4: Drywell Leak on First Floor Only

Scenario 4 is set up similar to Scenario 1 with the exception that the leak is instead postulated to originate from the primary containment access lock with subsequent release into the first floor. The results indicate that the entire building has a nearly uniform hydrogen concentration that reached a peak less than 4%. Similarly, the CO spreads uniformly at a peak slightly less than 8% on each of the floors. The mixture is not detonable and is not likely to cause the observed damage to the 1F1 Reactor Building.

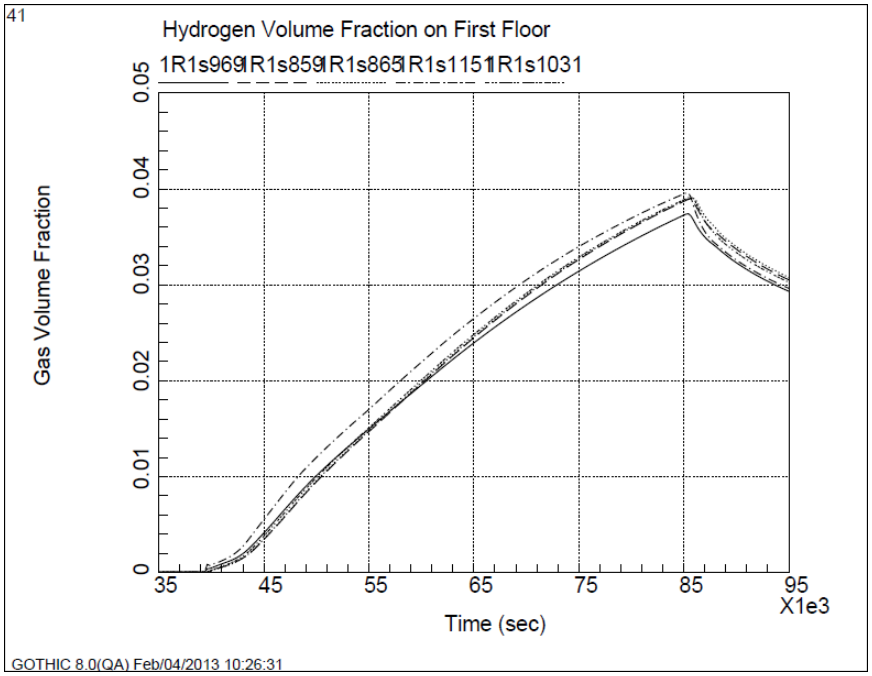

Figure 4-51
Hydrogen Concentration on First Floor

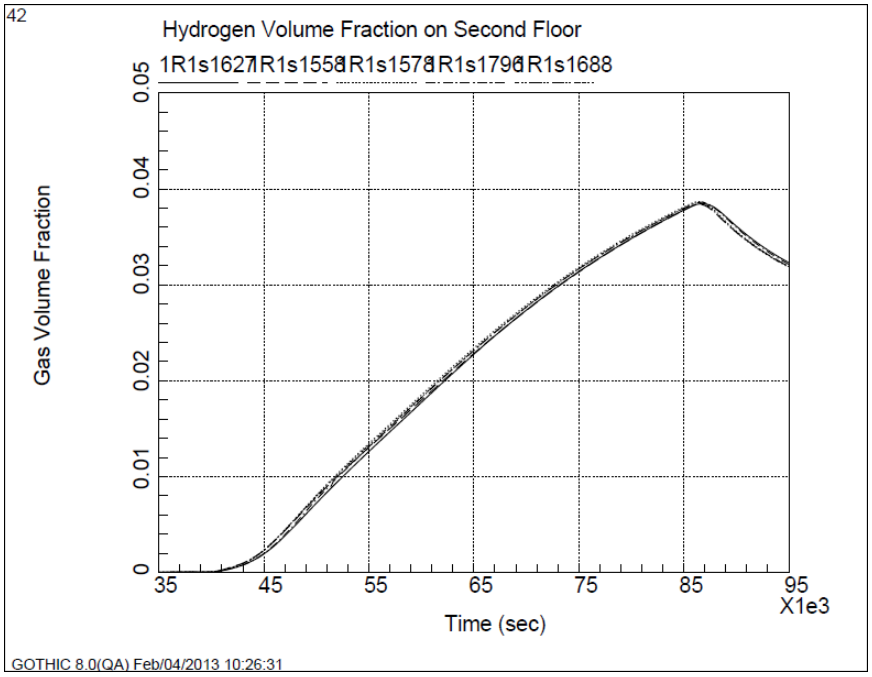

Figure 4-52
Hydrogen Concentration on Second Floor

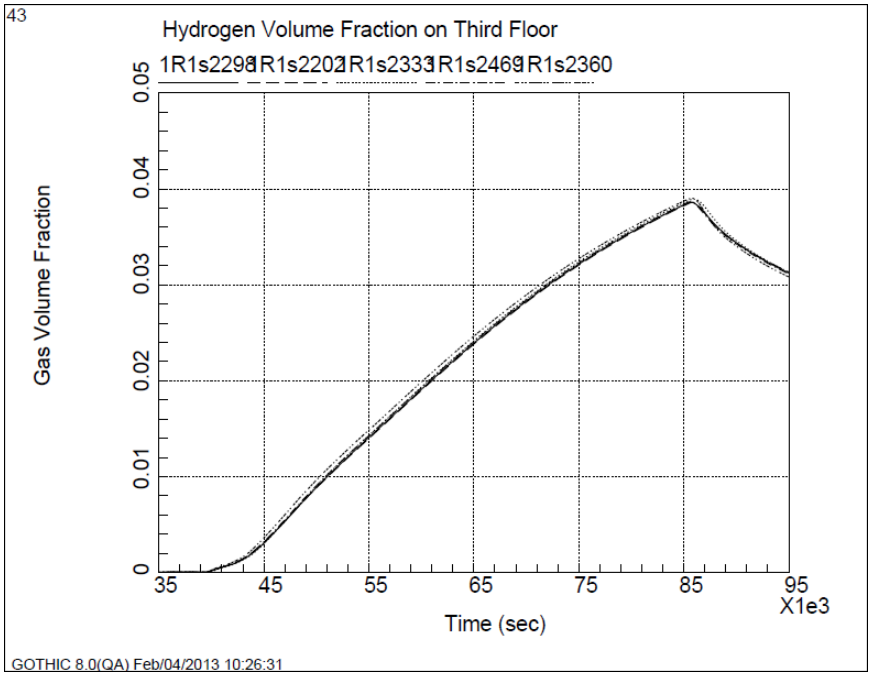

Figure 4-53
Hydrogen Concentration on Third Floor

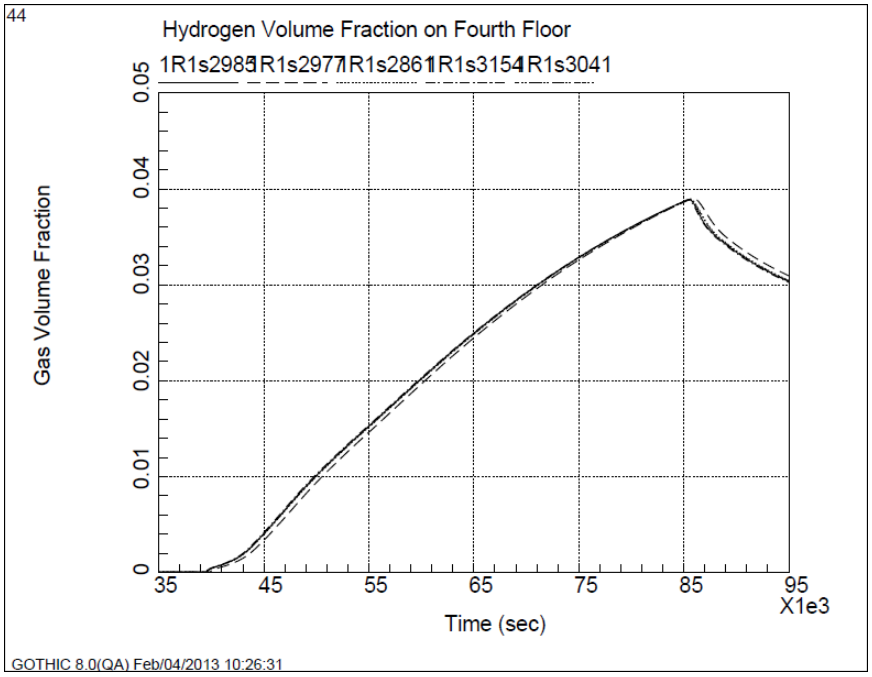

Figure 4-54
Hydrogen Concentration on Fourth Floor

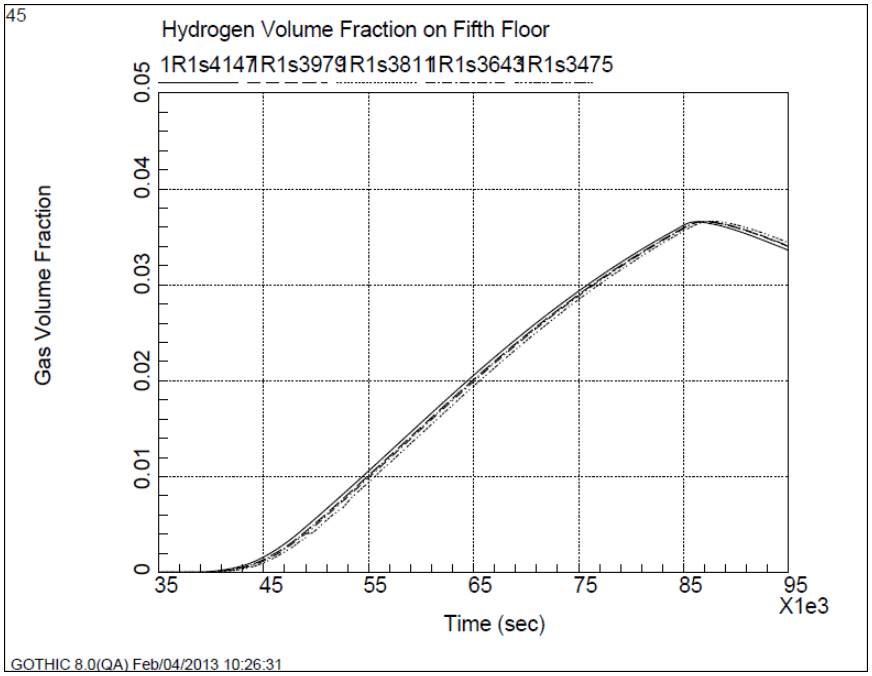

Figure 4-55
Hydrogen Concentration on Fifth Floor

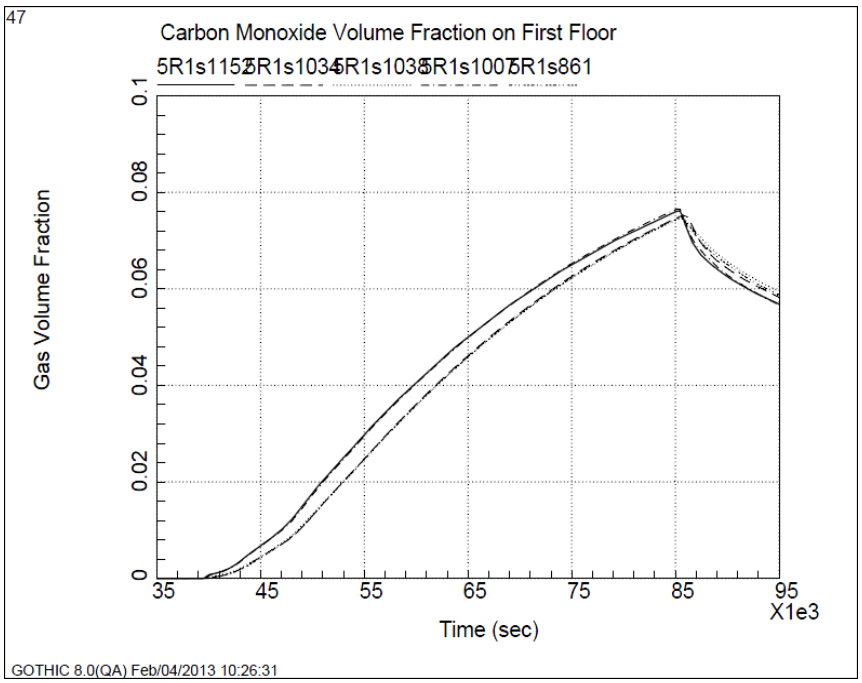

Figure 4-56
Carbon Monoxide Concentration on First Floor

4.7 Conclusions

For the given combustible gas and steam release from the drywell from the MAAP simulations, the results presented here indicate that a release via the drywell flange would be sufficient to

result in a detonation on the fifth floor. The combustible mixture is limited to the upper elevations of the reactor building consistent with the limited damage to lower elevations of the Reactor Building.

Backflow from the stack through the SGTS during the wetwell venting has a minimal effect on the concentrations in the fifth floor of the Reactor Building. However, the additional flow from the venting of the wetwell does result in explosive gas mixtures in the HVAC headers on the second through the fifth floors. A similar scenario could explain the explosion in 1F4 following the 1F3 wetwell venting provided that the HVAC system valve in 1F4 would allow the back flow from the stack.

If there was a failure of the valve on the tie line between the wetwell vent and the SGTS, the GOTHIC analysis indicates that the entire 1F1 Reactor Building would contain detonable gas mixtures throughout. Ignition on any floor would likely produce an explosion that involved the entire building. Since the 1F1 damage was mainly confined to the fifth floor, it is unlikely that this scenario occurred.

A release from the drywell into a lower level of the reactor building only results in the overall building hydrogen volume fraction being raised to less than 4%. This scenario results in a gas composition that could not sustain a detonation and therefore it is unlikely that this occurred.

4.8 Computer Files

Table 4-2
Files

File Name	Description
no_open_valves.zip	GOTHIC model for Scenario 1
SGTS_wwc.zip	GOTHIC model for Scenario 2
SGTS_ww_break.zip	GOTHIC model for Scenario 3
1Fleak.zip	GOTHIC model for Scenario 4
Each *.zip file contains:	
*.GTH	GOTHIC Model
*.SGR	Graphic Data File
*.SIN	Solver Input File
*.SOT	Solver Output File

5
1F1 AND 1F2 FLOODING

5.1 Introduction

The Fukushima Daiichi Nuclear power plants were subjected to extensive flooding in consequence to the large scale earthquake and subsequent tsunami. Seawater inundated the area surrounding the major buildings of the plant. This flooding was most severe in the area surrounding Units 1 through 4 (TEPCO Accident Report, 2012). Massive amounts of seawater flooded into 1F1 and 1F2 buildings, causing damage to emergency power systems (diesel generators, electrical equipment, etc.) resulting in a station blackout. The depth of floodwater around 1F1 and 1F2 buildings reached a maximum of 5.5 meters above plant grade (10 meters).

The purpose of this analysis is to simulate the flooding which occurred at Fukushima Daiichi 1F1 and 1F2. GOTHIC has the ability to model the environment inside the buildings affected by the flooding as a result of an external event (tsunami). This includes ingress of water from the outside by leaks through penetrations and failure of exterior doors. Internally, the progression of flooding is modeled consistent with traditional GOTHIC applications. Factors that affect the outcome of the flooding transient include inundation height, door leakage and failure, and ventilation locations. The location and size of leakage areas also affects the amount of water that becomes trapped in low elevation areas of buildings. These parameters are readily modified in GOTHIC.

Additionally, the use of 3-dimensional visualization of the flooding transient is presented as a demonstration of GOTHIC capabilities in flood modeling. Animations of the flooding simulation have been produced which provide an additional tool to quantify the local flooding and to investigate the effect of varying leakage flow areas.

The routes of the tsunami floodwater entering the building are presumed to be the building entrance/exit points, emergency diesel generator air supply louvers, above ground machinery hatches, building basement trenches, and ducts/penetrations for cables and piping. The buildings associated with 1F1 and 1F2 are listed in Table 5-1. Since the maximum inundation height around these buildings is 5.5 meters, only the basement and ground floors of buildings are included in the GOTHIC model. There is no modeling of HVAC systems, pipe networks, underground trenches or drainage systems. The physical displacement of these systems along with other small pieces of equipment is accounted for with volume porosity adjustments. The buildings included are represented geometrically with subdivided volumes in GOTHIC.

A flooding transient is implemented by connecting modeled buildings to a single large control volume which represents the environment surrounding 1F1 and 1F2. The connections represent the exterior openings in the buildings. The surrounding control volume is filled according to a tsunami input scheme which simulates the inundation height around 1F1 and 1F2. Atmospheric temperature and pressure is implemented in this volume using pressure and flow boundary conditions.

Table 5-1
Control Volumes

Control Volume Parameters						
Vol #	Description	Vol (m3)	Elev (m)	Ht (m)	Hyd. D. (m)	L/V IA (m2)
1	Basin/Atmosphere	100000.	0.	30.	100000.	DEFAULT
2s	Turbine Bldg 1 ground	31900.	10.2	6.	12.	DEFAULT
3s	Radwaste Bldg 1 roof	360.	14.7	3.1	5.	DEFAULT
4s	Reactor Bldg 1 ground	9700.	10.2	6.4	12.	DEFAULT
5s	Radwaste Bldg 1 ground	3700.	10.2	4.	8.	DEFAULT
6s	Reactor Bldg 1 basement	15800.	-1.23	10.4	18.	DEFAULT
7s	Radwaste Bldg 1 basement	6100.	1.4	7.7	13.	DEFAULT
8s	Turbine Bldg 1 basement	30100.	1.9	8.3	14.	DEFAULT
9s	Turbine Bldg 2 ground	51000.	9.	7.	13.	DEFAULT
10s	Radwaste Bldg 2 roof	488.	14.7	3.1	5.5	DEFAULT
11s	Radwaste Bldg 2 ground	3460.	10.2	3.7	7.	DEFAULT
12s	Reactor Bldg 2 ground	13800.	10.2	7.	13.	DEFAULT
13s	Radwaste Bldg 2 basement	8850.	-0.3	9.45	16.	DEFAULT
14s	Reactor Bldg 2 basement	27600.	-2.06	11.4	21.	DEFAULT
15s	Turbine Bldg 2 basement	48900.	0.3	8.7	14.	DEFAULT
16s	Fuel Storage Bldg ground rooms	720.	10.2	3.	5.6	DEFAULT
17s	Fuel Storage Bldg basement	7000.	-0.3	9.3	15.1	DEFAULT
18s	Fuel Storage Bldg roof	455.	14.2	3.	5.4	DEFAULT
19	Batch Oil Tank	443.	10.2	6.	6.	DEFAULT
20s	Reactor Bldg 2 corner stairs	2920.	-2.06	11.4	11.	DEFAULT
21s	Reactor Bldg 1 corner stairs	1380.	-1.23	11.4	8.	DEFAULT
22s	Service Bldg ground	4770.	10.2	6.	11.	DEFAULT
23	Turbing Bldg 2 Stairwell	155.	1.9	14.1	0.77	DEFAULT
24s	Fuel Storage ground	4190.	10.2	3.	5.	DEFAULT
25	SDG Air intake	191.	10.2	7.	3.2	DEFAULT
26	DG2A Air intake	191.	10.2	7.	3.2	DEFAULT

5.2 Assumptions

The model has been constructed using a limited amount of information supplied by TEPCO. As a consequence, results based on this model should be considered estimates and a demonstration of the type of flooding analysis that can be done with GOTHIC. The model may be readily modified to reflect more detailed information as it becomes available. Small flow paths (pipe and cable penetrations, HVAC, etc.) are largely excluded from the model with the exception of intake louvers and roof ventilation located on the diesel generator compartments. It is likely that these smaller potential flow-paths are negligible when compared to the larger flow-path areas presented by doors, hatches, and intake louvers. Detailed information on pipe penetrations and small passageways between rooms was not available. Transport of water into buildings and between rooms is provided by doors, stairwells, and hatches.

Figure 5-1 is a simplified drawing depicting the possible entry points for flood water. Structural drawings provide the location and size of doors, hatches, and stairwells but do not provide information on failure and leakage specifications. The absence of detailed information in this

regard has led to the development of a general suite of doors. The door types are listed in Table 5-3. The analyst may choose the leakage and size for a door and a door failure trip.

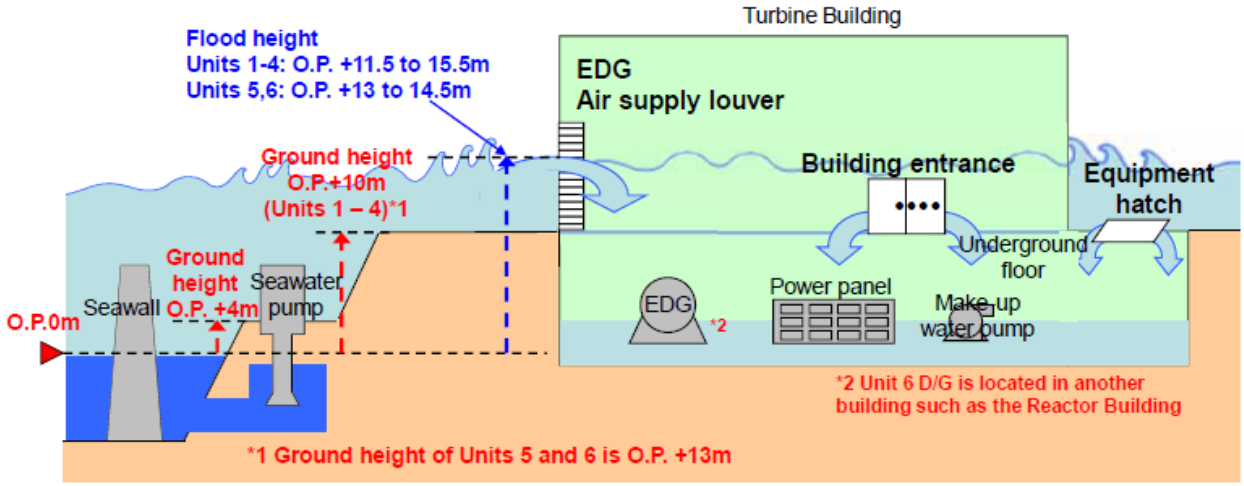

Figure 5-1
Flow Paths into Buildings (TEPCO Accident Report, 2012)

Although GOTHIC has the ability to model the hydrodynamic forces on walls and structures, this model does not included the details of the encroaching tsunami wave necessary to calculate hydrodynamic loads on the exterior of the building. It is assumed that the inundation occurs as a uniform run-up of seawater around 1F1 and 1F2 (TEPCO Accident Report, 2012). Hydrostatic pressure calculations provided by this model should be considered estimates. Thermal behavior is not considered in this model. It is assumed that thermal effects are not significant during the short duration of the flooding transient.

Accumulated water level in 1F1 and 1F2 torus rooms was found to be approximately 4 meters and 3.2 meters above sea-level as reported in (TEPCO 1F1 Torus, 2012) and (TEPCO 1F2 Torus, 2012) respectively. The maximum water level in the torus rooms was determined from TEPCO investigations many months after the accident (EPRI, 2013). Due to the presence of sediments, this water is believed to have penetrated the building from the exterior. The water in the 1F1 torus room was found to be radioactive, suggesting a leak may have formed in the torus. Other postulated sources of water are ingress into the reactor building through small leaks around doors and pipe/cable penetrations from surrounding rooms and buildings and leakage of emergency core cooling systems (ECCS). To this date, the flooding source for the torus rooms is not well known. This model assumes that all the accumulated water in the reactor building basements leaked in from the outside. Any water that leaks into the reactor building will likely drain to the reactor building basement (torus room). The location and size of small entries into the reactor buildings is unknown. In this model leakage into the reactor buildings is attributed to door gaps. A flow path cross-sectional area sufficient to allow the accumulation of water in the amount that was found in the 1F1 torus room is calculated. This calculation is based on the flooding transient implemented and upon the estimate of a flow resistance parameter for the leak.

5.3 Model Description

The model has been constructed with the input of only a few data points that are available. These data points have been made available as TEPCO continues to document their investigations in the aftermath of the event. As more information becomes available in the future this model can be modified to include any necessary changes.

1. Approximately 4 meters water (above sea level) in the 1F1 reactor building basement
2. Approximately 3.2 meters water (above sea level) in the 1F2 reactor building basement
3. Above ground hatches were found to be missing (washed away)
4. Damage to building entrances
5. Damage to intake louvers on diesel generator rooms
6. Maximum flood inundation height of 15.5 meters above sea level around 1F1 and 1F2

1F1 and 2 buildings are represented in GOTHIC by subdivided volumes. Figure 5-3 shows the noding diagram for the model. The noding diagram is shown without flow paths for clarity (there are 160 flow paths and 83 door components). The nodalization for each subdivided volume is sufficient to allow the proper placement of the main features inside each building. This level of detail is enough to account for the placement of walls, passageways, rooms, pits, and large pieces of equipment. The physical presence of finer details (i.e., small equipment, pipes, etc.) is accounted for with volume porosity. A typical value of 95% is used for volume porosity. Dimensions for buildings and flow paths are taken from the supplied drawings. In some instances dimensions were scaled from drawings. Table 5-2 lists the drawings that were used in the construction of this model. There are more than 20 subdivided control volumes in this model therefore only the figures depicting the plan views of 1F1 buildings are included. Figure 5-2 shows a general layout drawing of the 1F1 and 2 buildings.

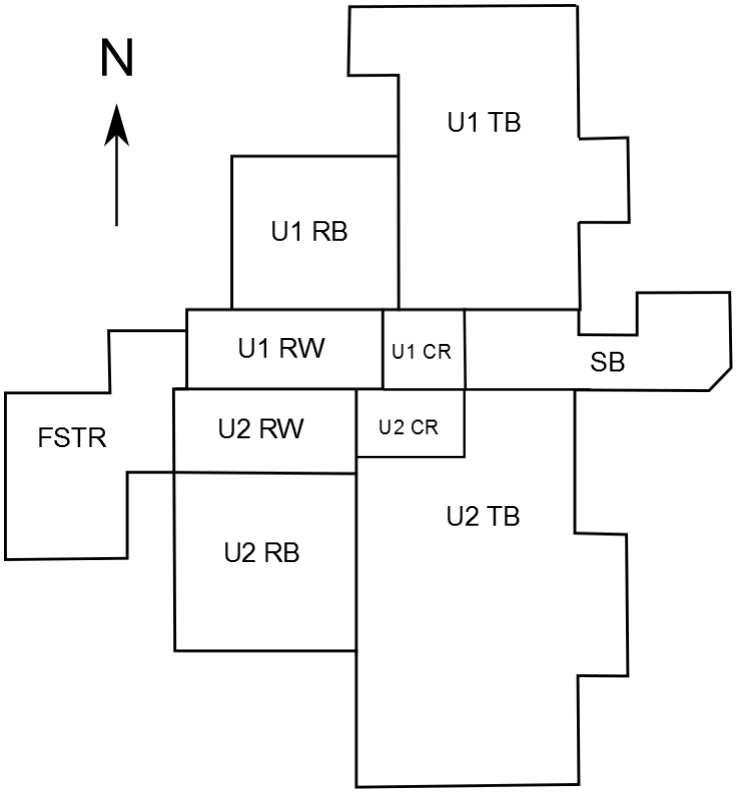

Figure 5-2
General Layout of 1F1 and 1F2

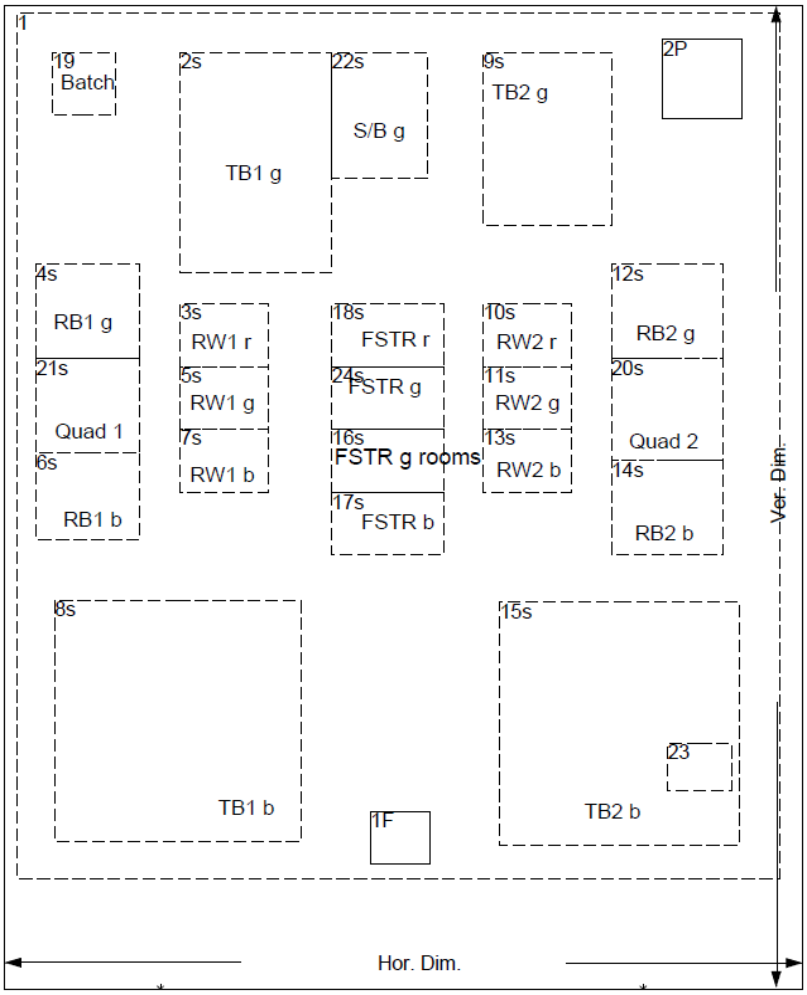

Figure 5-3
Noding diagram

Table 5-2
Reference Drawings

REF	Drawing I.D.	Description
1	G-192409	General Arrangement Turbine Building 1 Basement Floor Plan
2	G-192410	General Arrangement Turbine Building 1 Ground Floor Plan
3	G-192412	General Arrangement Turbine Building 1 Sections SH.1
4	G-192413	General Arrangement Turbine Building 1 Sections SH.2
5	G-192414	General Arrangement Reactor Building 1 Op. -1230 & Op. 10200 Floor
6	G-192417	General Arrangement Reactor Building Sections
7	G-192418	General Arrangement 1B Diesel Generator Room
8	G-192419	General Arrangement Radwaste Building 1 Plans
9	G-192420	General Arrangement Radwaste Building 1 Sections
10	G-199165	1F1 and 1F2 Plot Plan
11	G-199166	General Arrangement Turbine Building 2 Basement Floor Plan
12	G-199167	General Arrangement Turbine Building 2 Ground Floor Plan
13	G-199169	General Arrangement Turbine Building 2 Sections SH.1
14	G-199175	General Arrangement Reactor Building 2 Sections
15	G-199177	General Arrangement Radwaste Building 2 Plans
16	G-199178	General Arrangement Radwaste Building 2 Sections
17	G-199171	General Arrangement Reactor Building 2 Plans SH. 1
18	G-199172	General Arrangement Reactor Building 2 Plans SH. 2
19	1F1/2-FSTR-T	1, 2 FSTR Plans
20	VPF4096-001	1F1 Plot Plan

5.3.1 Turbine Buildings

The maximum reported inundation height of water (15.5 m above sea level) is below the second floor (~17 m above sea level) of the turbine buildings (TB), thus only the ground floor and basement levels are included in the model. In each TB there is a large condenser pit in the basement level. Figure 5-4 is a simplified drawing that shows the turbine/condenser equipment in the turbine building. There is a large opening in the ground floor into the basement level where the turbines are located above the condensers. This opening allows the passage of water from the ground level into the basement. The 1F1 and 2 Control Room (CR) buildings located adjacent to the turbine buildings are built into the same subdivided volumes as the turbine buildings. The basement level of the 1F1 and 2 CR buildings each contain a battery room and an electrical equipment room. The ground level of each CR building houses the cable vault. Flood height results for the CR building rooms are presented in the results section. The turbine buildings house electrical equipment such as switchgears, transformers, emergency control systems, etc.

Flooding water heights in areas containing electrical equipment are included in the results section.

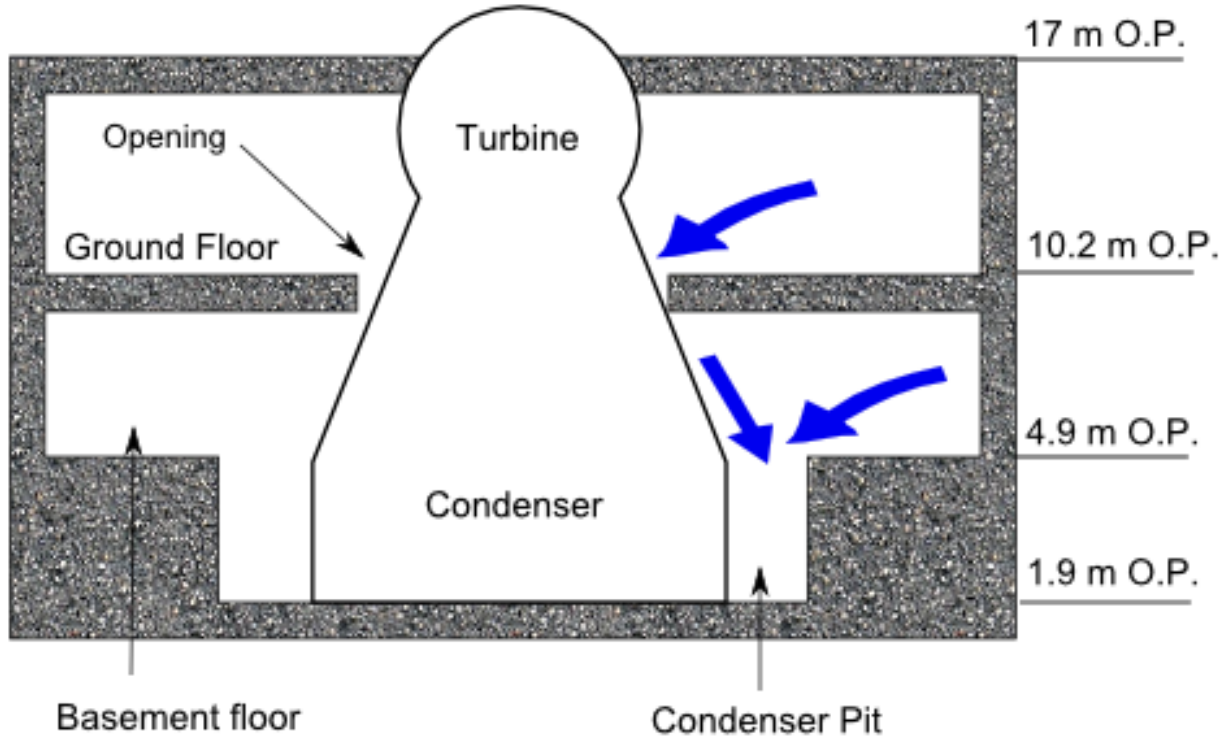

Figure 5-4
TB1 Drawing

The main path for water ingress into the turbine buildings is provided by the large roll-up doors located on the east face of the buildings on the ground floor. The east faces of the buildings were subjected directly to the incoming tsunami water. Because the roll-up doors are so large it is presumed they would present a sizable leakage flow path even when completely closed. However, through communication with TEPCO personnel, it has been reported that the large roll-up door on the ground floor of 1F1 turbine building (TB1-g) was open when the tsunami inundated the area. Thus, this door is modeled as open in the simulation. Visual observation of the 1F2 turbine building shows that the roll-up door was heavily damaged and the bottom third of the door was forced open by the flooding. This door is modeled as 1/3 open in the simulation. Figure 5-5 and Figure 5-6 show the subdivided volumes of the TB ground floor (TB1-g) and basement floor (TB1-b), respectively. Most water that enters the TB ground floor will drain to the TB basement level through a large opening in the floor surrounding the turbine condensers (see Figure 5-4). The TB basement level subdivided volumes have large condenser pits built in. The condenser pits have sumps but due to the loss of offsite power and station blackout, water accumulates in these large pits. There are stairwells from the ground level to the basement level in each TB. These are modeled as open vertical flow paths.

It has been well documented that the diesel generators with intake louvers were completely inundated (TEPCO Accident Report, 2012). The louvers, located at plant grade (10 meters above sea-level), allowed the diesel generator compartments to fill. The doors between the diesel

generator compartments and the turbine building are reported to be very tight, leak resistant doors; however these doors are included with a small leakage flow path in the model. The effects of diesel generator flooding on the plant are severe. The ingress of water into the turbine buildings from the DG compartments depends on the position of doors. It is presumed that the doors are closed, but leak. There are two diesel generators in TB1. They are the Standby Diesel generator (SDG) and the Emergency Diesel generator (EDG). The EDG, located at the south end of TB1-b, is liquid cooled and does not have air intake louvers. There is no direct path for water into the EDG from the outside. However, water may leak through doors connecting the EDG to the TB1-b. These doors are modeled as closed but allow leakage. The SDG, located at the southeast corner of TB1-b, is air cooled and has a large air intake louver located at plant grade. The intake louvers were heavily damaged and the SDG was completely inundated. One diesel generator in TB2, diesel generator 2A (DG2A), is located at the northeast corner of TB2 basement level. There is a door connecting DG2A to TB2-b which is reported to be a strong, tight door that is typically in the closed position. The DG2A has intake louvers which are reported to have been heavily damaged and the DG2A was completely inundated.

Reactor building personnel doors from the turbine building ground floor to the reactor building are supposed to be very tight. These doors are modeled as closed with very little leakage. There most likely are several small potential leak paths into the RB from the TB but these are not included in the model because the location and size of small penetrations is unknown. However, the effect of this leakage can be represented by adjusting the leakage on the RB personnel doors. Flow paths (FP) between the TB and RB can be seen in Figure 5-5. FP 113 and 114 are the RB north and south personnel doors. The FP markers shown in noding diagrams indicate the computational cell the flow paths are connected to. The RB personnel doors are type 10 door components as shown in Table 5-3.

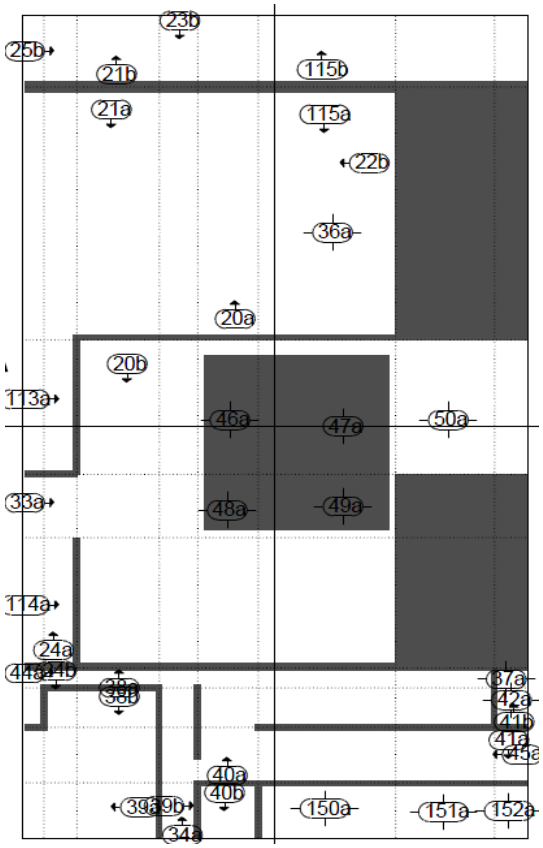

Figure 5-5
TB1-g Plan view

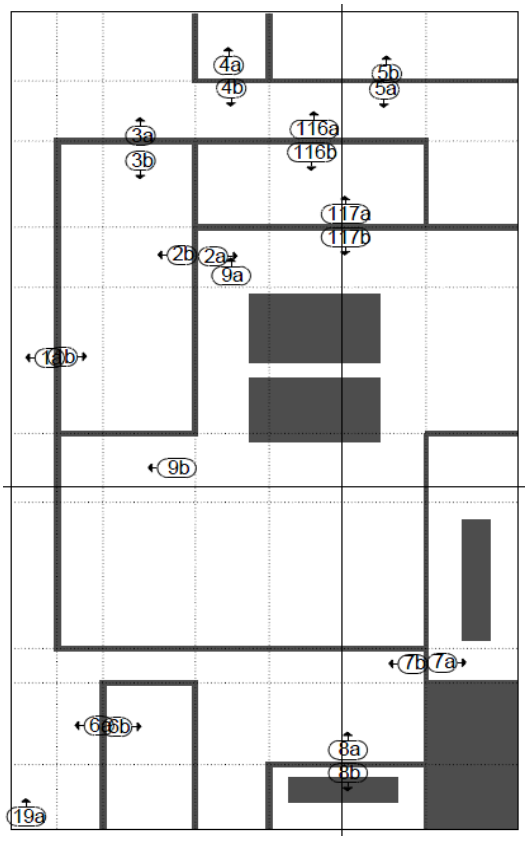

Figure 5-6
TB1-b Plan View

5.3.2 Reactor Buildings

Figure 5-7 and Figure 5-8 show the subdivided volumes of the 1F1 reactor building basement and ground floors (RB1-b and RB1-g). The RB basements have rooms at each corner that each contain a stairwell to the RB ground floor. Water that leaks into the RB ground floor will tend to drain into the basemnet via these stairwells. Each corner room in the RB basement has a door. Only one of these doors is open to the torus side of the RB basement (TEPCO comm.). In addition to stairwells there are also several hatches and penetrations from the RB ground floor into the basement. The location, size, and leakage of these potential flow paths is largely unknown so they are not accounted for in the model. However, due to the large flow path provided by stairs, small penetrations are assumed to be neglible. As previously mentioned, the RB basements were flooded and the accumulated water was measured to be 4 meters above sea-level in the RB1 basement and approximately 3.2 meters in the RB2 basement. The way in which the basements flooded is still unknown. One possibility is from leakage into the RB ground floor through leaking doors or penetrations from the TB or outside. This model accounts for leakage through the reactor bay personnel doors and the large equipment door on each RB. The leakage flow area necessary to flood the RB basements is calculated and presented in the results section.

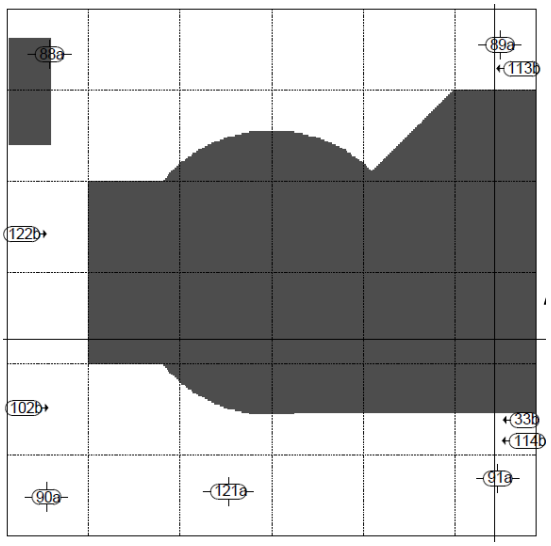

Figure 5-7
RB1-g Plan view

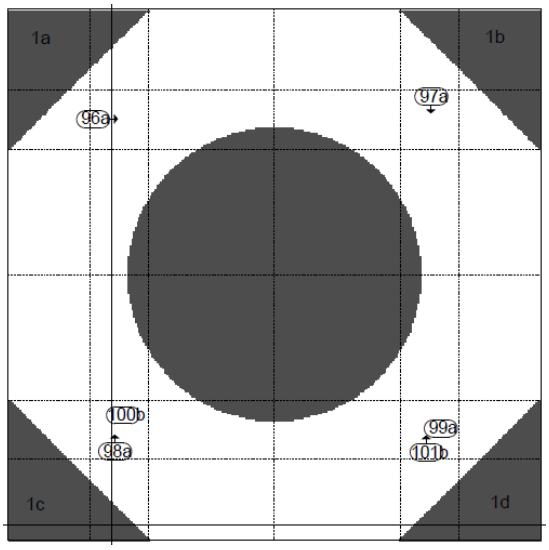

Figure 5-8
RB1-b Plan View

5.3.3 Service Building

Figure 5-9 shows the Service Building (SB) subdivided model. It has been reported that the main entrance door to the SB, shown as flow path 153 in Figure 5-9, failed (TEPCO comm.). This door is modeled with a trip which opens the door when the water level is 0.5 meters above the door threshold. Flow path 45 represents a large door which connects the SB to TB1-g. This flow path may allow a large amount of water to enter the TB since the SB likely flooded completely. The size and position of this door is unknown however the flow path area can be adjusted. In this model it is open.

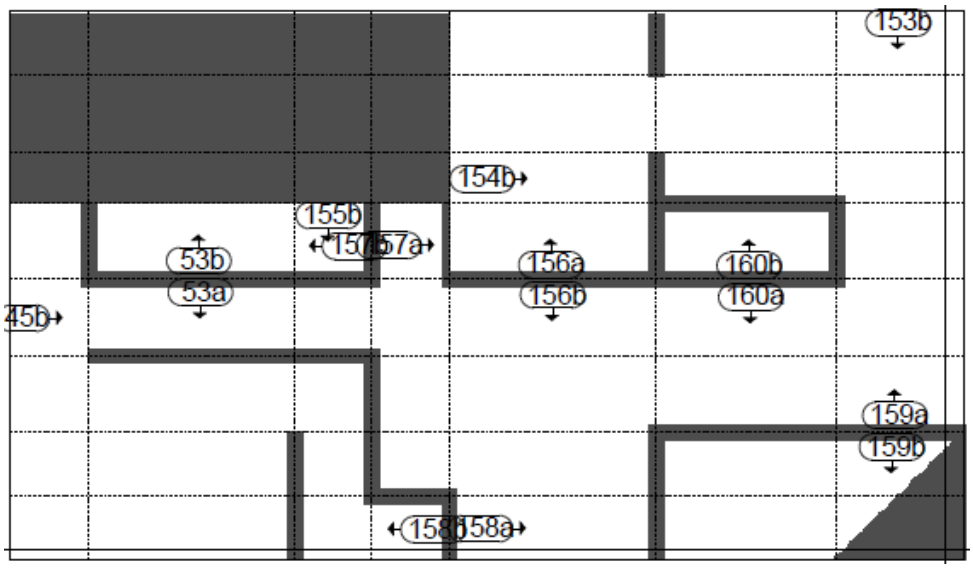

Figure 5-9
Service Building Plan View

5.3.4 Radwaste Buildings

The Radwaste buildings (RW) basement and ground floors are included in the model. Figure 5-10 and Figure 5-11 show plan views of these buildings modeled as subdivided volumes. Flow paths 61 and 136 shown in Figure 5-10 are open pathways to the FSTR building. All other doors are in closed position and allow leakage. A few rooms do not have doors as these rooms are accessible by hatches that are not included in the model.

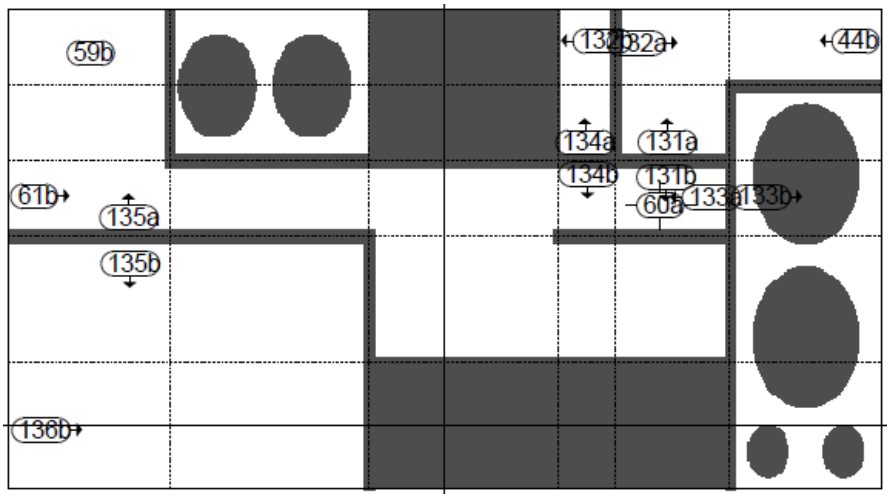

Figure 5-10
RWI-g Plan View

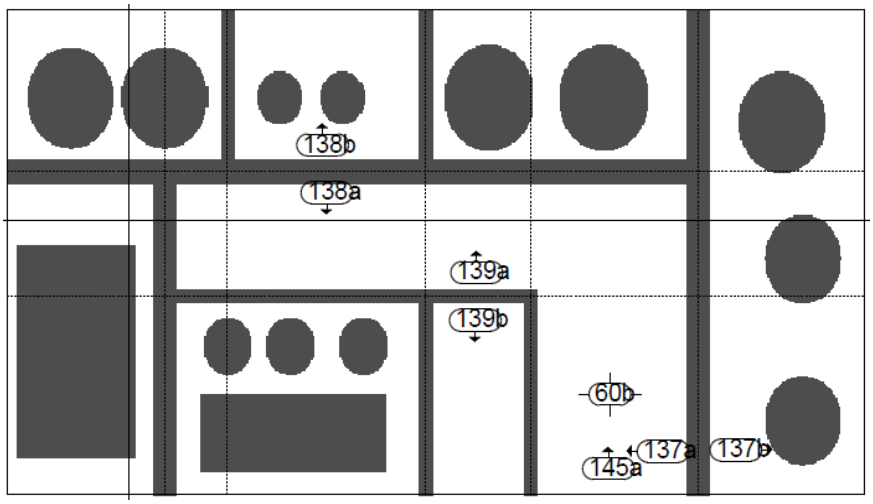

Figure 5-11
RW1-b Plan View

5.3.5 Fuel Storage Building

Figure 5-12 and Figure 5-13 show the Fuel Storage building (FSTR) ground and basement level subdivided volumes. Flow paths 61 and 136, shown in Figure 5-12, are pathways into the RW1 building. Flow paths 144 and 67 are pathways into RW2. There are no flow paths connected to the FSTR-B volume because the rooms therein are accessible by hatches that are not modeled.

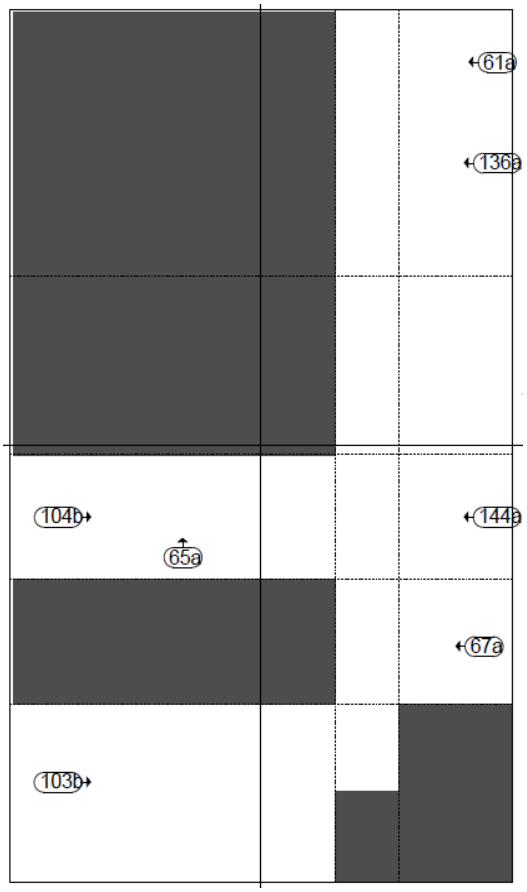

Figure 5-12
FSTR-G Plan view

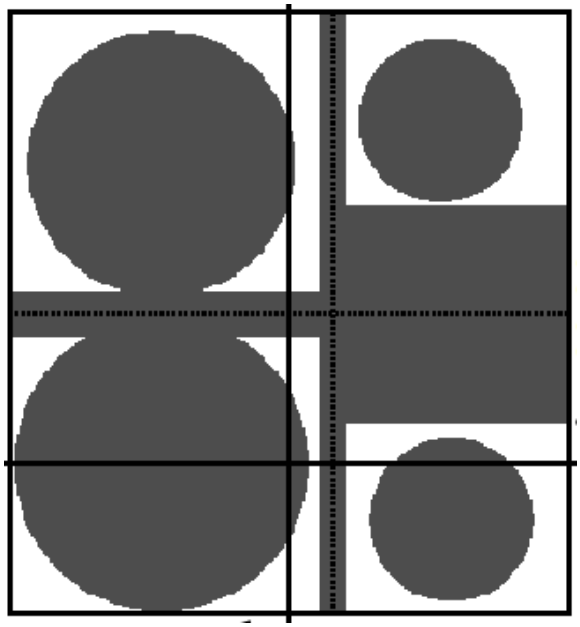

Figure 5-13
FSTR-B Plan View

5.3.6 Boundary Conditions

Flow BC and pressure BC are used to simulate conditions of flooding and atmosphere conditions. A pressure boundary condition is connected to the "basin" control volume such that it fills at constant atmospheric pressure. The flooding is implemented using a control variable function which regulates flow to match the known tsunami height. A flow boundary condition delivers flow proportional to this control variable. The tsunami height and transient are based on tidal height measurements (TEPCO Tsunami Survey, 2012). The temporal behavior of the tidal fluctuations is preserved in the implementation. The data was fit with a sine curve and the amplitude has been scaled to match the inundation heights reported around 1F1 and 1F2. The flooding transient built into the model utilizes the first positive wave of the function. The flooding is implemented using a table function, control variable, and flow boundary condition. The control variable regulates flow in the boundary condition in proportion to the difference between the specified height and the actual height. In this way the required height can be produced by a boundary flow condition with a negative feedback mechanism. Figure 5-14 shows a comparison of the inundation height (LL1), implemented as described above, to the desired height (DC1T).

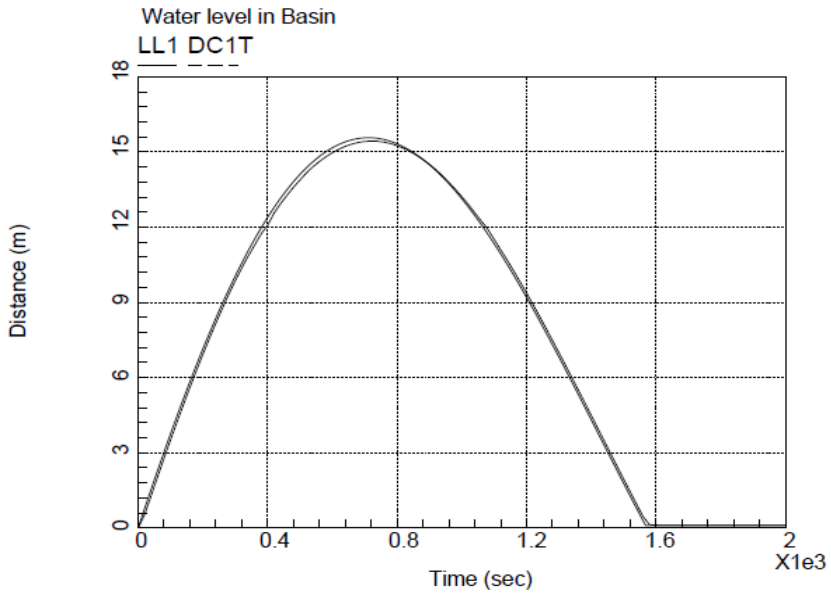

Figure 5-14
Inundation Height

5.3.7 Flow Paths

Louvers, vents, and hatches are implemented with flow paths. Leakage around doors is due to gaps around the perimeter of the door. It is assumed that all doors leak to some extent and this depends on the type of door. The amount of leakage is adjusted by specifying the loss coefficient associated with the closed position of each door. Table 5-3 lists the doors used in this model. For most purposes a leakage gap of 1 cm around the door perimeter is used. An exception is the reactor equipment doors. The leakage area for these doors has been calculated to allow the accumulation of water in the reactor building basements as measured after the event and reported in (TEPCO 1F1 Torus, 2012) and (TEPCO 1F2 Torus, 2012)**.** Doors can be set to trip open in

failure scenarios. However, because detailed information on door specifications is unavailable, the majority of doors in this model are set to either the open or closed position at the start of the transient. Internal doors that are called out in plant drawings are assumed to be closed as this is their default position (TEPCO comm.).

Table 5-3
Valve/door types

Valve/Door Types											
Valve Type #	Description	Valve Option	F Open Area (m2)	Opn Trv Crv	Cls Trv Crv	Full Open Cd	Flow Char Coef A	Flow Char Coef B	Flow Char Coef C	Flow Char Exp	Cd Mult Crv
1	Leaking Door	T OPEN	2.	2T		1.					3T
2	Sealed Door	Q OPEN	2.			0.59					
3	Leaking Double Door	T OPEN	3.	2T		1.					4T
4	Small RSD	T OPEN	9.	2T		1.					5T
5	Med RSD	T OPEN	15.	2T		1.					6T
6	Large RSD	T OPEN	30.	2T		1.					7T
7	Sm. Equipment Hatch	Q OPEN	4.			0.59					
8	Lg. Equipment Hatch	Q OPEN	16.			0.59					
9	Reactor Bay Equipment Door	T OPEN	27.	2T		1.					8T
10	Reactor Bay Personel Door	T OPEN	2.	2T		1.					9T
11	Conveyor Door	T OPEN	9.	2T		1.					10T
12	Diesel Gen. Leak Adj.	Q OPEN	9.			0.59					
13	Large RSD closed	T OPEN	30.	2T		1.					11T
14	Large RSD half open	T OPEN	30.	2T		1.					12T
15	Service Bldg door	T OPEN	16.	2T		1.					13T

5.4 Analysis

The purpose of this analysis is limited to determining the flooding behavior based on the extent a door is leaking/open and the door location. The amount of water flow and accumulation to any "room" in the model is calculated by GOTHIC. Hydrostatic loads and pressure differentials on doors may also be calculated using GOTHIC control variables. Only the accumulation of water during the flooding transient is presented herein. In order to avoid presenting the results of multiple combinations of door statuses (the actual status of doors in the model is largely unknown), the results of a single representative case are presented. The parameters for this case are described below.

5.4.1 Parameters

1. Diesel Generator doors are closed with leakage allowed. A significant source of water ingress was through diesel generator compartments. These were inundated severely but doors between DG and turbine buildings may have prevented leakage. It is unknown if the DG doors failed.
2. 1F1 Turbine Building (TB-1) ground level roll-up door is open. This door is reported to have been open when the tsunami water inundated the area (TEPCO comm.). The remaining external TB-1 doors are closed but allow leakage.
3. 1F2 Turbine Building (TB-2) ground level roll-up door is 1/3 open. This door appears to have been damaged during the flooding. The remaining external TB-2 doors are closed but allow leakage.

4. Reactor Building equipment doors are closed but allow leakage.
5. Reactor Building personnel doors are closed but allow leakage.
6. Each Reactor Building sub-basement has four entrances into basement (torus room). One quadrant of each mid-basement is open to the torus room in each RB basement.
7. Service Building (SB) Main entrance failure. SB double doors trip open when the water height is 0.5 meters above the door threshold.
8. Door between SB and TB-1 is halfway open (8 m^2). The flow area between the SB and TB-1 ground floor determines in part the flooding in the TB-1 ground floor.
9. Door between TB1 and TB2 ground level is closed but allows leakage.
10. Door between TB1 and TB2 basement level is closed but allows leakage.
11. Radwaste conveyor doors to the FSTR are open.
12. FSTR external doors are closed but allow leakage.

5.5 Results

5.5.1 1F1 Reactor Building

Three cases were considered for the 1F1 RB. In the first case, leakage into the RB ground floor is limited to small leakage gaps around the personnel doors and equipment door. In this case the accumulated water height in the reactor basement (torus room) is limited to 0.37 m from the basement floor (-0.86 m relative to sea level) which is much less than the measured amount of 5.23 m (4 m relative to sea level). Figure 5-15 shows the results of case 1.The measured amount of water for the 1F2 RB torus room is ~ 5.26 m from the basement floor. It may be a coincidence that both torus rooms are found to have similar amounts of accumulated water or it may be that they flooded in the same way and because the geometry of each torus room is similar the outcome of flooding is nearly the same.

In the second case, the gap leakage area for the personnel doors is calculated by trial and error to allow the measured water height to accumulate (5.23 m in RB1 torus room). The RB equipment doors are modeled with a 1 cm leakage gap around the perimeter. For ingress into the RB from the TB, the leakage area of the RB personnel doors is adjusted. In order to flood the torus room to a height of ~ 5.43 m, a leakage area for each personnel door of 0.23 m^2 is needed. This amounts to a leakage gap of ~3.8 cm around the door which is unlikely. If it is assumed that the 1F2 RB torus room flooded in the same manner as 1F1 then this scenario is more unlikely since the same treatment of doors for 1F2 yielded a height of only 1.36 m from the basement floor. The results for case 2 are shown in Figure 5-16.

The exterior conditions of RB1 and RB2 would have been similar since the tsunami inundation was likely the same for both buildings. Both the 1F1 and 2 RBs have large equipment doors on the ground floor. These large doors may present a significant leakage area. In case 3, the leakage area of the equipment door is adjusted to allow the measured amount of water to accumulate. A 0.5 cm leakage gap is applied to the personnel doors. The leakage area for the equipment doors is calculated to be 0.91 m^2. This amounts to a gap of ~5.5 cm on the sides and bottom of the door (inundation height is below the top of the door). This would be possible if the equipment door was pushed open by the water which depends on the type/strength of the door. Figure 5-17 shows the results for case 3. The dashed curve in Figure 5-17 is the water depth in the 1F2 RB

basement. The depth calculated is less than was measured. If the basement flooding was due to leakage around the equipment doors a larger leak area is needed for 1F2.

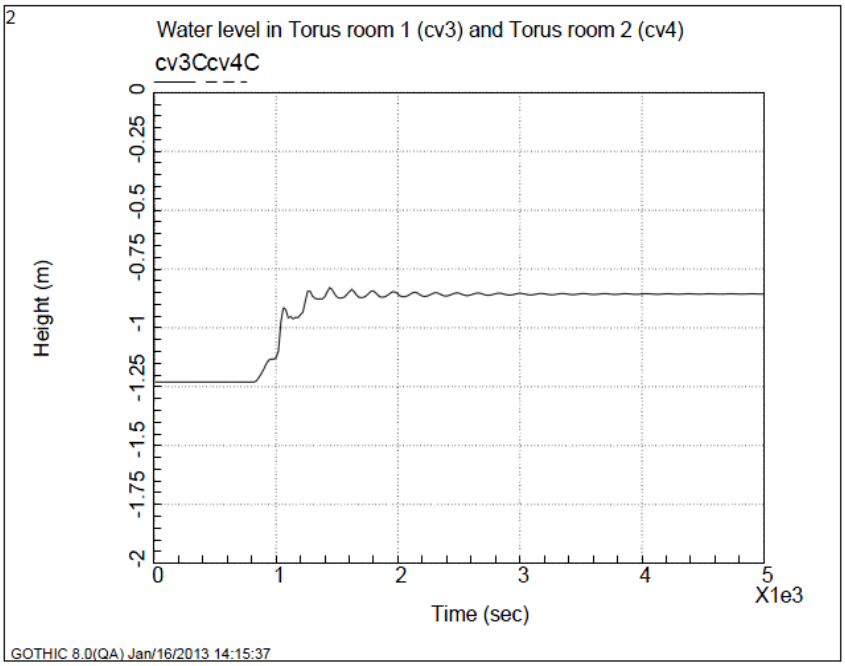

Figure 5-15
RB1 Torus Room Accumulated Water Height: Case 1

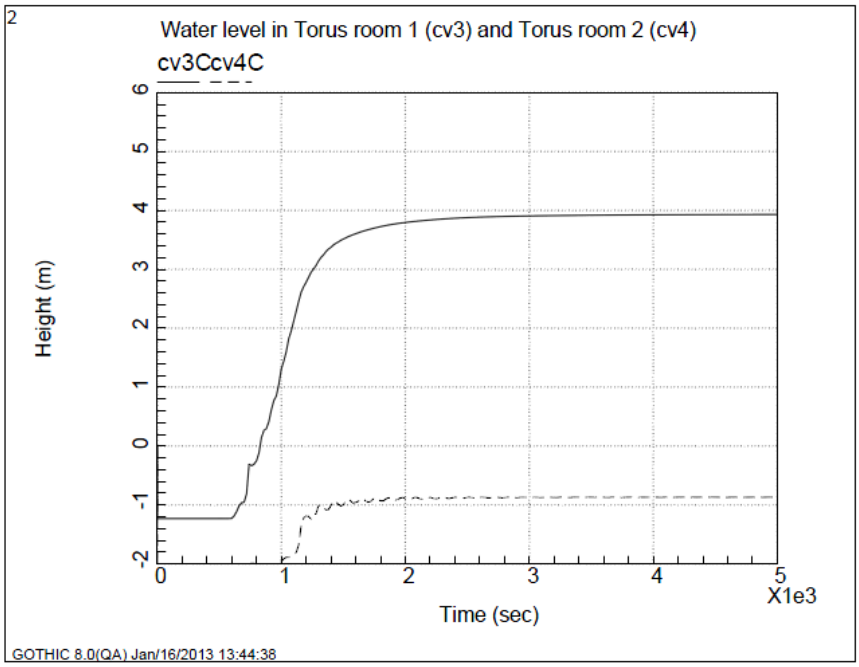

Figure 5-16
RB1 Torus Room Accumulated Water Height: Case 2

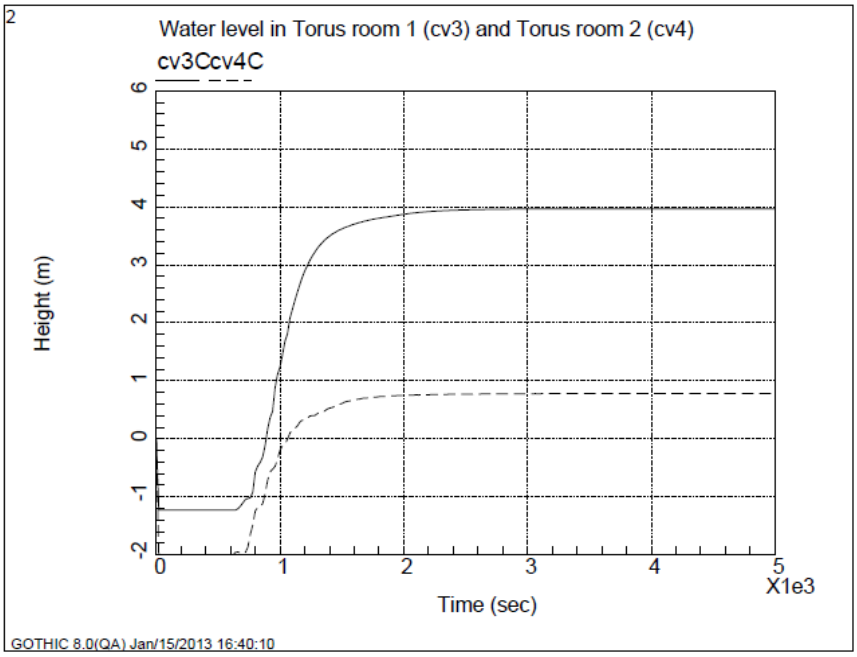

Figure 5-17
RB1 Torus Room Accumulated Water Height: Case 3

5.5.2 1F1 and 1F2 Turbine Buildings

As previously mentioned, the primary entrance points for water into the turbine buildings are the large roll-up doors located on the ground floors. An additional source of water for the 1F1 TB is the connection with the service building (SB). It will be shown in the next section that a large amount of water enters the SB via a failed door and then flows into the TB through a door that connects the two buildings. The results presented here are mainly for the 1F1 TB along with flood height results for areas containing electrical equipment in the 1F2 TB.

Figure 5-18 shows the flow into the TB via the large roll up door and through the connection with the SB. Flooding of the 1F1 TB is more extensive than in 1F2 TB because the roll-up door is open and there is an additional source of water via the SB. Figure 5-19 show the liquid depths inside the TB near these doors. Curve "58" of Figure 5-20 is the liquid depth in the SWGR (north section of the 1F1 TB ground floor) where the large roll-up door (RSD) is located. As can be seen, the SWGR is flooded extensively as soon as water enters the building. Curve "14" of Figure 5-21 is the liquid depth in the south section of the 1F1 TB ground floor. The door leading to the SB is located in this area.

Most of the water that enters the 1F1 TB ground floor drains to the basement level via stairwells and the large opening in the floor surrounding the turbine condensers. A large amount of water flows into the basement through the opening around the condensers as can be seen in Figure 5-22.

As mentioned in the Section 5.2, hydrostatic loads can be calculated using GOTHIC. For this model the hydrostatic load for a door is calculated by capturing the water height on each side of a door using control variables. Figure 5-23 shows the net hydrostatic load on the 1F1 RB north personnel door. The maximum load is approximately 14.5 kN.

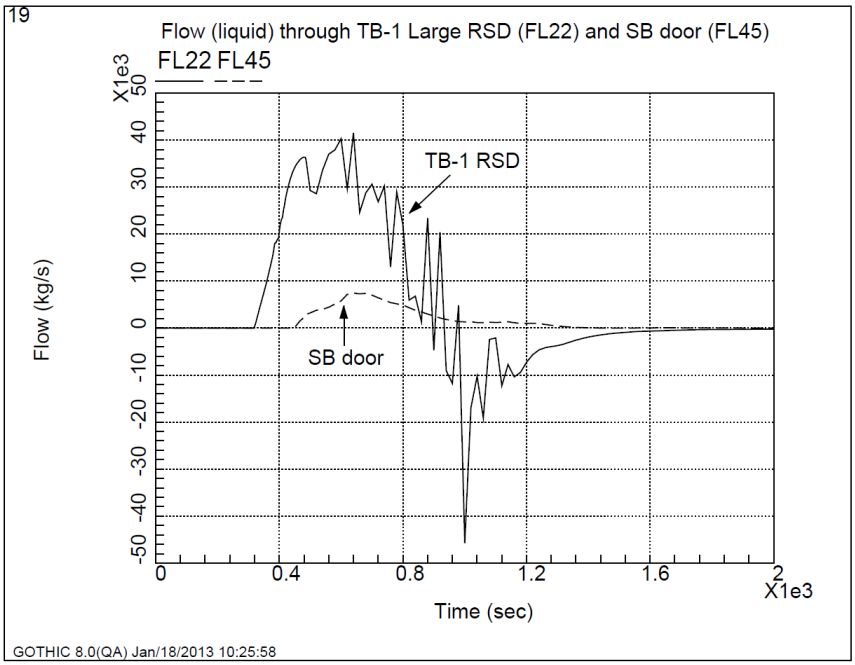

Figure 5-18
Flow through TB-1 Large RSD and SB Door

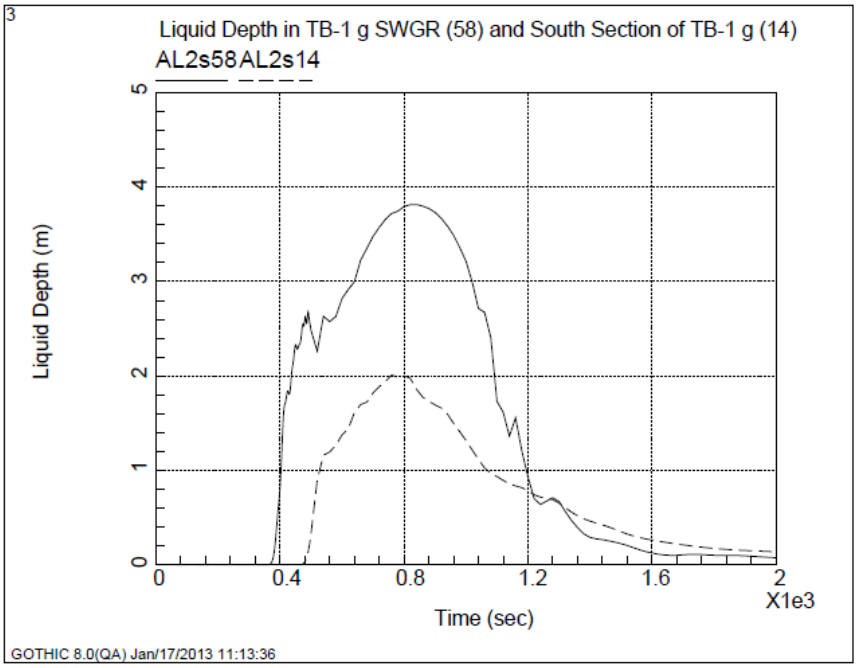

Figure 5-19
Liquid Depth in TB-1 g SWGR and South Section of TB-1 g

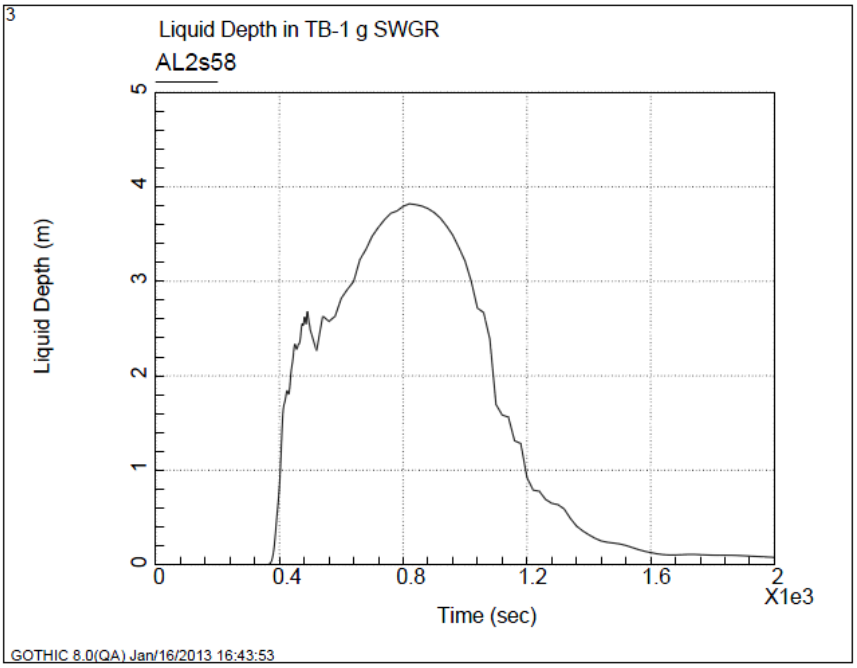

Figure 5-20
Liquid Depth in 1F1 SWGR

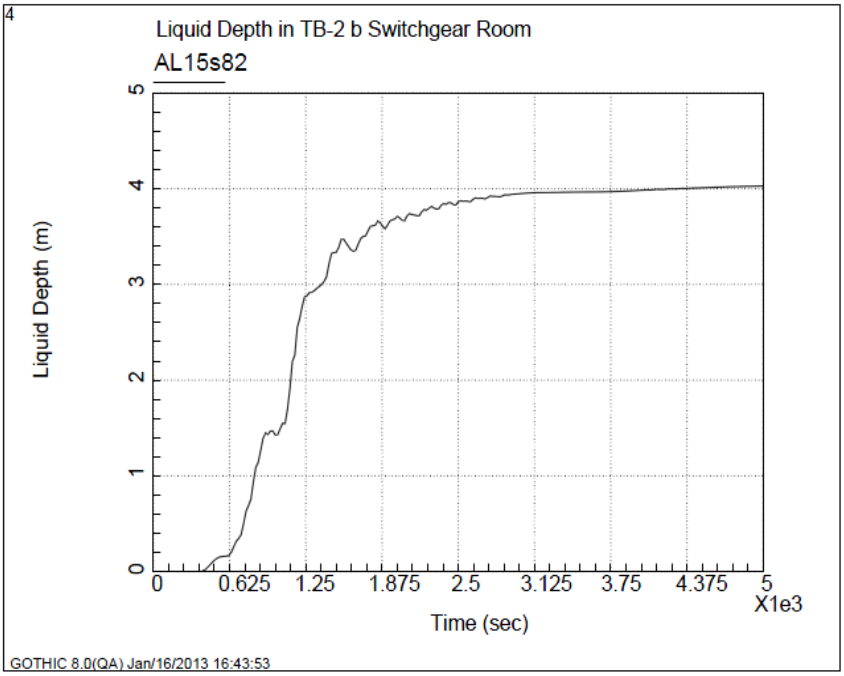

Figure 5-21
Liquid Depth in 1F2 SWGR

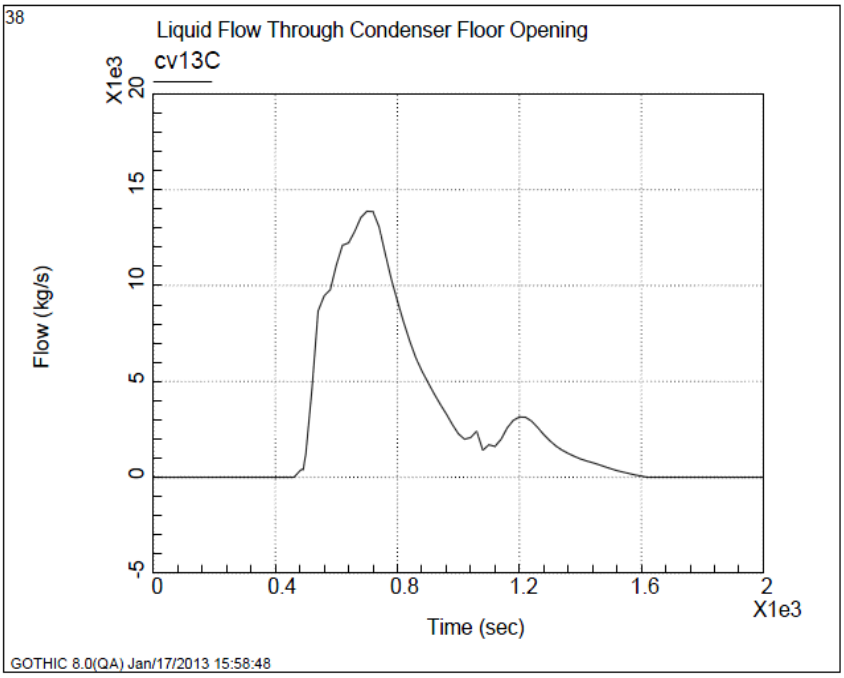

Figure 5-22
Flow into TB1-b around the Condensers

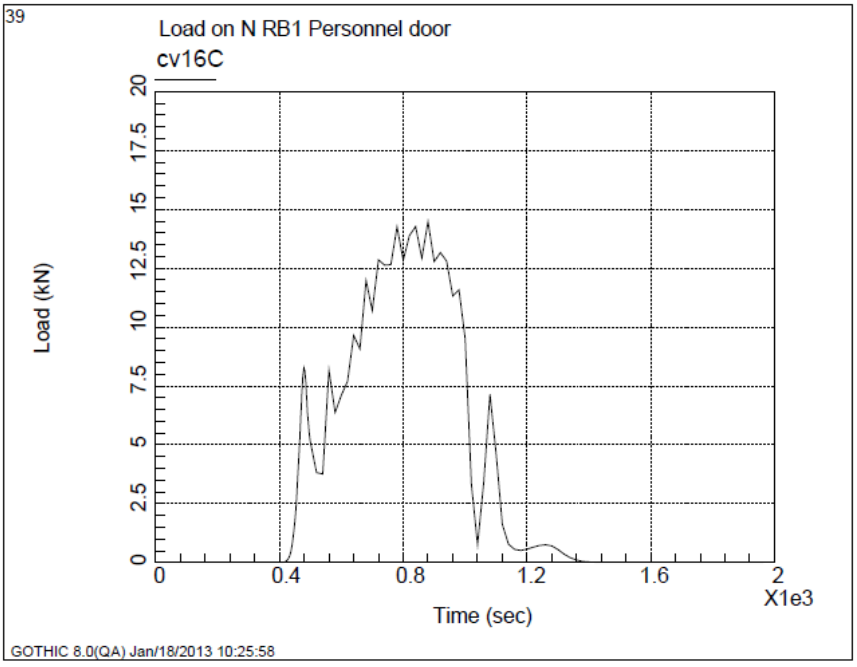

Figure 5-23
Load on 1F1 RB N Personnel Door

5.5.3 1F1 and 1F2 Service Buildings

The large external door (main entrance) of the Service building (SB) is known to have failed. It is reported that the doors are made of glass. The door likely failed due to the pressure differential across the door that developed as the height of water outside the building increased. A scenario such as this is modeled in GOTHIC using a trip that is associated with a door component. The trip has a set point of 0.5 m (liquid level) above the door threshold. Thus, when the flood water reaches this height the door is opened completely. Figure 5-24 shows the liquid flow through the SB main entrance. The flooding speed and length of transient make it difficult to resolve the trip action from Figure 5-24. Comparison of the pressure differential (Figure 5-25) across the door with the door flow (Figure 5-26) reveals that the door remains closed until a pressure differential of 4.9 kPa develops across the door, corresponding to a liquid height of 0.5 m above the door threshold. The figures indicate this happens 340 seconds from the start of the transient. The small amount of flow before this time is due to leakage. The average liquid level height for all the cells in the SB control volume is shown in Figure 5-27.

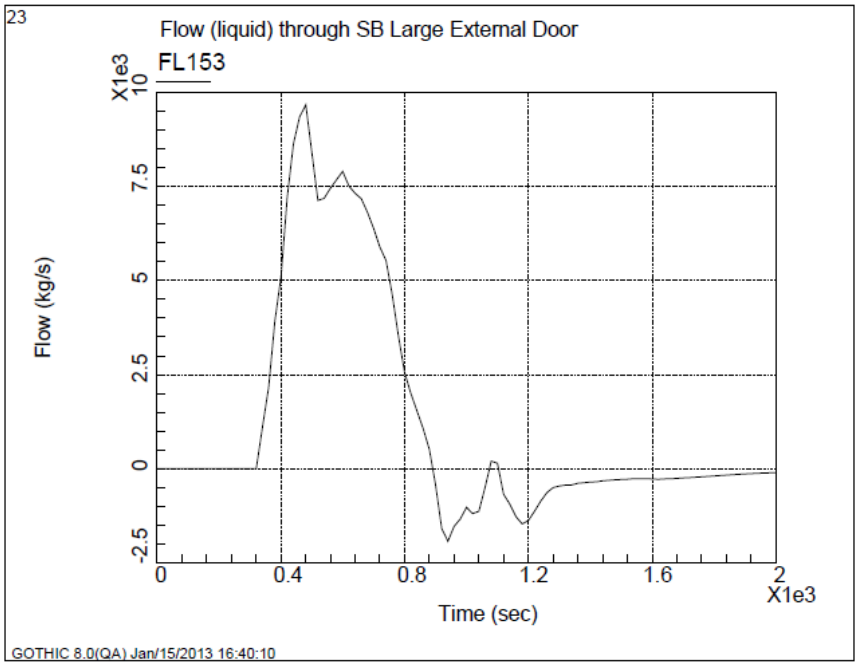

Figure 5-24
Liquid Flow through SB Large External Door

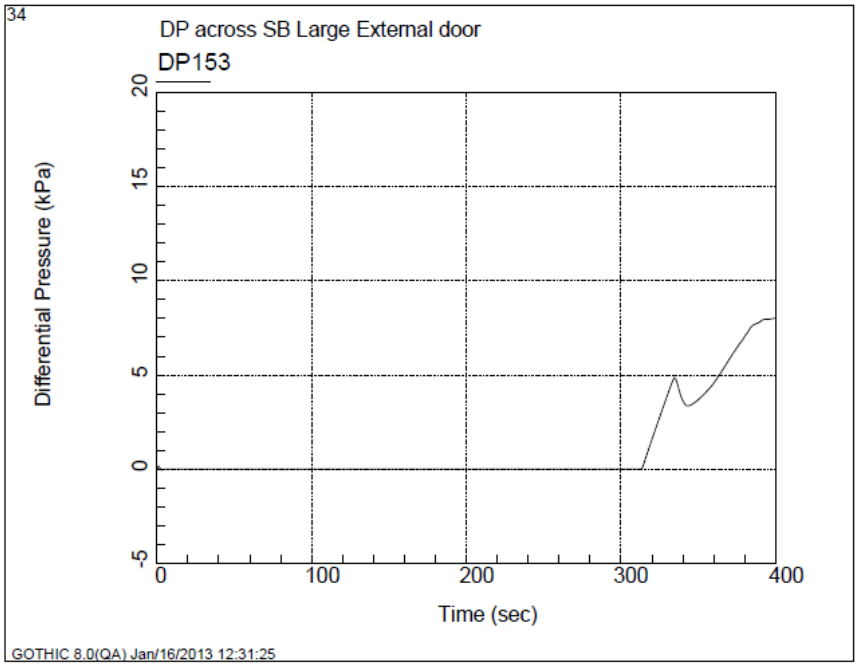

Figure 5-25
Differential Pressure across SB Main Door

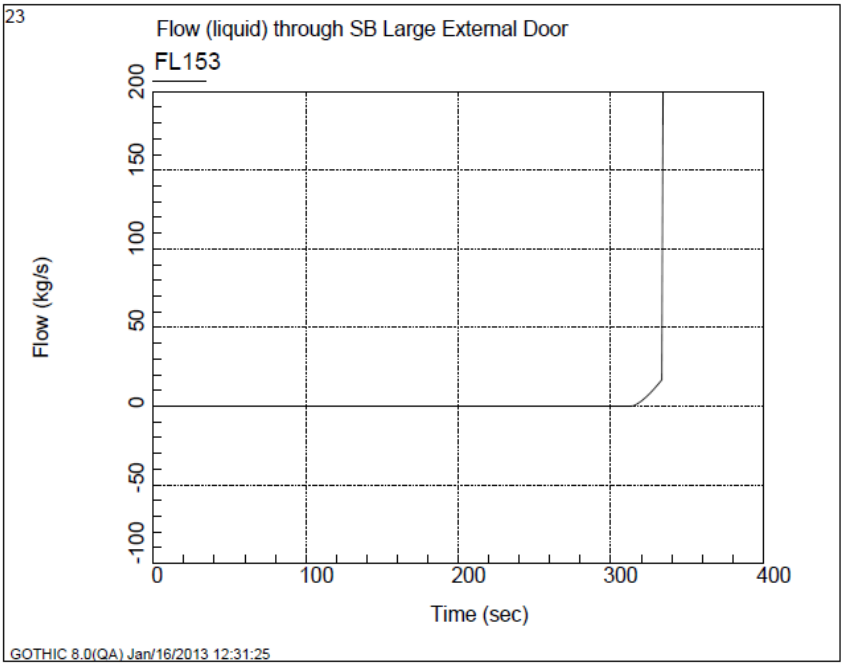

Figure 5-26
Liquid Flow through SB Large External Door

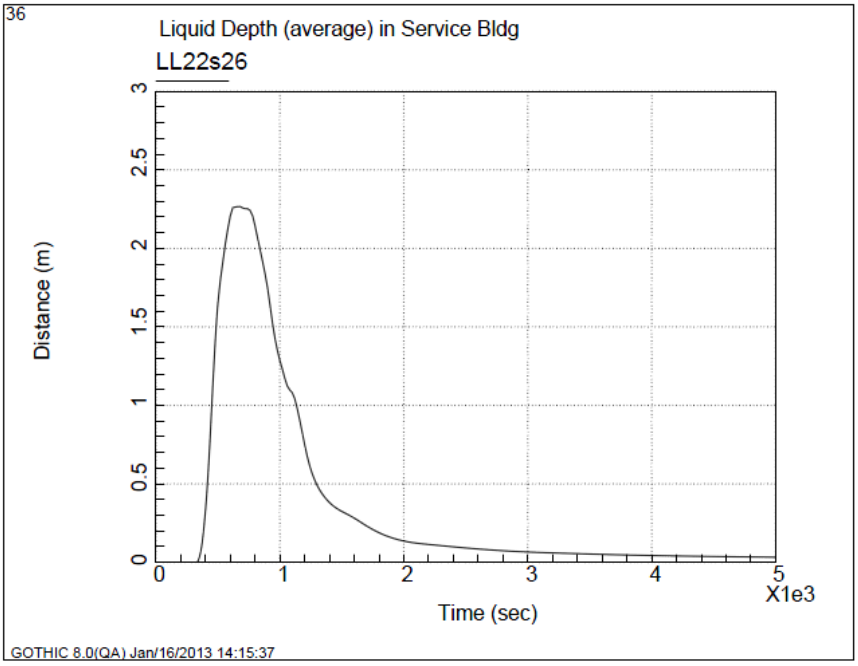

Figure 5-27
SB Average Liquid Depth

5.5.4 Diesel Generators

The emergency diesel generator (EDG) and diesel generator 2A (DG2A) are both located in rooms that have intake louvers and roof vents at plant grade (10 m). The low elevation of the intake louvers and roof vents allows water to rush into the diesel generator rooms and fill them almost completely. The interesting feature of the diesel generator rooms is the leakage associated with the doors between them and the adjacent turbine buildings. The leakage of these doors would allow additional ingress of water into the turbine building basements. In this model it is assumed that the doors remain closed, as they are reported to be "strong" (TEPCO comm.), but leakage through gaps around the perimeter is allowed. The gap around these doors is assumed to be 5 mm.

The door from DG2A (1F2) leads directly into the switchgear room (SWGR) of the 1F2 TB basement. Thus, if this door leaks then the SWGR will begin to flood immediately following DG2A flooding. Figure 5-28 shows the liquid flow through the DG2A door gaps into the SWGR. Figure 5-21 above showed the liquid depth in the SWGR. If the DG2A door does not leak there is a delay in time to when the SWGR begins to flood. Figure 5-29 is a closer look at the liquid depth in the SWGR as it begins to flood. Notice it starts to flood at ~370 seconds. Figure 5-30 shows the liquid depth in the SWGR when the DG2A door does not leak. In this case the SWGR begins to flood at ~600 seconds. There is approximately a 3.8 minute difference for the onset of flooding to the SWGR depending on the leakage from DG2A.

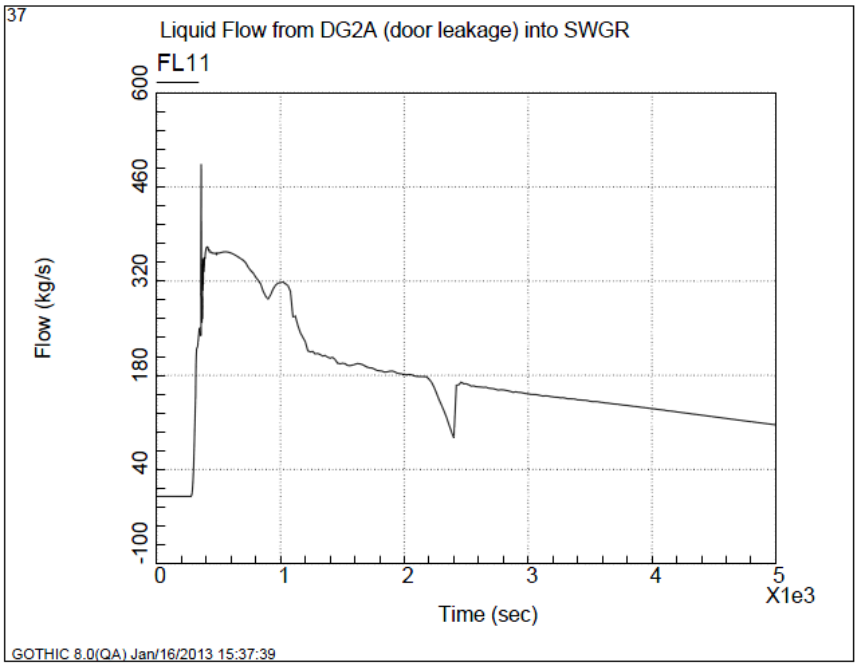

Figure 5-28
DG2A Leakage into SWGR

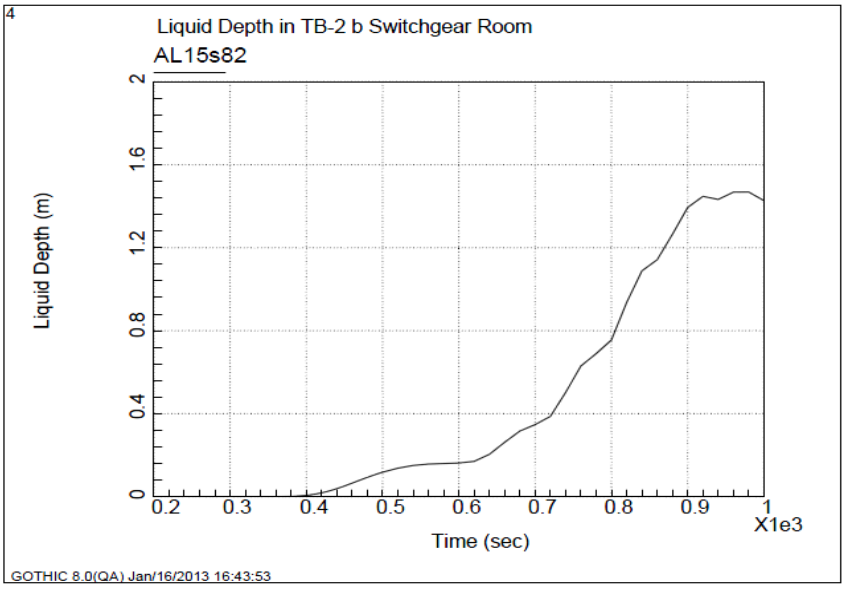

Figure 5-29
Liquid Depth in 1F2 SWGR with DG2A Leakage

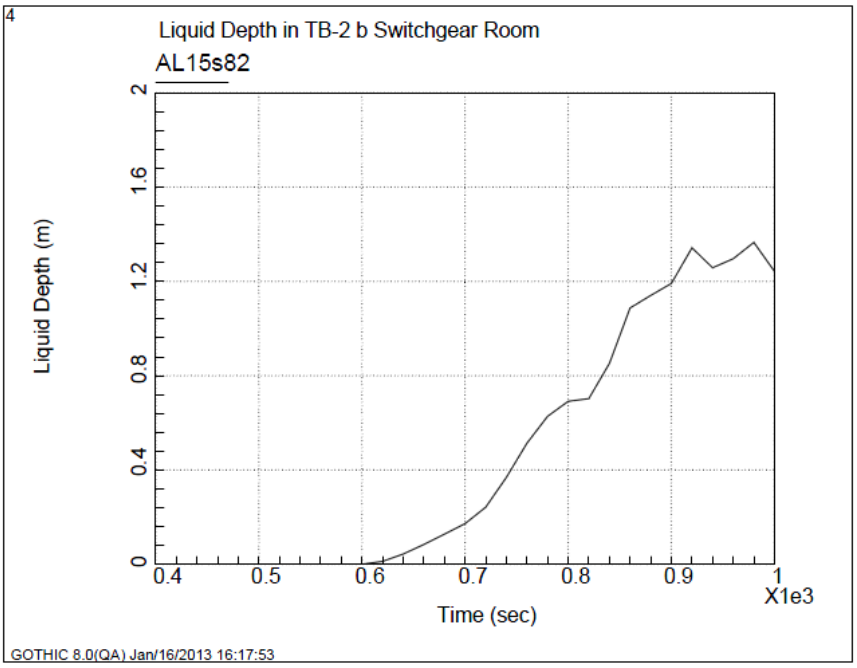

Figure 5-30
Liquid Depth in 1F2 SWGR without DG2A Leakage

5.5.5 1F1 Control Building

The sections of the control building (CR) that are affected by the flooding are the ground and basement levels. The cable vault room, located on the ground floor of the CR, begins to flood early in the transient because there is little to impede flow entering from the SB. Water has only to travel across the SB ground floor before it reaches the area of the cable vaults. The door between the cable vault and the SB is modeled as a type 3 (see Table 5-3) leaking double door. The leakage gap around the perimeter is assumed to be 5 mm on the sides and 1 cm for the bottom. It is unknown if this door failed but it is assumed to remain closed during the transient. Figure 5-31 shows the liquid depth in the cable vault.

The CR basement contains an electrical equipment room and a battery room. The electrical room is open to the TB1 basement level. The door between the electrical room and the battery room is modeled the same as the cable vault door. Figure 5-32 shows the liquid depth in the electrical equipment room. It can be seen from Figure 5-33 that water leaks into the battery room until a liquid depth equal to that in the electrical room is reached. Water that accumulates in the basement tends to level out among the various rooms and remains as there is no drainage feature included in the model.

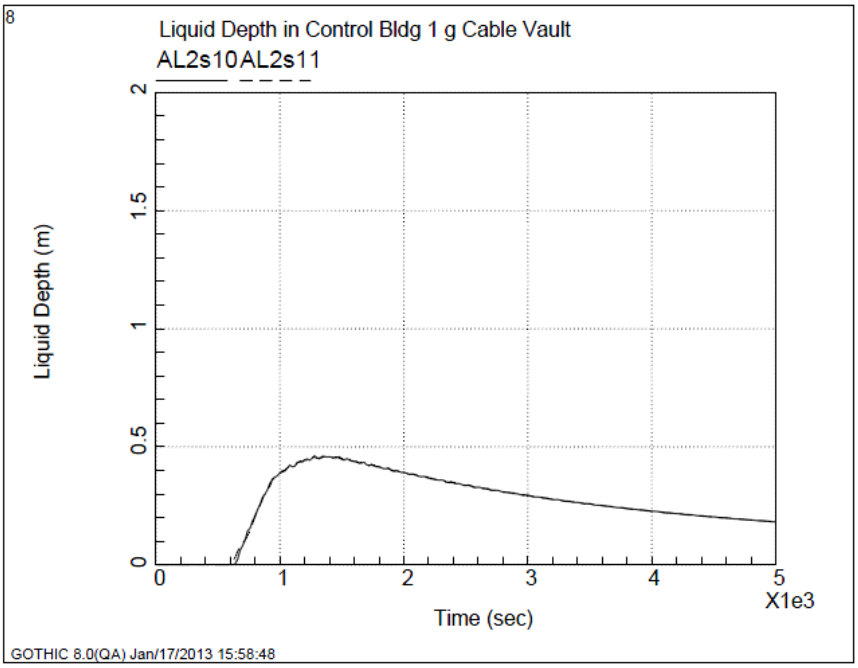

Figure 5-31
Liquid Depth in CR1 Cable Vault

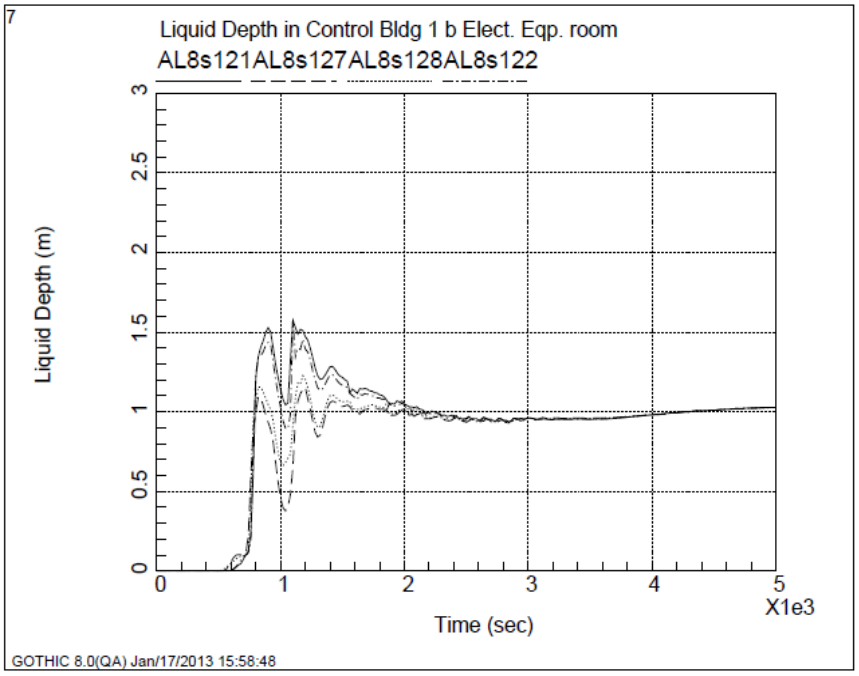

Figure 5-32
Liquid Depth in CR1 Electrical Equipment Room

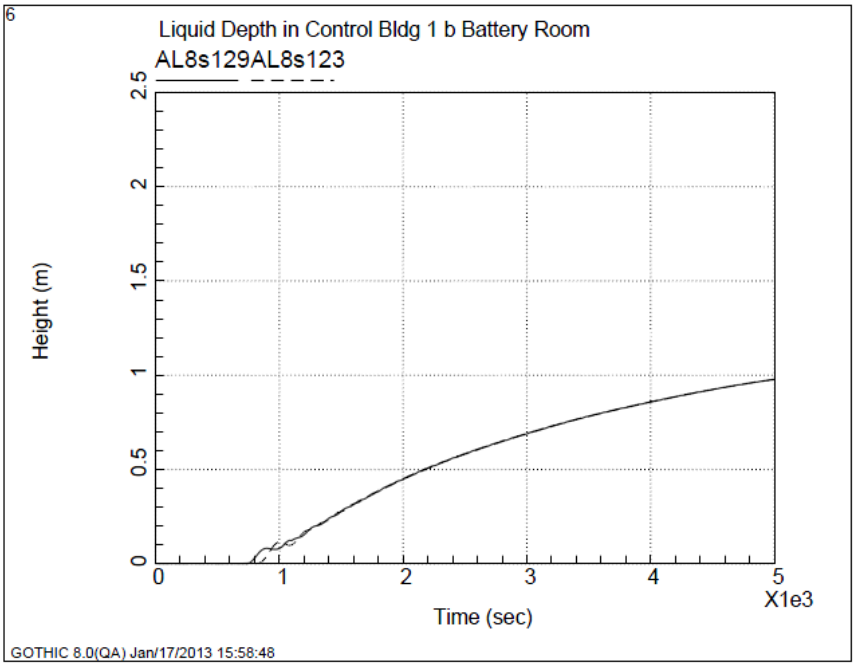

Figure 5-33
Liquid Depth in CR1 Battery Room

5.5.6 1F1 Radwaste Building

The Radwaste Building (RW) has three points of entry. There is a leaking double door from TB1-g on the east side and two open doors to the Fuel Storage Building (FSTR) on the west side. The RW ground floor begins to flood ~490 seconds into the transient. Figure 5-34 shows the liquid depth in the RW ground floor. Water first enters from the east side where a door connects the RW with the 1F1 TB. The flow through this door is small as the door is closed but allows leakage. The two doors on the west side to the FSTR are open and are large enough to move equipment through. They are modeled with 9 m^2 of flow area. Water enters through these doors after it has leaked into the FSTR.

Water that enters the RW ground floor tends to drain into the RW basement by way of a stairwell between the floors. Figure 5-35 shows a plot of liquid flow down into the basement through the stairwell. Figure 5-36 shows the liquid depth in the RW basement. Notice curve "15" (dashed line) on this graph increases slowly. This is the depth in a room on the east side of the basement modeled with a closed, leaking door. Water that drains into the basement accumulates there and eventually levels out among all the rooms with leakage.

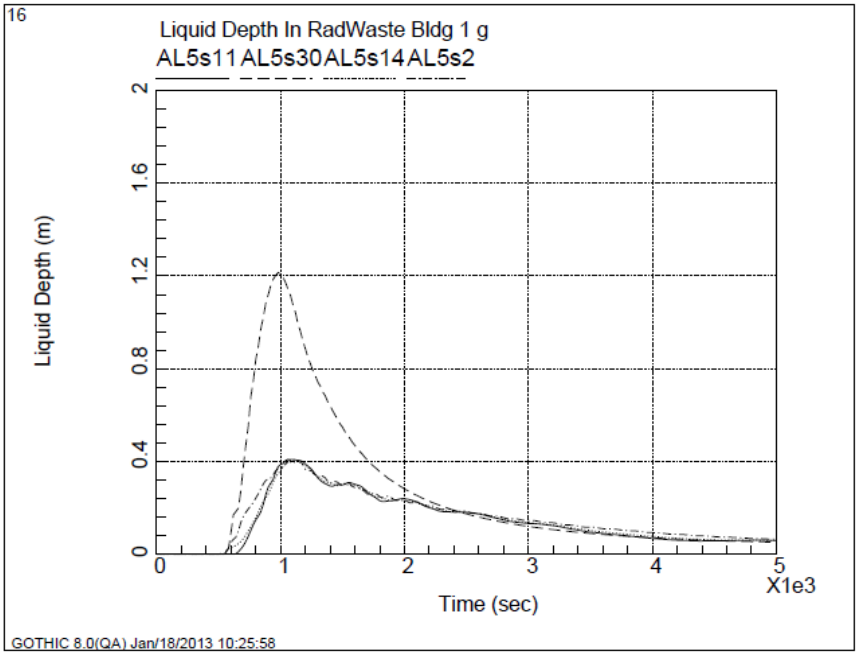

Figure 5-34
Liquid Depth in RW1 Ground Floor

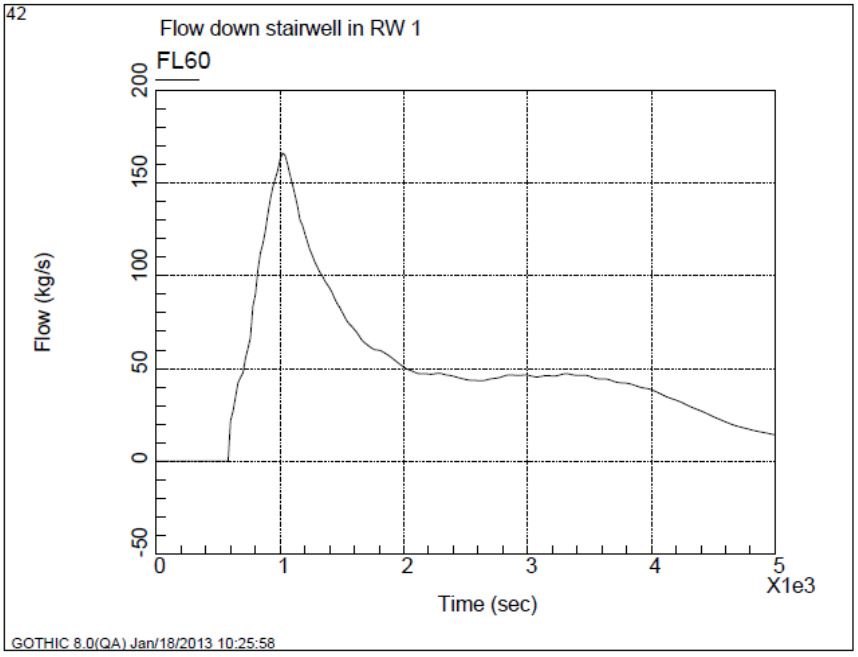

Figure 5-35
Flow Down Stairwell in RW-1

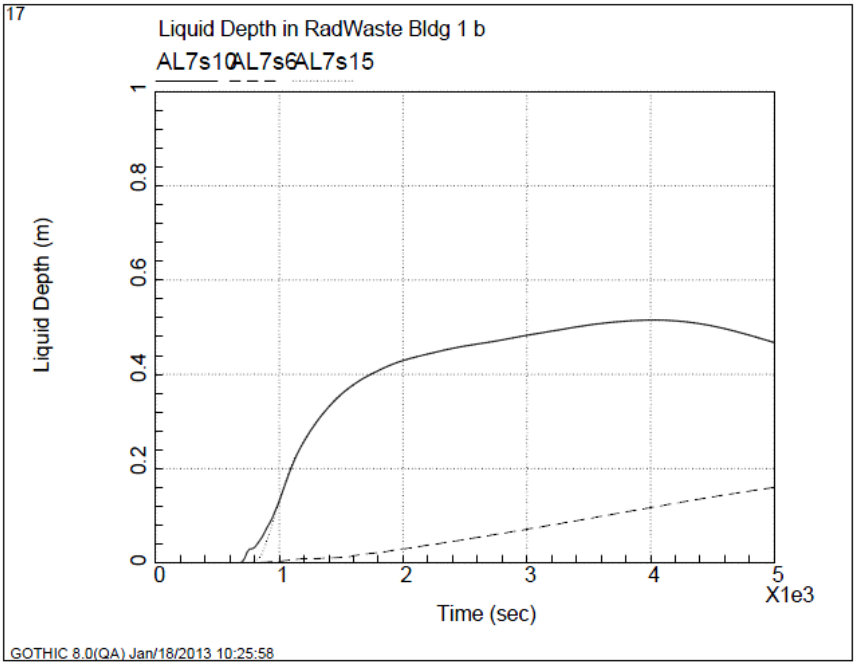

Figure 5-36
Liquid Depth in RW1 Basement

5.5.7 Fuel Storage Building

The fuel storage building (FSTR) has two large roll-up doors on the west face to the outside. In addition, it is connected with both the 1F1 and 2 Radwaste buildings (RW). All doors to the RW buildings are reported to have been open (TEPCO comm.). The two external doors on the west side are both large roll-up type doors. These doors are closed in the model but allow leakage due to gaps around the door perimeter. Figure 5-37 shows liquid depth in the FSTR. The depth is relatively limited (less than 0.5 m) because the external doors remain closed.

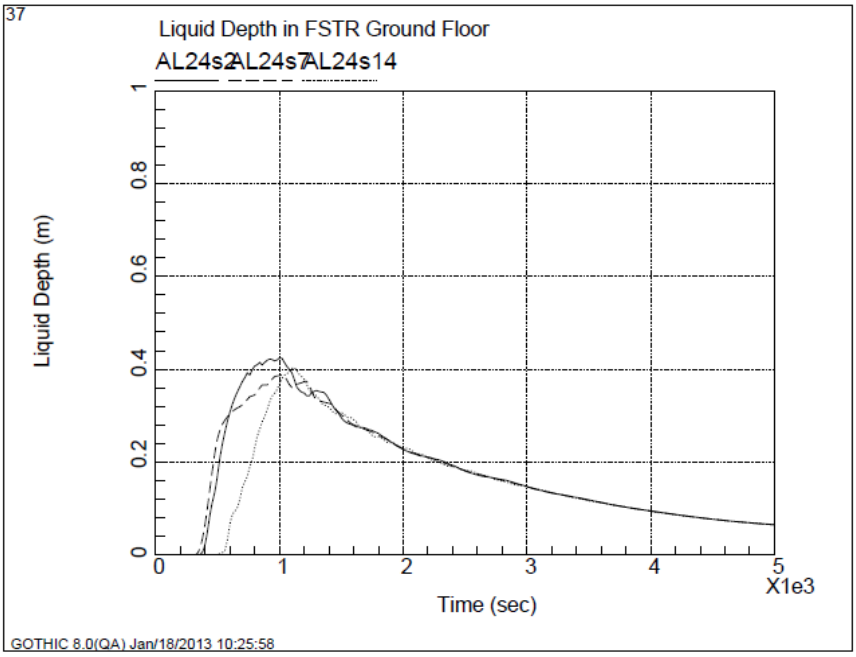

Figure 5-37
Liquid Depth in FSTR Ground Floor

5.5.8 3-D Visualization

Figure 5-38 is a frame shot from a 3-D transient visualization made using GOTHIC data files and TecPlot®. In this frame, water can be seen entering the building at various locations. The water movement is displayed using transparent isosurfaces. The isosurfaces visually define surfaces of equal depth. Three fixed depths are used here. An AVI file showing the transient can be viewed by following the link: Flooding simulation (NAI, Flooding Simulation, 2013).The animation has a time acceleration factor of ten. The URL is available in the reference section.

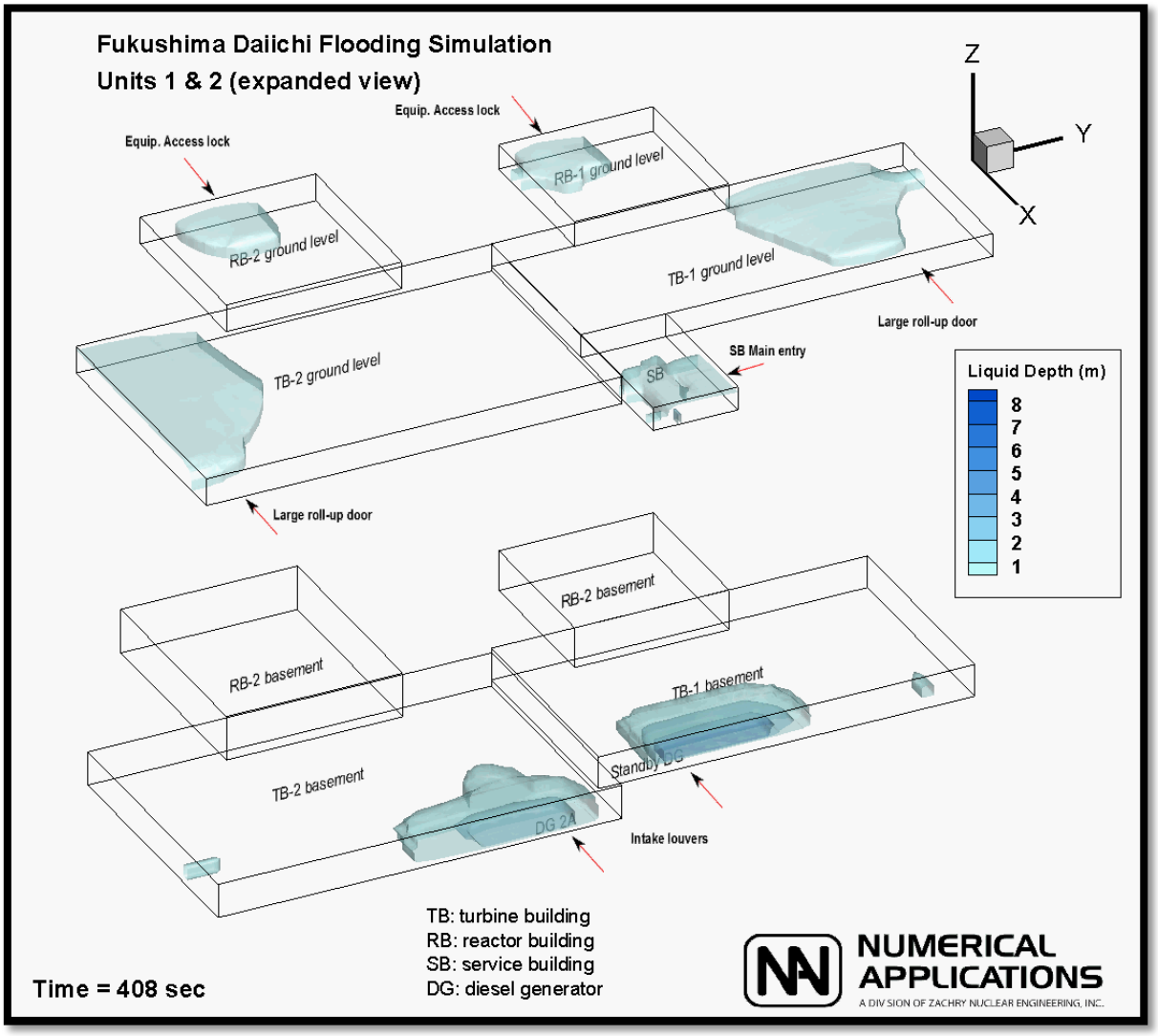

Figure 5-38
Frame from Animation

5.6 Conclusion

There is very limited information regarding the post-accident evaluation of local water levels in various areas of the plant building and the condition of potential leakage points. The majority of the analysis presented above is based on assumption of leakage areas and door failures. Consequently, the results are largely an indication of what could have happen rather than what did happen. The models and analysis demonstrate the ability of GOTHIC to simulate flooding and its potential value in preparing buildings for internal or external flood protection.

Large quantities of water entered the ground floor of the 1F1 and 1F2 Turbine Buildings primarily at three locations. The large roll-up doors located on the east side of each Turbine Building and the Service Building main entrance allowed a large amount of water to ingress into the turbine buildings. GOTHIC is used to track water as it flows through buildings and into rooms via leaking/open doors, hatches, and stairwells. This analysis demonstrates that a large

amount of water drained into the turbine building basements after entering the ground floor. The flow rates and accumulated water depths at locations internal to 1F1 and 1F2 confirm the presence of water where emergency equipment is known to have been disabled or destroyed.

Large amounts of accumulated water were found in the Reactor Building basements of 1F1 and 1F2. This analysis assumes that water entered into the reactor building ground floor through leakage around doors and subsequently drained into the basement. Three cases were analyzed for the purpose of calculating the required leakage area around doors that must be present to allow the reactor basements to flood to the amount measured. The way in which the reactor building basements flooded is still unknown. However, this work demonstrates that a likely source of water was due to leakage past the large equipment doors on the reactor building ground floor.

It has been shown that GOTHIC has the ability to quantitatively model flooding scenarios while offering the flexibility to specify parameters such as door components, trips, and control variables to accurately model the possible pathways for water. Through the use of line graphs and contour plots built into GOTHIC, the analyst can track water ingress and accumulation. 3-D transient visualization is also possible using GOTHIC data files and visualization software.

6
SIGNIFICANT OBSERVATIONS

The early phases of the events at 1F1 and 1F3 can be characterized as a small break or leak to the drywell. Based on the investigations described in this report, it was found that for this type of event, the containment pressure and temperature response is sensitive to phenomena not typically included in BWR design basis containment analysis. These include:

1. Mixing in the suppression pool with the potential for thermal stratification.
2. Mixing in the wetwell gas space with the potential for thermal stratification and steam concentration stratification.
3. Heat transfer from the drywell vents, header and downcomers to the wetwell gas space, with condensation in the vent system.
4. Heat transfer from the wetwell gas space to the torus room and surrounding structures.
5. Leakage between the drywell and wetwell gas space (steam bypass).
6. Mixing in the drywell with the potential for thermal and gas concentration stratification.

There may be other sensitive phenomena that have not yet been addressed in the investigations discussed here (e.g., drywell heat loss to the surrounding structure, heat loss to the flood water in the torus room and mixing between the drywell and the vent system).

The sensitivity of the containment pressure to details such as these may have implications for the understanding of the primary system response during the Fukushima events. The recorded containment pressure is a primary figure of merit for assessing the primary system analysis using MAAP or MELCOR for the Fukushima events. These primary system severe accident simulations address the containment response using methods typical for design basis analysis. If a more detailed containment model is coupled with the severe accident analysis codes, significant changes in the assumed progression of events may be necessary to match the recorded containment pressures.

Based on the studies of the 1F3 wetwell performance, the sequence of events emphasizes the potential importance of containment sprays to mitigate containment pressure rise in small break situations.

Consistent with previous investigations for buoyancy induced mixing, a hydrogen release to an open area, such as the upper level of the Reactor Buildings at Fukushima tends to a well-mixed condition at elevations above the release point. Backflow through the common stack has the potential to fill the HVAC ducts with detonable mixtures.

7
REFERENCES

Bonnet, J., & Seiler, J. (1999). Thermal-Hydraulic Phenomena in Corium Pools for Ex-Vessel Situations: the BALI Experiment. *Proceedings of the International Conference on Nuclear Engineering (ICONE 7).* Tokyo.

CBI NA-CON, Inc. (1987). *Mark I Containment Severe Accident Analysis.*

Cook, D. (1984). *Pressure Suppression Pool Thermal Mixing.* NUREG/CR-3471, ORNL/TM-8906.

EPRI. (2013). *Fukushima Technical Evaluation Phase 1 MAAP5 Analysis.* Palo Alto: EPRI.

FAI. (1992). *Severe Accident Management Guidance Technical Basis Report, Volume 2: The Physics of Accident Progression.*

FAI MAAP4. (1994). *MAAP4 - Modular Accident Analysis Program: User's Manual.*

FAI MAAP5. (2008). *MAAP5: Modular Accident Analysis Program, User's Manual.*

Gauntt, R., & Humphries, L. (1997). *Final Results of the XR2-1 BWR Metallic Melt Relocation Experiment.*

Gauntt, R., Kalinich, D., Cardoni, J., Goldmann, A., Phillips, J., Pickering, S., et al. (2012). *Fukushima Daiichi Accident Study.*

Henry, C. (n.d.). private communication.

Henry, R. (2011). *TMI-2: An Event in Accident Management for Light-Water-Moderated Reactors.* La Grange Park, Illinois USA: American Nuclear Society.

INPO. (2011). *Special Report on the Nuclear Accident at the Fukushima Daiichi Nuclear Power Station.*

Jahn, M., & Reineke, H. (1974). Free Convection Heat Transfer with Internal Heat Sources, Calculations and Measurements. *Proc. of the 5th Intl. Heat Transfer Conf.*, (p. Paper NC2.8). Tokyo.

JNES. (2012). *JNES MELCOR Analysis.*

Laine, J., & Puustinen, M. (2006). *Thermal Stratification Experiments with the Condensation Pool Test Rig, NKS-117.* Lappeenranta Univerisity of Technology, Finland.

Li, H., & Kudinov, P. (2009). *GOTHIC Code Simulation of Thermal Stratification in POOLEX Facility, NKS-196.* Royal Institute of Technology, KTH , Sweden.

Li, H., Kudinov, P., & Villaneva, W. (2010). *Modeling of Condesation, Stratification, and Mixing Phenomena in a Pool of Water, NKS-248.* Division of Nuclear Power Safety, Royal Institute of Technology, KTH, Sweden.

Li, H., Kudinov, P., & Villanueva, W. (2011). *Development and Validation of Effective Models for Simulation of Stratification and Mixing Phenomena in a Pool of Water, NKS-248.* Division of Nuclear Power Safety, Royal Institute of Technology, KTH Sweden.

Mizokami, S. (n.d.). *Private communication.*

Muller, C. (2006). Review of debris bed cooling in the TMI-2 accident. *Nuclear Engineering and Design, 236*, pp. 1965-1975.

NAI. (2013). *Flooding Simulation*. Retrieved from https://docs.google.com/file/d/0BzxErU0stSvGYl8zelVmV1BJZXM/edit?pli=1

NAI. (2013). *RCIC Discharge Animation*. Retrieved from https://docs.google.com/file/d/0BzxErU0stSvGcWVYcTVSUnJsZlE/edit?pli=1

NEA. (2000). *Carbon Monoxide-Hydrogen Combustion Characteristics in Severe Accident Containment Conditions.* Committe on the Safety of Nuclear Installations.

NRC CR-3486. (1986). *CR-3486 Hydrogen: Air: Steam Flammability Limits and Combustion Characteristics in the FITS Vessel.* Albuquerque: Sandia National Laboratory.

NRC CR-6920. (2006). *Risk-Informed Assessment of Degraded Containment Vessels. CR-6920.*

NRC Reg. 1.155. (1988). *Regulatory Guide 1.155: Station Blackout.*

NRC SOARCA. (2012). *State-of-the-Art Reactor Consequence Analyses, Volume 1: Peach Bottom Integrated Analysis.*

NRC WASH-1400. (1975). *Reactor Safety Study, An Assessment of Accident Risks in U.S. Commercial Nuclear Power Plants, WASH-1400.*

NSAC. (1980). *Analysis of the Three Mile Island-Unit 2 Accident.*

NUREG-0800. (2012, May). *Standard Review Plan for the Review of Safety Analysis Reports for Nuclear Power Plants: LWR Edition.* NRC.

OECD-NEA. (2012). *Benchmark Study of the Accident at the Fukushima Daiichi NPS Project, (BSAF Project).* Tokyo.

Patterson, B. (1979). *Mark I Containment Program, Monticello T-quencher Thermal Mixing Test, Final Report.* NEDO-24542, 79NED101.

TEPCO 1F1. (2012). Investigation on 1F2.

TEPCO 1F1 Torus. (2012). *Unit 1 Reactor Building Torus Room Investigation Result.*

TEPCO 1F2 Torus. (2012). *Investigation in the Torus Room on Unit 2 Basement Floor of the Reactor Building.*

TEPCO 1F3. (2012). *Investigation on 1F3.*

TEPCO. (2012). *MAAP Analysis.*

TEPCO Accident Report. (2012). *Fukushima Nuclear Accident Analysis Report.*

TEPCO p.c. (n.d.). Private communications with TEPCO.

TEPCO Tsunami Survey. (2012). *Tsunami Survey Results in the NPS Reproduction Analysis Using Tsunami Inversion.*

TEPCO (2013). Total Decay Heat Trend Based on ORIGEN-2 Analysis for 1F1, 1F2 and 1F3.

A
APPENDIX A

Attachment A.1 Drywell Model

A.1.1 Drywell Model

A subdivided drywell (drywell) model has been developed to produce a representative 3D modeling of the cylindrical and lower spherical portions of the drywell including the RPV, bioshield wall, and major flow paths for natural circulation that exist within the drywell as shown in Figure A-1 below. The drywell volume is divided into a central cylindrical volume (Volume 1s) and a volume representing the outer spherical portion of the lower drywell (Volume 2s). Figure A-1 shows the separate volumes used to model the drywell.

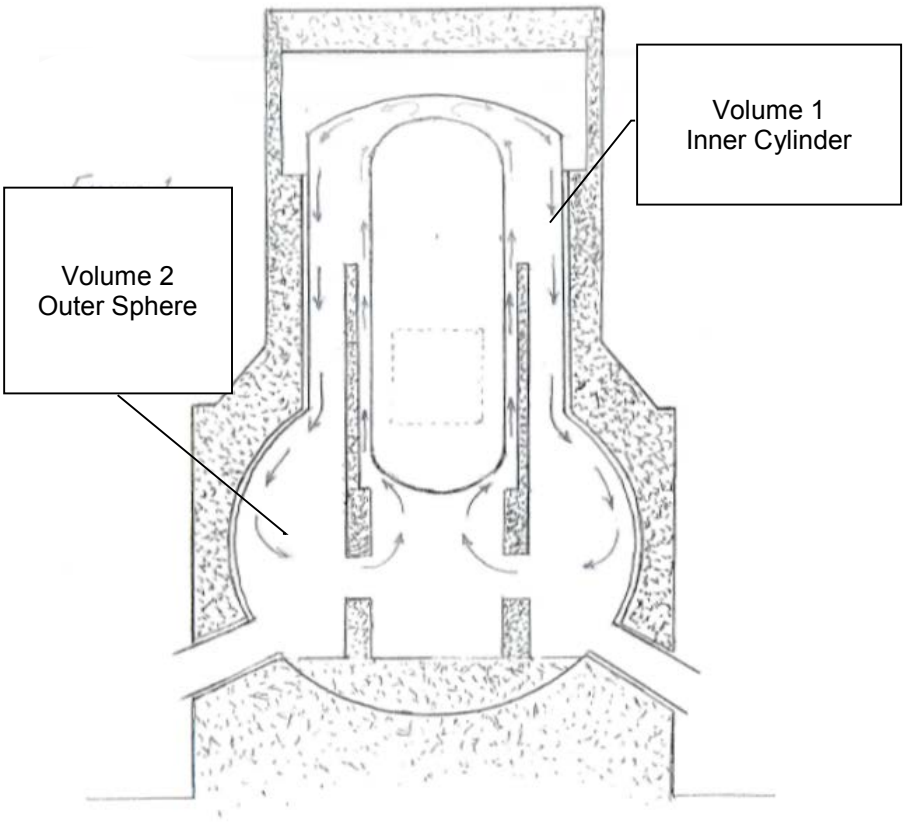

Figure A-1
Drywell Volumes

A.1.2 Primary Drywell Circulation Flow Paths

The GOTHIC modeling depicted in Figure A-2 and Figure A-3 below provides the basic flow paths to allow modeling of circulation within the drywell during the course of the accident. These two volumes are subdivided with sufficient detail to model the natural circulation paths

within the drywell. Natural circulation flows are established during the SBO phase and also by steam break-induced flows induced during the SBLOCA phase. The inner and outer drywell volumes are connected via 3-D flow connectors allowing unrestricted flow between the inner and outer portions of the lower spherical portion of the drywell.

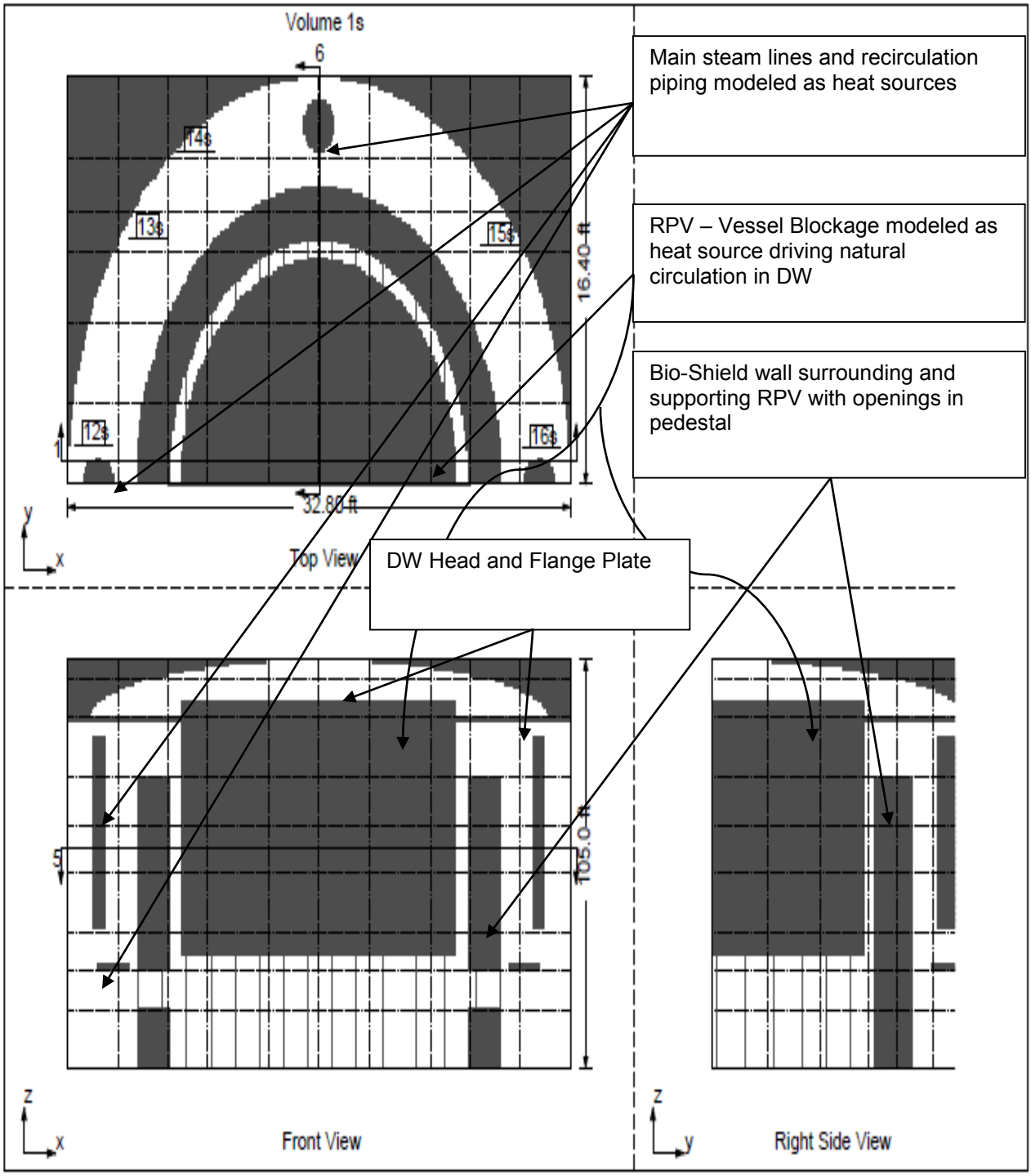

Figure A-2
INNER drywell Cylinder-volume 1s

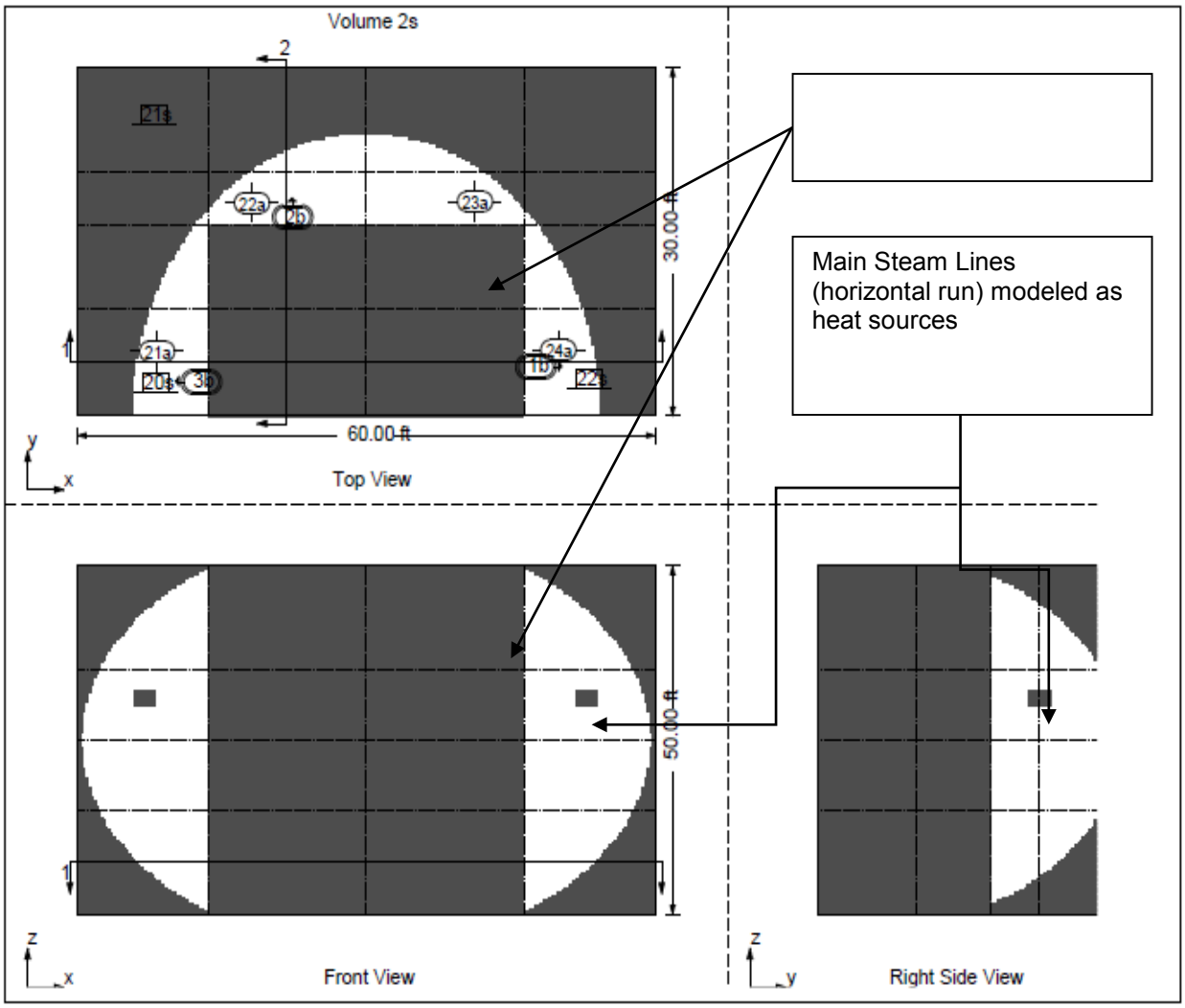

Figure A-3
OUTER drywell Sphere-volume 2s

Figure A-2 also shows the blockages representing the Reactor Pressure Vessel (RPV) and Main Steam piping within the drywell as well as the bioshield wall supporting and surrounding the lower RPV. The approximate 6 inch gap between the RPV and the bioshield wall creates a potential chimney effect as the hot vessel heats the surrounding air. This chimney effect will draw air into the lower pedestal region through openings to the lower regions of the drywell outside of the pedestal. This model configuration is intended to demonstrate the degree of mixing and/or stratification within the drywell with no forced circulation from the drywell cooler fans. However, the current model lacks specific dimensional parameters and therefore may only approximate the behavior of potential mixing currents.

A.1.3 Heat Sources and Sinks

The RPV vessel heat source is modeled as a multi-region conductor including the vessel metal wall, an estimated air gap the vessel insulation layer. During the early phase of the event with adequate liquid in the vessel for core coverage, the vessel internal temperature is expected to

remain at the saturation temperature for the SRV discharge (~288 °C). With the subsequent onset of fuel failure, the temperature can be adjusted to an internal temperature appropriate for fuel failure conditions (obtained from MELCOR results) and allow the conductor to model the resulting heat losses through the RPV wall and insulation. The RPV thermal behavior is modeled as two separate conductors allowing the internal temperature of the upper half and lower half of the RPV to be assigned separately. The heat contribution to the drywell from main steam lines and recirculation lines is also modeled with multiple conductors (similar to the RPV model) located at appropriate positions within the drywell. Estimates are used for the vessel insulation thermal properties.

The drywell metal liner is currently modeled as a heat conductor capable of removing heat from the drywell. The steel liner is model with a thickness typical for BWR's of this vintage and includes a 2 inch (approximate) air gap to the structural concrete that is several feet thick. Convective heat transfer to ambient air is assumed on the outside surface of the concrete. Although details specific to 1F1 would be beneficial here, the current model is deemed reasonable and not especially sensitive to potential differences in input parameters.

The drywell heat transfer model appears to provide a reasonable approximation of the overall heat load and serves to demonstrate the basic driving force for mixing in the drywell. Although details specific to the 1F1 drywell are needed, the current model provides reasonable predictions and demonstrates low sensitivity to potential differences in input parameters.

A.1.4 Localized Inputs for Vessel Leakage

The subdivided model of the drywell allows various postulated steam and hydrogen release scenarios to be modeled at specific locations within the drywell where such releases are speculated to occur. Postulated leakage flow paths representing the SRV Gasket failure or RPV instrument line rupture are modeled in order to assess the extent of mixing within the drywell. Boundary conditions and valved flow paths are modeled to simulate the scenario modeled with MELCOR [1], in which postulated leakage of vessel steam and hydrogen to the drywell occurs due to SRV gasket failure.

A.1.5 Localized Drywell Conditions- Results

The subdivided drywell model also allows predictions of localized temperature profiles within the drywell. Localized drywell temperature conditions can be used to evaluate the potential for temperature sensitive failure vulnerabilities at different locations within the drywell containment. Specifically, the investigation of local temperatures at the drywell head flange location can aid in assessment of the timing of the onset of temperature induced failure (flange leakage) at that location. Similarly, the model can provide localized temperatures at the location of any speculated steam leak into the drywell and the resulting temperature impact at various locations of suspected drywell containment failure.

The model also predicts the localized gas concentrations at various potential drywell leak locations to provide a definition of the composition of any postulated leakage path from the drywell to the Reactor Building. A valved flow path is included to simulate the MELCOR [1] scenario postulated leak from the drywell flange to the Reactor Building via the Refueling Pool Compartment above the drywell head. The validity of predictions of localized temperature and

gas concentration results using the current model are affected by the lack of plant-specific inputs discussed above.

A.1.6 References

1. JNES (2012) MELCOR Analysis
2. EPRI (2012) Fukushima Technical Evaluation Phase 1 MAAP5 Analysis

Attachment A-2 Unit 1 Scenario Model

A.2.1 1F1 Scenario Model

Two alternative scenarios for the 1F1 transient have been investigated using the MELCOR code and the MAAP code as presented in [1, 2]. Details of the 1F1-specific transient blowdown and hydrogen release assumed in either of these analyses have not been made available to date; attempts were made to reconstruct a reasonable representation of the scenarios based upon the limited information provided in those reports.

Reasonable agreement has been achieved in the effort to construct a representation of the scenario depicted within the MELCOR [1] analysis. The MELCOR analysis assumes hydrogen release via the SRV followed by hydrogen release to the drywell along with a steam leak through the SRV gasket. Due to the limited data presented, some assumptions and "reverse-engineering" were required to develop the steam and hydrogen releases via the SRV and RPV directly to the drywell postulated in this scenario. The releases used in the GOTHIC analysis should be considered as speculative approximations, however the GOTHIC results appear to provide a reasonable match to the MELCOR results and serve to demonstrate that the GOTHIC Drywell/Vent/Suppression Pool model provides reasonable predictions.

The 1F1 scenario used in the MAAP analysis presented in [2] differs from that used in the MELCOR analysis regarding the timing and amount of steam and hydrogen released to the containment. The MAAP scenario assumes an earlier hydrogen release to the drywell via an instrument tube rupture; subsequent steam and hydrogen release via an SRV gasket leak followed by hydrogen release from the RPV and the core/concrete interaction. Attempts to reverse-engineer the releases modeled in this analysis based upon the limited data in that report (including slightly more detailed information provided in [2]) were largely unsuccessful due to lack of critical steam release information within those reports. Furthermore, the scenario used for the MELCOR analysis was judged to be sufficiently different from that used for the MAAP analysis such that compensating the MAAP data with the release information used in the MELCOR analysis was not appropriate. Therefore no attempt was made to simulate the MAAP analysis using GOTHIC based upon the limited release data currently available to this analyst at this time.

A.2.2 Case Description- MELCOR1B

SRV flow to the suppression pool is implemented using eight flow paths representing half of the SRV quencher (8 flow paths was a remnant of the detailed modeling originally used in the subdivided suppression pool model simply carried over in the lumped model for convenience).The mass flow rate at Time = 0 is 1.6 lbm/s per flow path. This estimated flow rate is not particularly critical to the overall model performance since the suppression pool heat up alone produces limited containment pressure response. It is expected that suppression pool stratification is a more important factor. The extent of stratification is not predicted by this model but can be simulated by forcing elevated upper suppression pool temperature to values defined by judgment or other detailed suppression pool modeling.

SRV flow to the suppression pool is assumed to stop at about 13680 sec (3.8 hrs.). The 3.8 hour timing is based upon the abrupt peak in the wetwell hydrogen concentration as depicted in [1, 2].

RPV internal temperature excursion starts at about 7000 sec, ramping to 727 °C by 12000 sec and beyond based upon MELCOR RPV vapor space predictions [1].

The onset of hydrogen generation is assumed to start at 2.5 hrs. Based on Figure A-5, the integrated hydrogen generation plot appears to be somewhat "delayed" because the wetwell hydrogen concentration increase before the integrated hydrogen generation begins to increase. For the purposes of this scenario reconstruction, it has been assumed that there is some inconsistency within the plots on this figure and the hydrogen generation plot has been "shifted" ahead in time to be consistent with timing of the increase in the wetwell hydrogen concentration. The onset of hydrogen release, ignoring any delay between "generation" and "release" from the vessel, has been estimated from the plots to begin at about 2.5 hrs.

Initial hydrogen release via SRV. Based upon the fact that the secondary containment hydrogen concentration is greater than the drywell hydrogen concentration, it is assumed that a substantial portion of the initial hydrogen release is via the SRV flow directly to the suppression pool (with or without accompanying steam flow).

SRV gasket failure and release of steam and hydrogen to the drywell is assumed to start at 3 hrs based upon the MELCOR assumption of the onset of steam and hydrogen release to the drywell as depicted by Figure A-6. It may be reasonable to assume that the small leak to the drywell constitutes only a fraction of the flow passing through the SRV to the suppression pool. Since specific information regarding the steam and hydrogen to the drywell and the suppression pool, the following assumptions have been made.

- Beginning with the initial rapid suppression pool hydrogen concentration increase, all hydrogen release is assumed via the SRV steam discharge.
- The slightly delayed and less pronounced hydrogen increase in the drywell is assumed due to the hydrogen release after pressurization of the suppression pool and results in flow of wetwell gases into the drywell via the vacuum breakers.

Alternate Scenario - The onset of the direct release of hydrogen and steam to the drywell starts at 3 hrs as indicated in Figure A-6 It should be noted that this figure shows that an increase in hydrogen concentration in the drywell begins at the same time that the steam release to the drywell begins. This suggests that a steam/hydrogen release to the drywell occurs coincident with the onset of the hydrogen release to the suppression pool via the SRV discharge. This may account for the subtle increase in the slope of the drywell concentration increase within the first few minutes due to the early direct leakage of hydrogen into the drywell followed by the larger release from the wetwell when the wetwell vacuum breakers open. Figure A-6 also depicts a period beginning at about 3.3 hrs when the drywell hydrogen and steam concentration hold relatively stable for about 0.5 hrs. This may be indicative of a period when most of the vessel steam and hydrogen is released to the suppression pool via the SRV. This period is followed by a sharp increase in drywell hydrogen concentration due to direct leakage into the drywell. There is a gradual reduction in drywell hydrogen concentration as the steam release to the drywell dilutes the hydrogen and carries it to the wetwell. Although this is potentially a more accurate representation of the MELCOR scenario, it remains somewhat speculative. The scenario modeled in GOTHIC reproduces the major aspects of the MELCOR transient and is sufficient for the purpose of exercising the model and observing its performance.

Termination of SRV discharge to the suppression pool is assumed at about 3.8 hrs based on the concentration in the wetwell showing a peak at that point (Figure A-4 and Figure A-5).

Steam leakage to the drywell via SRV gasket continues at a rate defined by Figure A-6 until it nearly ceases at about 13 hours.

Hydrogen leakage to the drywell via the SRV gasket continues at a rate defined by Figure A-4 and Figure A-5 until it essentially ceases at about 13 hours.

Drywell leak via drywell head flange assumed at 17 hours.

The wetwell venting operation is performed at 24 hours until drywell pressure is reduced to ~4.14 kPa.

The reactor building explosion occurs approximately 1 hour after the wetwell venting operation is performed.

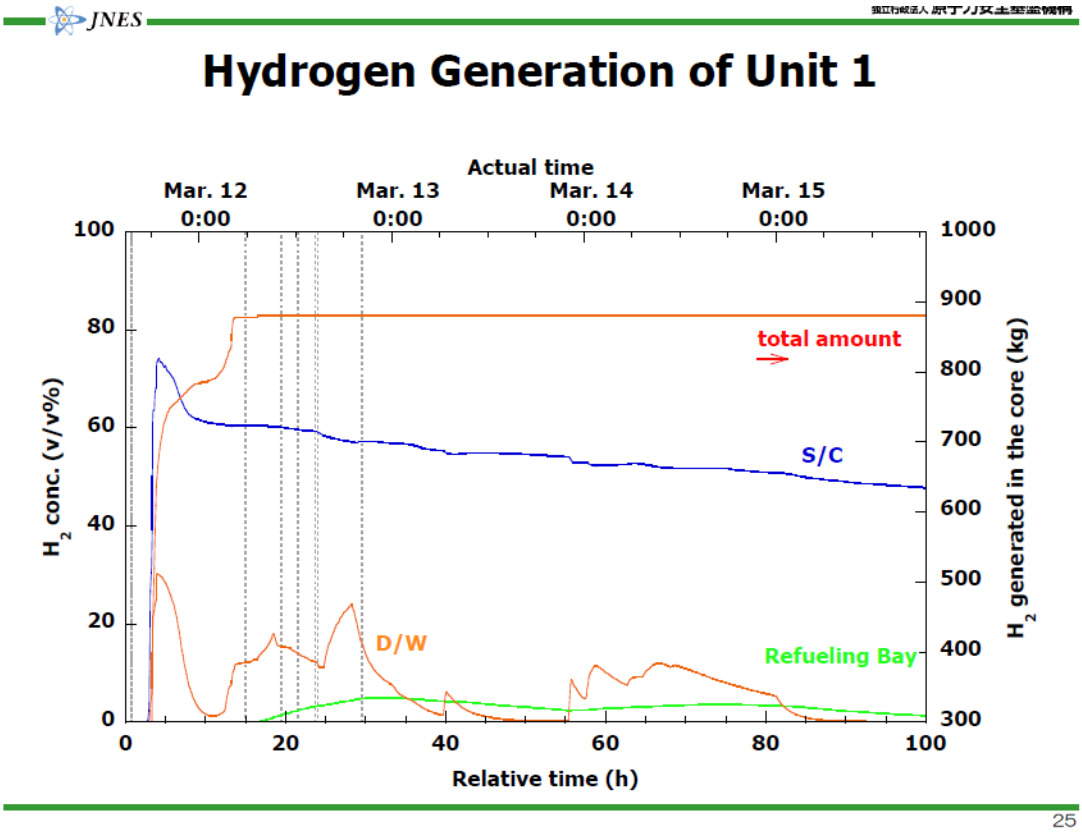

Figure A-4
S/C hydrogen Concentration

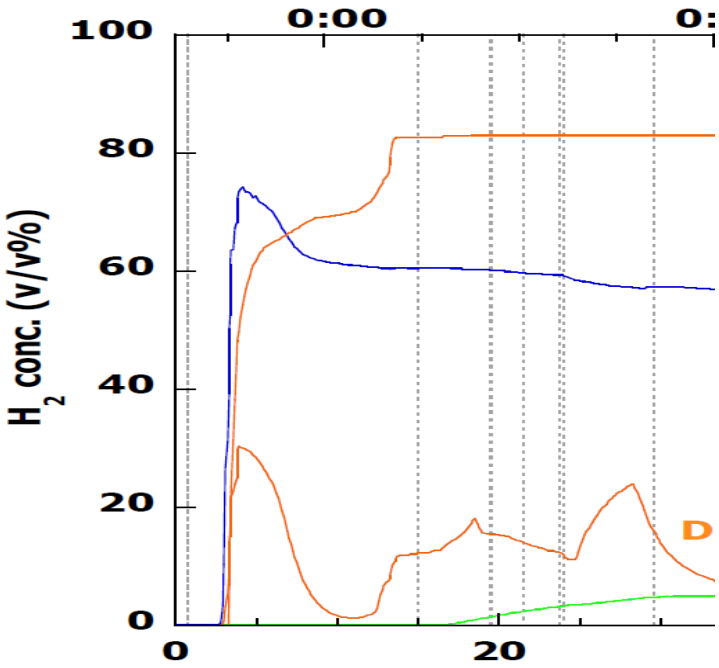

Figure A-5
Enlarged Portion of S/C hydrogen Concentration

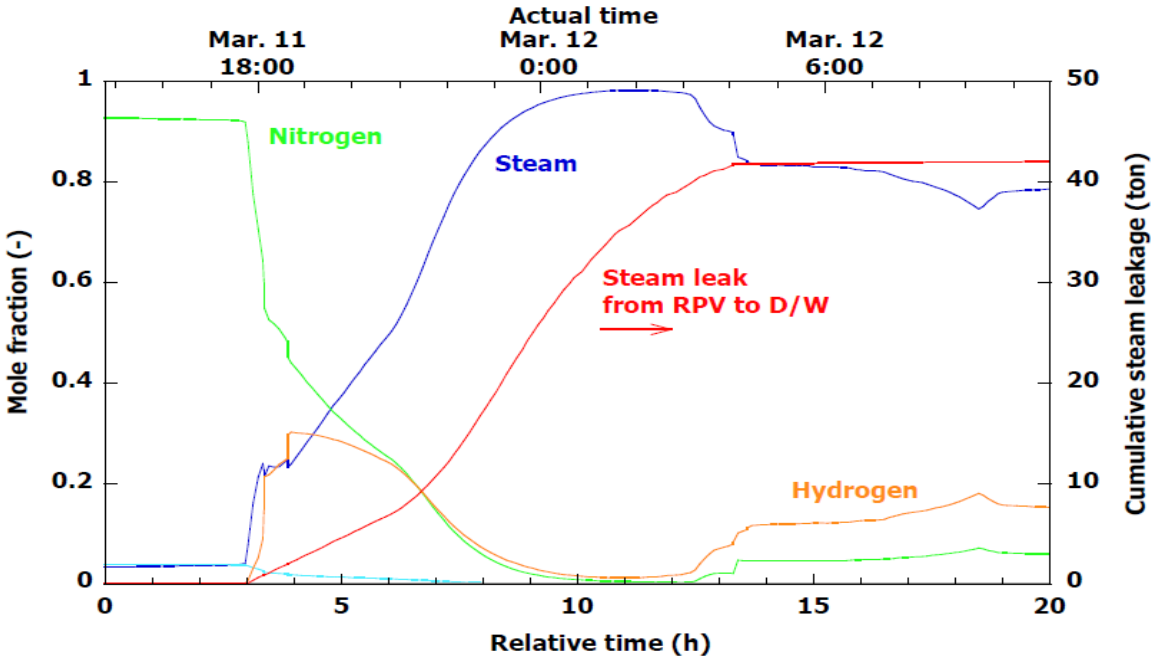

Figure A-6
Leakage through SRV

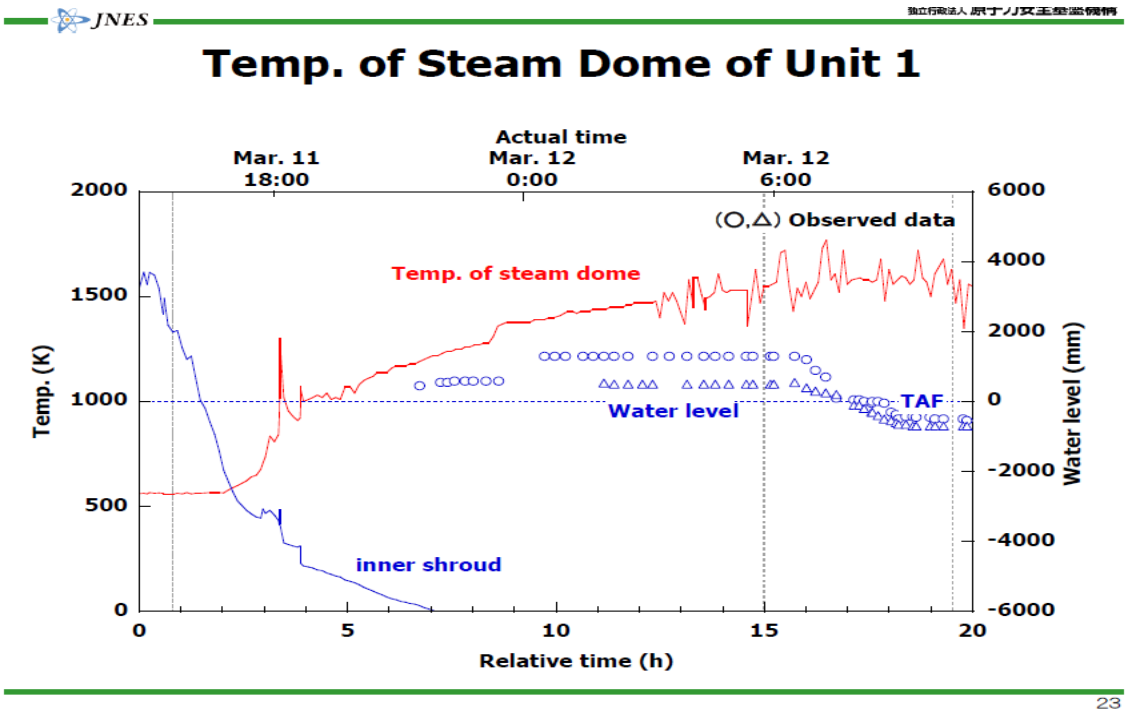

Figure A-7
MELCOR RPV Vapor Space Predictions

A.2.3 References

1. JNES (2012) MELCOR Analysis
2. EPRI (2012) Fukushima Technical Evaluation Phase 1 MAAP5 Analysis

Attachment A-3 GOTHIC Validation for Pool Stratification

To support the application of GOTHIC to the suppression pool performance studies, two validation exercises were completed as described in this section. This validation is in addition to the existing GOTHIC validation for buoyancy driven flows, previously in the vapor phase.

A.3.1 POOLEX

In boiling water reactor containment design, the suppression pool plays an important role as a heat sink to cool and condense steam released from the core vessel and/or main steam line during Loss of Coolant Accident (LOCA) or opening of safety relief valves in normal operation of boiling water reactors (BWRs). At lower steam flow rate conditions, there is a risk of thermal stratification above the discharge pipe exit. The unmixed thermal layers inside the suppression pool can keep the pool surface at higher temperature which reduces its pressure suppression capacity [2]

Hua Li and his research group from Royal Institute of Technology (KTH, Sweden) performed an extensive computational study about condensation, stratification and mixing phenomena in a pool of water [2, 3, and4]. Two and three dimensional GOTHIC models were generated and verification and validation studies were performed using POOLEX experiment results. Artificial oscillations and numerical diffusion were reported when direct steam injection and condensation was modeled using GOTHIC [2]. Li et al. proposed alternative methods to simulate the effect of steam injection referred to as Effective Heat Source (EHS) and Effective Momentum Source (EMS). Results were in good agreement with the experimental data. However, both alternative models were generated within the framework of the experimental measurements and may not be generally applicable.

The main objective of this work is to model direct steam injection and condensation in GOTHIC without the need of any alternative methods, simplifications, etc.

A.3.2 POOLEX STB-20 Experiment

In 2005, the POOLEX (POOL Experiment) project was performed at Lappeenranta University of Technology in Finland to investigate the behavior of the pressure suppression pool during a possible steam line break accident in Olkiluoto type BWRs [1]. As shown in Figure A-8, in such accidents a large amount of non-condensable (nitrogen) and condensable (steam) gas blow from the upper dry well to the condensation pool through the discharge pipes. Later, when the steam flow rate decreases and mixing inside the pool is not strong enough, thermal stratification of water in the condensation pool may occur [1].

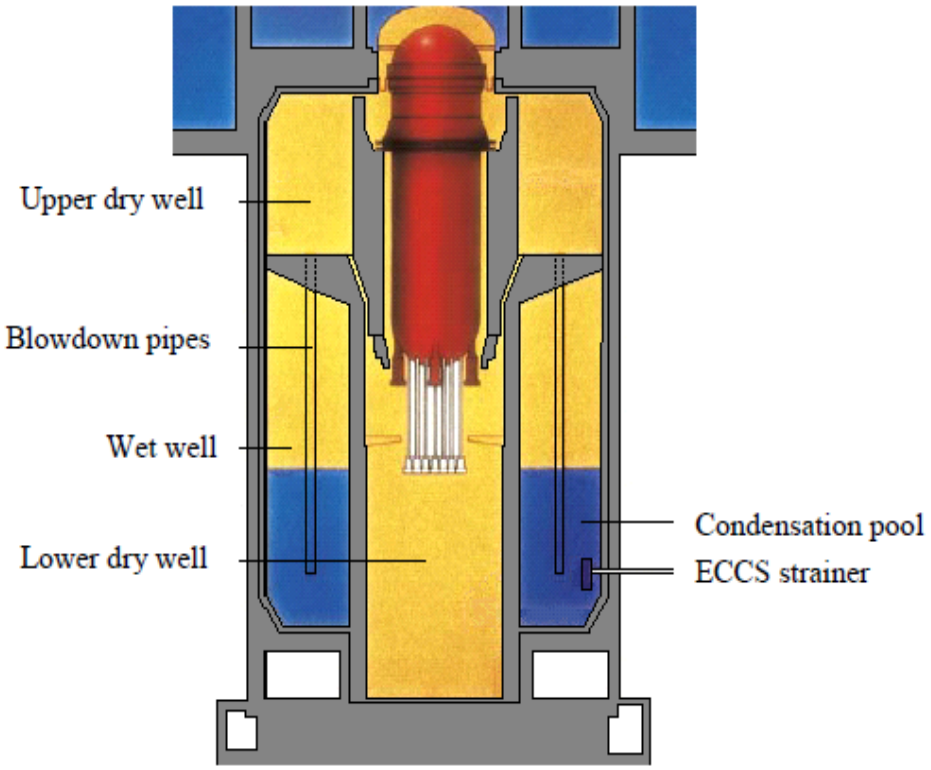

Figure A-8
Schematic of the Olkiluoto type BWR Containment [1]

The POOLEX test facility consists of a cylindrical stainless steel tank; 5 m in height with 2.4 m in diameter open to the lab atmosphere with a water pool that is 2.95 m deep. The vertical discharge pipe is 200 mm in diameter and submerged by 1.81 m into the pool. In the POOLEX STB-20 experiment, the steam flow rate was kept below a certain limit to limit mixing inside the pool. By doing so, the thermal stratification in a BWR suppression pool was investigated [1]. A schematic of the POOLEX test setup is given in Figure A-9. From Figure A-10, the experimental measurements showed that the bottom of the tank temperature remained close to its initial value of 30 °C, whereas at higher elevations the pool water temperature stratified up to 67 °C due to heat transfer from the steam condensation inside the discharge pipe

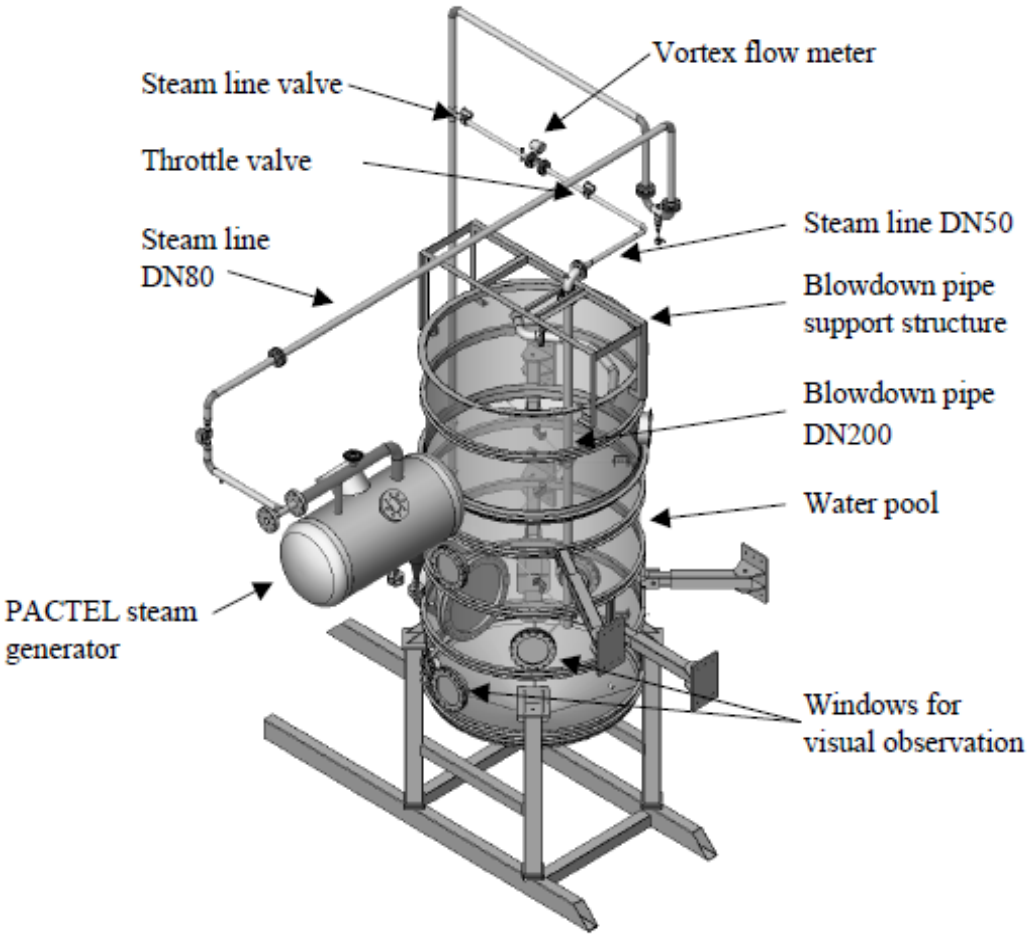

Figure A-9
POOLEX Test Rig [1]

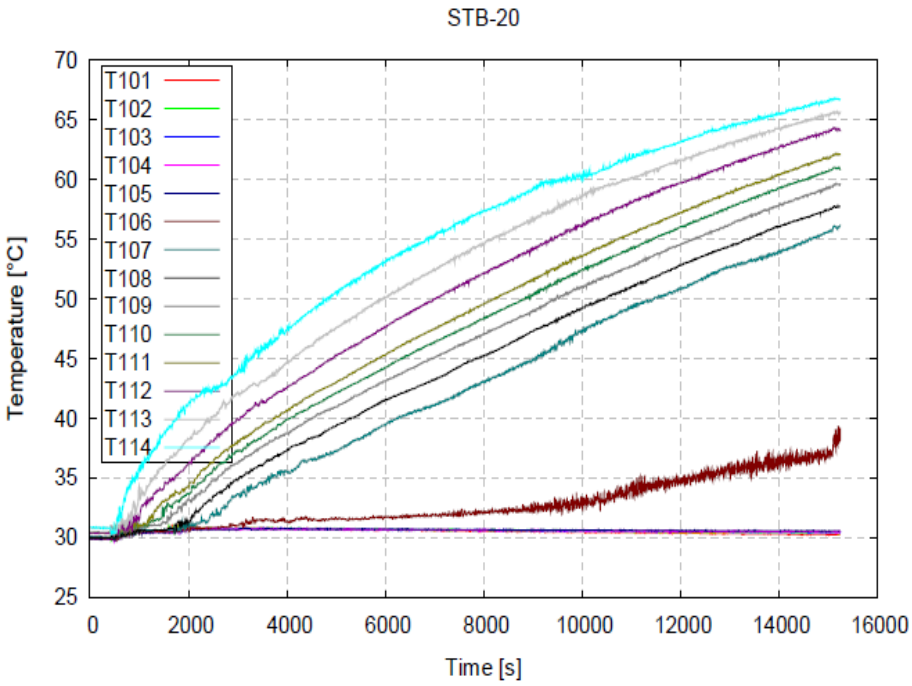

Figure A-10
STB-20 experiment measured data [1]

A.3.3 GOTHIC Integrated Steam Injection Model

According to the results and conclusions of Li et al. regarding GOTHIC models, it was essential to perform a benchmarking study to expand the qualification matrix of GOTHIC to investigate the need for improvements to model the observed thermal stratification. The GOTHIC models that were provided to NAI by KTH group members were reviewed.

Models which were generated in GOTHIC version 7.2b were rerun using version 8.0 without activating the "InterCell InterPhase Drag" option. Identical results were obtained with the previous runs. It was observed that the InterCell InterPhase Drag model introduced as an option in GOTHIC 8.0 tended to enhance the mixing and reduce the stratification.

When modeling the cylindrical pool as a 2D axisymmetric geometry, it is important to distribute the total volume in each cell according to the given geometric specifications. In the model presented here, wedge blockages are used to form a triangular region that represents a 10 degree sector of discharge pipe and water pool integrated model. The wedge shape blockages distribute the total volume in each cell automatically, so there is no need to calculate the volume porosity in advance.

As shown in Figure A-11, the lab atmosphere was modeled as a large single volume (104 m^3) maintained at 1 atm with Boundary Condition 1P. To maintain nearly constant temperature and humidity in the atmosphere volume a volumetric air mass flow inlet (100 m^3/s) at 24 °C and 50% humidity was specified for Boundary Condition 1F. In order to take in to account the natural circulation above the pool surface and its effect on pool surface temperature, the portion of lab atmosphere above the pool was emphasized with an individual cylindrical volume which is connected to the pool and the lab atmosphere with 3D connecters. The volume is subdivided

using the same wedge blockages ratio based on the 2D axisymmetric pool geometry. The discharge pipe wall was simulated with a plate blockage as shown in Figure A-12. A spanned thermal conductor was used to model the conduction through the pipe wall and the heat transfer (including condensation) on each side of the pipe wall. The DIRECT surface option with the DLM-FM condensation option was used on both sides of the pipe wall. Flow Boundary Condition 1F is used to specify the constant steam flow rate into the discharge pipe. The small lumped volume between the flow boundary condition and the discharge pipe was included to represent the steam line piping and to reduce pressure oscillations due to condensation inside the pipe, especially during the early part of the transient. The schematic of the GOTHIC model nodalization and the 2D axisymmetric discharged pipe and water pool meshing profiles are given in Figure A-11 and Figure A-12.

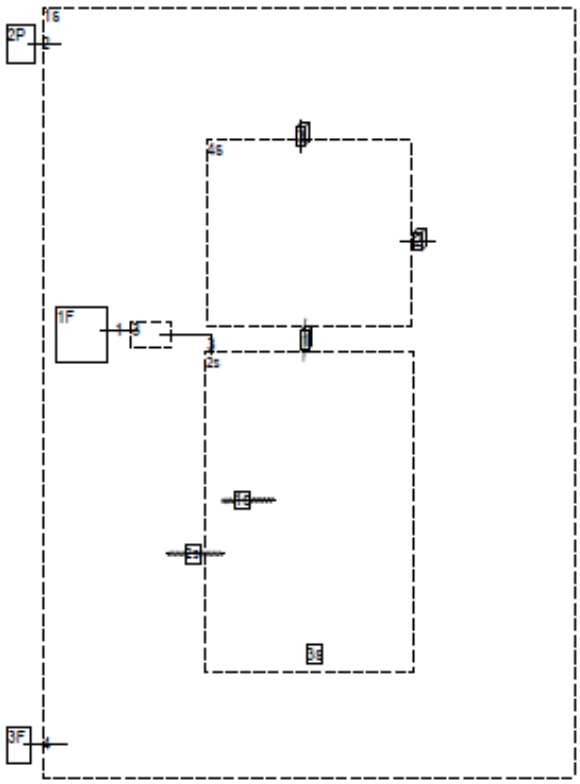

Figure A-11
GOTHIC model nodalization

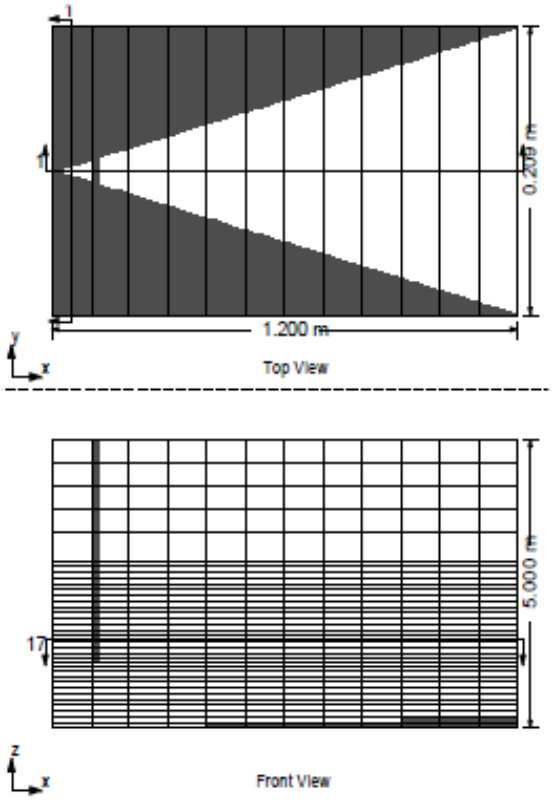

Figure A-12
Discharged pipe and water pool mesh

A.3.4 Results and Discussions

Bounded Second Order Upwind Method was selected as the differencing scheme to reduce potential numerical diffusion. Based on given transient boundary conditions, the integrated GOTHIC model was run and liquid temperature profiles were extracted at the same elevation points as in the experimental study [1]. As shown in Figure A-13 and Figure A-14, GOTHIC predictions demonstrate the thermal stratification inside the water pool and are in a good agreement with the experimental measurements (Figure A-10). Reasonable agreement with the data was achieved using currently available GOTHIC models without the need of any assumptions or EHS model.

The largest discrepancy between the GOTHIC results and the data was obtained around the elevation of the discharge pipe outlet. At this level, hot water from the condensed steam is entering the pool. The GOTHIC model for the test facility is for axisymmetric geometry. However, in the test the discharge pipe is off center by approximately 410 mm [1]. There could be additional circulation in the horizontal plane that cannot be captured in the 2-dimension model. Nevertheless, the overall top to bottom stratification is well predicted.

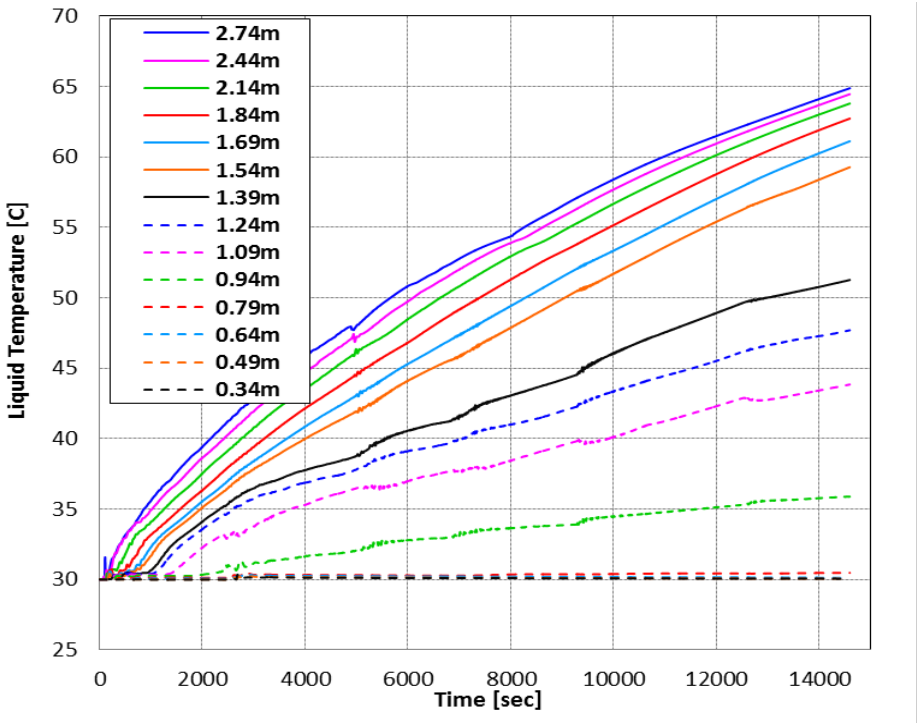

Figure A-13
GOTHIC temperature predictions of STB-20 test with direct steam injection simulation

As a part of the validation exercise, a grid sensitivity study was conducted to gauge the effect of grid size on the calculated thermal stratification. The number of cells in the liquid part of the coarse grid (Figure A-12) was refined along the axial (z) direction; only the number of cells right below and above the pipe was increased from 5 to 10. The aim was to capture condensed hot liquid mixing effect on the pool temperature stratification accurately at coarser mesh size. GOTHIC predictions were compared with the experimental data for the vertical temperature profile at 14,600 seconds. As shown in Figure A-14, GOTHIC thermal stratification predictions

were improved in the region just below the pipe outlet when the number of cells is increased. Otherwise, the results are about the same. When the grid spacing was increased from the base case (every other grid line removed), GOTHIC predicted near complete mixing in the tank, indicating that a minimum grid resolution is required to predict the stratification.

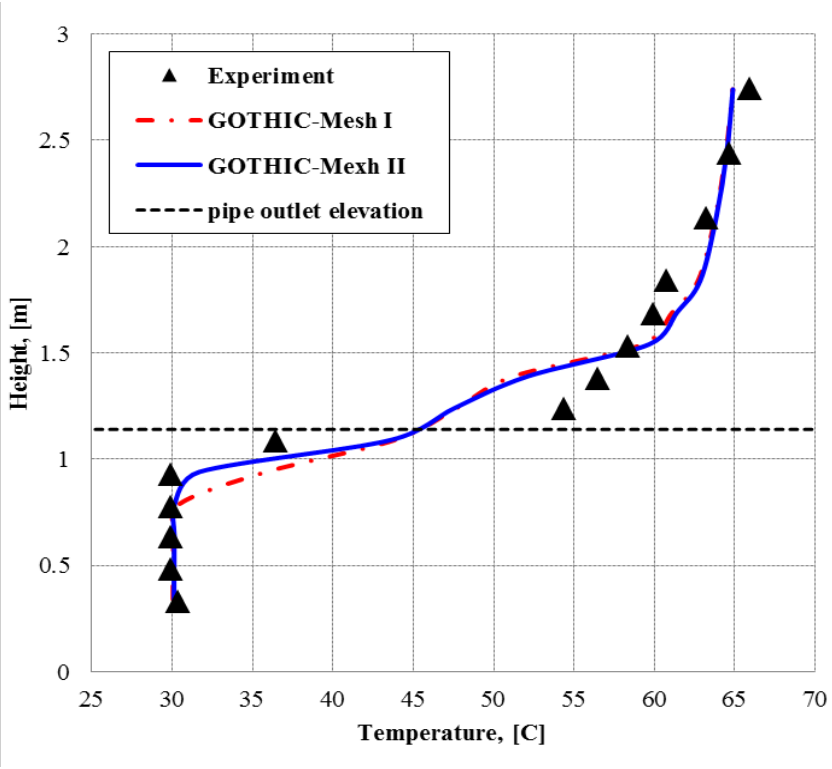

Figure A-14
GOTHIC vertical temperature predictions with different grid resolutions

Comparing the results generated here with those from Li, et al, it is clear that the simulation of stratification can be sensitive to rather small changes in the modeling approach. This sensitivity was observed in the conduct of the noding sensitivity study. When the model with the finest grid was first run, the GOTHIC results showed near complete mixing of the entire pool throughout the transient. It was found that using an iterative solution method for the reduced set of cell equation solved by GOTHIC rather than a direct matrix reduction technique restored the stratification. Apparently, the accumulated round-off error in the direct solution method was sufficient to induce and maintain a significant circulation loop in the pool. This round-off error in a direct solution naturally increases with the number of cells. For the iterative method used in GOTHIC, local round-off error is independent of the number of cells.

In Li et al.'s study, the water pool and the discharge pipe were modeled using separate volumes and connected by heat conductors for the pipe wall and a flow path for the pipe exit. A single lumped volume was used for the discharge pipe. The simplified treatment of the discharge pipe results in incomplete condensation within the pipe and discharge of a small amount of steam into the pool. Steam bubbles that enter and condense in the pool provide an extra buoyancy source that results in over mixing, especially in the early part of the transient. The vapor flow at the bottom of the discharge pipe is evident in Li et al.'s work [2]. With the integrated pipe model

used in this study, the steam discharge into the pool was eliminated, except for the very early portion of the transient. By doing so, not only was the number of flow path connections reduced but also the discharged pipe was modeled with subvolumes on the same grid as the water pool. This allows for more detail in the condensation behavior as the steam progresses through the discharge pipe and provides more consistent treatment of the momentum equations at the bottom of the pipe. Although the GOTHIC flow path momentum models are nearly consistent with the momentum treatment for cell faces in a subdivided model, there are minor differences to accommodate the more general features of the flow paths.

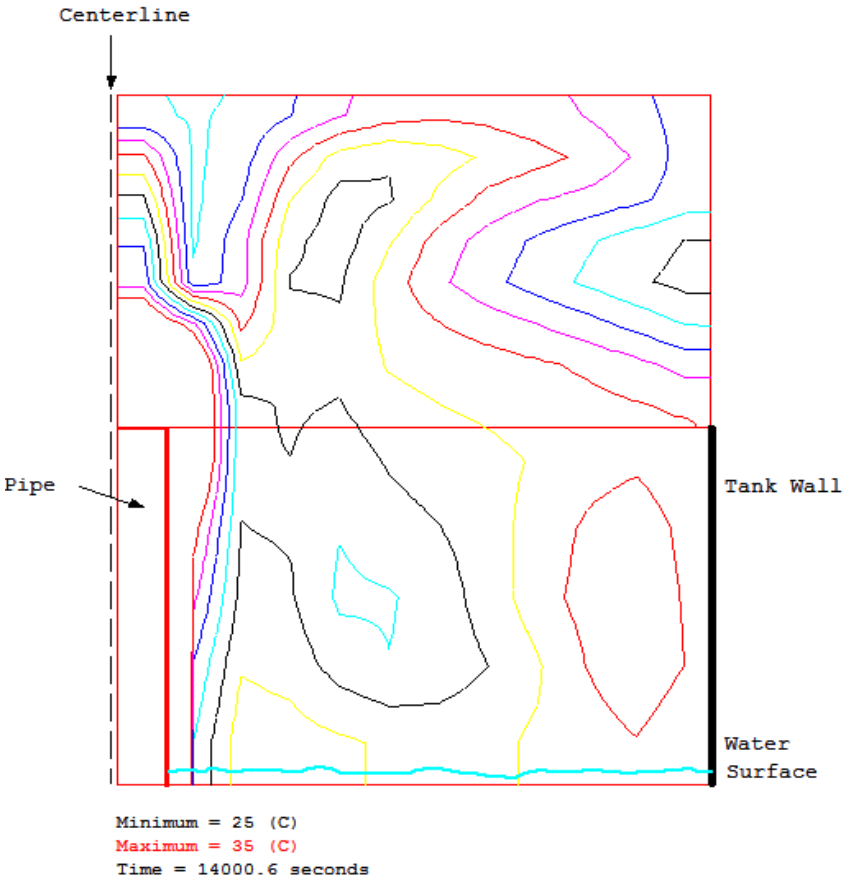

Figure A-15
GOTHIC Vapor Temperature Contours Above the Pool Surface

Finally, in Li et al.'s work, the lab atmosphere was modeled as a large lumped volume at constant room temperature and it was connected to the pool surface with a 3D connecter. This method, however, can misinterpret the heat transfer calculations between the air and vapor above the pool; setting a volume of air at constant 24 °C temperature above the pool can result in an under-prediction of the surface temperature. Therefore, in this study, the atmospheric region right above the pool surface was modeled by subdivided volumes to capture the heat transfer effect correctly. As shown in Figure A-15 and Figure A-16, the vapor above the pool surface/inside the room atmosphere mixes through natural circulation due to density differences, and the vapor temperature reaches up to 35 °C. This approach provides more realistic simulation in terms of heat loss and its effect on the pool surface temperature predictions.

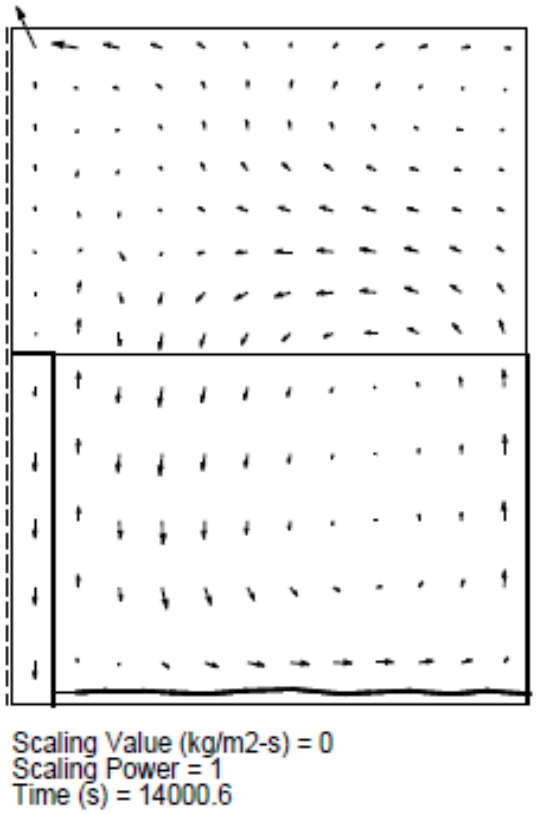

Figure A-16
GOTHIC Mass flux profile above the pool surface

A.3.5 Summary

In this study the GOTHIC model performance on condensation, stratification and mixing phenomena in a pool of water was investigated. GOTHIC models for the POOLEX STB-20 tests, with different grid refinements, were compared against the transient temperature distribution in the pool and the vertical temperature profile after 14,600 seconds of continuous steam injection. Contrary to the experience reported by Li [2], the integrated model for the discharge pipe gave reasonable results without resorting to special treatment of the heat and momentum source. Increasing the number of cells in the pool generally provided more accurate predictions compared to the experimental data. In summary, it is concluded that current GOTHIC models are capable of capturing the steam condensation in a discharge pipe and the thermal stratification inside the water pool correctly.

A.3.6 Acknowledgment

The present work benefited from the input of Dr. Walter Villanueva and his research group from Royal Institute of Technology (KTH), who provided their GOTHIC models and assistance to the research summarized herein.

A.3.7 References

3. J. Laine and M. Puustinen (2006), Thermal Stratification Experiments with the Condensation Pool Test Rig, NKS Report, Lappeenranta University of Technology, Finland. NKS-117.
4. H. Li and P. Kudinov (2010), Effective Approaches to Simulation of Thermal Stratification and Mixing in a Pressure Suppression Pool, CFD for Nuclear Reactor Safety Applications (CFD4NRS-3) Workshop, Bethesda, MD, USA.
5. H. Li, P. Kudinov and W. Villanueva (2010), Modeling of Condensation, Stratification, and Mixing Phenomena in a Pool of Water, NKS Report , Division of Nuclear Power Safety, Royal Institute of Technology, KTH, Sweden, NKS-225.
6. H. Li, P. Kudinov and W. Villanueva (2011). Development and Validation of Effective Models for Simulation of Stratification and Mixing Phenomena in a Pool of Water, NKS Report , Division of Nuclear Power Safety, Royal Institute of Technology, KTH, Sweden, NKS-248.
7. EPRI (2012), GOTHIC Thermal Hydraulic Analysis Package Technical Manual, Version 8.0 (QA), Palo Alto, CA, USA

Attachment A-4 Monticello SRV Discharge Test

A.4.1 Introduction

Tests were conducted at the Monticello nuclear plant in 1978 to evaluate the performance of the T-quenchers under extended Safety Relief Valve (SRV) operation [1, 2]. Two tests were conducted. In the first test steam was released to the Mark I pressure suppression pool from a single SRV. The transient temperature response at various locations in the pool was recorded. The second test was similar but included the operation of one Residual Heat Removal (RHR) loop. The validation report here is for the first of these tests.

A.4.2 Test Description

The Monticello wetwell is shown in Figure A-17 and Figure A-18.

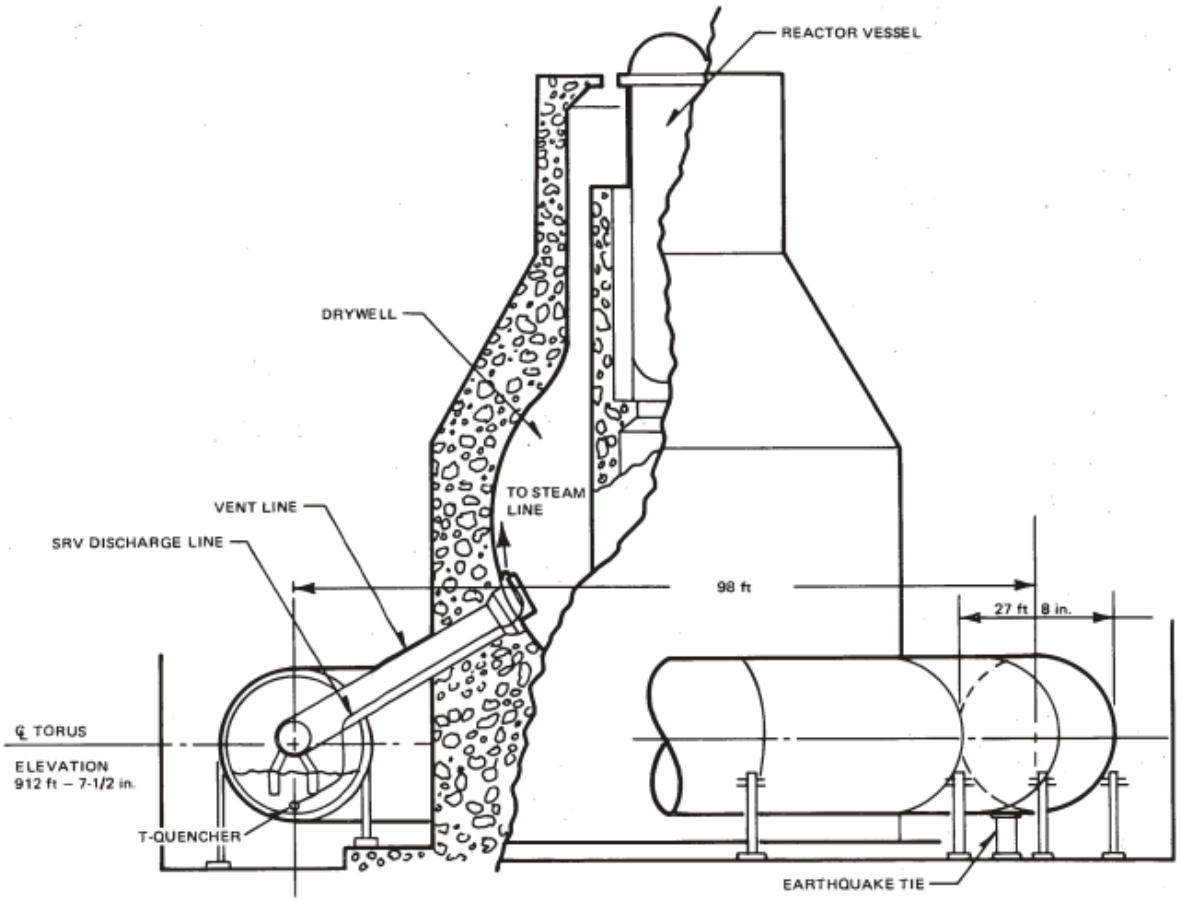

Figure A-17
Monticello Plant Configuration [2]

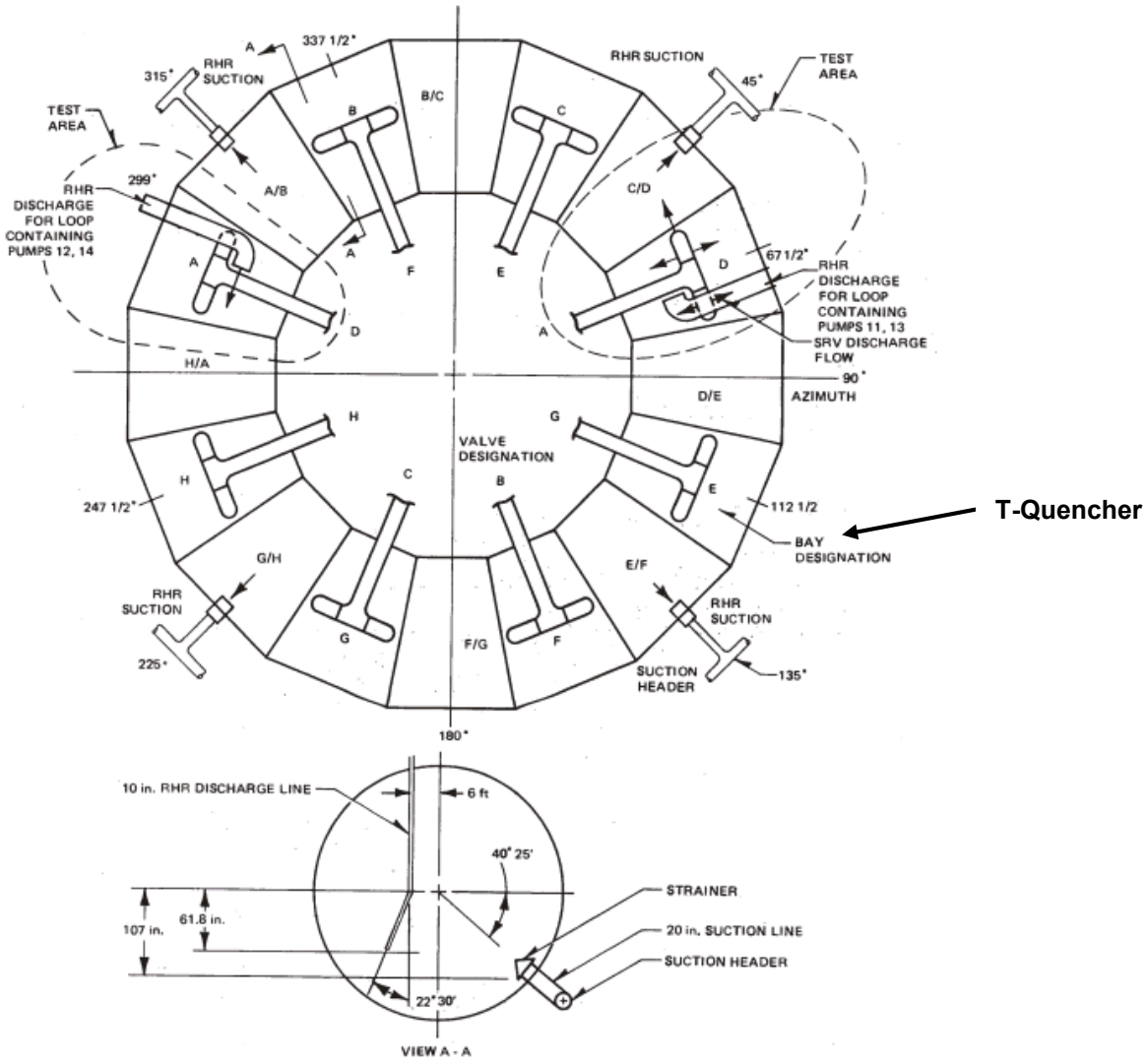

Figure A-18
Wetwell Configuration [2]

The wetwell is constructed of 16 piping segments to create a torus. Each segment is referred to as a "Bay" with the letter designations shown in Figure A-18. There are 8 T-Quenchers evenly spaced around the torus. The details of a T-Quencher are shown in Figure A-19. The holes have an estimated diameter of 3/8". One end of the T-Quencher (Zone E) has 40 holes; the other end has no holes. This arrangement was intended to promote circulation around the torus.

For this test, there was 69,000 ft^3 of water in the torus at 52.1 °F. Steam, at 1193.6 Btu/lbm, was continuously injected at 208.5 lbm/s for 11 minutes and 7 seconds through the T-Quencher in Bay D. The temperature was measure at 23 locations around the torus include lower, upper and mid-pool elevations using Resistance Temperature Detectors (RTD).

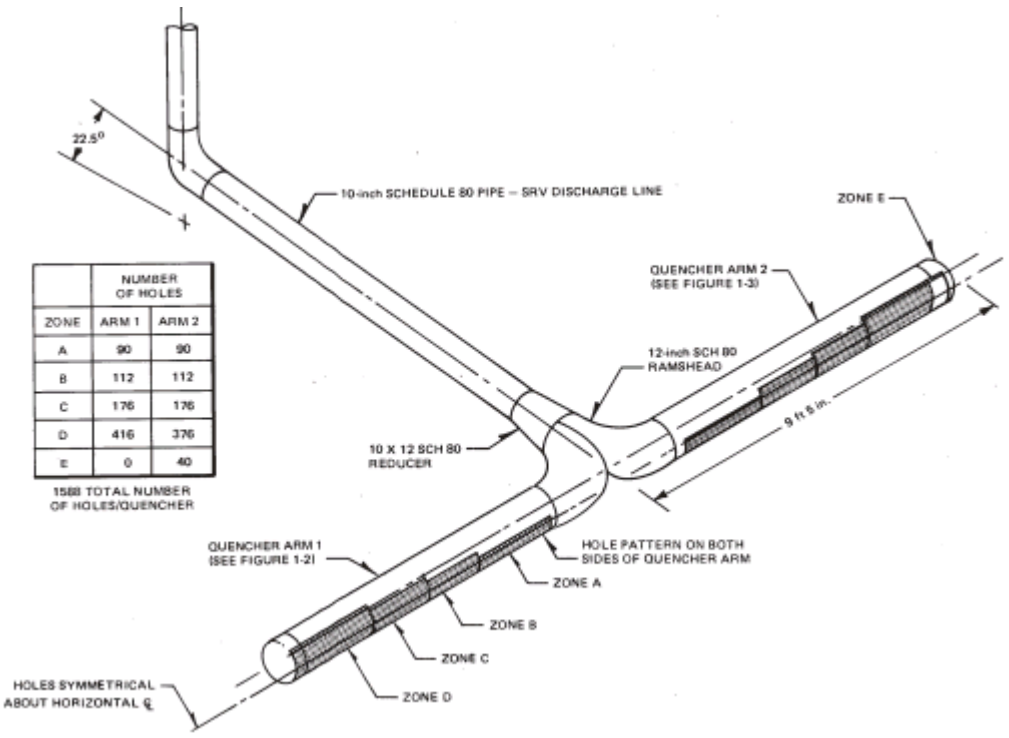

Figure A-19
T-Quencher Details [2]

A.4.3 GOTHIC Model

The overall noding diagram for the wetwell is shown in Figure A-20. For 3D modeling, GOTHIC is restricted to rectangular coordinates. Curved geometries are modeled using blockages from which volume and area porosities and hydraulic lengths are obtained. The GOTHIC 3D modeling capabilities includes an option for a torus blockage. However, to simplify the modeling and to allow finer grid resolution without excess computation time, the torus was treated as a cylinder, represented by Volume 1. A 3D connector connects one end of the cylinder to the other end. With this modeling approach the full turn of the torus is modeled but the curvature is ignored. Since the flow distribution is expected to be dominated by buoyancy forces (rather than momentum), the curvature effect should be small.

Volume 2 represents the SRV tail pipe leading to the T-Quencher and Volume 3 represents the T-Quencher pipe. The T-Quencher is connected to the nearby cell in the pool volume using 3D Connectors 2 and 3 for the holes on either side of the T-Quencher. Although this modeling approach does not directly account for the increasing number of holes towards the T-Quencher ends, it does give a uniform distribution of the steam injection over the length of the T-Quencher pipe as presumably intended by the hole pattern.

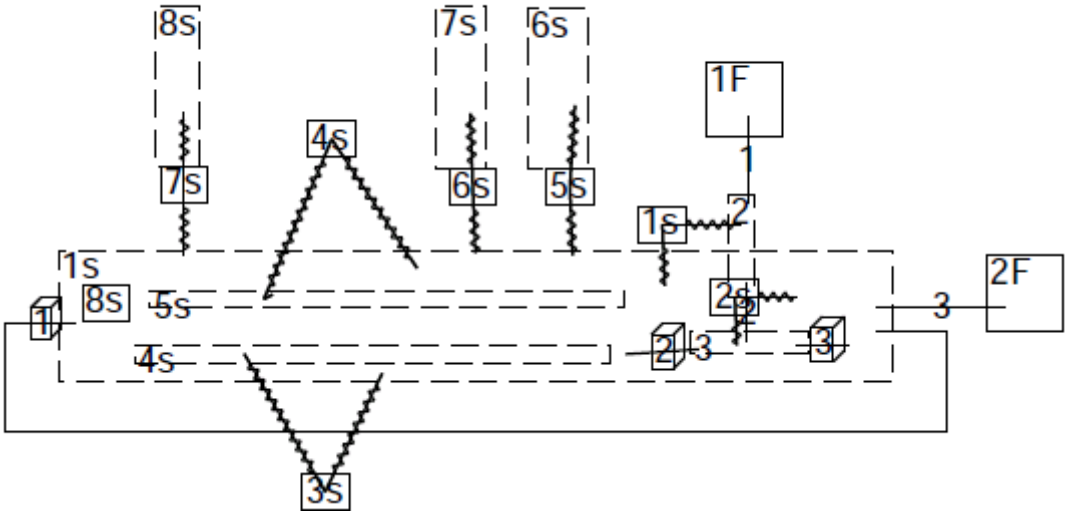

Figure A-20
Overall Noding for Wetwell

Volumes 4 and 5 represent the water in the submerged portion of the vents. The water in the vents participates in the heat up of the pool via conduction through the vent pipe but it is not free to move with the pool water in the buoyancy induced convection currents. Volumes 6, 7 and 8 model the vent support columns in the pool. Similar to the water in the vents, the water in the pool can be heated but does not move with the bulk pool flow. The three modeled supports are the ones to which some of the RTD's were attached. The mounting of the RTD's was not described in the available test documentation and it was considered that the measured temperatures may be somewhat influenced by the stationary water inside the support columns.

Conductors were included to model the heat transfer across the tail pipe to the torus air space (#1s), across the tail pipe to the pool (#2s), across the submerged vents (#4s and #5s), across the support tube walls (#6s, #7s and #8s) and the torus shell (#8s).

The conductors were included in an attempt to improve comparisons between the GOTHIC predictions and the data. However, in the end, it was found that these had only a small effect on the pool behavior. A larger effect was due to the fluid dynamic drag imposed by the structures in the pool. Distributed loss factors were included to account for the drag from the vents, vent supports, SRV tail pipes, T-Quenchers, T-Quencher support structure and the torus ribs between bays that extend into the pool.

The 3D noding for the unrolled torus is shown in Figure A-21. The uniform grid line spacing in the x (circumferential) direction is 2.1 ft. The uniform grid line spacing across the torus tube is 5.5 ft. The grid line spacing in the vertical direction is 1 ft. in the pool with coarser spacing in the air space (2-5 ft.).

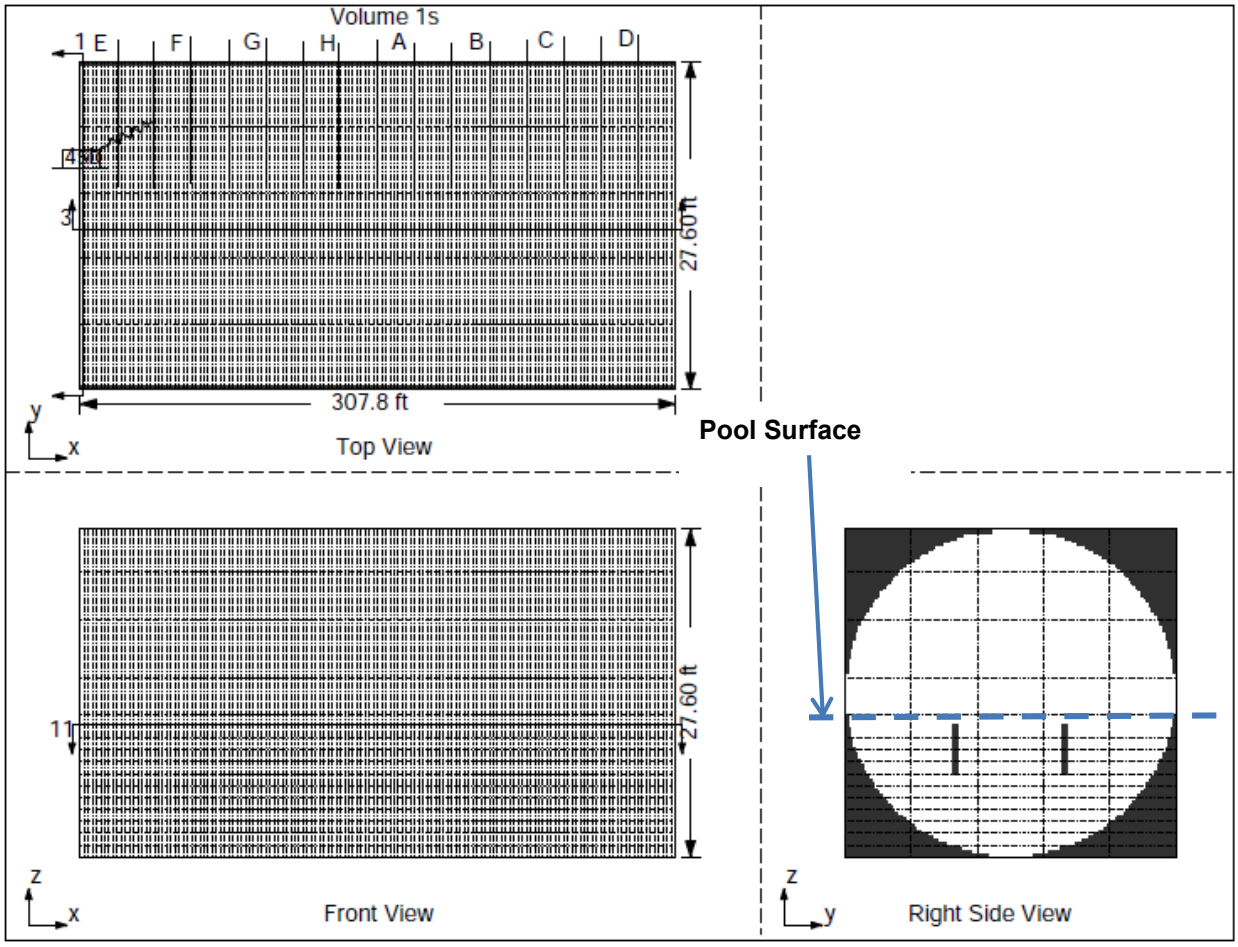

Figure A-21
3D Torus Noding

A.4.4 Results

The graphs that follow show the temperature transients in the upper pool, pool mid-level and lower pool. The torus tube ID is 27.7 ft. and the water level is 10.95 ft. Except for Bay D, the RTDs were mounted at 38" (3.2 ft.), 80" (6.7 ft.) and 122.4" (10.2 ft.) from the bottom of the pool. More RTDs were used in Bay D where the active SRV discharge was located. Mid-level RTDs were mounted at 66" (5.5 ft.) and 95.5" (8.0 ft.) instead of 80". Results are shown for Bays D, C, B and H in Figure A-22 through Figure A-33.

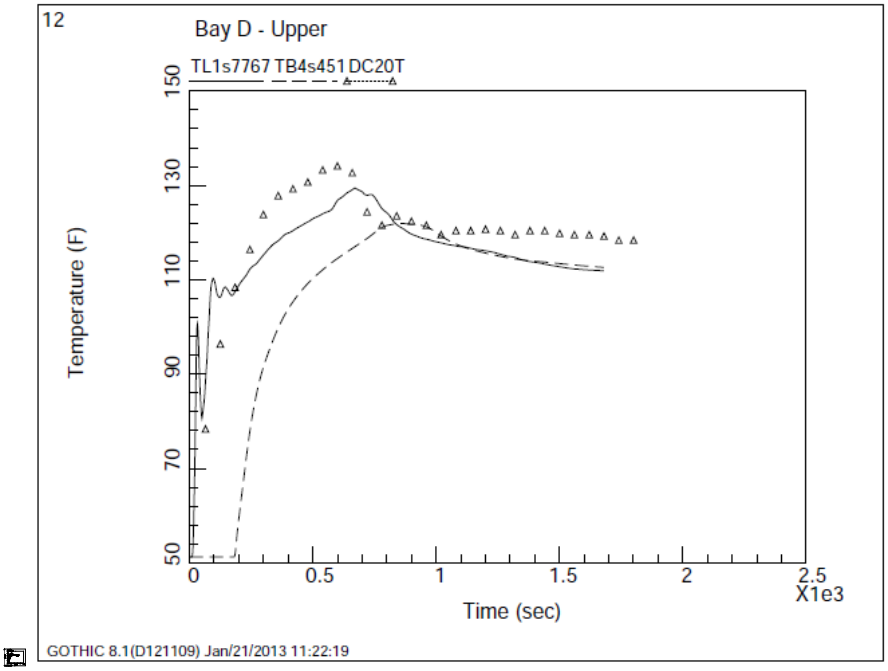

Figure A-22
Bay D Upper Level

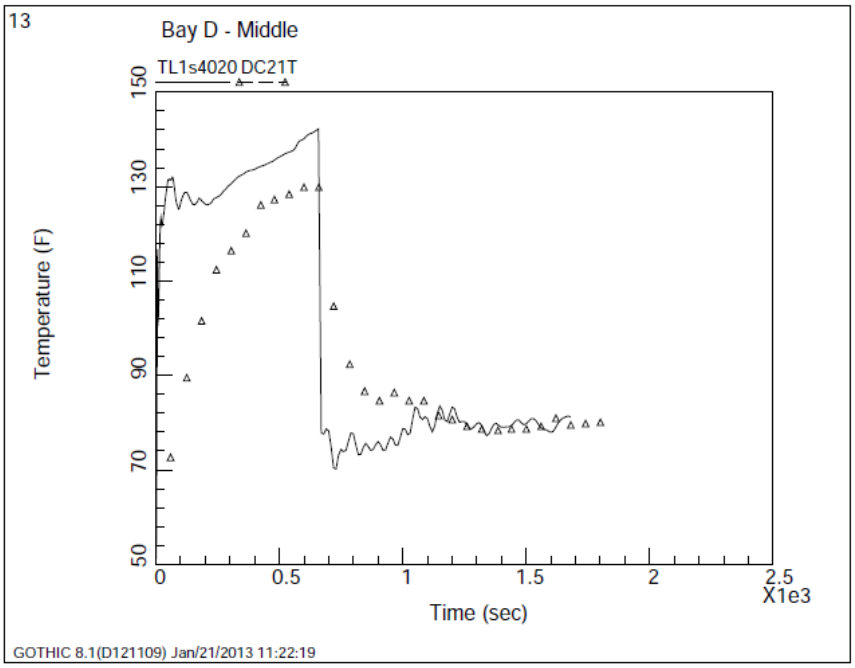

Figure A-23
Bay D Mid-Level

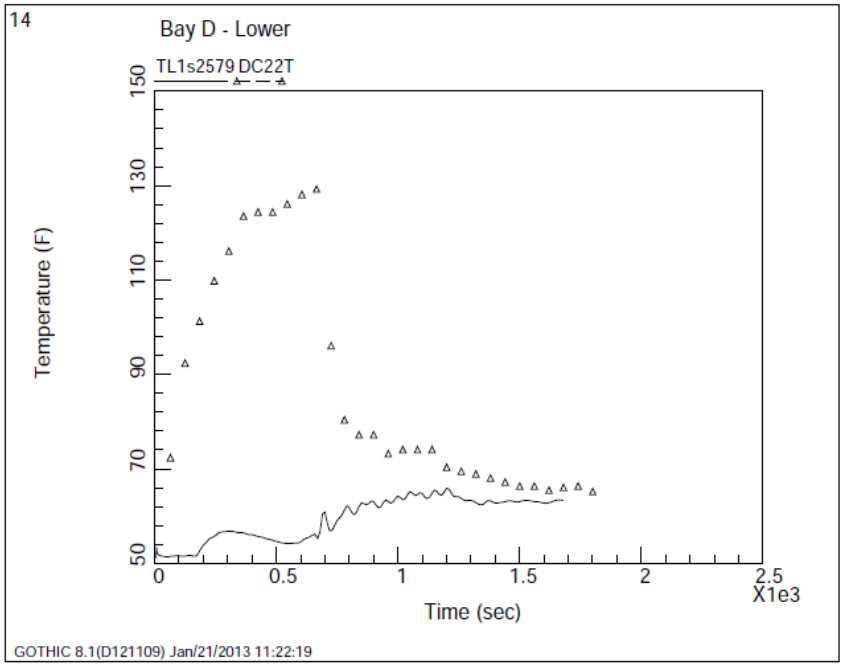

Figure A-24
Bay D Lower Level

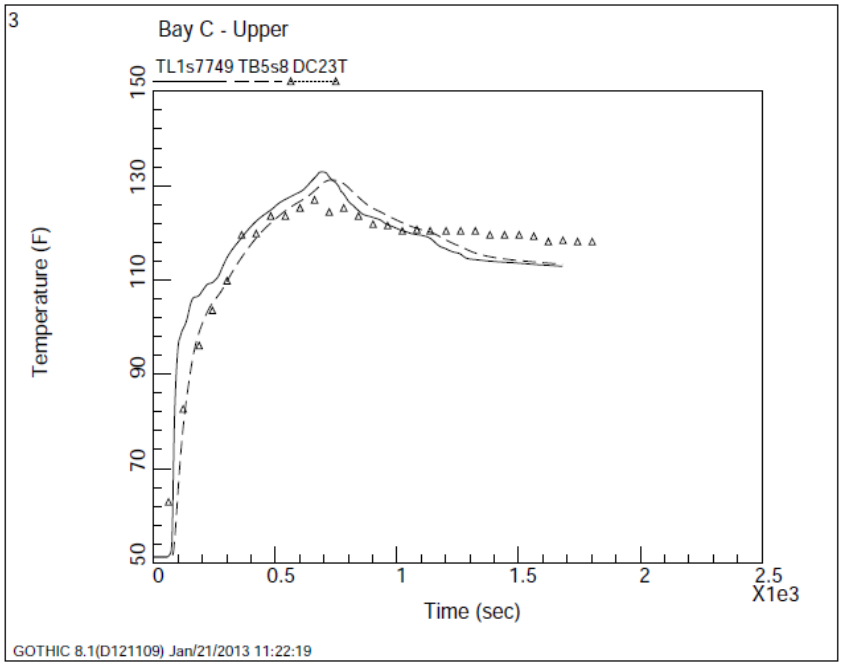

Figure A-25
Bay C Upper Level

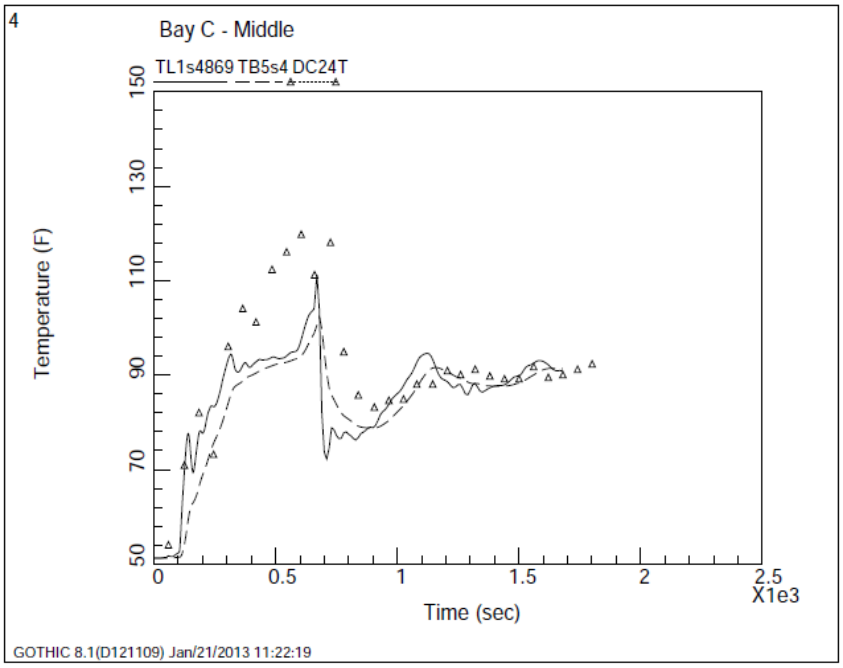

Figure A-26
Bay C Mid-Level

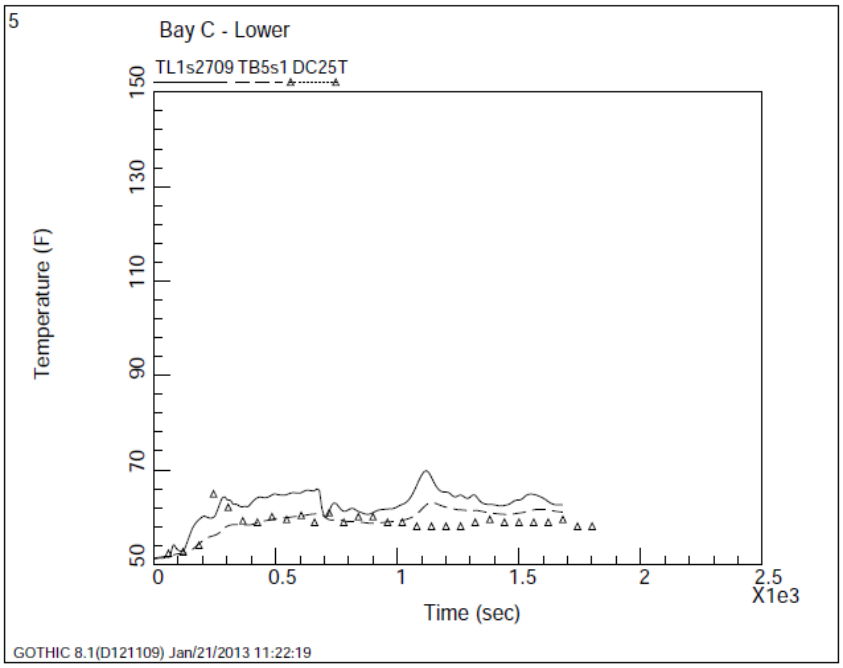

Figure A-27
Bay C Lower Level

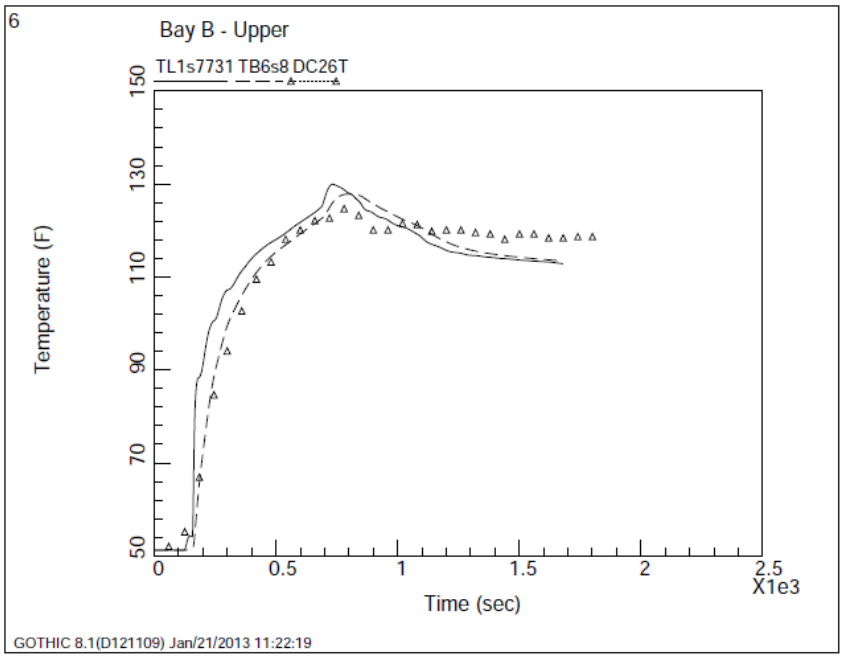

Figure A-28
Bay B Upper Level

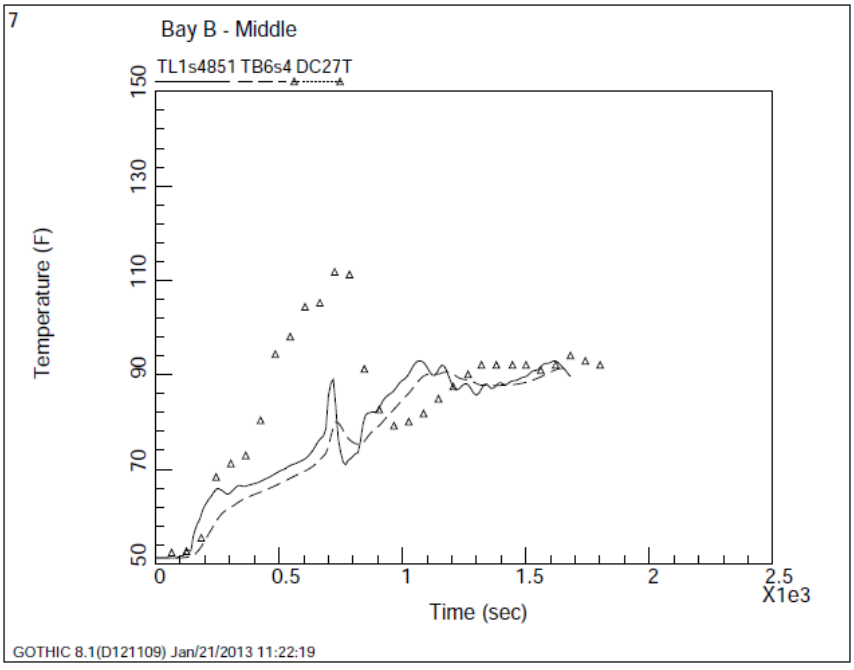

Figure A-29
Bay B Mid-Level

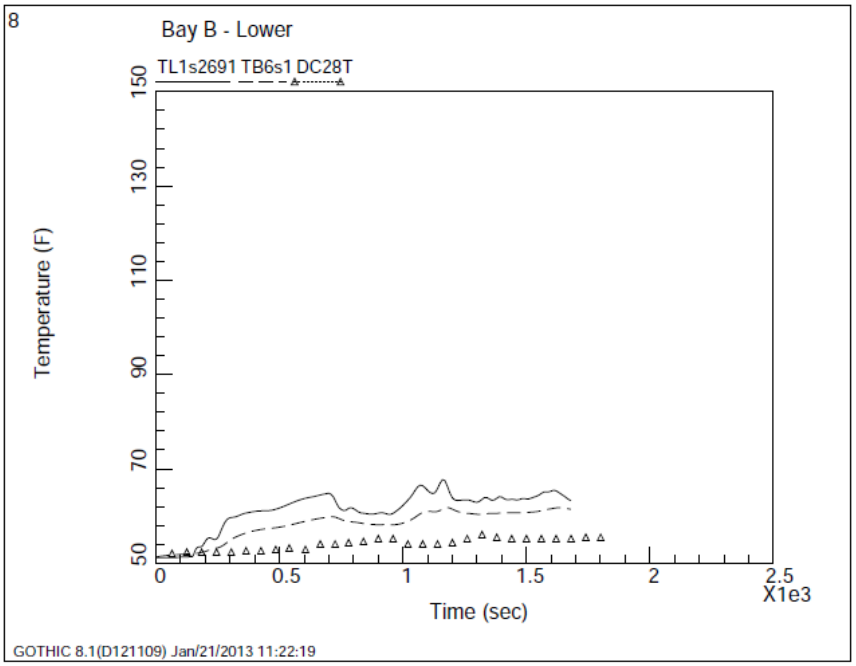

Figure A-30
Bay B Lower Level

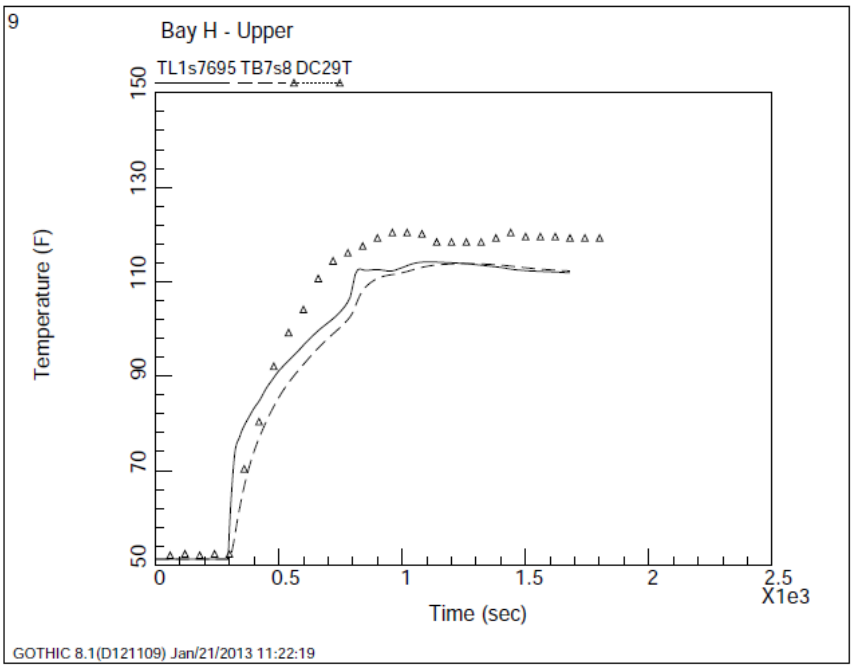

Figure A-31
Bay H Upper Level

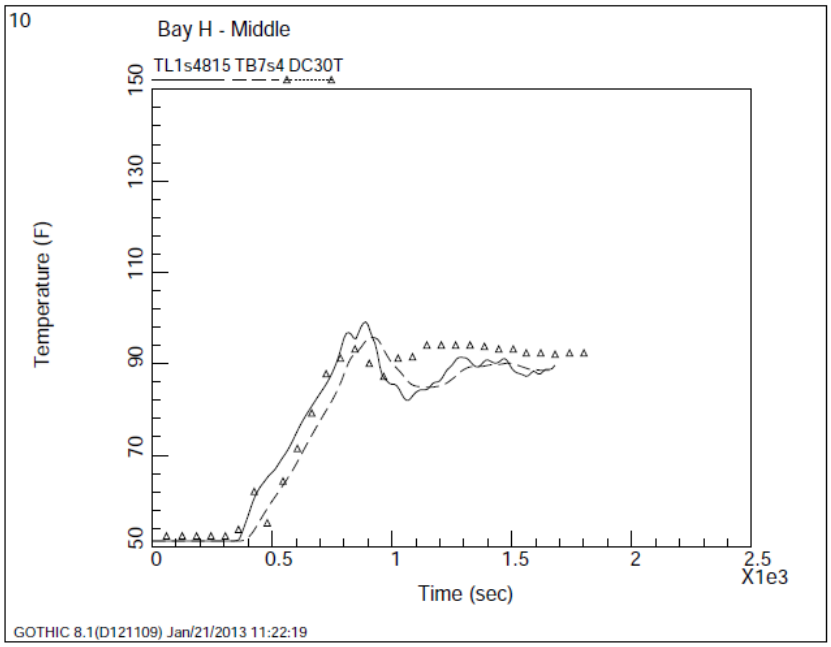

Figure A-32
Bay H Mid-Level

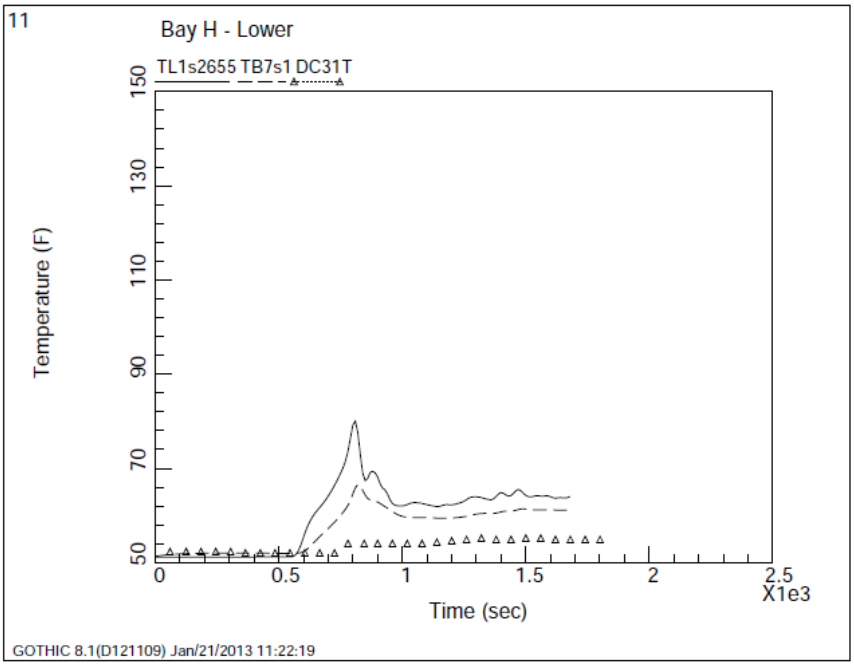

Figure A-33
Bay H Lower Level

In general, there is reasonable agreement between the data and the GOTHIC results. It must be recognized that the measured temperature is for the small volume in close contact with the RTD while the GOTHIC results are a cell average value for a cell that is over 10 ft^3. In regions of strong temperature gradients, the cell average temperature may differ substantially from the value at the measurement location. To illustrate, the temperature distribution at 600 seconds is shown in Figure A-34

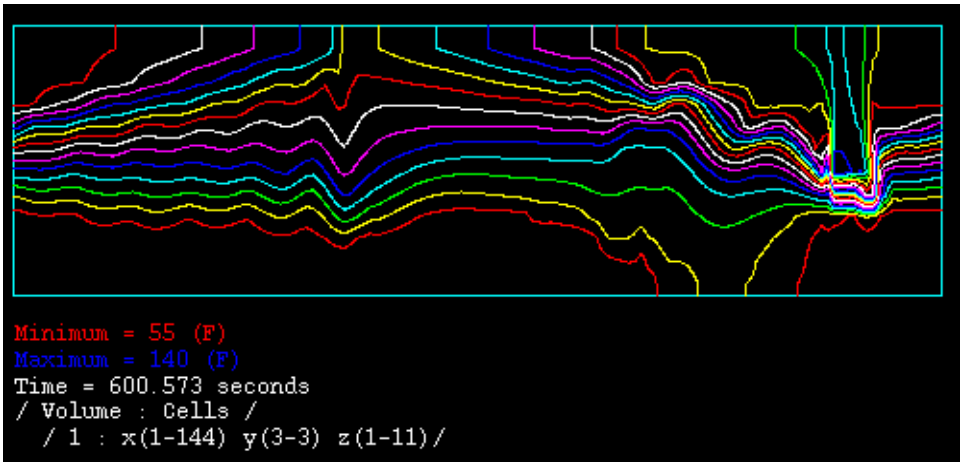

Figure A-34
Temperature Distribution at 600 seconds

The arrival time of the temperature rise in each of the bays is well predicted. After the steam injection was terminated, GOTHIC maintains the stratification but the top to bottom difference is somewhat less than indicated by the data. Although, there is general agreement with the transient development at the various locations, there are some notable exceptions. The worst agreement is at the lower level in Bay D. In this bay, the measurements indicate that during the steam injection, the temperature at the lower level is about the same as at the mid-level. This may be a bit surprising considering that the lower level RTD is located about 2 ft. below the T-Quencher. Inspection of the GOTHIC results indicates that local convection loops develop throughout the pool and especially in Bay D as shown in Figure A-35. Apparently, the lower RTD in bay D is located in a local convection loop with down flow from the high temperature region above. These local convection loops depend strongly on the local geometry details that are not captured in the relatively coarse grid used in this simulation.

Figure A-36 is a frame shot of a TecPlot® animation showing the wetwell liquid temperature profile at 600 seconds. This animation can be viewed by following the link Monticello_animation [3]. The URL is available in the reference section. The animation shows a thermal plume that evolves during the discharge. The plume distributes laterally throughout the suppression pool until a nearly uniform thermal stratification of the pool occurs.

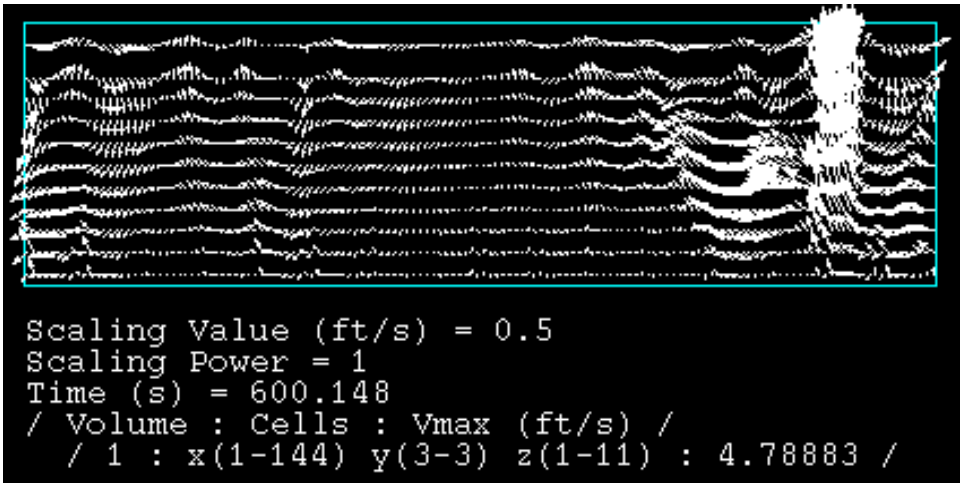

Figure A-35
Velocity Pattern Distribution at 600 seconds

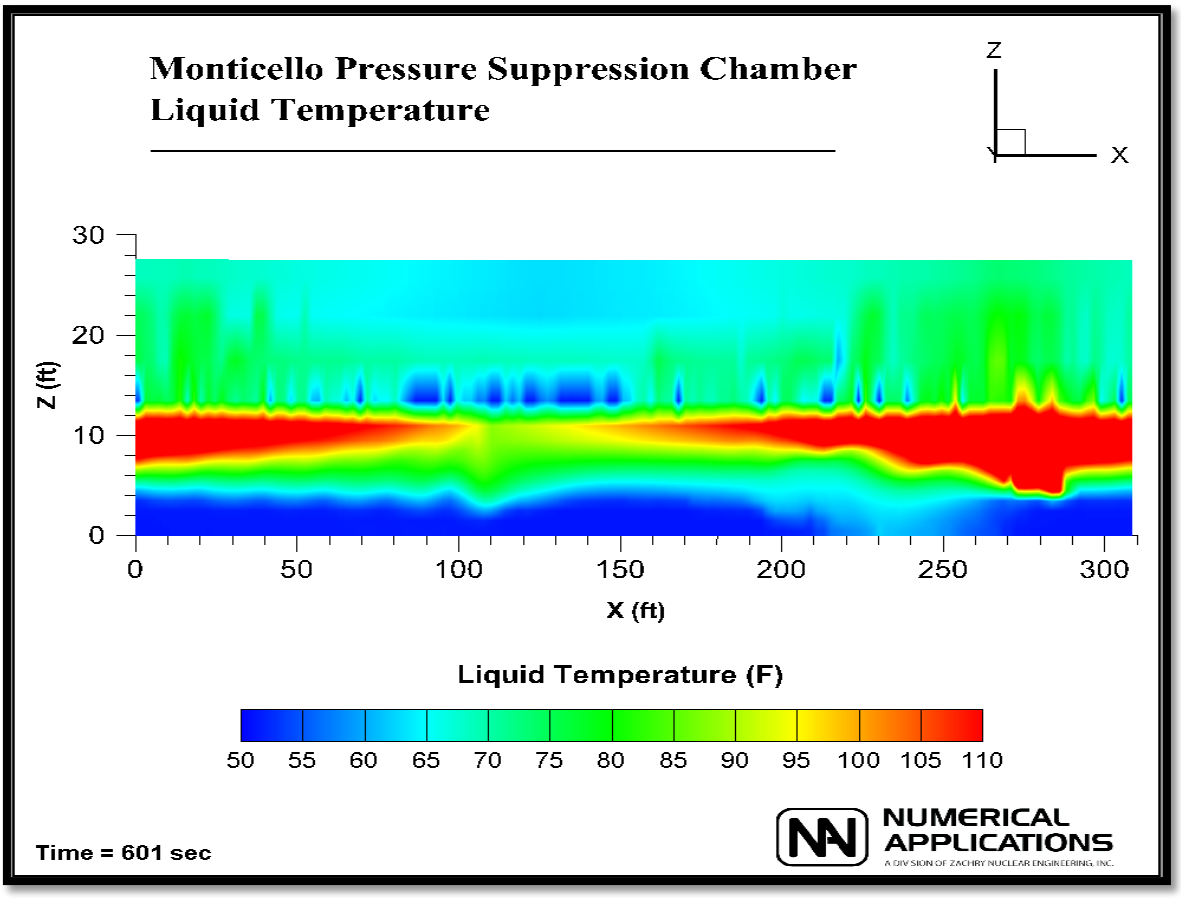

Figure A-36
TecPlot Frame Showing Thermal Plume at 601 Seconds

A.4.5 Conclusion

Allowing for differences due to local versus cell average conditions, overall, GOTHIC gives good agreement for the transient development of the temperature distribution and the thermal stratification that develops and persists after the steam flow has been terminated.

A.4.6 References

1. Cook, DH, "Pressure Suppression Pool Thermal Mixing", NUREG/CR-3471, ORNL/TM-8906, October 1984.
2. Patterson, BJ, "Mark I Containment Program, Monticello T-Quencher Thermal Mixing Test, Final Report", NEDO-24542, 79NED101, August 1979.
3. NAI. (2013). *Monticello Animation* Retrieved from https://docs.google.com/file/d/0BzxErU0stSvGSmp1a3VSYThueUk/edit?pli=1

Attachment A-5 Browns Ferry Nuclear Plant (BFNP) Unit 2 Test

A.5.1 Introduction

In discussion regarding the possibility of stratification of the suppression pool in the Fukushima Unit 3 at the Fukushima Daiichi Technical Evaluation Project Review in November, Bill Williamson from TVA [1] recounted an incident at the Browns Ferry Nuclear Plant (BFNP) Unit 2 that indicated the potential pool stratification under long term steam release from the RCIC exhaust. The Reactor Core Isolation Cooling (RCIC) system of BFNP Unit 2 reactor was in test mode for pressure control from 16:05 on 6/28/1991 until 03:13 on 6/29/1991 (40,080 seconds). The outboard Main Steam Isolation Valves (MSIVs) were closed and the Reactor Pressure Vessel (RPV) pressure was about 5,840 kP (850 psia). During the test, neither the pool temperature indicator nor the gas space temperature monitor showed much of an increase in temperature. However, when the 2A Residual Heat Removal (RHR) pump was started, the Suppression Pool (SP) temperature indicator rose rapidly from 30.6 °C to 48.9 °C (87 to 120 °F). When the Suppression Chamber (SC) air temperature recorder was tapped, the indicated temperature jumped from 34. 5 to 65. 6 °C (94 to 150 °F). Hand calculations indicate that the energy deposited in the pool by the RCIC exhaust was enough to raise average pool temperature to 48.9 °C (120 °F).

The pool temperature response indicates a high likelihood of pool stratification. TVA provided sufficient information for the test conditions to allow a simulation with GOTHIC as described in this section.

A.5.2 Test Description

During the test the MSIV's were closed. The RPV pressure was maintained at 5,962 kPa by the RCIC system for 40,080 seconds. Procedures require that the drywell pressure be maintained below 111.7 kPa and the pressure difference between drywell and suppression chamber is between 7.9 and 9 kPa. To meet these requirements, Drywell (DW) venting was started at t = 4080 seconds followed by intermittent venting during the remainder of the test. The required venting to limit the drywell pressure increase indicates that there was substantial heating of the suppression chamber gas space and steam generation by pool evaporation.

For RCIC in test mode with RPV at high pressure and SP at low pressure, the RCIC steam flow is discharged into the SP at 3.08 kg/s (6.8 lbm/s). The free volume of the DW and vent system is 4,847 m^3 (171,000 ft^3) and the total volume of the Wetwell (WW) is 7,209 m^3 (254,000 ft^3)

The pool temperature instruments are located near the bottom of the SP (2.03 m (6.66 ft) above the torus bottom). The lower end of the RCIC exhaust sparger is at 1.84 m (6.0 ft) above the pool bottom. Normal SP level is 4.51 to 4.59 m (14.8 to 15.1 ft) above the torus bottom.

Drawings provided by TVA were used to estimate the geometric parameters needed for a 3D GOTHIC model. As shown in Figure A-37, the total vertical RCIC pipe length is 3.2 m (10.5 ft). The sparger section of the exhaust pipe has 1440 uniformly spaced 12.7 mm holes (0.5 in) (40 rows, 24 holes per row).

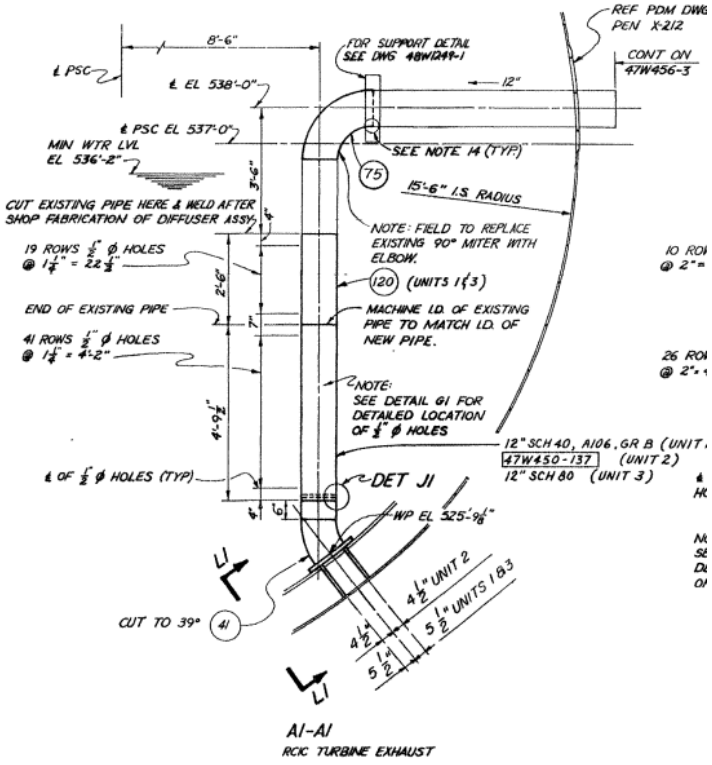

(a)

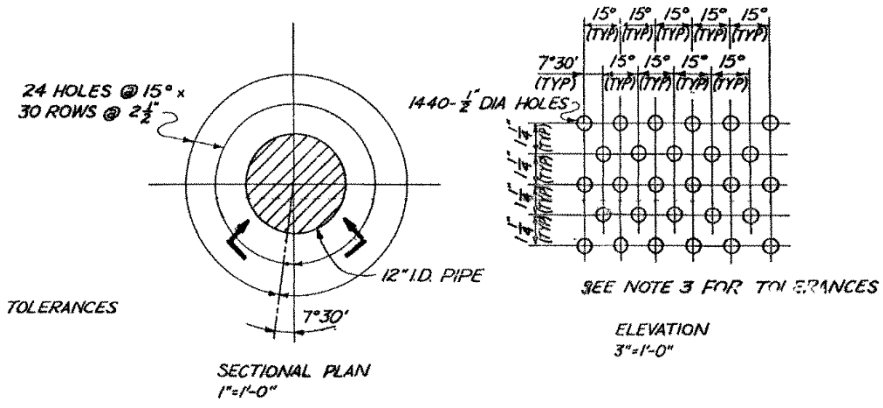

(b)

Figure A-37
BFNP Unit 2 Technical Drawings of Suppression Pool (a) and RCIC Sparger (b)

A.5.3 BFNP Unit 2 3D GOTHIC Model

Similar to previous GOTHIC Fukushima Unit 3 and Monticello analyses, the containment model was designed to address the stratification inside the suppression pool during the steam release through RCIC sparger. The GOTHIC model is shown in Figure A-38. The nominal grid spacing in the pool is 0.2 m in the vertical direction, 5.2 m circumferentially and 1.89 m across the torus minor diameter. The vertical grid spacing at the pool elevation is 0.4 m to capture steam/gas temperature right above the pool surface. The model considers only the constant steam injection

through the RCIC sparger. The mixing induced by the RHR pump at the end of the test was not modeled because there was insufficient information for this phase of the test.

For 3D modeling, GOTHIC is restricted to rectangular coordinates. Curved geometries are modeled using blockages from which volume, area porosities and hydraulic lengths are obtained. To simplify the modeling and to allow finer grid resolution without excess computation time, the torus was treated as a cylinder and only 1/2 of the total suppression chamber was modeled, taking advantage of geometric symmetry. The symmetry plane cuts through the center of the RCIC sparger. The steam injection rate was scaled down accordingly.

To approximate the pressure transient, the model includes one-half of the drywell and vent system. Flow Paths 2 and 3 connect the Vent volume to the drywell and wetwell, respectively. Flow Path 4 represents the vacuum breaker line between the wetwell gas space and the drywell. Valve component 1V models the vacuum breakers.

As shown in Figure A-38, subdivided Volumes 1s and Volume 2s represent the 1D DW and 3D WW geometries. Lumped Volume 3 represents the DW Vent and Volume 4 represents the Torus Room. A conductor was added to allow heat transfer from the interior of the vent system (drywell vents, header and downcomers) to the wetwell gas space. Conductors were also added for heat transfer between the wetwell gas space and the Torus Room and between the Torus Room air and the Torus Room concrete walls.

Volume 5 represents the RCIC Pipe. Volume 6 represents a portion of the remaining RCIC exhaust line. This volume was included represent some of the remaining RCIC system and to act as a surge volume that helps to limit high pressure oscillations due to collapsing steam bubbles in the exhaust line. Volume 5 represents the submerged RCIC Sparger. The RCIC exhaust sparger volume was subdivided in z-direction and its grid spacing was kept identical to the axial grid spacing of the suppression pool region in the WW Volume 2s. The Sparger volume is connected to the pool with nine Flow Paths (FP) spanning the range of the sparger length. Each FP has an equivalent diameter and flow area based on given geometric parameters and total number of openings at each elevation (Figure A-37 (b)).

The assumed initial conditions were 30 °C (86 °F) and 101.3 kPa (14.7 psia). Steam was injected from boundary condition 1F into the RCIC pipe at 1.54 kg/s (3.4 lbm/s) (1/2 scaled down RCIC steam exhaust flow). The steam enthalpy is estimated at 2,785 kJ/kg based on the measured RPV pressure (5,962kPa) (saturation conditions assumed). The steam flow rate remained constant throughout the transient. The simulation was run for 43,200 seconds (12 hours), slightly longer than the actual test. However GOTHIC results are compared at the exact test measurement time. Results are discussed and compared with the measured values in the following section.

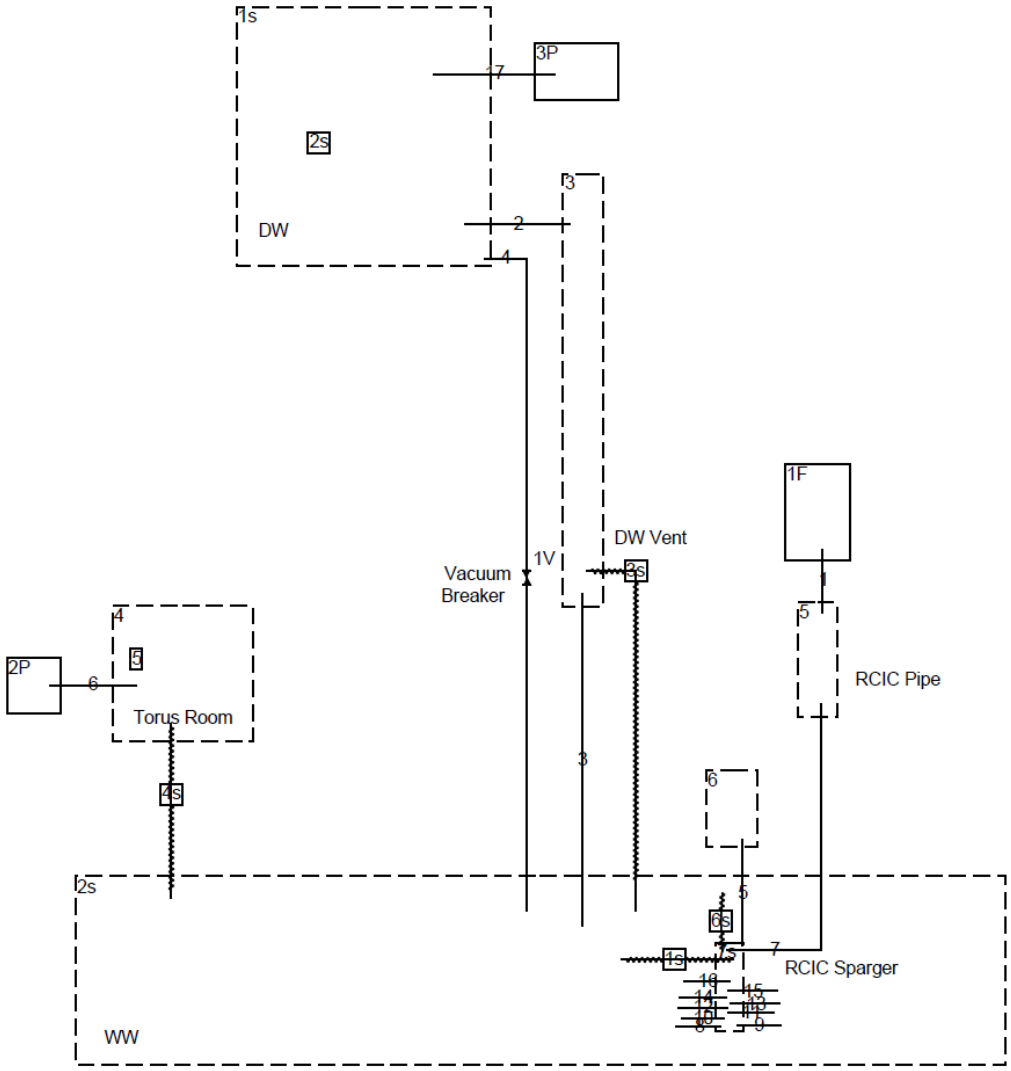

Figure A-38
GOTHIC 3D Model Nodalization

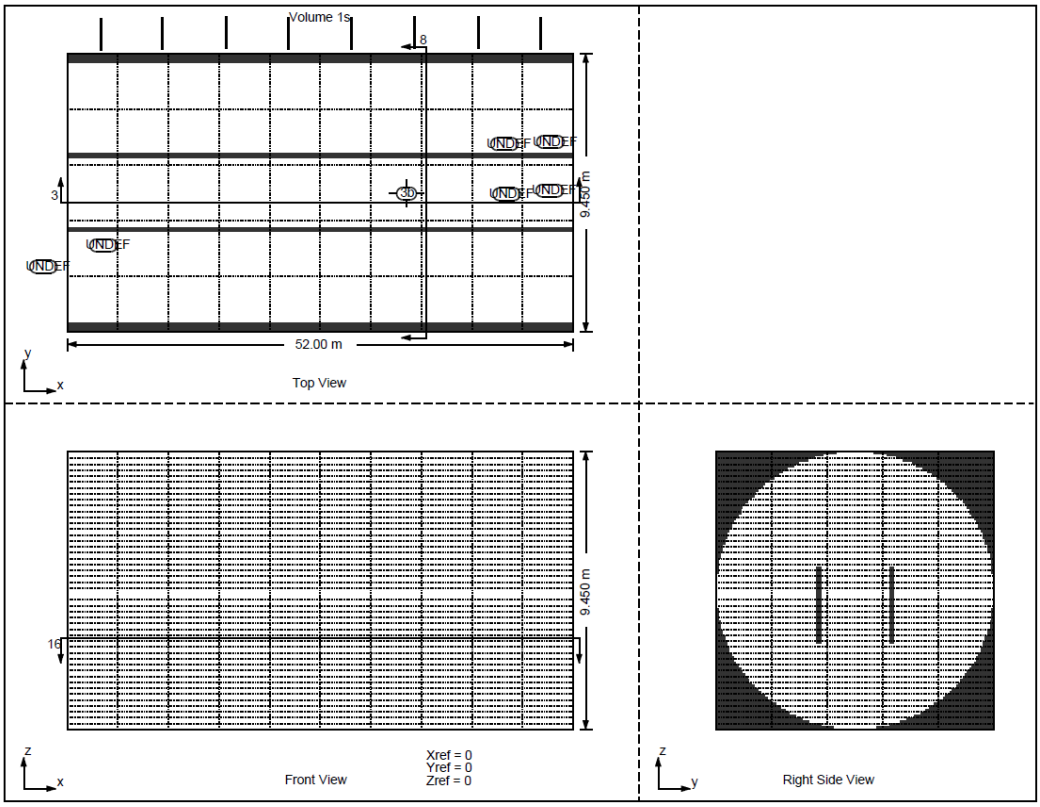

Figure A-39
GOTHIC 3D Model Suppression Pool Mesh

A.5.4 BFNP Unit 2 3D GOTHIC Model Results

The GOTHIC suppression chamber and suppression pool temperature predictions are compared with the plant measurements. As shown in Figure A-40, the SC steam/air temperatures at the top of the torus and above the pool surface increased almost linearly throughout the transient. The temperature difference between the top of the torus and near the pool surface remains within a 0-2 °C range, which indicates the atmosphere above the SP, was well mixed throughout the test. According to GOTHIC predictions, at t = 40,080 s the steam/air temperature near the pool surface reached 64.2 °C in good agreement with the BFNP Unit 2 plant measurement of 65.6 °C.

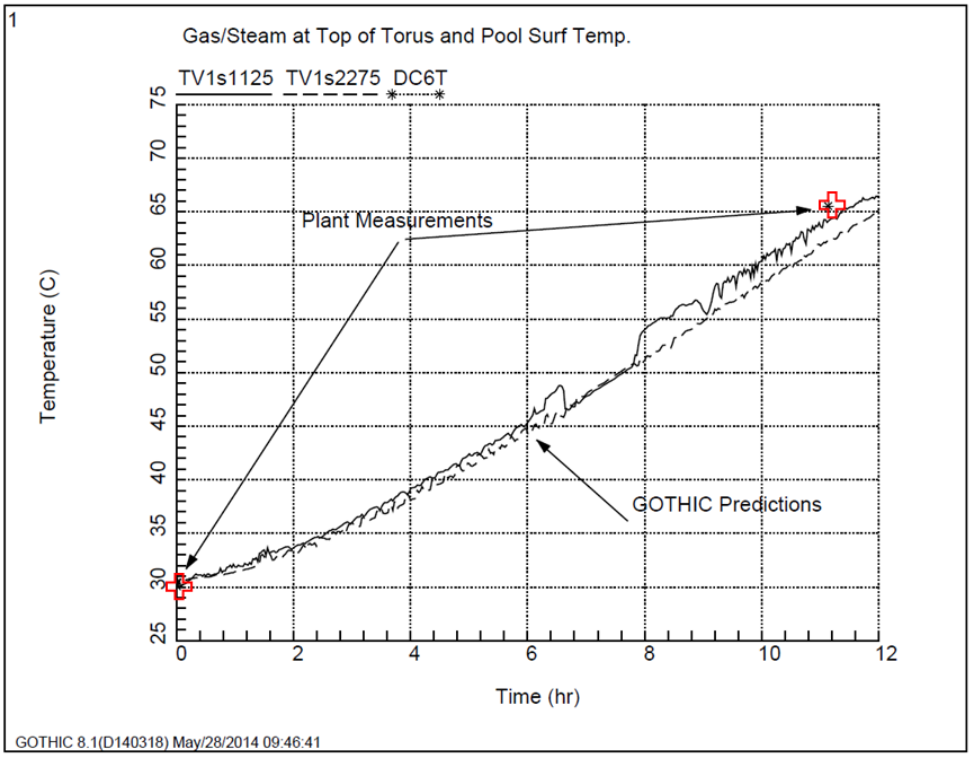

Figure A-40
GOTHIC Temperature Gas/Steam Predictions at Pool Surface and Torus

As shown in Figure A-41, the GOTHIC suppression pool (SP) temperature predictions at different elevations demonstrate the thermal stratification in the pool. From Figure A-42, steam is released from only the first two levels of the RCIC sparger (3.7 m and 3.5 m above from the pool bottom) into the SP. As a result, the water temperature above 3.5 m is well mixed and increases to about 66 °C while the pool bottom temperature remained at its initial value of 30 °C.

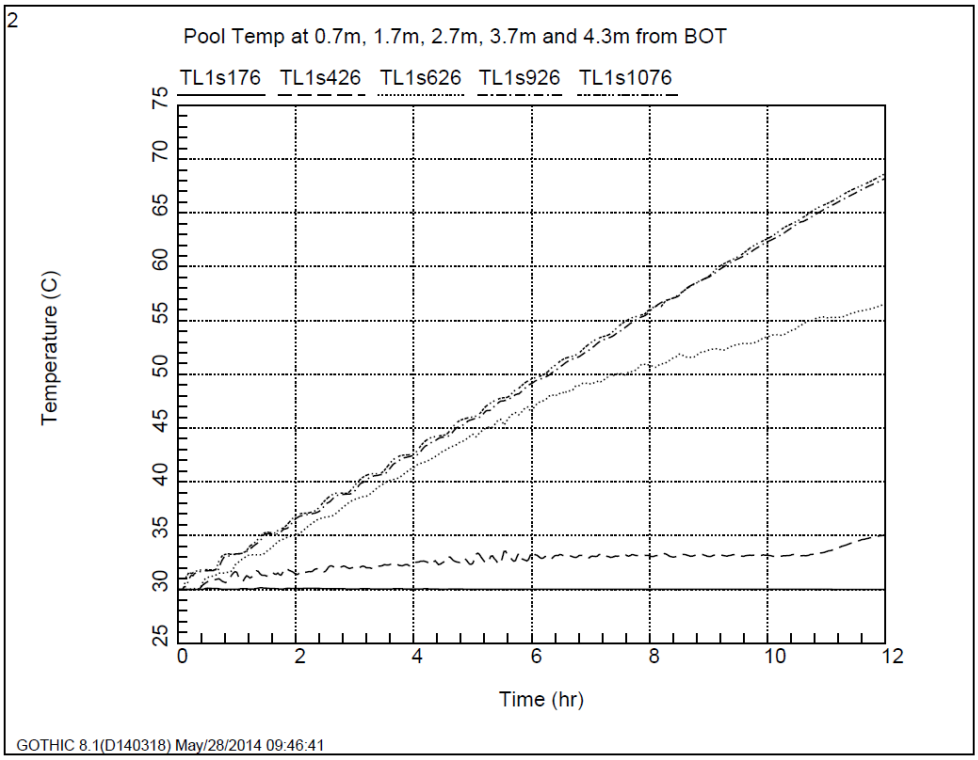

Figure A-41
GOTHIC Temperature Predictions of Suppression Pool

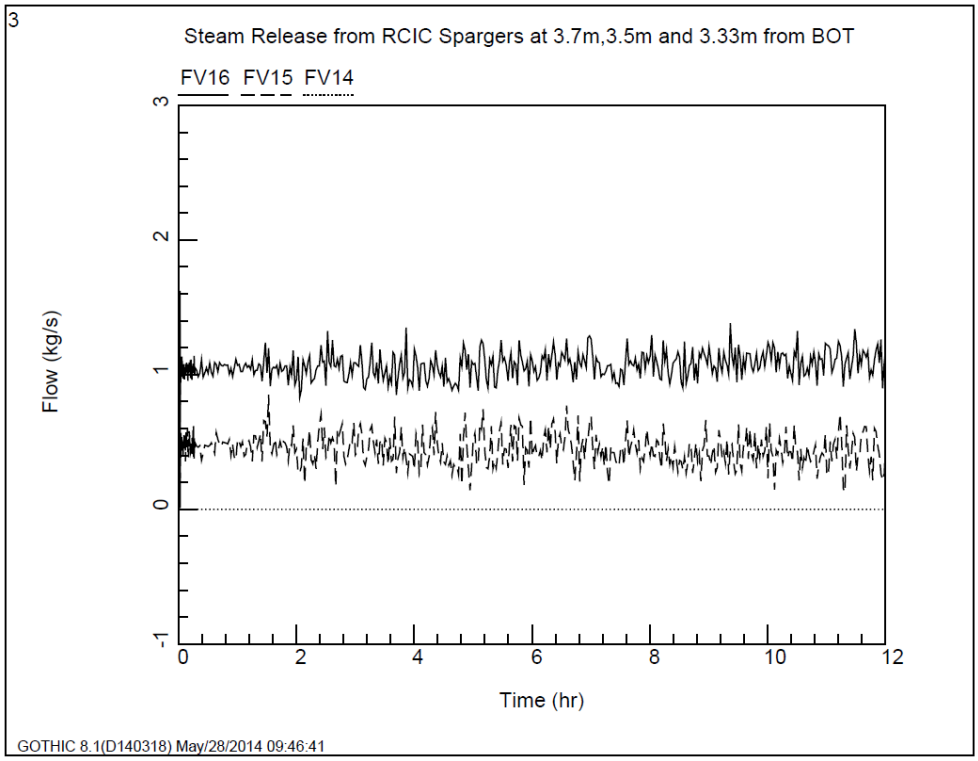

Figure A-42

GOTHIC Pool Steam Release Predictions from RCIC Sparger

Figure A-43 and Figure A-44 show the suppression pool liquid velocity vectors and temperature contour profiles, respectively. The vector plot confirms that there is substantial mixing between the hot liquid/steam and the pool water at higher elevations. At around 40,100 s, the SP temperature is stratified from 30 °C to 66.4 °C between the pool bottom and pool surface.

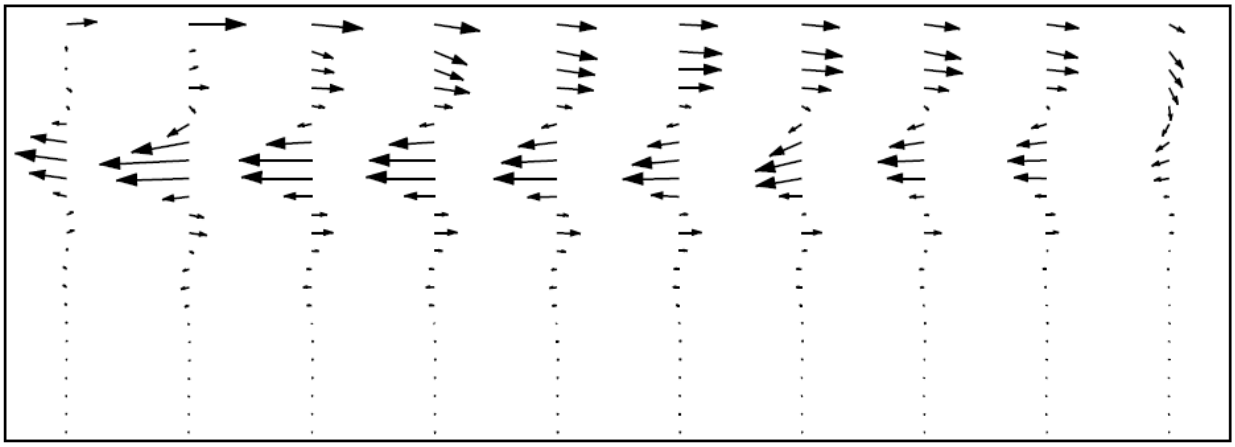

Scaling Value (m/s) = 0
Scaling Power = 1
Time (s) = 40101.1
/ Volume : Cells : Vmax (m/s) /
/ 1 : x(1-10) y(3-3) z(1-23) : 0.0703262 /

Figure A-43
GOTHIC Velocity Vector Predictions of Suppression Pool Mixing

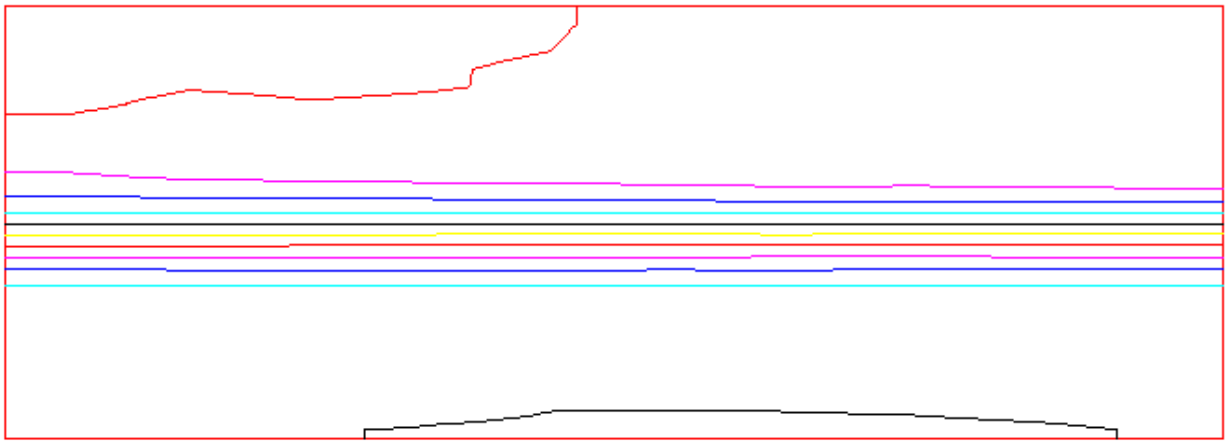

Minimum = 30 (C)
Maximum = 66.3636 (C)
Time = 40101.1 seconds
/ Volume : Cells /
/ 1 : x(1-10) y(3-3) z(1-23)/

Figure A-44
GOTHIC Temperature Contour Predictions of Suppression Pool Stratification

The increase in pool surface temperature heats the suppression chamber (SC) steam/gas atmosphere and increases its pressure. As shown in Figure A-45, the SC pressure linearly increased until it reached 120 kPa. The DW venting started at around 4.8 hours when the pressure difference between SC and DW reached 7.9 kPa (1.15 psi). The DW pressure increased linearly until it reached its pressure limit of 111.7 kPa. During the RCIC testing, DW venting wasn't as continuous as it is predicted in GOTHIC. Instead, venting was reported as on and off during the event. In addition, earlier venting was stated during the RCIC testing than predicted by the GOTHIC model. It should be noted that the GOTHIC model was not intended to predict the drywell venting since there is limited information available about how the venting was performed. Hence, in GOTHIC simulations venting didn't started until the DW pressure operating limit was reached.

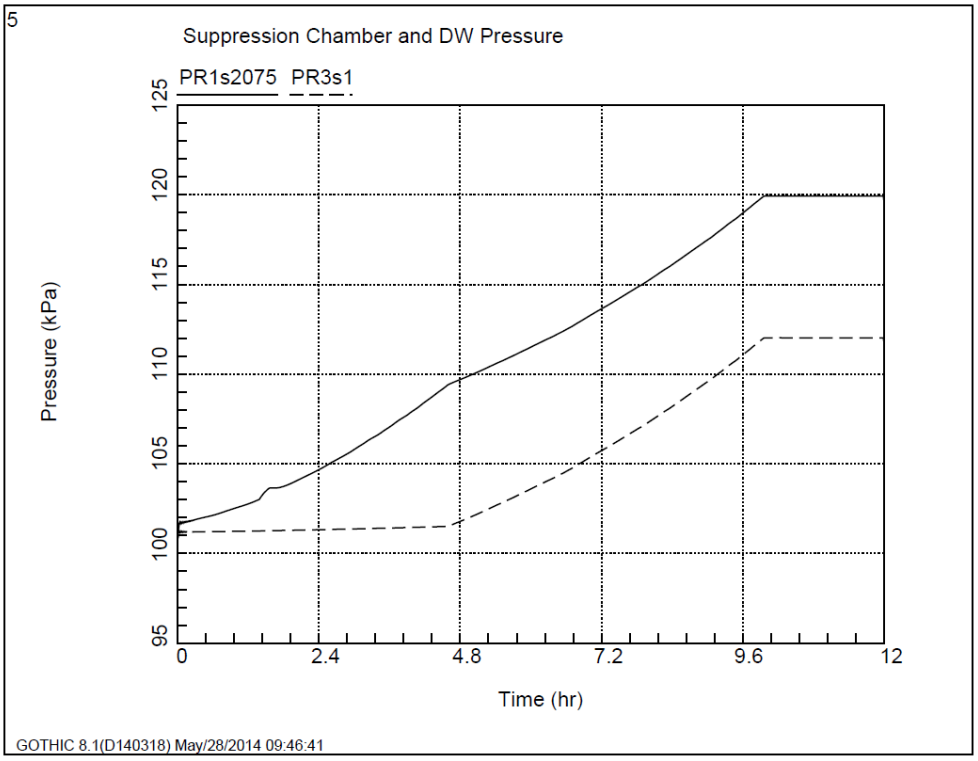

Figure A-45
GOTHIC Pressure Predictions of Suppression Chamber and Drywell

A.5.5 Conclusion

Allowing for differences due to simplifications in modelling, overall, GOTHIC gives good agreement with the limited measurements available from the test. The stratification indicated in the test was confirmed in the GOTHIC simulation.

A.5.6 References

1. Email from Bill Williamson of TVA to Tom George of NAI, November 25, 2013

Attachment A-6 Event Timeline

A.6.1 Introduction

A timeline of the events at Fukushima Daiichi Units 1 and 3 is provided in this section. In this first phase of the project, only relevant information from 1F1 and 1F3 are used. The information used to build this timeline has been made available in [1, 2]. Events are listed with the date and Japan Standard Time (JST).

During review of the timeline, recall that 1F1 is a BWR/3 and is equipped with Isolation Condensers (ICs). In contrast, 1F3 is a BWR/4 that is equipped with a Reactor Core Isolation Cooling (RCIC) system. The IC and RCIC serve similar functions by have several important design differences that must be considered in performing analysis. Refer to standard texts on BWR systems for a summary of these two systems.

A.6.2 1F1 Event Timeline

3/11 14:46

Automatic reactor scram due to the earthquake.

3/11 14:47

Main Steam Isolation Valves (MSIV) closed. All control rods were inserted. The scram caused the average power range monitor (APRM) readings to drop suddenly. It was confirmed that the scram went normally. Reactor Pressure Vessel (RPV) pressure increased due to the closure of MSIV.

Due to the loss of off-site power, two Emergency Diesel Generators (EDGs) started up automatically at 14:47. The voltage data was within the normal range. Also due to the loss of off-site power, the emergency bus lost power temporarily until the EDGs started up. As a result, the reactor protection system lost power, and the main steam isolation valves (MSIVs) closed automatically.

3/11 14:52

Isolation Condensers (IC) (A) and (B) started automatically. An operator confirmed the auto startup of the ICs was due to a rise in reactor pressure. Operation of IC's led to RPV pressure decrease. Pressure then increased due to the stop of IC. Changes in the pressure are presumably due to intermittent IC operation.

3/11 15:03

ICs (A) and (B) were stopped manually. The Main Control Room recognized that it would be unable to prevent exceeding the 55℃/h reactor water temperature drop rate.

3/11 15:05

Torus cooling by Containment Cooling System (CCS) (B) started (stopped later due to SBO).

3/11 15:11

Torus cooling by CCS (A) started (stopped later due to SBO).

3/11 15:17

IC(A) restarted

3/11 15:17 – 15:34

IC(A) was started and stopped repeatedly. The Main Control Room recognized that one IC system was enough to maintain the reactor pressure at 6 to 7 MPa.

15:17 started / 15:19 stopped
15:24 started / 15:26 stooped
15:32 started / 15:34 stopped

3/11 15:37

A Station Black out (SBO) occurred because of the Tsunami. This caused torus cooling by CCS (A) and (B) to stop. The status indicator of the IC failed, and operators were unable to check whether the IC valve (3A) was opened or closed. The normal heating, ventilation, and air conditioning (HVAC) system shut down when normal power was lost; however, the primary containment isolation system (PCIS) isolation signal, triggered by the low reactor water level (L-3) or the safety protection system power loss caused the standby gas treatment system (SGTS) to automatically start up, allowing negative pressure to be maintained in the PCV.

3/11 18:18

2A and 3A valves of IC (A) system were opened. Some of the DC power supplies for the Main Control Room came back. An operator opened the valves (MO-2A, 3A). An operator identified the generation of steam. However, the quantity of steam generation was small and subsided. The small amount of steam suggests the opening of IC valves was very limited.

3/11 18:25

MO-3A valve of IC (A) system was closed. Operators estimated that IC had malfunctioned. Considering that the pipe lineup needed to supply water for the shell side had not been formed, an operator set the MO-3A valve to a “closed” state at 18:25

3/11 20:07

The operation of RPV venting was not performed; however, between 20:07 on March 11 and 2:45 on March 12, RPV pressure was depressurized. It is presumed that leakage of the gas phase occurred. There is the possibility for failure of in-core monitors and the gasket seal used in the SV/SRV flange.

3/11 20:50

The lineup of alternative water injection into the RPV by Diesel Driving Fire Protection Pump (DDFP) was implemented. It is presumed that water injected by the DDFP did not reach the RPV because of high RPV pressure.

3/11 21:30

MO-3A valve of IC (A) system was opened. An operator tried re-opening the MO-3A valve because Diesel Driven Fire Pump (DDFP) was in service and refilling water could be supplied to the IC shell side if needed. An operator recognized the generation of steam. As the operating condition of IC after SBO is unclear, it is presumed that the IC malfunctioned after the tsunami.

3/12 1:25

An operator confirmed that the DDFP had stopped. It is presumed that water injected by DDFP did not reach to the RPV, because RPV pressure was unknown during DDFP operation. It is presumed that water injected by DDFP did not reach to the RPV because of high RPV pressure.

3/12 4:00

Batch injection of fresh water through the Fire Protection System (FP) line into RPV by the fire truck was implemented. The discharged total amount of fresh water was 1.30 m^3. Fresh water stored in the fire engine was injected. However, this was temporarily halted due to field radiation level increase etc. Note: the amount of water actually injected into the RPV is still not clear.

3/12 5:46

Injection of fresh water through the FP line to the RPV via fire truck restarted. Fresh water injection using the FP tank as a source continued. Note: the amount of water actually injected into the RPV is still not clear.

3/12 10:17

After 10:17, operators excited the solenoid valve of the small vent valve of the Secondary Containment (S/C) vent line (AO valve) three times. The Main Control Room (MCR) tried opening the small vent valve of S/C at 10:17, 10:23, and 10:24 on March 12. However, the MCR was unable to confirm whether the small vent valve of S/C (AO valve) was open or not. Although the Instrumental Air system (IA), which supplies air to AO valves, had stopped due to loss of AC power, operators excited the solenoid valve, hoping that residual pressure in the IA might open the valve. It is presumed that the small vent valve of the S/C (AO valve) was not opened.

3/12 14:30

Primary containment vessel (PCV) pressure decrease was confirmed. A temporary compressor was connected to the Instrument Air-System (IA) and was started at around 14:00. This allowed the opening of the large vent valve of S/C. D/W pressure decrease was confirmed at 14:30 and was deemed to be due to radioactive material release through venting. It is presumed that the

PCV venting before 14:00 was not successful, but it is presumed to have occurred at some time between 14:00 and 14:30.

3/12 14:53

Injection of fresh water into the RPV by fire truck had finished. The total amount of fresh water discharged was 80 m^3. The amount of water actually injected into the RPV is still not clear.

3/12 15:36

An explosion occurred at the 1F1 Reactor Building (R/B). This event cause the delay of sea water injection

3/12 19:04

Injection of sea water through the FP line into the RPV by fire truck started. The fire brigade completed connecting three fire engines in series to form a water injection line, using the reversing valve pit of 1F3 as a water source. They started sea water injection at 19:04. The amount of water actually injected into the RPV is still not clear.

3/12 21:45

Fire pump stopped and sea water injection into the RPV stopped.

3/12 23:50

Sea water injection into RPV by fire pump restarted.

3/14 1:10

Fire pump stopped due to no water in the pit.

3/14 20:00

Sea water injection into RPV by fire pump restarted.

A.6.3 1F3 Event Timeline

3/11 14:46

Earthquake occurred

3/11 14:47

Automatic Reactor Scram due to the earthquake.

3/11 15:05

The Reactor Core Isolation Cooling (RCIC) system was started manually.

3/11 15:25

RCIC shut down automatically (reactor water level high (L-8)).

3/11 15:38

SBO occurred. Although all the AC power supplies were lost, the DC power supply remained intact and available. RCIC and HPCI, both of which use DC power for operation control were available.

3/11 16:03

RCIC was started manually.

3/12 11:13

DDFP started up automatically. The startup of the DDFP was a test operation and it was uncertain that formation of the S/C spray line was completed at this time. It is presumed that the S/C spray was not implemented.

3/12 11:36

RCIC shut down automatically (tripped). DDFP stopped. The reason why RCIC stopped is unclear. Note: at 5:08 on March 13, operators tried to start up the RCIC but the mechanical structure of the steam stop valve was dislocated and they could not start it up.

3/12 12:06

Alternative S/C spray by DDFP started.

3/12 12:35

HPCI started up automatically (reactor water level low (L-2)).

3/12 20:36

Reactor water level became unknown due to the loss of power supply to the reactor water meters. The flow rate setting of the HPCI was raised slightly to monitor the operational state with the reactor pressure and HPCI discharge pressure, etc.

3/13 2:42

HPCI was stopped manually. Personnel at the Emergency Response Center (ERC) and MCR feared that steam leakage would occur due to equipment damage caused by HPCI system turbine revolution speed decrease. Note: From 2:00 on March 13, reactor pressure, which had remained stable at approx. 1MPa, began to decline.

3/13 3:05

Main control room received the report that the alternative water injection line by DDFP into the reactor had been established. (Shift to the alternative water injection line into the RPV from alternative S/C spray line.) The exact time when S/C spray by DDFP stopped was unclear. This is the time when the main control room received the report. It is presumed that water by DDFP did not reach to the RPV at that time due to high RPV pressure

3/13 5:08

Alternative S/C spray by DDFP started (Shift to the alternative S/C spray line from the alternative water injection line into the reactor).

3/13 7:39

Alternative D/W spray by DDFP started (Shift to the D/W spray line from S/C spray line. Both S/C spray and D/W spray were in service at this time.) It was assumed that each S/C spray and D/W spray operated at a flow rate equal to half of the injection rate during previous S/C spray.

3/13 7:43

Alternative S/C spray by DDFP stopped

3/13 8:40 - 9:10

Water injection by DDFP through alternative water injection line was formed. Alternative D/W spray by DDFP stopped. D/W spray line was shifted to the alternative water injection line into the RPV. The exact time was unclear, but it is presumed that D/W spray stopped at 8:55 judging from a sharp increase in PCV pressure. Also, it is presumed that water injection did not reach to the reactor.

3/13 8:41

The large S/C vent valve was opened. The formation of a vent line was completed, except for the rupture disk.

3/13 9:08

Depressurizing operation of the RPV was started by Safety Relief Valves (SRV). Operators discovered the depressurization of the RPV. When members of the recovery team were connecting batteries to open an SRV, two SRVs showed half-open signal and RPV pressure declined. At 9:50 operators opened SRV. However depressurization had occurred before completion of the operation of opening SRV. Thus, the exact time of RPV depressurization is still unknown, but it is presumed that SRV was opened at 9:08.

3/13 9:20

PCV pressure decreased. ERC judged that venting had occurred at around 9:20, from 637 kPa at 9:10 to 540 kPa at 9:24. A PCV venting line, excluding the rupture disc was established by

opening the large vent valve (AO valve) of the S/C at 8:41. However, it is presumed that venting was started at 9:20, since PCV pressure started to decrease at the time. PCV pressure decrease was confirmed at around 9:20.

3/13 9:25

Injection of fresh water through the FP line into RPV by fire truck was started. Note: It is presumed that water injection began at 9:25 because RPV pressure had been too high to inject water till around 9:08 on March 13. The amount of water injected by alternative water injection line is unclear. Water injection was possible starting at around 9:08 after depressurization of the RPV because alternative water injection line into the RPV was established sometime between 8:40 - 9:10. However, the exact time of water injection is still unknown. Therefore, it is presumed that water injection began at 9:25.

3/13 11:17

It was confirmed that the large vent valve (AO valve) of the S/C had been in a "closed" state due to a decrease in pressure of the operational air cylinders.

3/13 12:00

RPV pressure increased. The lamps of SRVs were going off.

3/13 12:04

RPV pressure decreased. Operators found that the wiring for batteries had come off. Operators restored the wiring and opened an SRV. Note: The detail of SRV operation is unclear. The fact is that the RPV depressurization started as written in the strip chart record. SRV operation started to decrease RPV pressure. This report did not notice the exact timing when SRV was opened. It might be possible to judge the SRV opening time based on depressurization behavior of RPV pressure written on the chart record. Figure A-46 shows the 1F3 RPV pressure chart record for March 13, 2:00 to 13:00. [1].

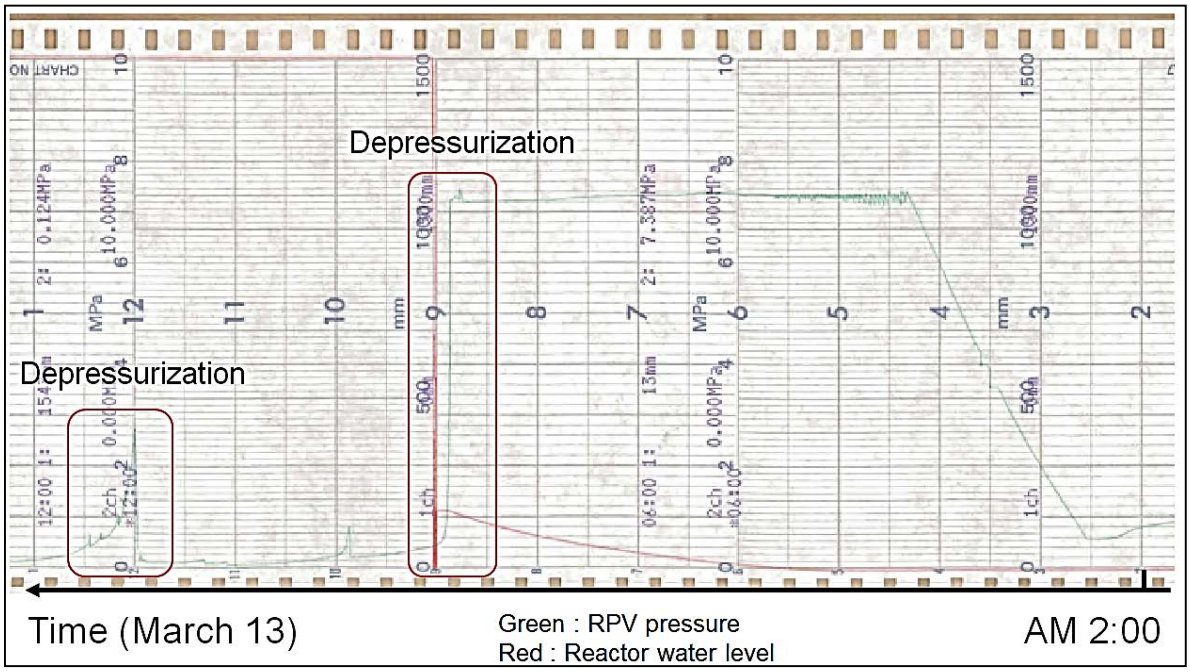

Figure A-46
1F3 RPV Pressure Chart Record

3/13 12:20

Injection of fresh water by fire truck was interrupted due to depletion of a water source. The operation of changing the water source from fresh water to sea water was started. It is presumed that there was no interruption in water injection into the RPV because DDFP kept operating during the change in water sources for water injection by fire truck.

3/13 12:30

Opening operation of the large PCV vent valve (AO valve) of S/C was implemented.

3/13 13:12

Sea water injection by fire truck through the FP line into RPV was started.

3/13 14:30

D/W pressure increased.

3/13 19:00

A temporary air compressor was connected to the Instrument Air (IA) system in order to open the PCV vent valve.

3/13 21:10

The Emergency Response Center (ERC) judged that the large S/C vent valve (AO valve) was opened. Opening operation of the large S/C vent valve was started around 15:00 on March 13 and PCV pressure decrease was observed around 20:30. Reduction of D/W pressure was observed. It is presumed that the large vent valve (AO valve) of the S/C opened at 20:30 judging from the PCV pressure drop.

3/13 22:15

DDFP which had injected water into RPV was confirmed to have stopped (Out of fuel).

3/14 0:50

D/W pressure increased. It is presumed that venting which started at about 21:10 on March 13th terminated at this time based on the increase of D/W pressure.

3/14 1:10

The pump of the fire truck was halted in order to supply water to the reversing valve pit at 1F3.

3/14 3:20

The supply to the reversing valve pit had finished and the injection of sea water into RPV by fire truck restarted

3/14 3:40

The large S/C vent valve (AO valve) was opened. However, it is presumed that the venting was not implemented, as the D/W pressure did not fluctuate.

3/14 5:20

Opening operation of the small vent valve (AO valve) of S/C was started.

3/14 6:10

The small S/C vent valve (AO valve) was opened.

3/14 11:01

An explosion occurred in the Reactor Building and injection of sea water by fire truck was halted due to the explosion.

3/14 11:55

D/W pressure increased. It is presumed that the venting which started at 5:20 on March 14th terminated at 12:00, based on the increasing trend of D/W pressure.

3/14 15:30

Injection of sea water into RPV by fire truck restarted.

3/14 16:30

D/W pressure decreased. It is presumed that venting occurred at 16:00 based on the D/W pressure trend. This venting is presumed to have terminated at 21:04 based on the increase trend of D/W pressure.

3/14 19:20

Injection of sea water into RPV by fire truck stopped (Out of fuel).

3/14 19:54

Injection of sea water into RPV by fire truck restarted.

3/14 20:40

D/W pressure increased. It is presumed that the venting which started at 16:00 on March 14th terminated at 21:04 based on the increasing trend of D/W pressure.

3/14 21:14

Sea water injection by fire truck into the 1F3 RPV was stopped in order to increase the amount of water injected into the 1F2 RPV.

3/15 2:30

Sea water injection by fire truck restarted. Note: This was not considered in TEPCO's analysis published on March 2012 (TEPCO Accident Report, 2012), because it had not been revealed when TEPCO conducted the analysis.

3/15 16:00

The large and small vent valves (AO valve) of the S/C were confirmed to be closed due to failure of the small generator which had energized solenoid valves in the air supply line for the vent valves.

3/15 16:05

The large S/C vent valve was opened. Opening operation of the large PCV vent valve (AO valve) of S/C was conducted.

3/16 1:55

The small S/C vent valve was opened. Opening operation of the small PCV vent valve (AO valve) of S/C was conducted.

3/17 21:00

It was confirmed that the large S/C vent valves were closed. Note: To some extent, TEPCO presumed in the MAAP analysis that the vent valve was opened when PCV pressure decreased and the vent valve was closed when PCV pressure increased with or without the operation of venting. Closure of the large PCV vent valve (AO valve) of the S/C was confirmed. The closure of the valve was confirmed following the opening of the vent at 16:05 March 15th. However, it is presumed that the valve was not closed based on the behavior of the D/W pressure.

3/17 21:30

Opening operation of the large PCV vent valve (AO valve) of S/C was conducted.

3/18 5:30

Closure of the large PCV vent valve (AO valve) of S/C was confirmed. Opening operation of the large PCV vent valve (AO valve) of S/C was conducted.

3/19 11:30

Closure of the large PCV vent valve (AO valve) of the S/C was confirmed.

3/20 11:25

Opening operation of the large PCV vent valve (AO valve) of the S/C was conducted.

A.6.4 References

1. OECD-NEA. (2012). Benchmark Study of the Accident at the Fukushima Daiichi NPS Project, (BSAF Project). Tokyo.
2. TEPCO Accident Report. (2012). Fukushima Nuclear Accident Analysis Report.

The Electric Power Research Institute, Inc. (EPRI, www.epri.com) conducts research and development relating to the generation, delivery and use of electricity for the benefit of the public. An independent, nonprofit organization, EPRI brings together its scientists and engineers as well as experts from academia and industry to help address challenges in electricity, including reliability, efficiency, affordability, health, safety and the environment. EPRI also provides technology, policy and economic analyses to drive long-range research and development planning, and supports research in emerging technologies. EPRI's members represent approximately 90 percent of the electricity generated and delivered in the United States, and international participation extends to more than 30 countries. EPRI's principal offices and laboratories are located in Palo Alto, Calif.; Charlotte, N.C.; Knoxville, Tenn.; and Lenox, Mass.

Together…Shaping the Future of Electricity

3002005295

Electric Power Research Institute
3420 Hillview Avenue, Palo Alto, California 94304-1338 • PO Box 10412, Palo Alto, California 94303-0813 • USA
800.313.3774 • 650.855.2121 • askepri@epri.com • www.epri.com